The αvβ6 Integrin in Cancer

Daniel James Marsh

A thesis submitted to the University College London for the degree of Doctor of Philosophy in the faculty of Biomedical Sciences, Department of Oncology,

UCL Cancer Institute,
University College London

Abstract

The epithelial restricted αvβ6 integrin is known to have minimal expression in healthy tissue and to be upregulated in cancer and healing wounds. This thesis explores the role of αvβ6 in cancer and tests the hypothesis that αvβ6 has a prognostic and therapeutic utility in cancer.

Using immunohistochemistry, increased αvβ6 expression was found in non-melanoma skin cancers (NMSC), particularly in morphoeic type basal cell carcinoma. In cell culture experiments, αvβ6 was found to activate TGF-β and promote myofibroblast differentiation, producing a tumour stroma rich in smooth muscle actin (SMA). These findings prompted a study of αvβ6 and SMA as prognostic indicators in oral squamous cell carcinoma (OSCC). A study of 282 cases of OSCC found that although αvβ6 was not a prognostic marker, patients with high SMA levels had a highly significant increased risk of disease specific mortality (HR 3.06 [CI 1.65-5.66], $p<0.001$).

Next, the utility of αvβ6 as a target was explored through the development of a single chain antibody fragment (scFv) specific for αvβ6. The scFv was tested for the delivery of targeted magnetic fluid hyperthermia (MFH), an experimental cancer treatment based on the generation of heat by magnetic nanoparticles when placed within an alternating magnetic field. The αvβ6-specific scFv (B6.3) was manufactured and high ligand specificity confirmed on ELISA and FACS analysis. B6.3 was successfully conjugated to two alternative iron nanoparticles. *In-vitro* studies demonstrated increased cellular uptake of scFv-nanoparticle complexes and greater cellular toxicity on exposure to MFH compared to nanoparticles alone.

In conclusion, αvβ6 is a potential target for therapy in NMSC and OSCC. SMA is found to be an independent prognostic marker in OSCC and αvβ6 identified as a pro-invasive factor in morphoeic BCC. Finally, the production αvβ6 specific scFvs and use for *in-vitro* MFH potentiates the development of αvβ6 targeted MFH cancer therapy.

Declaration of Originality

I, Daniel James Marsh, declare that the research for this thesis is original and that the ideas were developed by me in conjunction with my supervisors. Where information has been obtained from other sources I confirm that this has been indicated in the thesis.

Contents

Page

List of Figures

Chapter 1

Chapter 2

Chapter 3

Chapter 4

Chapter 5

List of Tables

Chapter 1

Chapter 2

Chapter 3

Chapter 4

Chapter 5

List of Abbreviations

A375B6	β6 transfected human melanoma cell line
Ab	Antibody
A/C	Alternating current
ADEPT	Antibody directed enzyme prodrug therapy
AK	Actinic Keratosis
ANOVA	Analysis Of Varience
AMF	Alternating magnetic field
ATP	Adenosine TriPhosphate
A375	Human melanoma cell line
B6.3	anti αvβ6 scFv antibody
BMGY	Buffered Glycerol-complex Medium Yeast
BMMY	Buffered Methanol-complex Medium Yeast
BCC	Basal cell carcinoma
BSA	Bovine Serum Albumin
C	Constant domain
CDR	Complementarity determining region
CEA	Carcinoembryonic antigen
COOH	Carboxyl group
COSHH	Control of Substances Hazardous to Health
CT	Computerised tomography
Cy3	Cyanine 3
Da	Dalton
DAB	Diaminobenzidinetetrahydrochloride
ddH_2O	Double-distilled water
DMEM	Dulbeccos Modified Eagle Medium
DNA	Deoxyribonucleic acid
DTT	Dithiothreitol
IMAC	Expanded bed adsorption immobilised metal affinity chromatography
EBA	Expanded Bed Adsorption
ECL	Enhanced Chemiluminescence
EDC	N-ethyl-N'-(3-diethyl-aminopropyl)-carbodiimide
E. coli	*Escherichia coli*
EDTA	Ethylenediamine tetraacetic acid
EGFR	Epidermal growth factor receptor

EGTA	Ethylene glycol tetraacetic acid
ELISA	Enzyme-linked immunosorbent assay
EMT	Epithelial Mesenchymal Transition
ERK	Extracellular signal Related Kinases
FAK	Focal Adhesion Kinase
Fab	Fragment released from papain digestion of IgG
Fc	Constant fragment
FCM	Fibroblast Conditioned Medium
FCS	Fetal Calf Serum
FDA	Food and Drug Administration
Fe	Iron
FITC	Fluorescein isothiocyanate
FR	Framework region
FPLC	Fast pressure liquid chromatography
Fv	Variable region fragment
g	gram
hr	hour
H	Heavy chain
HGF	Hepatocyte Growth Factor
HFF2	Human foreskin fibroblast cell line
HIFU	High Intensity Focused Ultrasound
HNSCC	Head and neck squamous cell carcinoma
HPV	Human papilloma virus
hsMFE-23	Humanised stabilized MFE-23
HSP	Heat Shock Protein
HSP -70	70kDa Heat Shock Protein
Hz	Hertz
Ig	Immunoglobulin
IGF-IR	Insulin like Growth Factor Receptor 1
kA/m	kiloAmpere/metre
K_D	Dissociation constant
kDa	kiloDalton
KHz	kiloHertz
l	litre
L	Light chain
LB	Luria Bertani (Broth)
LAP	Latency Activated Peptide
LTBP1	Latent TGFβ Binding Peptide 1

M	molar
MAb	Monoclonal antibody
MACH	Magnetic Alternating Current Hyperthermia
MAPK	Mitogen Activated Protein Kinase
MCM	Myofibroblast Conditioned Medium
MES	2-(4-morpholino) ethanesulphonic HCL
MEM	Minimal Essental Medium
MFE-23	Murine anti-CEA antibody
MFH	Magnetic fluid hyperthermia
MMP-9	Matrix metallopeptidase 9
MOPS	3-[N-morpholino]propanesulfonic acid
MRI	Magnetic resonance imaging
MTT	3-(4,5-Dimethylthiazol-2-yl)-2,5-diphenyltetrazolium
MW	Molecular weight
MWCO	Molecular Weight Cut Off
MHz	Mega hertz
µg	Microgram
mg	Milligram
min	minute
µM	micromolar
mM	millimolar
µl	microlitre
ml	millilitre
N	Nitrogen
NH_2	Amine group
NHS	N-hydroxysuccinimide
NMSC	Non melanoma skin cancer
Oe	Oersted
OD	Optical density
OSCC	Oral Squamous Cell Carcinoma
Pax	Paxillin
PAK	P21 activated kinase
PBS	Phosphate buffered saline
PCR	Polymerase chain reaction
PEG	Poly(ethylene) glycol
PET	Positron emission tomography
P. pastoris	*Pichia pastoris*
RGD	Arginine – Glycine - Aspartate

RES	Reticuloendothelial system
RNase A	Ribonuclease A
Rpm	Revolutions per minute
RT	Room temperature
s	second
SAR	Specific absorption rate
SCC	Squamous Cell Carcinoma
scFv	Single chain fragment variable
SDS	Sodium dodecyl sulphate
SDS-PAGE	SDS-polyacrylamide gel electrophoresis
SF	Scatter Factor
SiRNA	Small interfering RNA
SPIONs	Superparamagnetic iron oxide nanoparticles
TBE	Tris borate EDTA
TGF-β	Transforming Growth Factor β
TNF	Tumour Necrosis Factor
Tris	*tris*(hydroxymethyl)aminomethane
Tris-Cl	*tris*(hydroxymethyl)amino methane and hydrochloric acid
UV	Ultraviolet
V	Variable domain
V	Voltage
VB6	human keratinocyte cell line overexpressing αvβ6
VEGF	Vascular endothelial growth factor
V_H	Heavy chain variable domain
Vin	Vinculin
V_L	Light chain variable domain
v/v	Volume to volume
w/v	Weight to volume
YPD	Yeast Peptone Dextrose
YPDS	YPD with Sorbitol
YT	Yeast Tryptone
Zyx	Zyxin

Acknowledgements

This PhD would not have been possible without Professor Kerry Chester who has supported me throughout and whose friendship I value dearly. I remain indebted to Jag Chana for his help with getting the project off the ground and for all the clinical training he has provided during my time in research. Thanks must also go to Tim Meyer for his critical review and support. I also would like to thank Professor Gareth Thomas and all at the Centre for Tumour Biology at Barts and The London School of Medicine for allowing me to use their facilities.

Thank you to Professor Richard Begent for allowing me to pursue my PhD in his laboratory and to others in the laboratory whose help was invaluable. In particular, Dr Heide Kogelberg, Dr Berend Tolner, Dr Kim Vigor, Helen Lowe and Lynda Robson for their practical assistance. Thanks also to Professor Quentin Pankhurst, Dr Paul Southern and Mathew Kallumadil at the Royal Institution of Great Britain for help with developing and setting up the MACH machine.

I would like to acknowledge the Restoration of Appearance and Function Trust, the Royal College of Surgeons of England, BASO and the Peter Samuels Fund at the Royal Free Hospital for the financial support provided during my studentship.

Finally, I would like to thank my wife Rosie for her never-ending patience and support.

Chapter 1

Introduction

1.1 The αvβ6 Integrin

1.1.1 Background

Integrins are heterodimeric molecules that span the membrane of cells provide a direct connection between the extracellular matrix and the intracellular cytoskeleton potentiating bidirectional communication between the internal cell environment and the surrounding extracellular components (Akiyama *et al* 1995). As well as mediating cell adhesion, integrins are involved in development, immune responses, leukocyte signalling, haemostasis, cancer and integrins are receptors for many bacteria and viruses.

The basic structure of an integrin consists of alpha and beta subunits that are non-covalently associated with an extracellular globular domain and a long cytoplasmic tail (figure 1.1). The intracellular component of integrins contains the carboxy termini of the alpha and beta domains, is less than 60 amino acids in length and interacts with the cellular cytoskeleton through a series of protein kinase mediated reactions. All integrins except one (α6β4) bind to and regulate the intracellular actin monofilament system which in turn regulates cell motility. The extracellular domain of the integrin is globular in shape and contains the ligand binding site which coordinates the interaction of the cell with the external environment (Hynes 2002).

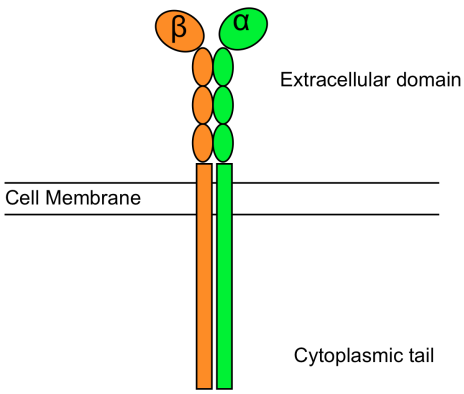

Figure 1.1 - Generalised integrin structure showing α and β subunits spanning the cell membrane

So far there are known to be 24 possible combinations of the 18 alpha and 8 beta subunits that make up the integrin family all of which, on binding to ligand activate a series of intracellular signaling pathways (figure 1.2). Integrins have previously been identified to play an important part in cellular survival (Meredith *et al* 1993), proliferation, regulation of gene expression (Werb *et al* 1989) and tumour progression (Guo and Giancotti 2004).

Altered integrin expression has been reported in many tumours and has long been known to play a role in the progression of squamous cell carcinoma (SCC) of the skin and head and neck (Jones *et al* 1993 and 1997, Lyons and Jones 2007). SCC develops due to abnormal changes in the epithelium as keratinocyte cells undergo differentiation to become the protective cells on the outer layer of our skin or mucosa. Prior to undergoing differentiation, the basal layer of stratified squamous epithelium is anchored by integrins which interact specifically with proteins making up the extracellular matrix of the basement membrane. Abnormalities in integrin function alter the way cells interact with their local environment and these molecules have been implicated in the development and progression of SCC (Watt 2002).

Interactions between integrins and the intracellular actin based cytoskeleton are complex however an overview is given in figure 1.2 and table 1.1 below.

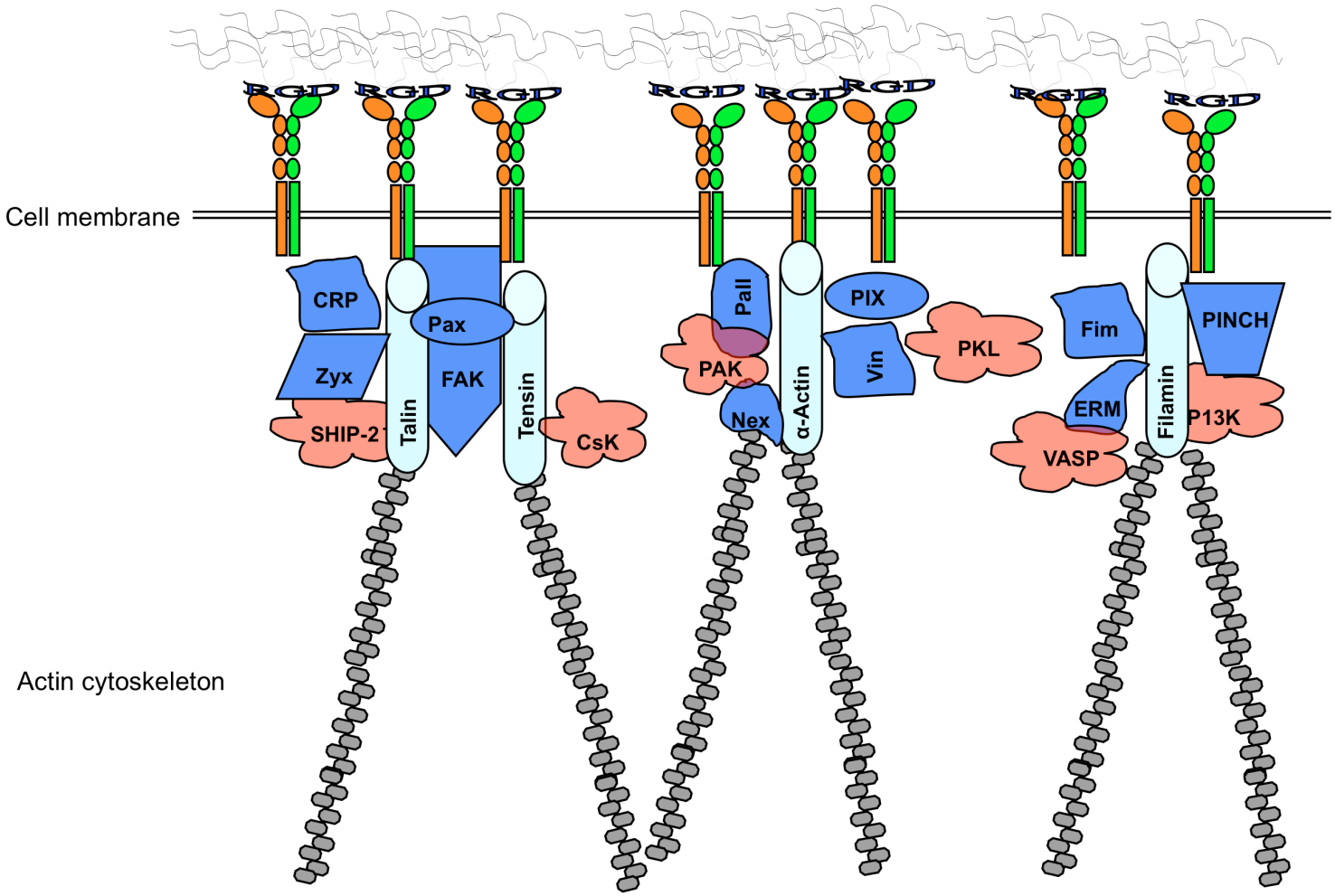

Figure 1.2 - Pathways involved following integrin binding to ligand showing adaptor proteins (pale blue) linking integrins to actin filaments, enzymes (red) and other integrin associated proteins in dark blue.

Integrin associated protein	*Proposed Function*
FAK Focal Adhesion Kinase	An intracellular tyrosine kinase protein - mediates signal transduction pathways initiated either at the sites of cell attachment or at growth factor receptors.
Vin Vinculin	A key regulator of Focal Adhesions and interacts with talin and α-actinin
Talin	Actin-binding protein essential role in inside-out integrin activation and early coupling of extracellular ligand-bound integrins to the cytoskeleton through recruitment of other proteins such as paxillin, vinculin, α-actinin, tensin, and zyxin
PAK P21 activated Kinase	Regulation of the Erk pathway, acting primarily at the level of Raf-1 and involved with Rac-mediated actin reorganization of the membrane of migrating cells
Pax Paxillin	Localizes to focal adhesions possibly through a direct association with ß-integrin tails or an intermediate protein 'X' such as vinculin and actopaxin that bind actin directly to regulators of actin cytoskeletal dynamics such as the ARF GAP, PKL, the exchange factor PIX and the p21-activated kinase, PAK.
Zyx Zyxin	Focal adhesion protein which shuttles between the focal adhesion and the nucleus, influences actin assembly and organization as well as cell motility
SHIP2 Src homology 2 (SH2) domain-containing inositol 5-phosphatase 2.	Catalyses the dephosphorylation of phosphatidylinositol 3,4,5-trisphosphate [PtdIns(3,4,5)P3] to phosphatidylinositol 3,4-bisphosphate. Interacts with cell cytoskeleton proteins including venexin.
CSK	Negative regulatory kinase for SFK. Leads to enhanced phosphorylation of FAK and paxilllin, enhanced cell scattering, rearrangement of actin cytoskeleton and increased cell adhesion/migration and invasiveness.
Tensin	Negatively regulates actin assembly by capping the barbed end of filaments and controls the transmission of force between actin cytoskeleton and focal adhesions.
Nex Nexilin	Actin filament binding protein localised at cell matrix adherens junction.
Pall Palladin	Binds directly to F-actin, crosslinking actin filaments into bundles,
PIX PAK-interacting exchange factor	PIX strongly stimulates PAK activity and is important for PAK recruitment and localization to focal complexes and focal adhesions.
PI3K phosphatidyl inositol 3-kinase	Activated form, PtdIns(3,4,5)P_3, targets various kinases to influence mitogenic signalling, cell survival and cytoskeletal remodelling.
PKL paxillin kinase linker	On cell adhesion to fibronectin and rac activation, PKL is phosphorylated by Src and/or FAK allowing localization to focal adhesions and for paxillin binding

ERM ezrin–radixin–moesin proteins	Interact via their FERM domains with signaling molecules including phosphatidylinositol 3-kinase or a Rho-specific guanine nucleotide dissociation inhibitor (GDI).
Fim Fimbrin	Actin crosslinker contributing to cell mechanics in a myosin-II-dependent manner allowing for cell contractility and modulating change in cell-shape.
VASP vasodilator-stimulated phosphoprotein	Enhances actin polymerization, localises at the tips of actin fibers.
Fil filamin	Actin crosslinker protein. Cells lacking filamin expression exhibit unstable surfaces, are incapable of locomotion, and have impaired mechanical resistance
PINCH Cysteine-histidine rich protein	Forms complex IPP with integrin-linked kinases and Parvins which act as regulators of gene transcription or cell–cell adhesion.

Table 1.1 - Descriptions of the role of integrin associated proteins shown in figure 2.2

In normal human epidermis, the most abundant integrins are α2β1 (a collagen receptor), α3β1 (primarily a laminin receptor) and α6β4 (a laminin receptor) (Watt 2002). The αvβ5 integrin (a vitronectin receptor) is expressed at lower levels, the α5β1 integrin (fibronectin receptor) and αvβ6 integrins (receptor for tenascin and fibronectin) are either expressed at low levels or undetectable in normal epidermis, but are upregulated during wound healing in vivo.

In general, as keratinocytes move through the layers of the epidermis, integrin expression is downregulated from a maximal expression at the basement membrane to minimal or negative expression at the superficial stratum corneum (Figure 1.3).

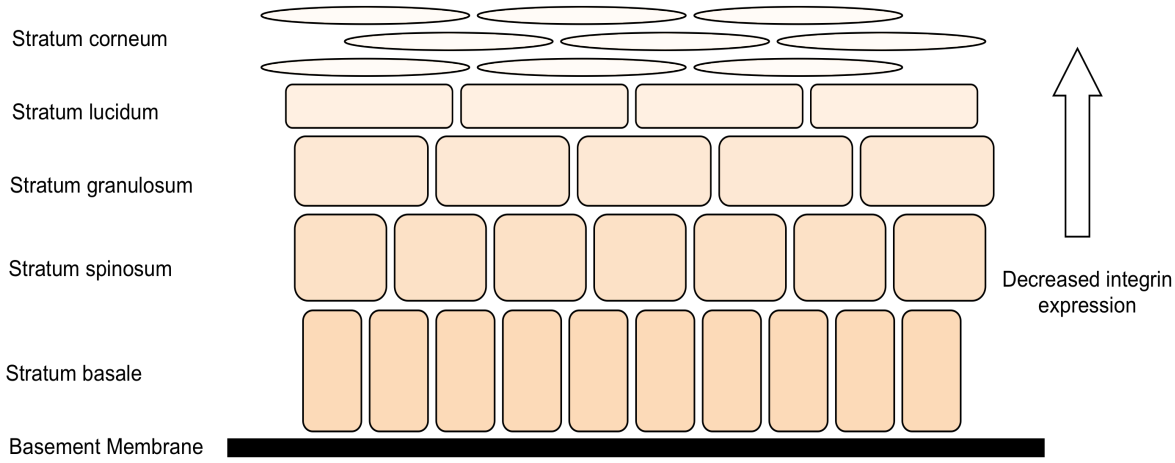

Figure 1.3 - Layers of epidermis showing morphological change in epidermal cells and the decreased expression of integrins moving from the basement membrane to the skin surface.

Examining SCC sections using immunohistochemistry staining for integrin expression reveals variations between sections within the same tumour and between different tumour samples. Occasionally, complete loss of a particular integrin occurs throughout a tumour, whereas expression of other integrins in the same tumour seems normal (Jones 1993).

Integrin overexpression, when integrins are expressed throughout the tumour mass, is frequently seen and has been shown to correlate with poor prognosis as in the case of α6β4 (Rabinovitz and Mercurio 1996, van Waes *et al* 1995) and αvβ6 (Thomas *et al* 2006). The αvβ6 integrin is of particular interest as it is not constitutively expressed in normal healthy epithelium but is upregulated in healing wounds and in carcinogenesis (Breuss *et al* 1995). Furthermore, as αvβ6 is expressed solely on epithelial cells, the integrin has generated much interest as a novel target for epithelial cancer therapies.

1.1.2 αvβ6 and wound healing

In vitro studies have shown that αvβ6 is important for coordinating keratinocyte interaction with fibronectin, tenascin and vitronectin, which are important constituents of the early wound matrix (Busk *et al* 1992, Koivisto *et al* 1999). Maximal expression of αvβ6 was seen relatively late during mucosal and dermal wound healing, after the two migrating edges of the wound epithelium have joined (Haapasalmi *et al* 1996). Workers have also shown that in the re-epithelialisation of normal human wounds there is a switch in integrin expression from αvβ5 to αvβ6 (Clark *et al* 1996). Further studies have shown that αvβ6-dependent upregulation of the type IV collagenase MMP-9 facilitates cell movement by allowing keratinocytes to detach from the basement membrane (Thomas *et al* 2001).

Although exact mechanisms for regulation of αvβ6 turnover in wound healing are not yet fully understood, the integrin may be important in the late stabilisation of wounds through a TGFβ mediated pathway. TGFβ is important in wound healing for the regulation of re-epithelialisation, suppression of inflammation, deposition of extracellular matrix and formation of scar tissue (Verrecchia *et al* 2002). It is possible that expression of αvβ6 in wound healing may alter the rate of repair or morphology of the wound. In vivo work using a transgenic mouse which constitutively expresses αvβ6 found that these mice healed without significant scarring and rates of wound healing and TGFβ levels were similar to controls (Hakkinen 2004). Interestingly, the same group noted that mice overexpressing αvβ6 spontaneously developed chronic skin ulcers containing activated fibroblasts and macrophages, and these ulcers expressed higher levels of TGFβ compared to normal skin in the same mice. These data suggest that in situations of chronic inflammation, the fibrosis and ulceration that occurs may be αvβ6-mediated.

1.1.3 αvβ6 activates TGFβ

The transforming growth factor β family consists of three isoforms (TGFβ 1,2,3) that are involved in modulation of inflammation, inhibition of growth, regulation of ECM turnover and cancer metastasis (Yang 2010). The TGFβs are secreted in inactive form with the larger TGFβ molecule non covalently associated with the latency associated peptide (LAP) and in most cases, this complex is joined by a third protein, the latent TGFβ binding protein 1 (LTBP1). The exact mechanisms for activation of TGFβ are incompletely understood however it is known that LAPβ1 contains the tripeptide sequence RGD and that LAPβ1 is a ligand for αvβ6 (Wipff and Hines 2008). Binding of the LAP peptide to αvβ6 integrin has further been shown to activate TGFβ1 (Munger *et al* 1999) and TGFβ3 (Annes *et al* 2002). The αvβ6 dependent LAP mediated activation of TGFβ depends on a conformational change in the latent TGFβ and not on the cleavage of LAP from TGFβ. Studies using cells expressing mutant β6 could only activate TGFβ when the β6 was able to interact with actin in the cell cytoskeleton via phosphorylation of adaptor proteins including FAK and paxillin (Munger *et al* 1999). Thus the activation of TGFβ1 through binding of LAPβ1 to αvβ6 is further dependent on the ability of the αvβ6 to interact with the actin cytoskeleton.

Upregulation of TGFβ has previously been shown to be both a promoter and inhibitor of carcinogenesis (Elliott and Blobe 2005, Akhurst and Derynck 2001) so evidence that αvβ6 upregulates TGFβ further suggests the cytokine has a complex role in the development of cancer. It is possible that in the early stages of tumour growth, TGFβ is inhibitory and that as the cancer grows, TGFβ becomes a tumour promoter which may explain the differences described as to it's effects (Elliott and Blobe 2005).

1.1.4 αvβ6 and the promotion of carcinogenesis

In common with other αv integrins, when binding to ligand, αvβ6 recognises the arginine-glycine-aspartate (RGD) tripeptide motif. It is through this motif that αvβ6 interacts with the extracellular matrix and one mechanism by which the integrin modulates cellular motility, migration and invasion. Carcinogenesis involves

disruption of normal interactions with the cell's milleu which is characterised by disrupted cytoskeletal organisation and altered adhesion dependent responses. One suggested mechanism for the promotion of carcinogenesis is the phenotypic change in cell type from epithelial to the more invasive mesenchymal type. Bates *et al* (2005) showed that αvβ6 overexpression was associated with a change in colon carcinoma cells from epithelial to mesenchymal type. Others have shown that αvβ6 is overexpressed at the leading edge of oral SCC tumours suggesting that the integrin is upregulated as tumours become more invasive (Regezi *et al* 2002). Recently, blockade of the αvβ6 integrin has been shown to inhibit tumour progression *in vivo* using human pharyngeal cancer xenographs in mice (van Aarsen et al 2008). Table 1.2 lists tumour types shown to express αvβ6.

Tissue	**No of Tumours**	**% Expressing αvβ6**	**Reference**
Oral SCC	40	100	Regezzi et al 2002
	11	100	Impola et al 2004
	40	100	Jones et al 1997
	38	94.7	Hsiao et al 2010
	30	90	Breuss et al 1995
	5	80	Hamidi et al 2000
Oesophagus	56	68	Van Aarsen et al 2008
Pancreas	34	100	Siphos et al 2004
Breast	45	100	Arihiro et al 2000
Skin	49	84	Van Aarsen et al 2008
Cervix	85	59	Hazelbag et al 2007
	46	92	Van Aarsen et al 2008
Endometrial carcinoma	126	42	Hecht et al 2008
Lung	51	50	Smyth et al 1995
	271	56	Elayadi 2007
Gastric	38	47	Kawashima et al 2003
	300	36.7%	Zhang et al 2008
Colon	488	38	Bates et al 2005

Table 1.2 - Published data on αvβ6 expression levels in various epithelial malignancies

Ramos *et al* (2007) showed that transfecting β6 into poorly invasive Oral Squamous Cell Carcinoma (OSCC) cells enhanced tumour growth rate five fold compared to non transfected cells when injected into nude mice. The same group showed the β6-transfected cells invaded deep into muscle whereas the non transfected cells did not cross the muscle fascia suggesting β6 promotes invasion in OSCC cells. More recently Ramos *et al* (2009) have suggested that αvβ6 expression in OSCC cells may trigger epithelial to mesenchymal transition (EMT) which causes cells to become more invasive. This finding is in agreement with Bates *et al* (2005) who described the role of αvβ6 in EMT in colon carcinoma.

It has been suggested that one other possible mechanism by which αvβ6 promotes invasion is through the upregulation of proteases or collagenases including matrix metallo- proteases (MMP) 3 and 9. MMPs are a family of zinc dependent endopeptidases that act to degrade the components of the extracellular matrix (Munshi and Stack 2006). Thomas *et al* (2001) used OSCC cells retrovirally transfected with β6 cDNA and found this cell line to be significantly more invasive through Matrigel® in Transwell® invasion assays compared to controls with low levels of αvβ6. The mechanism for the increased invasion was described to be through αvβ6-dependent upregulation of the type IV collagenase MMP-9 (and to a lesser extent MMP-2). In a similar study using colon carcinoma cells, αvβ6 has been shown to regulate MMP-9 by a process modulated through the extracellular- regulated kinase (ERK) binding to the β6 cytoplasmic tail (Niu *et al* 2002). More recently, Fouchier *et al* (2007) described the involvement of αvβ6 in the adhesion of HT29-D4 adenocarcinoma cells to fibrinogen that had been processed by MMP9 in the presence of high concentration of Mn2+. This process was shown to occur via the activation of the Extracellular Signal Regulated Kinase (ERK)/ Mitogen Activated Protein Kinase (MAPK) pathway and MMP9.

The HS1 associated protein HAX-1 has also been implicated as a partner for αvβ6 in the promotion of carcinogenesis. Ramsay *et al* (2007) found that the interaction between HAX-1 and αvβ6 was important for the clathrin-mediated endocytosis of the receptor and influenced the invasive behaviour of OSCC cells. Evidence is emerging

that the rate of clathrin mediated receptor recycling is important in determining the invasive capacity for the cell and the ultimately the rate of cancer progression (Lanzetti and DiFiore 2008). So it is by several mechanisms that αvβ6 has been shown to be important in cancer progression.

1.1.5 αvβ6 as a prognostic indicator

Interestingly, αvβ6 has been shown to be expressed in leukoplakia, a premalignant lesion of the oral mucosa as well as in salivary gland neoplasias (Westernoff *et al* 2005). This observation suggests that the integrin may play a role in the progression from normal mucosa to malignancy (Hamidi *et al* 2000). Furthermore, upregulation of αvβ6 is associated with increased cellular invasion and more aggressive carcinomas so it is conceivable that patients with tumours expressing higher levels of αvβ6 may have a worse prognosis than those with low levels of the integrin.

Bates *et al* (2005) showed that αvβ6 enhanced the tumorigenic properties of colon carcinoma and in an analysis of 488 colorectal carcinomas that the β6 subunit was associated with significantly poorer prognosis. The same group also showed that distant metastases were also strongly positive for β6 suggesting the integrin is associated with disease progression and a poorer prognosis. Expression of αvβ6 has also been described in the lymph nodes of patients with gastric carcinoma (Kawashima *et al* 2003). Other workers have shown αvβ6 to be expressed in gastric carcinomas and interestingly, overexpression was found to correlate with reduced survival in gastric carcinoma patients (Zhang et al 2008).

Overexpression of αvβ6 has also been shown to be an unfavourable prognostic marker in cervical carcinoma. Hazelbag *et al* (2007) looked at paraffin fixed specimens of cervical SCC from 86 women who had undergone radical hysterectomy and found that high levels of αvβ6 expression was significantly associated with more advanced disease at time of resection. Furthermore, patients with tumour cells that stained strongly for αvβ6 on immunohistochemistry had a shorter overall five year survival rate.

1.2 Oral Squamous Cell Carcinoma

Squamous Cell Carcinoma (SCC) is a malignant tumour of epithelial cells which is locally invasive and prone to distant metastases if left untreated. The epithelium is in effect our barrier to the external environment and it is the epithelial cells which constitute the external and internal linings of the body. Common sites for SCCs to arise are on the epidermal layer of the skin, the lining of the cervix, the oesophagus and the mucosal surfaces of the head and neck aero digestive tracts. The prognosis of SCC very much depends on the site, for example epidermal SCC if detected early enough is treated by surgical excision which is frequently curative. In contrast, when SCC arises in the head and neck region, 5 year survival rates are less than 50% and there have been little improvement in the mortality figures over the past 30 years.

Overall, greater than ninety percent of oral cancers are SCC's with the remaining ten percent made up from lymphomas, adenocarcinomas, salivary gland tumours, sarcomas and other rarer tumour types. Worldwide there are an estimated 405,000 new cases of oral squamous cell carcinomas (OSCC) every year. Every year there are approximately 320,000 deaths from OSCC, resulting in an average incidence rate of 8.8 and 5.1 per 100,000 males and females. These figures place OSCC as the eighth leading cause of death from cancer worldwide (Shibuya *et al* 2002). There are large regional variations in the level of OSCC, the highest incidence being in Somme, France with an average rate of 43.1 new cases per 100,000 in men and 4.7 cases per 100,000 in women. In women, the highest incidence of OSCC is found in Bangalore, India, with an average rate of 11.2 cases per 100,000. The lowest incidence for males was reported in Quito, Ecuador, with an average of 2.4 new cases per 100,000 and the lowest worldwide incidence for females was reported in Kangwha County, Korea, with an average rate of 0.5 per 100,000 (Parkin *et al* 2002). In the United States of America, The National Cancer Institute's Surveillance, Epidemiology and End Results Program (SEER) reported that between 1997 and 2002, the median age of oral and oropharyngeal cancer diagnosis was 63 years, and the median age at death was 68 years (Ries *et al* 2005).

As with many cancers, tobacco use is a major risk factor and in 1957, Wynder and Bross first identified cigarette smoking to be an independent risk factor for oral and

oropharyngeal cancer. Later, tobacco and alcohol were confirmed to be the two major risk factors for the development of oral cancers and were even seen to be synergistic in effect (Choi and Kahyo 1991, Brennan *et al* 1995, Lewin et al 1998). Other risk factors for the development of OSCC include presence of premalignant oral lesions, betal quid chewing, age, diets lacking antioxidants, genetic factors, exposure to UV-light, immunodeficiencies, anaemias and poor oral health (Reichart 2001). The human papilloma virus (HPV) has recently been identified in over 95% of invasive cervical cancers (Bosch *et al* 2002) and HPV has also been implicated as a risk factor for HNSCC (Ragin 2007). Figure 1.4 shows a buccal intaoral squamous cell carcinoma.

Figure 1.4 – Typical appearance of oral squamous cell carcinoma.

1.2.1 Current Management of Oral Cancers

1.2.1.1 Imaging

Combined with thorough physical examination, pan endoscopy and a tissue diagnosis, improvements in imaging techniques have lead to a huge increase in the accuracy of preoperative staging of patients with OSCC. Current imaging modalities include computerised tomography (CT) and magnetic resonance imaging (MRI) with the choice of scan being determined by the location of the tumour and what information is being sought. Newer spiral CT imaging allows for accurate three dimensional images which can be obtained in a shorter time period and are useful for guided biopsies of deep seated tumours. Positron Emission Tomography (PET)/CT combines image data from intravenously injected radioactive 2-[18F]-fluoro-2-deoxy- D-glucose (FDG) with anatomical data from the CT scan. By merging the excellent sensitivity of PET with the spatial resolution of CT, accurate images can be obtained of metabolically active tumours, especially in patients who have undergone therapy (Sachelarie *et al* 2005).

MRI is often used in place of CT when detailed soft tissue images are required as the modality offers improved contrast by which blood vessels, masses, and adjacent soft tissues are easily differentiated (Hoover *et al* 1987). Disadvantages of MRI include the length of time taken to obtain the images, often patients with OSCC have other co-morbidities and cannot lie still for the required time period. Patients with cardiac pacemakers, metallic cochlear implants or cerebral artery aneurysm clips cannot be placed in the strong magnetic field of an MRI machine due to risk of implant malfunction (Pavlicek *et al* 1983, Klucznik *et al* 1993). The use of contrast agents improves the efficiency of both CT and MRI scans and recently superparamagnetic iron oxide nanoparticles have been used to improve contrast in MRI imaging of cancers of the liver and lymph nodes. Contrast agents in current use are taken up non specifically either by tissues with a higher metabolic rate or simply accumulate in organs which are acting to remove them from the circulation (DeBondt *et al* 2007). Work continues to produce contrast agents which can be specifically targeted against cells or molecules produced by cancers to improve the efficacy of conventional imaging techniques (reviewed by Atri 2006).

1.2.1.2 Therapy

A unifying thread in OSCC is the poor overall survival for those patients with advanced, recurrent or metastatic disease. Oral cancers have been classified by the American Joint Committee on Cancers (AJCC) and is based on the Tumour Node Metastasis (TNM) system:

Stage 0	Carcinoma in situ
Stage I	Tumour < 2cm diameter
Stage II	Tumour 2 – 4 cm in diameter
Stage III	Tumour > 4cm diameter Tumour diameter <2cm with single ipsilateral lymph node (LN) <3cm in diameter Tumour 2 – 4cm diameter with single ipsilateral LN <3 cm in diameter. Tumour > 4cm with single ipsilateral LN <3cm in diameter
Stage IVa	Tumour invades adjacent structures Tumour invades adjacent structures with single ipsilateral LN <3cm Tumour of any size with ipsilateral LN 3-6cm diameter or multiple ipsilateral LNs all under 6cm or multiple bilateral/contralateral LNs all under 6cm diameter
Stage IVb	Any tumour size with any LN >6cm in diameter
Stage IVc	Any tumour, any nodal status with distant metastasis

Patients with stage I/II early disease can usually be cured with chemoradiotherapy and or surgery, however, by the time most patients present to their doctor, most will already have locally or regionally advanced disease (Cohen *et al* 2003). The treatment goal for patients with Stage III/IV locoregional disease is organ preservation and cure. One of the reasons patient's with OSCC have such a poor prognosis is that at the time of presentation metastatic spread may have aready occurred and irrespective of therapy, locoregional failure is the most common pattern of disease progression. To improve the outcome for patients with OSCC, a multidisciplinary approach is adopted involving surgeons, oncologists, radiotherapists, occupational therapists, speech therapists, dieticians and other allied healthcare professionals.

Although the outlook for patients with advanced OSCC remains poor, there has been some improvement with the use of new chemotherapy programs and of combined chemoradiotherapy regimens. The Meta-Analysis of Chemotherapy on Head and Neck Cancer (MACH-NC) Collaborative Group recently reported a 4% overall survival improvement in OSCC at 5 years compared to controls (Pignon *et al* 2000). More recently, a large phase 2 trial looking at combined chemotherapy regimen of cisplatin, fluorouracil and docetaxel in stage III/IV OSCC showed an improvement in median overall survival of 18.8 months, as compared with 14.5 months with cisplatin and fluorouracil alone (Vermorken *et al* 2007). However, these are modest improvements and 5-year survival in OSCC remains at less than 50%, which comes with the heavy price to pay of all the acute side effects associated with chemo and radiotherapy (Cooper *et al* 2004, Bernier *et al* 2004).

In OSCC, the median survival time for patients with metastatic disease is just 6-8 months and in those with treatment-refractory disease the median survival time is just 3 months, for these patients, the only treatment is palliative. Several randomized clinical trials have shown a 30% to 40% response rate in stage IV disease (Forastiere *et al* 1992, Gibson *et al* 2004) however there has been no improvement in mean survival time. The standard treatment for recurrent and/or metastatic OSCC remains combination chemotherapy with either cisplatin/fluorouracil or a platinum/taxane regimen (Cohen *et al* 2003).

Research on new avenues of treatment in OSCC has focused on developing therapies against specific molecular targets that are over expressed in cancerous cells. One such target is the Epidermal Growth Factor Receptor (EGFR) family which is upregulated in over 90% of head and neck SCC (Albanell *et al* 2001) and high expression levels are associated with adverse prognosis (Chung *et al* 2006, Mrhalova *et al* 2005, Smid *et al* 2006). Cetuximab is a monoclonal antibody against the EGFR receptor and has been shown to improve the median duration of survival (49 months versus 29.3 months) in a large multicenter phase III trial. The trial involved 424 patients with locoregionally advanced HNSCC who were randomized to receive either radiotherapy alone or radiotherapy in combination with weekly cetuximab during radiotherapy (Bonner *et al* 2006). A smaller randomised phase III trial comparing cetuximab with cisplatin to cisplatin alone in patients with recurrent or metastatic HNSCC failed to show any significant increase in overall survival time (Burtness *et al* 2005).

Gefitinib and erlotinib are orally administered EGFR selective tyrosine kinase inhibitors (TKI) which are approved by the Food and Drug Administration for the treatment of Non-small cell lung cancers. Knowledge that the EGFR is upregulated in HNSCC has lead to the use of these TKI's in phase I/II clinical trials. Cohen *et al* (2003) set up a phase II trial, using gefitinib as a single agent in patients with recurrent or metastatic HNSCC and found overall survival to be 29% at 1 year and mean survival time was 8.1 months. Erlotinib has also been evaluated in a single agent phase 2 study in previously treated patients with stage IV HNSCC and showed a median overall survival of 6 months, and a 1-year survival of 20% (Soulieres *et al* 2004). These studies show a minimal increase in survival time compared to patients receiving standard therapy and as such do not represent a major improvement in prognosis.

The Cyclooxygenase (COX) 2 receptor is known to be involved in tumour progression and is upregulated in several carcinomas including OSCC (Chan *et al* 1999, Grau *et al* 2004). Celecoxib is a selective COX2 receptor inhibitor which has been shown to inhibit the proliferation of OSCC cells both in vitro and in vivo (Bock *et al* 2007). Vascular endothelial growth factor (VEGF) is another attractive target for anticancer therapies in a number of cancers including HNSCC. Kyzas *et al* (2005)

found that high VEGF expression was associated with higher clinical stage and worse overall survival in retrospective review of 69 OSCC patients. *In vivo* studies combining the monoclonal anti VEGF antibody Bevacizumab (Avastin) with the chemotherapeutic agent paclitaxel further showed a dramatic reduction in tumour size compared to when each agent was applied separately (Fujuita *et al* 2007).

Other promising therapies are antibodies directed against the insulin like growth factor type 1 receptor (IGF-IR) (Garcia-Ecchevaria *et al* 2004) and immunotoxins which target the epithelial cellular adhesion molecule Ep-CAM (Stoecklein 2006). The therapeutic efficacy of the human anti IGF-IR monoclonal antibody IMC-A12 alone and in combination with the EGFR blocking antibody Cetuximab has been in HNSCC tumor xenografts. The study showed that use of IMC-A12 in combination with Cetuximab resulted in 44% of the tumour xenographs showing complete regression. (Barnes *et al* 2007).

1.3 Non Melanoma Skin Cancers

Non melanoma skin cancer (NMSC) is the most common human malignancy and can be divided into basal cell carcinomas (BCC) and SCC. BCC is the most common human malignancy and although most are indolent and treated with simple excision there exists a small subset of Morphoeic type BCC which are highly aggressive, occur mainly in the head and neck region and are prone to recurrence (discussed in detail in chapter 3). In the UK, there are over 62,000 new cases of BCC and SCC registered per year although this number is thought to be much higher due to incomplete registration (Cancer Research UK, *CancerStats: Incidence UK*. 2004). SCC is the second most common type of skin cancer and is responsible for the highest number of deaths from cutaneous malignancy after melanoma (Weinstock1989, Bernstein *et al* 1996). Cutaneous SCCs are a heterogenous group of tumours with many distinctive characteristics that can affect diagnosis and appropriate patient management. Of interest are the premalignant skin conditions such as Actinic Keratosis or Bowens disease which may be described as SCC in situ or early SCC. These early types of SCC have not yet invaded across the basement membrane and if left untreated it is

estimated up to 20% of these will become malignant (Callen *et al* 1997). There are multiple histologically distinct variants of true SCCs and the behaviour of these subtypes varies considerably, with some being relatively indolent and others exhibiting a high propensity for aggressive and frequently metastatic behaviour. (Barr 1991, Lohmann and Solomon 2001). Although the majority of cutaneous squamous tumours can be treated with simple excision, there is a subset of patients who either present with advanced disease or who have particularly aggressive phenotype of squamous tumour.

For a Caucasian child born in the United States in 1994, the lifetime risk of developing NMSC was estimated to be 28% - 33% for BCC and 7% - 11% for SCC (Miller and Weinstock 1994). The rates of cutaneous SCC appear to vary widely depending on skin type, geographical location and reporting levels by healthcare professionals. Cutaneous SCC rates per 100,000 of population have been reported at 1332 for males living in Queensland, Australia (Buettner and Raasch 1998) compared to 25 per 100,000 in Welsh men (Holme *et al* 2000).

The incidence of NMSC is increasing rapidly. For Caucasians living in Europe, the U.S., Canada, and Australia there has been an annual increase of 3–8% per year in the rates of NMSC over the past 40 years (Green 1992). The rates of SCC have also been shown to double with every 8-10 degree decline in latitude as one approaches the equator (Giles *et al* 1988) as the exposure to UV light also increases with proximity to the equator (Fears 1983). As people age, the incidence of NMSC increases, possibly due to prolonged exposure to UV light – the risk of developing SCC for patients over 75 years old is approximately 35 times higher than for those aged 50 to 55 years old (Holme 2000).

The increases in skin cancer rates seen over the past 40 years have been attributed to changes in lifestyle, increased sun exposure, aging populations, increased skin cancer awareness and depletion of the ozone layer through greenhouse gas emissions. It has been estimated that a 10% reduction in the thickness of the ozone layer results in a 20% increase in UV-radiation and a corresponding 40% increase in skin cancers (Oikarinen and Raitio 2000). Chronic UV exposure as a major risk factor for NMSC is further evidenced by the fact that over 80% of tumours arise on sun exposed areas

of the skin. The commonest sites for NMSCs include backs of hands and forearms, lips, nose, upper aspect of the back, the face and tops of the ears (Buettner and Raasch 1998).

Other risk factors for NMSC include pale complexion, fair or red hair, skin types I and II (Fitzpatrick 1988), previously damaged skin areas such as burn scars. Chemical exposure such as arsenic, coal tar and tobacco, immunosuppression and genetic disorders such as xeroderma pigmentosum have all been linked with increased risk of SCC (Diepgen and Mahler 2002). Patients who have already had a NMSC are at increased risk of developing a second tumour, as are those who have a premalignant lesion such as Actinic Keratosis (AK) or Bowens disease (SCC in situ). A study by Frankel *et al* (1992) found that of all patients with NMSC, 52% developed a second lesion in the five years after the original diagnosis. It is also estimated that around 5–20% of AKs will transform into SCC within 10–25 years (Marks *et al* 1988) and that the risk of malignant transformation for an average patient with AKs followed up for 10 years would be 6-10% (Dodson *et al* 1991).

1.4 Antibodies

Antibodies are glycoprotein immunoglobulins that bind antigens and are produced by B-cells. An antigen can be defined as a substance that can be bound by an antibody molecule through its antigen-binding sites or epitopes. The high specificity of antibodies for their target ligand raises the potential for their use as agents to deliver targeted cancer therapy. This became a possibility when the fusion of cancer and immune cells to create hybridomas allowed for the production of designer cancer specific monoclonal antibodies (Köhler & Milstein, 1975)

1.4.1 Antibody structure

Antibodies have a basic structure of four polypeptide chains, two identical light (L) chains and two heavy (H) chains. Each L chain is bound to a H chain by non-covalent interactions and disulphide bridges and the H chains are bound to one another by covalent disulfide bridges and non covalent hydrophilic and hydrophobic interactions

to form the classic Y shaped molecule (Poljak 1973, Davies *et al* 1975). The five classes of human immunoglobulin IgM, IgG, IgD, IgA and IgE are defined by differences in their heavy chains.

The H and L chains can be further divided into variable (V) and constant (C) regions (Dreyer and Bennet 1965; Hilschmann and Craig 1965) and these in turn are folded into globular domains (Poljak *et al* 1972). The ligand specificity found on antibodies is due to complement determining regions (CDRs) located in the V region, three of which are found on the H chain (V_H) and three on the L chain (V_L). These CDR loops are hypervariable in amino acid length and sequence, accounting for the huge diversity in ligand recognition seen with antibodies (Wu and Kabat 1970; Kabat and Wu 1971).

Ryle and Porter (1959) further showed that digestion with the enzyme pepsin cleaves the Fc portion from the whole antibody. The Fc portion is involved in complement fixation and interaction with other components of the immune response. Between each Fab and Fc portion lies a proline rich "hinge" region, 25 amino acid residues long and containing interchain disulfides bridges (Dayhoff 1972). Proteolytic cleavage of the whole antibody with the enzyme papain releases two identical fragments (Fab) of around molecular weight 50,000 which contain the Antigen binding portion of the molecule (Porter 1959). The architecture of the Fab fragments is of a framework of fairly constant residues in a beta sheet formation that link the three CDR regions.

1.4.2 Fv antibody fragments

The antigen binding Fab fragments can further be digested by pepsin to produce Fv fragments of around molecular weight 30,000. These Fv fragments consist of V_L and V_H chains held together by non covalent bonds and were shown have the same association constant as whole Fab suggesting the antigen binding ability of antibodies is independent of the Fc region (Inbar *et al* 1972). The small size of Fv fragments and the retention of full antigen binding capabilities makes them an interesting tool in the

development of immunotherapeutic applications. Furthermore, the small size of Fv's allows greater tumour penetration, improved pharmacokinetics and a reduction in antigenicity of the fragments compared to whole antibodies (Sedlacek *et al*., 1983). Development of expression systems using *E. coli* has allowed for the production of fully functional Fv fragments (Skerra and Pluckthun 1988) with similar binding affinities to whole antibodies, however these early systems failed to produce fragments stable in physiological conditions. Work to improve the stability of these Fv fragments lead to the introduction of chemical cross-linking of the variable domains and introduction of intermolecular disulfide bonds (Glockshuber *et al* 1990).

1.4.3 scFvs

Huston *et al* (1988) first utilised *E. coli* bacteria to produce recombinant V_H - V_L complexes joined by the synthetic polypeptide linker (Gly-Gly-Gly-Gly-Ser)3 and these complexes were termed single chain Fv's (scFv's). Bird *et al* (1988) also used synthetic flexible linkers joining the carboxyl terminus of V_L to the amino terminus of V_H to create scFv's and found them to be comparable in antigen affinity and specificity to the monoclonal antibodies from which their sequences were derived. Since that time, scFv and Fab antibody fragments have been generated from many existing monoclonal antibodies (MAbs) and, due to their small size, have been shown to have improved tissue penetration and clearance (Colcher *et al* 1998). Figure 1.5 shows various designs of engineered antibodies.

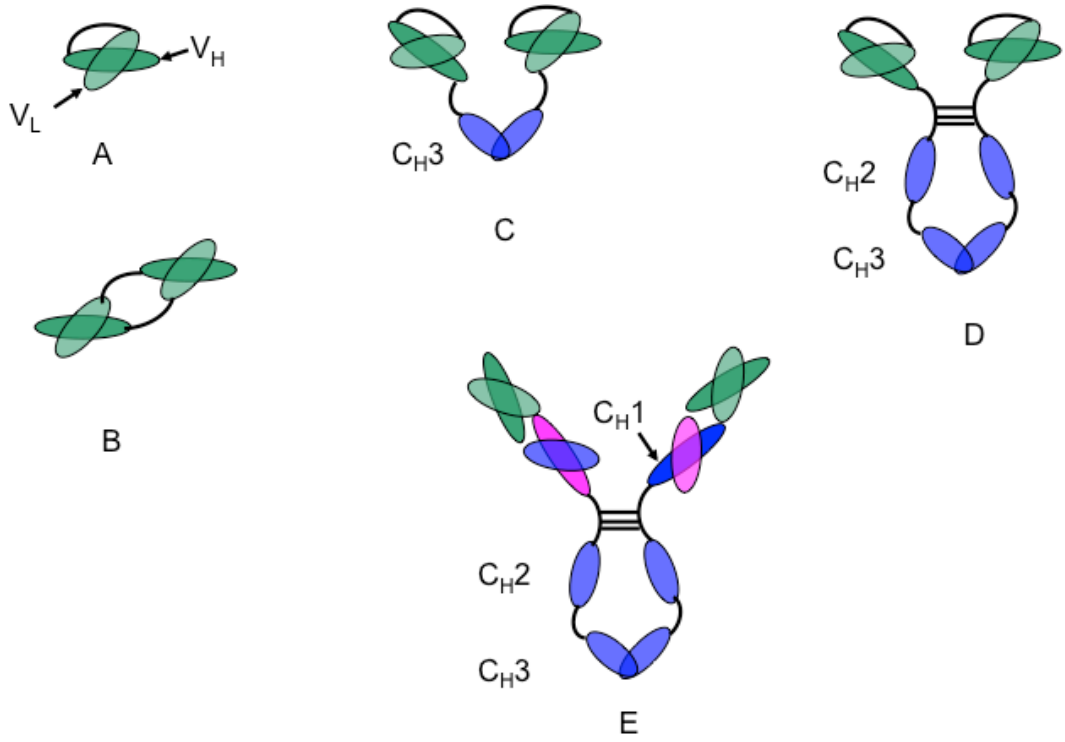

Figure 1.5 - Schematic representation of various engineered antibody fragments A) scFv (25KDa), B) Diabody (55KDa), C) Minibody (80KDa), D) scFv-Fc (105KDa), E) Intact Ab (150KDa)

The development of display techniques using filamentous bacteriophage technology allowed for the selection of high affinity scFv's from a library of millions of scFv's displayed on the coat proteins of bacteria (McCafferty *et al* 1990). Phage display involves the use of polymerase chain reaction to amplify V_L and V_H regions of antibodies, making it possible to create large numbers of different scFvs. These regions are randomly combined and then used to construct to large repertoires of scFvs that are displayed on the surface of bacteriophage. The virus like phage particles can contain single stranded DNA encoding for bacterial coat proteins. When phage enters the bacteria, the DNA is replicated, phage particles assembled and secreted into culture media without lysis of the bacterial cell. Antibody fragment DNA can then be spliced to the gene sequence for a phage coat protein, resulting in a phage surface expressed scFv fusion protein.

Clackson *et al* (1991) originally created phage display libraries from B cells extracted from the spleens of immunised mice and used these to successfully select antigen-specific scFv's. Subsequently, phage libraries have been made from human B cells

taken from individuals immunized with antigen (Persson 1991), exposed to infectious agents (Burton *et al* 1991), with cancer (Cai and Garen 1995) or even with autoimmune diseases (Graus *et al* 1997). However, one of the most successful uses of phage display has been for the selection of antibodies recognising specific antigens which have similar affinity to antibodies developed from hybridoma techniques. Furthermore, by using the selected scFvs as the basis for new libraries, the affinity can be further increased to levels greater than would be naturally found in the immune system (reviewed by Adams and Schier 1999).

There are two main types of phage library: naive or immune. The naive libraries are derived from natural unimmunised human rearranged V genes (Marks *et al* 1991, Sblattero and Bradbury 2000), synthetic human V genes (Griffiths *et al* 1994) or shuffled V genes (Soderlind et al., 2000). Immunised libraries are generated from the V genes from immunised humans or mice and tend to have much higher affinities for the antigen than when using naïve libraries (reviewed by Bradbury and Marks 2004). Refinements in the use of phage display technology have led to the production of high affinity, human scFvs directed against a wide range of antigens.

Recently, human phage antibody libraries have been used in the production of a fully human anti TNF α antibody, Adalimumab (Humira) which is Food and Drug Administration (FDA) approved for the treatment of rheumatoid arthritis. Currently, there are several other antibody constructs in advanced clinical trials which have been discovered using phage display technology (Hoogenboom *et al* 2005).

1.4.4 Antibody Engineering for Therapy

Antibodies can be used either to block biological functions, to trigger an immune response against a cell they are bound to or as delivery agents to target cytotoxic agents, drugs or radioisotopes against specific antigens (Wu and Senter 2005, Weiner 2010). To improve usefulness of antibodies in the treatment of disease, they have been manipulated to vary the molecular size, pharmacokinetics, immunogenicity, specificity, valency and effector functions (Batra *et al* 2002). Currently there are 32 antibody-based products approved by the FDA for human use in the clinic, 85% were

the result of antibody engineering and of those, 90% were for the treatment of cancer or immunological disease (Dubel 2007).

Antibody engineering began with the creation of Fab, Fv and scFv fragments as described in above. The benefit of these small fragments being reduced immunogenicity and their small size with rapid clearance made the fragments ideal for imaging modalities such as radioimmmunotherapy (reviewed by Wangler *et al* 2007). However the small size and the monovalency of scFvs has limited their therapeutic potential due to the rapid clearance of these antibody fragments from the circulation. To improve the clinical applications of scFv's various strategies have been employed including the formation of dimers either spontaneously or through the use of covalent disulphide bonds or peptide linkers (Hollinger *et al* 1993, Wu *et al* 1996, Goel *et al* 2000).

The discovery that camels and llamas (*sp Camelidae*) have antibodies consisting only of heavy chains and that the variable region (V_HH) is capable of independently binding antigen has led to the development of a further class of antibody fragment termed nanobodies. Nanobodies are 15KDa in size and recognise antigen through long CDR loops which seek out cryptic epitopes inaccessible to larger V_H V_L pairings. In addition, the greater thermal and intracellular stability of nanobodies has led to their investigation as potential targeting agents (Muyldermans 2001, Revets *et al* 2005)

To improve the serum half life and stability of scFvs, they can be reinserted into whole antibodies or fused to Fc portions to enable the new complexes to bind complement and trigger host immune responses (Persic *et al* 1997, De Lorenzo *et al* 2004). Much of the early work in designing antibodies for therapy was based on mouse antibodies which led to the development of Human-Anti-Mouse-Antibody response, particularly with repeated administrations. To reduce the immune response, chimeric antibodies were developed in which mouse VH and VL domains were fused with human Fc portions. Unfortunately, although less immunogenic, these mouse-human chimeric antibodies generated an immune response termed Human-Anti-Chimeric-Antibody response (reviewed by Mirick *et al* 2004). Other options to limit human immune responses to engineered antibodies include grafting of murine CDR

regions onto human antibody frameworks (ie the amino acid sequences between the CDR regions in human antibodies)

Another approach to 'humanise' engineered antibodies whilst maintaining efficacy and affinity is to exchange for human residues, only the external residues of the murine antibody, leaving the CDR and internal residues of murine origin. A successful approach to humanise the murine anti CEA antibody MFE-23 was employed by Graff *et al* (2004) who compared the crystalline structure of MFE-23 with that of TR1.9 – a fully human antibody. The group identified 28 human residues on TR1.9 that were >30% solvent accessible and substituted these residues into MFE-23, the newly humanised hMFE-23 retaining full affinity for it's ligand CEA.

1.4.5 MFE-23

Phage display has been used to produce the scFv MFE-23 which is directed against CEA, an oncofoetal protein expressed in several cancers including colon cancer (Chester *et al* 1994). The scFv MFE- 23 was developed from a filamentous phage expression library of random murine V_H V_L domain pairings obtained from a CEA immunized mouse. MFE-23 was also the first scFv to be used in patients and has been used in several clinical trials firstly to improve imaging of secondary tumour deposits in patients with colon cancer (Begent *et al* 1996). A second clinical trial used radiolabelled MFE-23 and a hand held gamma radiation probe to detect the presence of liver metastases during surgery (Mayer *et al* 2000). Furthermore, the scFv has been previously well characterised and it's structure and behaviour in vitro and in vivo described (Boehm *et al* 2000, Lee *et al* 2002 and Sainz-Pastor *et al* 2006).

1.4.6 Rational Structural Based Antibody Design

With the advent of X ray crystallography it has become possible to study the macromolecular structure of proteins, enzymes and nucleic acids. This ability has lead to the development of rational approaches to drug and antibody design based on a knowledge of the precise structure of therapeutic targets (Scapin 2006). Combining

knowledge of the macromolecular structure with the ability to substitute amino acid sequences into precise positions within the CDR loops of scFv's or Fab gives a further avenue of approach in antibody design. This technique of grafting peptide epitopes newly synthesised or cut from known antigens into antibody CDR loops is known as antibody antigenisation and was first described by Zanetti (1992). This technique takes advantage of the fact that the Fv regions are held in β pleated sheet conformation principally by the framework regions (FRs) and the CDR loops often protrude beyond these confines. Thus it is possible to insert novel peptides into the CDR loops without disturbing the overall conformation of the Fv region (Figure 1.6).

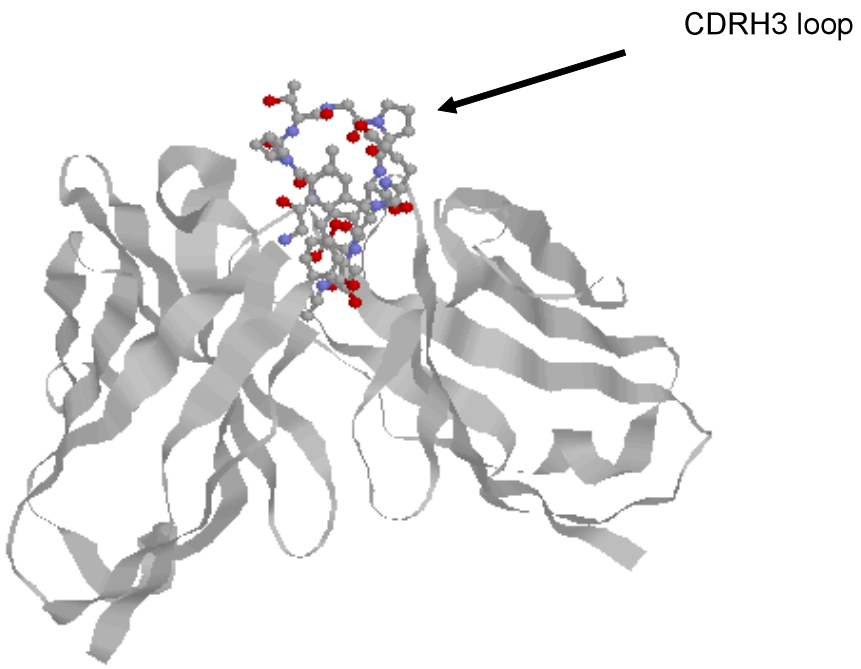

Figure 1.6 - Ribbon model of shMFE-23 showing position of CDR3 loop and site for peptide insertion.

This hypothesis was tested by inserting a B cell epitope for the malarial parasite into the third CDR loop of the VH chain of a murine antibody which was then used to successfully immunise rabbits and mice against the malarial parasite (Billetta *et al* 1991). Further examples of this approach include the insertion of RGD repeat loops into the CDR region of a chimeric mouse-human heavy chain immunoglobulin which

was subsequently shown to bind at RGD recognition sites on the αvβ3 integrin expressed on tumour cell lines (Lanza *et al* 1997).

Taking a rational structural based approach to antibody design allows the alteration of the specificity of well-characterised whole antibodies or antibody fragments that are known to be safe in human trials and can speed the time taken from bench to bedside.

1.5 Nanotechnology and Cancer

1.5.1 Background

Nanotechnology is a rapidly developing field involving the interdisciplinary study of materials that are between 100 to 10,000 times smaller than the size of a human cell. Collaborations between engineers, physicists, biologists and medics have led to some striking advances, particularly in the area of nanomaterial research. Advances in nanotechnology are providing us with unprecedented abilities to study and manipulate molecular interactions at a sub cellular level leading to the development of new strategies to image and treat human disease. The past ten years have seen the establishment of specific centres for research into nanotechnology, such as the Nanotechnology Characterisation Laboratory in the USA and London Centre of Nanotechnology – a joint venture between University College London and Imperial College London. In America, an estimated $6 billion has been invested in nanotechnology research and this investment is beginning to show some returns (Cai and Chen 2007, Mazzola 2003).

Nanotechnology has the potential to make the great advances in the arena of cancer research. Current cancer therapies include aggressive surgery to excise the tumour and any known metastases combined with chemo or radiotherapy often with high associated morbidity. In essence the problem of treating cancer is that it often is detected too late to provide treatment and the treatments we have do not differentiate sufficiently between healthy and cancerous cells. The goal of cancer treatments is

therefore to detect cancers earlier before they have had chance to develop and spread to distant parts of the body then, when detected to treat only the cancerous cells, leaving as much normal tissue undisturbed as possible

1.5.2 Nanoparticles for Targeted Cancer Theranosis

The term theranosis is used to refer to molecular complexes that can be used for both therapy and diagnosis of disease. Nanotechnology research has been focussed on producing devices capable of targeting cancerous cells and using these devices to improve cancer imaging and to deliver anti cancer therapies directly to the cancer cells. Tumour targeting can be passive or active, for example the rapid growth of tumours often means they have a poorly developed vascular supply with leaky capillary beds and a poor lymphatic drainage (Maeda and Matsumura 1989, Jain 1988). This is in comparison to the normal well organised functional tissue architecture of capillary arterioles and venules. Vessel wall structure is also abnormal in tumours (McDonald and Choyke 2003, di Tomaso *et al,* 2005). Large inter-endothelial junctions, increased numbers of fenestrations, vesicles, and a lack of normal basement membrane are often found in tumour vessels (Dvorak *et al* 2000). It is becoming increasingly thought that the increased permeability of tumour vasculature compared to normal vasculature means circulating molecular complexes are more likely to leak from the circulation into the tumour (Fukumura and Jain 2007). Furthermore, the size of molecular complexes directly influences the biodistribution of these complexes (Schipper *et al* 2009). Linking toxic agents to suitable nanomaterials may thus increase the toxin's uptake at the tumour and the reduced lymphatic drainage may further encourage accumulation of the agent at the tumour site.

One problem with passive delivery of nanoparticles is that these particles are recognised as foreign and mopped up by the reticuloendothelial system (RES) and by macrophage phagocytosis. Use of hydrophilic particle coatings such as polyethylene glycol (PEG) and dextran can minimise phagocytosis and maximise the time nanoparticles can remain in the circulation (Lin *et al* 2009, Hu *et al* 2006).

Other forms of passive targeting include 'Tumour Activated Prodrug Therapy' which uses enzymes present in the local tumour environment to activate an intravenously delivered prodrug complex. An example of this is the use of doxyrubicin-human albumin conjugates which are activated by specific matrix metallo proteases produced by melanoma cells, causing the local release of activated doxyrubicin at the tumour site (Mansour *et al* 2003). Direct intratumoural injection is another method of passive targeting and this has been used to deliver various toxic or imaging agents including mitomycin (Nomura *et al* 1998), the attenuated adenovirus ONYX-015 which kills cells with mutated p53 (Khuri *et al* 2000) and ferromagnetic nanoparticles (Johannsen M *et al* 2006). Magnetic nanoparticles have been used to passively target tumours by attaching drugs to particles, delivering the complexes intravenously and using an externally placed magnet over the tumour to target the nanoparticles-drug complexes (Alexiou *et al* 2003).

Active cancer targeting is an attractive concept which uses specific targeting agents such as antibodies to deliver nanoparticles directly to cancer cells which can then be used for cancer imaging and therapy. This concept will be explored throughout this thesis.

1.5.3 Magnetic Nanoparticles

Magnetic nanoparticles are ferric particles between 5 – 100 nm in size (compared to the average cell diameter of 10000 nm) and have characteristics between molecular and solid states, combining chemical accessibility in solution with physical properties of the bulk phase (Siegel 1999). Most research has focussed on the use of iron oxide nanoparticles, made from magnetite (Fe_30_4) or maghemite (γFe_20_3) principally due to the biological stability and ease of manufacture of these particles. Magnetic nanoparticles of magnetite or maghemite are synthesized through the alkaline co-precipitation of Fe^{2+} and Fe^{3+} aqueous salt solutions. The control of size, shape and composition of nanoparticles depends on the type of salts used, Fe^{2+} to Fe^{3+} ratio, and pH of the media (Sjogren *et al* 1994). The magnetic properties of nanoparticles can vary greatly and are dependent on the size and interactions between

the particles which is in turn dependent on the manufacturing conditions (reviewed by Boyer *et al* 2010).

The aim of the manufacturing process of magnetic nanoparticles is to produce a ferro-fluid whereby the particles are held in colloid form and retain fluid characteristics even in high magnetic fields (Charles and Poppelwell 1980). To reduce hydrophobic interparticulate interactions, prevent aggregation and to ensure the particles are remain in suspension, the particles are given a stabilising surface coating. Various coatings are available including polymeric complexes such as polyethylene glycol (Hu *et al* 2006), dextran (Berry *et al* 2003), polyvinylpyrrolidone (D'Souza *et al* 2004), fatty acids (Sahoo *et al* 2002) and inorganic materials such as the surfactants sodium oleate and sodium carboxymethylcellulose (Sun *et al* 2007) or silica (Tartaj *et al* 2002).

The magnetic properties of material can be described by the relationship between the magnetic field (H) and the magnetic induction (B). Ferromagnetism describes the phenomenon of permanent magnetism seen when unpaired electron spins align themselves spontaneously in the absence of a magnetic field. Iron is a ferromagnetic material however when it is ground down to tiny particles, less than 15nm in size, the particles no longer display ferromagnetism after removal of the magnetic field. Particles below the 15nm size are described as displaying paramagnetic properties in that they behave as ferromagnets when an external magnetic field is applied however on removal of the field, no permanent magnetism remains. Superparamagnetic Ion Oxide Nanoparticles (SPIONs) are particles of magnetite or maghemite that are stable in and dispersed in solution until an external magnetic field is applied, at which point they become ferromagnetic in behaviour until the field is removed (Bonnemain 1998, Cantillon-Murphy *et al* 2010). The precise behaviour of SPIONs when placed in a magnetic field depends on both the size and the temperature of the particles (Kallumadil *et al* 2009).

1.5.4 Nanoparticles for imaging

Magnetic Resonance Imaging (MRI) exploits the magnetic properties of the large numbers of hydrogen ions present in the tissues of the body to provide high quality non invasive images. When a large pulsed radiofrequency magnetic field is applied to hydrogen ions in the body, changes in the alignment of hydrogen ions are detected by pick-up coils within the scanner and these are converted to images. The different tissue types are distinguishable essentially due to the differences in water and hence hydrogen ion content between tissue types (Elster and Burdet 2001). To improve the accuracy of MRI scanning, it is useful to be able to enhance the contrast between different tissue types using contrast agents. SPIONs are now routinely used as contrast agents because of their superparamagnetic properties that cause a reduction in the signal generated by MRI, improving the contrast between different tissue types.

Superparamagnetic iron oxide nanoparticles such as dextran magnetite have been used to provide negative contrast when imaging the liver using MRI scans as they have higher molar relaxivities and can be used at lower concentrations (Stark *et al* 1988). These agents are useful for imaging the liver and spleen as magnetic nanoparticles accumulate in the reticuloendothelial (RES) system of the liver and spleen which has been described as passive targeting. The RES is defined as the cell family comprising bone marrow progenitors, blood monocytes and tissue macrophages, one function of which is to recognise and remove unwanted autologous or foreign material from the blood stream (Hume *et al* 2002). This is done through opsonisation when circulating plasma proteins known as opsonins attach themselves to the surface of foreign material. The opsonins are then recognised by circulating monocytes or fixed macrophages within the RES causing phagocytosis/endocytosis of the foreign material, eliminating them from the circulation and causing the accumulation of foreign material within organs of high phagocytic activity. This is what happens when dextran coated paramagnetic particles are delivered intravenously leading to their accumulation within the liver and spleen and the improved imaging of these organs using MRI scanners.

There is minimal associated toxicity with iron accumulation and in vivo tests have shown that the iron oxide component of the nanoparticles will be naturally recycled. The human body contains around 3-4 g Fe, for example, in the proteins ferritin, hemosiderin, transferritin, and hemoglobin. As the magnetic nanoparticles start to break down, any soluble Fe becomes part of this normal Fe pool, and given that a clinical dose would likely include just a few milligrams of Fe per kilogram body weight, the prospect of Fe overload is highly unlikely.

Active targeting of nanoparticles for imaging has also been achieved using particles conjugated to RGD peptides in integrin positive liver cancers (Chen *et al* 2010). Furthermore, Lee *et al* (2009) have successfully conjugated iron nanoparticles to RGD peptides and shown effective siRNA uptake in breast cancers which over-express integrins demonstrating potential for both imaging and therapy. Yang *et al* (2009) have used single chain epidermal growth factor receptor antibody conjugated nanoparticles for improving in vivo MRI imaging of mouse pancreatic tumours.

1.5.5 Magnetic Fluid Hyperthermia

'Quae medicamenta non sanat; ferrum sanat. Uae ferrum non sanat; ignis sanat. Quae vero ignis non sanat; insanabilia reportari oportet'

'Those diseases medicine cannot cure, the knife cures. Those diseases the knife cannot cure, fire cures; and those that fire cannot cure are to be reckoned totally incurable'
Hippocrates c.420 BC

The earliest description of using heat as a therapy for breast tumours is a reference in the Egyptian Edwin Smith surgical papyrus dated 3000 BC, a more well known proponent of medical hyperthermia is Hippocrates (460-370 BC) who describes the use of cautery as a treatment (Breasted 1931). Since the 17th century there have been numerous reports of tumour regressions in patients suffering with infectious fever (Storm 1983) and in 1898, Westermark described using temperatures of 42-44ºC to

treat inoperable carcinomas of the uterus. There has recently been an increase in interest shown in hyperthermia as a cancer therapy as evidenced by increasing numbers of randomised controlled trials looking at the effects of hyperthermia combined with either radio or chemotherapy (van der Zee 2002).

Clinical hyperthermia can be delivered either locally, regionally or as whole body hyperthermia and heat can be induced by electromagnetic field technique, ultrasound, or perfusion methods. The rationale underlying clinical hyperthermia is the fact that temperatures over 42.5ºC are cytotoxic for tumour cells (Dewey 1977 and 1994), especially in the local environment of the tumour where there is low pO2 and low pH due to insufficient blood perfusion. Orgill et al (2005) have shown that by heating cells to 45°C, intracellular proteins become unfolded, cell membranes are disrupted and cell death swiftly follows. Hyperthermia has been used successfully to treat localised prostate cancers using high intensity focused ultrasound (HIFU) (Chaussy and Thuroff 2001, Uchida *et al* 2002) and has been shown to improve survival in advanced head and neck cancers when combined with radiotherapy (Valdagni and Amichetti 1994). However, a major technical problem with hyperthermia is the difficulty of heating the local tumour region to the intended temperature without damaging normal tissue.

The potential to use tiny particles of magnetic material and alternating magnetic fields to deliver clinical hyperthermia was first explored by Gilchrist *et al*. in 1957. The group injected microscopic particles of magnetite into primary tumours of the bowel in dogs, in the expectation the particles would accumulate in the lymph nodes which drained the tumour. The nodes were then dissected out and exposed to an alternating magnetic field of strength 200±240 Oersted (Oe). It was found that a concentration of 5mg of magnetite per gram of lymph node tissue yielded a temperature increase of 14ºC in 3 min. Two years later, the same group conducted an in vivo study using rabbits in which inguinal lymph nodes were successfully targeted with heat (Medal *et al* 1959). Total necrosis of the nodes was reported after 3 min of heating at 470 Oe. This early work, based on lymphatic uptake of microscopic ferromagnetic particles, clearly proved that it was possible to heat tissue in vivo using heat generated when magnetic particles are placed within alternating magnetic fields.

The mechanism by which heating takes place is by the power absorption of magnetic particles when they are exposed to an A/C magnetic field (Jordan 1993). The important factor for magnetic heating experiments is the specific absorption rate (SAR), which is determined by SAR = C × ΔT/Δt, where C is the specific heat capacity of the sample and T and t are the temperature and time, respectively. SAR is very sensitive to the material properties. While in multi-domain particles the dominant heating is hysteresis loss due to the movement of domain walls, this is not the case with small, single domain particles. The two main contributing mechanisms of SAR in single domain magnetic nanoparticles are the Brownian (rotation of the entire nanoparticle) and Néel (random flipping of the spin without rotation of the particle) relaxations (Kotitz 1995, Pakhomov 2005). The transition between the two mechanisms occurs between 5-12 nm for various materials, but it also varies with frequency (Mornet 2004).

There are several alternative ways to deliver magnetic particles to tumours, either via an artery that feeds a tumour, intravenously or via direct injection into the tumour. In 1976, Rand *et al* injected particles of iron oxide suspended in silicon into the renal arteries of dogs which were then sacrificed and the kidneys placed within a 570 Oe, 20 KHz alternating magnetic field. Temperature measurements showed the ex vivo kidneys heated to 12ºC per minute. In 1994, Mitsumori *et al* tested dextran coated magnetite particles suspended in lipiodol or in a degradable starch microsphere. Earlier work had shown that such particles generated significant heat upon exposure to an alternating magnetic field (Tazawa *et al* 1988). The study reported an increase of over 12ºC after 10 min of heating, in vivo, in a rabbit kidney following direct arterial injection.

The dextran coated particles used by Mitsumori *et al* were 75nm in diameter with a 7.4 nm magnetite core. Suspensions containing particles less than 100nm in diameter are defined as magnetic fluids, can be heated by weaker magnetic fields and are generally less likely to cause heating of peripheral tissues. This may be an advantage over the use of larger multi-domain particles, which may require stronger field conditions for heating (Jordan *et al* 1997, Pankhurst *et al* 2009)). Advantages of delivering particles intra arterially is that the particles are more likely to be well distributed throughout the tumour, providing a uniform distribution of heat. Further,

the poor venous drainage of tumours will favour retention of particles within the tumour for repeated hyperthermia therapies (Vaupel 2000, Lin *et al* 2010).

Magnetic particles can also be directly injected into tumours, this was first investigated by Rand in 1982. The group used ferromagnetic particles suspended in normal saline and directly injected these into the renal pelvis of 24 rabbits containing unilateral implanted renal carcinomas. On exposure to a magnetic field of 1000 Oe alternating at 2 kHz, tumour temperatures of 55ºC were obtained. Histological examination of the tumours 3 days after heating revealed complete tumour destruction.

The direct intratumoural injection approach was used by Chan *et al* (1997), who used mice containing implanted subcutaneous hind-limb tumours and reported a tumour/body differential of 6.5-8.5ºC on exposure to a 7.15 kA/m magnetic field alternating at 0.85MHz. The tumours were infiltrated with supraparamagnetic colloidal iron oxide particles by direct intratumoural injection. It was found that a tumour iron concentration of only 0.5-1.0 mg/g was needed to produce this differential heating.

An in vitro study by Hilger *et al* (2000) examined the effect of magnetic thermoablation in cow muscle. In this study, 50-180 mg of magnetite particles (1 micron diameter) suspended in 0.3mL of physiologic saline containing 1% Tween 80 were directly injected into prepared cylindrical cavities within samples of fresh cow muscle and exposed to a 6.5 kA/m magnetic field, alternating at 400 kHz. Temperature increases of up to 87ºC were recorded within 15mm from the particle deposits. It was suggested that lesions up to a volume of 0.131 cm^3 could be treated using a dose of 180 mg of particles. Although the author was investigating the technique for use in the ablation of muscle lesions and the cooling effects of blood flow were absent, the principle of generating localized tissue heat with magnetic particles and externally applied magnetic fields was again demonstrated. Hilger *et al* (2001) have also tested direct intratumoural injection on immunosuppressed mice containing implanted human breast adenocarcinoma, as a model of the potential treatment of human breast cancer. In this work, a ferrofluid containing 10 nm magnetite particles was directly injected into the tumours, which were then exposed to

a 6.5 kA/m magnetic field alternating at 400 kHz. Mean tumour temperatures of 63ºC were recorded after 2-3 min of heating and all tumours showed histological evidence of necrosis.

Recently, Balivada et al (2010) have compared the results of AMF exposure on mice with melanoma tumour xenographs using porphyrin coated magnetic nanoparticles which were delivered either intravenously or directly intratumorally. The group found a significant reduction in tumour size in both groups after exposure to AMF suggesting the intravenous route may be a possibility however they also noted significant amounts of nanoparticles in the lungs and liver of the tumours.

Since 2001, there have been several phase 1 clinical trials of magnetic fluid hyperthermia using direct injection of magnetic nanoparticles. In 2006, Johannsen *et al* reported promising results from a feasibility study involving 10 patients with locally recurrent prostate cancer treated with magnetic fluid hyperthermia. In 2007, Maier-Hauff and colleagues treated patients with recurrent glioblastoma multiforma using combination of radiotherapy and magnetic fluid hyperthermia. Patients received 4-10 repeated hyperthermia treatments and a mean temperature increase of 44.6°C was achieved intratumourally. There were signs of local tumour control, no toxic or adverse effects of the therapy and the study concluded that magnetic fluid hyperthermia can safely be used in glioblastoma multiforma patients.

An advance on either intra vascular injection of particles or on direct tumour injection would be the use of targeted particles. This was first explored by Suzuki *et al* (1995) who described the attachment of monoclonal antibodies to magnetite particles, using polyethylene glycol with terminal carboxy or amino groups. Analysis of the cells after incubation determined that 90 pg of magnetite had been adsorbed per tumour cell, four times the amount compared to control cells.

In 2005, deNardo *et al* attached 20nm poly ethylene coated nanoparticles to monoclonal antibodies and used these constructs in vitro and in vivo experiments. Using a 153KHz alternating magnetic field (AMF) at strengths of 700, 1000, 1300 Oe significant reductions in tumour growth were seen compared to controls with no

treatment. This early work demonstrates the potential for developing a system using antibody-nanoparticle complexes to deliver targeted magnetic fluid hyperthermia.

1.6 Research Aims

The overarching hypothesis for this research is that the αvβ6 integrin is a clinically useful target in oral squamous cell carcinoma and non melanoma skin cancers. This thesis aims to test the hypothesis in several ways. Firstly, expression levels of αvβ6 in pre malignant actinic keratoses and basal cell carcinomas of the skin will be examined. The clinical utility of αvβ6 will be tested by determining whether the integrin is an independent prognostic marker in oral squamous cell carcinoma. Finally, a single chain antibody fragment specific to αvβ6 will be designed, produced and tested for its ability to deliver nanoparticles to αvβ6 expressing cells for the delivery of targeted magnetic alternating current hyperthermia.

Chapter 2

Materials and Methods

2.1 Materials and suppliers

Buffers	*Formula*
Tris-borate (TBE) stock (10x)	100mM Tris, 10mM Boric acid, 1.25 mM EDTA
10x DNA loading buffer for agarose gels	2.7 ml glycerol, 0.3 ml TBE buffer (10x), 1% SDS, 1ml 0.5 M EDTA, pH 8.0
DNA loading buffer	0.25% bomophenol blue, 0.25% xylene cyanol FF, 30% glycerol in dd H_20
DNA Markers in loading buffer	Marker 10 µl, loading buffer 10 µl, dd H_20 80 µl
2 x SDS-PAGE loading buffer	1.25mM Tris-HCl, pH 6.8; 20% (v/v) glycerol, 2% (v/v) β-mercaptoethanol; 0.1% (w/v) bromophenol blue; 0.1% (w/v) SDS
1 x SDS PAGE running buffer	25mM Tris-HCl, 192 mM glycine, 20% (w/v) SDS
5x SDS loading buffer	250mM TrisHCl pH6.8, 10%SDS, 30% Glycerol, 5% β-mercapitalethanol, 0.02%bromophenol blue
1 x transfer buffer	25 mM Tris-HCl, 192 mM glycine,, 20 % (v/v) methanol
Coomassie gel stain	0.1% (w/v) Coomassie Blue R-250, 45% (v/v) methanol; 10% (v/v) glacial acetic acid
Coomassie gel destain	30% (v/v) methanol, 10% (v/v) glacial acetic acid
NEBuffer 4	50 mM potassium acetate, 20 mM Tris-acetate, 10 mM Magnesium Acetate, 1 mM Dithiothreitol
Qiagen buffer P1 (resuspension)	50mM TrisCl, pH 8.0, 10mM EDTA, 100µg/ml Rnase A
Qiagen buffer P2 (lysis)	200mM NaOH, 1% SDS (w/v)
Qiagen buffer P3 (neutralisation)	3.0 M potassium acetate, pH 5.5
Qiagen buffer QBT (equilibration)	750 mM NaCl, 50 mM MOPS, pH 7.0, 15% isopropanol (w/v), 0.15% Triton® X –100 (v/v)
Qiagen buffer QC (wash)	1.0 M NaCl, 50mM MOPS, 15% isopropanol
Qiagen buffer QF (elution)	1.25 M NaCl, 50 mM TrisCl, pH 8.5, 15% isopropanol (v/v)
Direct Purification Buffer	50mM KCl 10mM Tris-HCl (pH 8.8 at 25°C) 1.5mM MgCl2 0.1% Triton® X-100
TE Buffer	10mM Tris-HCl (pH 7.5) 1mM EDTA
10X T4 ligation buffer	400 mM Tris-HCl, 100 mM $MgCl_2$, 100 mM DTT, 5 mM ATP (pH 7.8 at 25°C).

Table 2.1 – Solutions for protein manipulation and analysis

Media	*Formula*
2x YT broth	16g tryptone, 10g yeast extract, 5g NaCl. Made up to 1l with dH_20 then autoclaved. For 2x YT Agar, add 15g agar prior to autoclaving
Luria Bertani Broth (LB)	10 g tryptone, 5 g yeast extract, 10 g NaCl. Complete to 1 L with dH_20. Autoclave. For LB Agar, add 15 g/L agar prior to autoclaving.

Table 2.2 - Media for bacterial growth

Media	*Formula*
Yeast Extract Peptone Dextrose Medium (YPD)	Dissolve 10 g yeast extract and 20 g peptone in 900 ml dH_20. Autoclave. When cool add 100 ml 20% glucose solution. Store at 4°C. For YPD agar add 20 g/L agar prior to autoclaving.
YPD with sorbitol (YPDS)	Dissolve 10 g yeast extract, 20 g peptone and 182.2 g sorbitol in 900 ml dH_20. Autoclave. When cool add 100 ml 20% glucose solution. Store at 4°C. For YPDS agar add 20 g/L agar prior to autoclaving.
Buffered Methanol-complex Medium (BMMY)	Dissolve 10 g yeast extract and 20 g peptone in 900 ml dH_20. Autoclave. When cool add 100 ml 1M potassium phosphate buffer, pH 6.0, 100 ml 13.4% YNB, 2 ml 0.02% biotin, 100 ml 5% methanol. Store at 4°C.
YPD medium/glucose primary culture medium	Dissolve 4 g peptone, 4 g yeast extract, 3 g glucose into 230 ml dH_20. Autoclave.
Basic salt medium	Dissolve 5.4 g $CaSO_4$, 87.6 g K_2SO_4, 70.2 g $MgSO_4$: 7H2O, 54 g $(NH_4)_2SO_4$ and 300 ml Glycerol into 5.0 L dH_20. Autoclave.
Sodium hexametaphosphate	Dissolve 150 g in 1 L dH_20. Filter sterilise.
Secondary culture medium	300 ml basic salt medium 30 ml sodium hexametaphosphate, 1 ml trace elements (see Table 2.6). Filter sterilise.
Fermentation medium	4.7 L basic salt medium, 1 L sodium hexametaphosphate, 1 ml anti-foam, 24 ml trace elements. Autoclaved in fermentor.
Limited glycerol feed	300 ml glycerol, 300 ml dH_20. Autoclave. Add 7 ml sterile

	trace elements.
Limited methanol feed	2 L methanol, 24 ml sterile trace elements.

Table 2.3 – Yeast growth media and solutions

Buffers	***Formula***
Keratinocyte Growth Medium (for VB6 cells)	450mls αMEM (Invitrogen), 50mls 10% Fetal calf serum, 5mls Penecillin/streptokinase, 7.5mls 20Mmol Glutamine, 250µl Insulin, 2mls Hydrocortisone, 500µl EGF, 5mls Adenine, 500µl Cholera Toxin
A375B6 Culture Medium	500mls DMEM media (Lonza Biowhittaker, Woking, UK), 10% FCS, Pen/Strep and 2mMol glutamine
HT29 Culture Medium	500mls McCoys 5A media (Lonza Biowhittaker, Woking, UK), 10% FCS, Pen/Strep and 2mMol glutamine
Trypsin	Versene EDTA and trypsin
Freezing Medium	1ml dimethyl sulphoxide (DMSO) with 9ml foetal calf serum

Table 2.4 - Solutions for tissue culture

Buffers	***Formula***
0.1 M Sodium hydrogen phosphate buffer pH 9.0	14.1g Na_2HPO_4 dissolved in 1l dH_20. Adjusted to pH 9.0 with NaOH.
Glycine 25mM	Dissolve 0.18g glycine into 100mls 1xPBS
MES buffer 0.5M	Dissolve 106.6g 2-(4-morpholino)ethanesulphonic HCl in 1l dH_20. Adjust to pH 6.3 with Na_2CO_3
MES buffer 0.1M	Dissolve 21.3g 2-(4-morpholino)ethanesulphonic HCl in 1l dH_20. Adjust to pH 6.3 with Na_2CO_3
EDC/NHS activation buffer	Dissolve 0.6mg 1-ethyl-3-(3-dimethlaminopropyl)-carbodiimide hydrochloride and 1.2mg N-hydroxysuccinimide in 200µl 0.5M MES buffer
Activation Buffer for cyanogen bromide conjugation	0.1M Sodium hydrogen phosphate buffer pH9. Filter to sterilise

Table 2.5 – Solutions for nanoparticles-scFv conjugation

Buffers	*Formula*
$FeCl_3$ standard	Dissolve in 1 litre H_20
Lysis buffer	50 mM NaOH 0.2g dissolved in 100ml H_20
Iron Releasing Buffer	Dilute 3.5ml of 4M HCl into 10ml H_20. Add to 10ml solution of 0.45g $KMnO_4$ dissolved in H_20
Iron Detecting Buffer	Dissolve in 5mls H_20 0.015g ferrozine, 0.015g neocuproine, 0.96g ammonium acetate and 0.9g ascorbic acid.

Table 2.6 - Solutions for Ferrozine Assay

All experiments were in accordance with HSE guidance on COSHH and carried out following standard guidelines for good laboratory practice. The work was carried out within the Department of Oncology, Royal Free and University College Medical School, at The Cancer Institute, University College London and at the Centre for Tumour Biology, Institute of Cancer, Bart's and the London School of Medicine and Dentistry, UK.

2.1.1 Chemicals and reagents

All chemicals were of AnalaR grade and purchased from VWR-BDH Ltd (Gillingham, Dorset, UK) or Sigma-Aldrich Company Ltd (Poole, Dorset, UK), unless otherwise stated. Buffers, solutions and antibiotics were prepared using distilled de-ionised water (dH_20; Elga, UK), unless otherwise stated.

2.1.2 Superparamagnetic Nanoparticles

Chemicell FluidMAG-DX® magnetic nanoparticles were purchased from Chemicell GmbH, Berlin, Germany. Resovist® nanoparticles were purchased from Bayer Schering Pharma, Newbury, UK.

2.1.3 Glassware and disposables

All glassware used was washed with tap water and detergent followed by rinsing with dH_20. All plastic-ware was purchased from VWR-BDH Ltd (Gillingham, Dorset, UK), unless otherwise stated.

2.2 Methods

2.2.1 Manipulation of bacterial DNA

2.2.1.1 Expression Vectors and Primers

The plasmid hsMFEpCTCON (C.P. Graff *et al* Protein Eng.Des.Sel. 2004, 17, 293-304, available in the laboratory) was used as template for PCR amplification. The bacterial expression vector pUC119HIS was a kind gift from the MRC Laboratory of Molecular Biology, Cambridge, UK. Primers were obtained from MWG Biotec (Ebersberg, Germany), dissolved at concentrations of 100pM/µl and stored at –20ºC.

2.2.1.2 PCR

PCR reactions were carried out using the Taq PCR Master Mix Kit (Qiagen GmbH, Hilden, Germany) kit.

Template		40 µl
Primers	– forward	0.5µl
	- back	0.5 µl
PCR Master mix		50 µl
dd H_20		9 µl
Total reaction volume		100 µl

Cycling carried out using Biometra Personal Cycler in steps as follows : Initial, 94ºC for 2 minutes; Denaturing, 94ºC for 30 seconds, Annealing 50ºC for 60 seconds, Elongation 72ºC for 7 minutes cycled 30 times with final elongation step 72 ºC for 7 minutes.

First PCR reaction amplified the 5'end of the 6.2.2. DNA sequence using primers hsMFE sense and 6.2.2. antisense with hsMFEpCTCON plasmid as template. The second PCR reaction amplified the 3' end of the 6.2.2. DNA sequence using primers hsMFE antisense and 6.2.2. sense with plasmid hsMFEpCTCON.

PCR reactions were carried out using varying amounts of template which had been diluted 1:1000. Amounts used were 1µl, 2µl, 3µl, 4µl, 5µl.

Following purification of the PCR products (see below), the 5' end of the 6.2.2. DNA sequence was diluted to 1:100 and the 3' end of the 6.2.2. DNA sequence was diluted to 1:1000 with dd H_20. A third PCR reaction was set up to assemble the whole 6.2.2. DNA sequence using the partly overlapping products from the first two reactions as templates with the primers hsMFEsense and hsMFE antisense. This reaction used varying amounts of 2µl, 5µl and 10µl of both templates. The resulting PCR product was then purified using the Wizard Purification Kit (Promega, Madison, WI, USA) following the manufacturer's instructions.

300µl of PCR product was transferred to a 1.5ml microcentrifuge tube and 100µl of direct purification buffer was added and mixed with 1ml of purification resin by vortexing three times over 1 minute. The mixture was transferred to a Wizard PCR Prep Minicolumn then 2ml of 80% isopropanol was added and the slurry pushed through the column with a syringe plunger. The Minicolumn was then transferred to a 1.5ml microcentrifuge tube and centrifuged for 2 minutes at 10,000 x g before 50µl of water was added to elute the DNA by final centrifugation for 20 seconds at 10,000 x g.

2.2.1.3 PCR for site-directed mutagenesis

Site-directed mutagenesis was performed using the QuikChange® Site-Directed Mutagenesis Kit (Stratagene, Cambridge, UK) using a set of complementary primers overlapping the region to be mutated. Melting temperatures (T_m) of the primers to determine annealing temperatures in PCR amplifications were estimated using the following equation:

$$T_m=81.5 + 0.41(\%GC) -675/N-\%mismatch$$

Where N is the primer length in bases, and % GC and % mismatch are whole numbers.

Amplification was carried out according to manufacturer's protocols in 600 µl snap-fit thin-walled tubes (Bio-Rad Laboratories, UK). Briefly, 5 µl (5 ng) of template plasmid DNA was added to 5 µl 10 X reaction buffer (consisting of 100 mM KCl, 100 mM $(NH_4)_2SO_4$, 200 mM Tris-HCl (pH 8.8), 20 mM $MgSO_4$, 1% Triton® X-100, 1 mg/ml nuclease-free bovine serum albumin), 1 µl dNTP mix, 1.25 µl each oligonucleotide (125 ng), and sterile dH_2O to 50 µl. One microlitre of *PfuTurbo*® DNA polymerase (2.5 U/ µl) was then added to each reaction. Reactions were incubated at 95°C for 30 s followed by 12 cycles of PCR as follows: 95°C for 30 s, 55°C for 1 min, 68°C for 2 min/kb plasmid length (reaction times were between 12-13.2 min).

2.2.1.4 Agarose Gel Electrophoresis

For agarose gel electrophoresis, Agarose MP was supplied from Roche Diagnostics (Lewes, East Sussex, UK). DNA Molecular Weight Markers II (*Hind* III-digested λ DNA) and IX (*Hae* III-digested φx174 DNA) were purchased from Roche Diagnostics Ltd (Lewes, East Sussex, UK). Figure 2.1 shows sizes of standards.

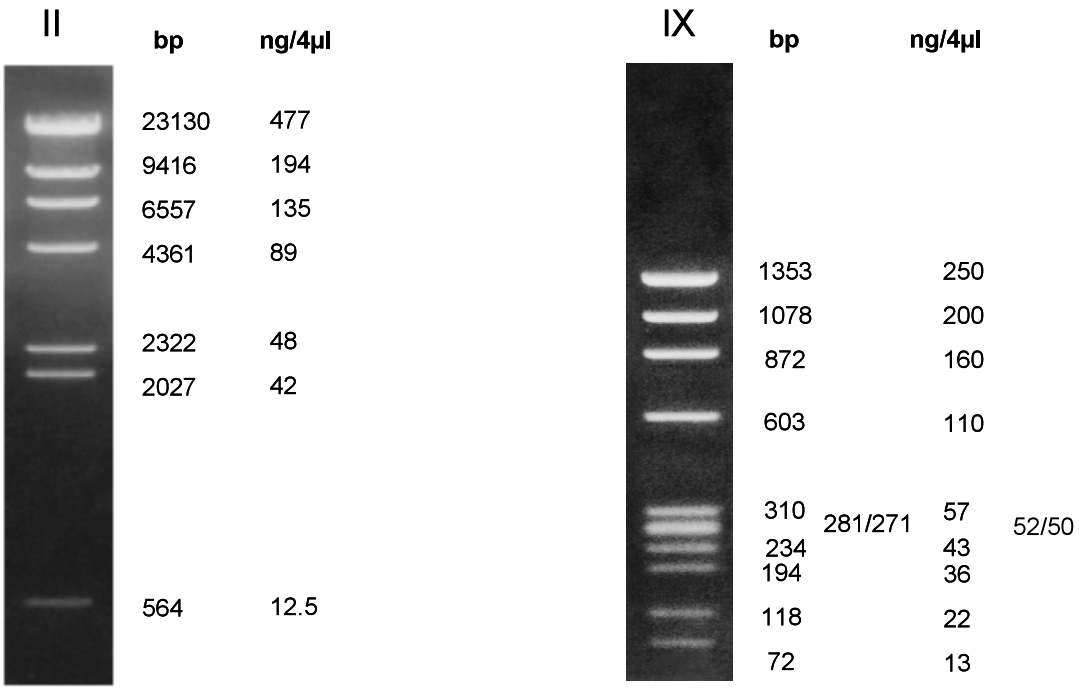

Figure 2.1 - DNA Markers II and IX shown run on 1% agarose gel with relative sizes and ng of DNA in 4µl

Gel electrophoresis was conducted using 1% horizontal slab gels run on a Hi-Set mini electrophoresis unit (Anachem, UK). Gels were made up using 0.5mg of agarose MP (Roche Diagnostics, UK) dissolved in 50ml 1x TBE buffer (Table 2.1) by microwave heating. 5 µl ethidium bromide was added to the solution after cooling to a temperature that allowed the glassware to be comfortably handled and the gel poured into the electrophoresis unit with appropriate well forming units.

For agarose gel electrophoresis, 10x DNA loading buffer (Table 2.1) was added to the DNA at a ratio of 2µl buffer to 8 µl DNA and this solution was applied to the gel. In all cases, electrophoresis was carried out using 1x TBE buffer at a constant 50 mV powered with the Pharmacia LKB-GPS 200/400 powerpack (Pharmacia, UK). Bands were visualised using a UVP transilluminator (Genetic Research Instrumentation Ltd, Essex, UK) prior to photography using a DS34 polaroid direct screen instant camera (Genetic Research Instrumentation Ltd, Essex, UK) and black and white Polaroid film type 667.

2.2.1.5 Purification of DNA from Agarose

DNA was extracted using the QIAEX II Agarose Gel Extraction Protocol (Qiagen GmbH, Hilden, Germany). After agarose gel electrophoresis desired DNA bands were excised with a scalpel and the gel was placed in a 1.5ml microcentrifuge tube. The gel was then weighed and Buffer QX1 (Table 2.1) was added to the tube at a ratio of 1:3 volumes which was then incubated at 50ºC for 10 minutes with vortexing every 2 minutes. The sample was then centrifuged for 30s at 10,000 x g, supernatant removed and the pellet washed once with Buffer QX1 then twice with Buffer PE (Table 2.1) to remove residual salt contaminants. The pellet was air dried for 30 minutes until white. The DNA was eluted in 20µl dH_20 prior to centrifuging for 30 sec and the supernatant then pipetted into a 1ml tube. This final step was repeated once.

2.2.1.6 PCR Product and Plasmid Digestion

Restriction site enzymes were used to cut the 6.2.2. PCR product and the plasmid vector VLpuc119 (available in the laboratory). To test the enzymes, a small scale digestion was carried out using 1µl plasmid (3.8µg), 0.5µl NcoI, NotI digestion enzymes (New England Biolabs, Ipswich, MA, USA), 1µl NEBuffer 3, 1µl BSA (10%) and 6µl dd H_20. All digestion took place at 37°C over 4 hours using the PCR personal cycler. Successful digestion was verified by 1% Agarose Gel electrophoresis.

Large scale digestion was then performed using 5µl plasmid (19µg), 2.5µl NcoI, NotI digestion enzymes (New England Biolabs), 5µl NEBuffer 3, 5µl BSA (10%) and 30µl dd H_20**.** PCR product digestion was conducted using 35µl PCR product, 2.5µl NcoI, NotI digestion enzymes (New England Biolabs), 5µl NEBuffer 3 and 5µl BSA (10%). Purification of digestion products was performed using 1% agarose gel electrophoresis and DNA eluted from the gel using Qiagen Gel Extraction Kit as above.

2.2.1.7 Protein Ligation

Ligation of digested PCR product and digested VLpuc119 vector was performed at differing ratios of vector to insert 1:1, 1:3, 1:5, 3:1 and a control of vector only. In each case, 10ng of vector were used, with the appropriate amount of digested PCR product, 2µl 5x DNA buffer was added to the reaction mixture and the volume made up to 10µl with ddH_2O, then 10µl T4 DNA Ligation Buffer was added followed by 1µl T4 DNA Ligase. The mixture was then incubated for 30 minutes at room temperature.

2.2.1.8 Phenol Extraction of DNA from Ligation Mixture

In a 1.5ml microcentrifuge tube, 21µl ligation mixture was added to 81µl dd H_20 and to this, a further 100µl of Phenol:Chloroform Isamyl alcohol were added. The sample was vortexed for one minute and then centrifuged for 3 minutes, 14,000 x g at room temperature. The upper aqueous phase was then carefully transferred to a clean tube to which 100µl dichloromethane was added, the sample vortexed then again centrifuged at 14,000 x g for 3 minutes. The DNA containing upper phase was taken and 1/20 vol of 3M NaAc (pH5.6) added prior to DNA being precipitated by adding 1 vol of isopropanol. The whole mixture was then vortexed for 1 minute and centrifuged for 10 minutes at 14,000 x g before discarding the supernatant. The sample was then washed with 70% ethanol, supernatant carefully removed and the DNA pellet allowed to air dry overnight. The following morning, the sample was solubilized in 5µl dd H_20.

2.2.2 Bacterial Protein Production

2.2.2.1 Microbial strains

The bacterial strain TG1 was a kind gift from Professor Robert Hawkins (Cancer Research UK Department of Medical Oncology, Paterson Institute of Cancer Research, Manchester, UK). TOP10F' and the wild-type yeast strain X-33 were obtained from Invitrogen (UK).

2.2.2.2 Transformation of phenol extracted ligation mixture by electroporation

Electrocompetent TG1 cells were defrosted on ice. 1 µl of plasmid (1:1000 dilution) was added to 50 µl of thawed cells and the sample then transferred into 0.2 cm cuvettes (BioRad Laboratories, Hemel Hempstead, UK) pre chilled on ice. Cuvettes were then individually pulsed at 2.5kV, 25 µFD, 200 Ω using the Bio-Rad Micropulser (Bio-Rad Laboratories - as above) and after electroporation, 0.5 mls 2YT, 1% glucose (no ampicillin) was added and the cuvettes incubated at 37 ºC for 1 hr. Following this, 100 µl of the culture was plated onto agar with 2YT, 1% glucose, 100µg/ml ampicillin and plates were then incubated overnight at 37ºC.

2.2.2.3 PCR Colony screening

Individual bacterial colonies were picked from agar plates using autoclaved wooden sticks and split half to grow in 2x YT/1% glucose/100µg/ml ampicillin and half for PCR colony screening. For screening, cells were suspended in 50 µl dd H_20, heated at 100ºC for 10 minutes, centrifuged and 40 µl were used in PCR reaction as above with primers hsMFE sense and hsMFE anti-sense. However, for this PCR reaction we used a total volume of 50µl only.

2.2.2.4 Plasmid Extraction

This was carried out using the QIAGEN Plasmid Midi Extraction Kit (Qiagen GmbH, Hilden, Germany). Cells were grown overnight at 37ºC shaking at 300 x g from 60 µl starter culture in 30 mls 2xYT, containing 1% glucose and 100µg/ml ampicillin contained in sterile 250 ml flasks. Bacterial cells from culture were centrifuged at 6000 x g for 15 minutes at 4ºC and the pellet re-suspended in 4ml Buffer P1 (Table 2.1) before adding 4mls Buffer P2 and incubating at room temp for 5 min. Next, 4mls chilled Buffer P3 was added and the mixture incubated on ice for 15 min before centrifuging at 20,000 x g for 30 min at 4 ºC and removing the plasmid containing supernatant. Centrifugation was repeated at 20,000 x g for 15 min at 4ºC and the supernatant was immediately applied to QIAGEN-tip 100 columns which had been primed using 4ml Buffer QBT. The column was next washed twice with 10mls Buffer QC prior to DNA elution using Buffer QF and the eluate collected in a clean 15ml centrifuge tube.

To precipitate DNA, 3.5mls isopropanol was added to the elute and the sample centrifuged at 15,000 x g for 30 min at 4ºC. The supernatant was carefully removed and the pellet washed with 70% ethanol at room temperature by centrifugation at 15,000 x g for 10 min before again removing the supernatant and air drying the DNA pellet overnight. Finally the DNA was dissolved in 100 µl dH_20.

2.2.2.5 Determination of DNA yield after purification

This was quantified using optical density measurements on a spectrophotometer (CECIL CE2041 2000) at wavelength of 260 nm using a quartz cuvette. The spectrophotometer was zeroed using dd H_20 and samples of purified DNA diluted 1:1000 before taking readings at 260 nm. DNA purification was calculated using the following formula:

$$[DNA] = (Optical\ Density_{260} \times 50 \times dilution\ factor)\ \mu g/ml$$

Optical $Density_{260}$ of 1.0 is equivalent to [DNA] of 50 μg/ml

2.2.2.6 Protein Expression

Single colonies from transformed *E.coli* cells were selected from agar plates and cultured overnight at 37ºC, 225 x g in 5mls 2YT, 1% glucose, 100μg/ml of ampicillin. Cells were harvested by centrifuging at 3,900 x g for 20 min then re-suspended in 5mls 2YT, 100μg/ml ampicillin, 5μl β-D-thiogalactoside (IPTG) (1M stock) and grown overnight at 30ºC with shaking at 225 x g. The culture was again centrifuged at 3,900 x g and the supernatant containing expressed protein decanted into clean polypropylene tubes.

2.2.2.7 Protein Concentration

500μl supernatant following protein expression was loaded onto Vivaspin 500 centrifugal concentrators (Sigma Aldridge, UK) with membrane pore size of 10,000 Da MWCO. This was centrifuged at 15,000 x g for 20 minutes and the protein concentrated to a volume of 5μl prior top loading for SDS-PAGE electrophoresis or Western blot analysis.

2.2.2.8 SDS PAGE Electrophoresis

Samples for electrophoresis were made up using 200 µl of supernatant containing the expressed protein and this was mixed with 67µl of 5x SDS PAGE reducing buffer in 1ml microcentrifuge tubes. Protein denaturation was achieved by heating for 10 min at 99.9ºC in the Biometra Personal Cycler. Samples were loaded onto two 12% Tris-Glycine pre-cast mini gels (Invitrogen, Paisly, UK) and run on an Xcell II™ Mini-Cell system (Invitrogen) in 1 x SDS PAGE Running Buffer at a constant 35mA (125V, 5W) for 1.5 hrs using a PowerEase® 500 power supply (Invitrogen). Protein molecular weight marker (See Blue®) was obtained from Invitrogen and run in lane 1 (figure 2.2). After electrophoresis, one gel was stained using Coomassie blue and one loaded for Western blot analysis. Gels for staining were soaked for one hour in Coomassie blue at room temperature on a shaker then transferred into Destain to soak overnight.

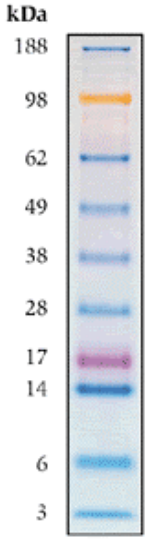

Figure 2.2 :-See Blue® marker after subjection to SDS- PAGE with apparent molecular weights (From Invitrogen catalogue).

2.2.2.9 Western blot analysis

Gels from electrophoresis were transferred onto 0.45 μm polyvinylidene difluoride (PVDF) membrane (Bio-Rad Laboratories, as above) which had been pre-soaked in methanol. The gel was placed next to the membrane and inbetween eight sheets of blotting paper (Whatman, Maidstone, UK) pre soaked with 1x Transfer buffer and then into an XCell II Blot Module (Invitrogen, as before). The Module was placed in the XCell Mini Cell System and run at 125 mA (25V, 17W) for 1.5 hrs using 1x transfer buffer.

Following protein transfer from gel to membrane, the membrane was removed and blocked for 1hr at room temperature in 5% Marvel (Marvel, UK) dried milk powder made up with PBS. After 1 hr on the shaker, membrane was washed three times in 0.1% (v/v) Tween-20 in PBS followed by three times with PBS. Next, the membrane was stained with 20 μl mouse anti-tetra-His antibody (Qiagen, 100μg/1ml stock) in 20mls 1% Marvel in PBS for one hour under shaking, then washed four times in Tween/PBS followed by four times in PBS. Secondary staining was achieved using 20μl sheep anti-mouse IgG antibody (GE Healthcare) again dissolved in 20mls 1%Marvel/PBS and left for 1 hour at room temperature under shaking.
Finally, the membrane was washed again four times in Tween/PBS and proteins visualised using DAB solution (0.25 mg/ml 3,3'- Diaminobenzidine tetrahydrochloride, 0.5μl/ml H_20_2 in dH_20). When protein bands became visible after 20mins, the reaction was stopped by rinsing the membrane in dH_20 and membrane was then air dried.

2.2.3 Protein Production in Yeast

2.2.3.1 Linearisation of plasmids for homologous recombination with X-33 yeast genome

pPICZα-B based plasmids (or modified pPicZαB vector) containing insert DNA were linearised for transformation into the X-33 yeast genome. 10 μg (approx. 10 μl) of plasmid DNA was digested with 4 μl *Pme* I (40 units; New England Biolabs) for 2 h at 37°C in the presence of 5 μl 10 X NEBuffer 4 (Table 2.1), 5 μl BSA (10 x BSA; final concentration 100 μg/ml), and completed to 50 μl with sterile dH_20. Reactions were stopped by heat inactivation at 65°C for 20 min and digested DNA was purified by phenol:chloroform extraction and precipitated

2.2.3.2 Preparation of electro-competent yeast cells

Yeast wild-type X-33 strain was purchased from Invitrogen (UK) and prepared for electroporation following protocols by Invitrogen (UK). Five millilitres of YPD media (Table 2.3) was inoculated with X-33 cells picked from agar stabs (EasySelect™ *Pichia* Expression Kit; Invitrogen, UK) and the inoculated culture was grown overnight at 30°C, 250 x g in an orbital shaker. The next day, 500 ml YPD was inoculated with 0.5 ml overnight culture and grown at 30°C, 250 x g until an OD_{600} of between 1.3-1.5 (~16 h).

Cultures were centrifuged at 1,500 x *g* for 5 min at 4°C and pellets resuspended in 500 ml ice-cold sterile dH_2O. Cells were centrifuged as before, followed by resuspension of the pellet in 250 ml ice-cold sterile dH_2O. The cells were again centrifuged and the pellet resuspended in 20 ml ice-cold sterile 1 M sorbitol. The process was repeated once more and cells resuspended in 1 ml ice-cold sterile 1 M sorbitol. The cells were stored on ice and used the same day.

2.2.3.3 Electroporation of electro-competent yeast cells

Eighty microlitres of freshly prepared X-33 electrocompetent cells were added to 10 µl of linearised plasmid DNA and incubated on ice for 1 min. Cells were transferred to a pre-chilled 0.2 µm cuvette (Biorad) and pulsed once using the pre-set 'Pic' setting on BioRad MicroPulser™ (Bio-Rad Laboratories Ltd., Hemel Hempstead, U.K.) for 5 ms at 2000 V. One millilitre of ice-cold, sterile 1 M sorbitol was immediately added to the mixture, the contents of the cuvette were transferred to a sterile 15 ml tube and the cells were incubated at 30°C for 2 h with no shaking. Transformed cells were spread onto YPDS plates (Table 2.3) containing Zeocin™ (100 µg/ml) in 10, 25, 50, 100, and 200 µl aliquots and incubated at 30°C for 4-5 days until colonies formed. At this time, ten clones were picked and streaked onto fresh YPDS Zeocin™ plates and incubated for 2-3 days until colonies formed.

2.2.3.4 Protein expression in yeast

Individual colonies were picked from YPDS plates (Table 2.3) containing 100 µg/ml Zeocin and inoculated into 5ml BMGY medium (Table 2.3) and grown until an OD_{600} of 2-5 at 30°C, 250 x g (approximately 16 h). Overnight cultures were centrifuged for 5 min at 3,000 x *g* (room temperature) and pellets were resuspended in BMMY (Table 2.3) with the addition of 1 % casamino acid, pH 6.0 medium to a final OD_{600} = 1 (approximately 50 ml). Cultures were expressed at 30°C, 250 x g with the addition of 100% methanol for a final concentration of 0.5% (v/v) every 24 h for a total of 96 h. At this time cultures were centrifuged for 10 min at 3,000 x *g* and supernatants were filtered through 0.2 µm Nalgene filters and stored at either 4°C for immediate purification or at -80°C. Glycerol stocks were made for high expressers by mixing 900 µl of culture with 100 µl sterile glycerol, followed by storage at -80°C.

2.2.3.5 Seed lot preparation for P. pastoris fermentation

Single colonies growing on YPDS-zeocin plates were streaked out onto the freshly prepared YPDS-zeocin plates and grown at 30°C until colonies formed (1-2 days) in an empty incubator which had been sprayed with 80% (v/v) ethanol in sterile dH_20. Colonies were picked from the plates and used to inoculate 50 ml sterile YPDS-zeocin. The culture was grown at 30°C, 250 x g in an empty incubator which had been sprayed with 80% (v/v) ethanol until an OD_{600} = 15-25 (approximately 48 h). At this time the culture was centrifuged in a sterile centrifuge tube for 10 min at 3,000 x *g* and moved into a laminar flow cabinet. The pellet was resuspended in 25 ml sterile YPD and dispensed in 1 ml aliquots into cryovials (Nunc) for storage at -80°C.

2.2.3.6 Fermentation of P. pastoris X-33 cells

Fermentations of *P. pastoris* X-33 cells were carried out with the help of Dr. Berend Tolner (UCL Cancer Institute, London) using a Bioflo 3000 Batch/Continuous Bioreactor (New Brunswick Scientific, Edison, NJ, USA). One frozen vial containing 1 ml of seed lot was used to inoculate a 250 ml primary culture of YEPD Glucose medium (Table 2.3) and the culture was grown overnight at 30°C at 180 x g (OD_{600}=12). Concomitant with this, fermentation medium was prepared by mixing 5 L basic salt medium in the fermentor and 1 L sodium hexametaphosphate (*see* Table 2.4).

Five millilitres of the primary culture was used to inoculate a 0.2 μm filter-sterilised (Nalgene Ltd., UK) secondary culture comprised of 300 ml basic salt medium, 30 ml sodium hexametaphosphate, and 1 ml trace elements (Table 2.3). The secondary culture was grown overnight at 30°C at 180 x g (OD_{600}=5). The 10 L fermentor, with remaining basic salt medium, was autoclaved and the remaining sodium hexametaphosphate was added, along with 1 ml anti-foam (Sigma-Aldrich Ltd., UK) and 24 ml trace elements. The fermentor pH was set to 5.0, regulated by a base solution of 100% NH_4OH and an acid solution of 10% ortho phosphoric acid. The

dissolved oxygen probe was set to 40%. The run was started upon addition of the complete secondary starter culture.

A limited glycerol feed (made up of an autoclaved mixture of 300 ml 100% glycerol with 300 ml water and 7 ml trace elements) was started immediately upon a sharp increase in dissolved oxygen (approximately 23-24 h) and the pH was reset to 6.5. One hour after the start of the limited glycerol feed, 11 ml of limited methanol feed (made up of 2000 ml methanol and 24 ml trace elements) was directly injected into the fermentor. Flow rates of glycerol and methanol feeds were altered during the run and are given in Table 2.7. The fermentation run was stopped after approximately 72 h post inoculation, at which time the cells were harvested by centrifugation at 11,300 *x g* for 1 h. Cleared supernatants were filtered through 0.2 μm Nalgene vacuum filters (Millipore UK) and either immediately purified or stored at -80°C.

Time post limited feed start (h)	***Flow rate glycerol (ml/h)***	***Flow rate methanol (ml/h)***
0	120	0
1.0	120	0
1.5	100	0
2.0	80	0
2.5	60	0
3.0	40	0
3.5	20	0
4.0	0	10
6.0	0	20
8.0	0	30
10.0	0	42-45

Table 2.7 - Flow rates for addition of glycerol and methanol during yeast fermentation

2.2.3.7 Purification of scFv after large scale Pichia production

Supernatant from the Pichia fermentation was purified using expanded bed adsorption immobilised metal affinity chromatography IMAC (GE Healthcare)).

Firstly, the expanded bed adsorption column was connected to the spectrophotometer and zeroed with water. Next, the column was charged with 0.1 M copper sulphate solution at flow rate of 300 cm/h. Unbound ions were washed off with dH2O until

UV signal returned back to baseline. Ten column volumes of loading buffer (Table 2.1) were then run through the column.

Before application to the column, the Pichia supernatant diluted 1:1 with 2 M NaCl in 2x PBS, then loaded onto the charged EBA column at flow rate 300 cm/h. Following this, loading buffer was run through until the UV signal reached baseline. To remove contaminants, 40 mM Imidazole wash buffer was applied to the column at a flow rate 300 cm/h. Next, the column flow was reversed and the target histidine-tagged scFv proteins were eluted from the column by application of 200 mM Imidazole elution buffer to the column at flow rate 150 cm/h fraction. Peak fractions were analysed on a spectrophotometer at OD280, those containing protein were further concentrated by application to a 1 ml Ni^{2+} charged HiTrap IMAC HP column (GE Healthcare).

2.2.3.8 Size exclusion chromatography

Purification of the concentrated scFv fractions continued using size exclusion chromatography with an AKTA™ FPLC system (GE Healthcare) loaded with a Superdex 75 column (125 ml bed volume) (GE Healthcare). Protein samples were loaded via the 2 ml injection loop at a constant flow rate of 2 ml/min PBS, fractions were collected and peak fractions pooled prior to western blot analysis as in section *2.2.2.9.*

2.2.3.9 Quantification of protein post purification

Protein concentration was determined spectrophotometrically on a Cecil CE2041 2000 series spectrophotometer using the equation:

$$A_{280}=\varepsilon 280 \times c \times l$$

- A_{280} is the absorbance of protein samples at 280 nm
- ε280 is the extinction coefficient (0.1%, 280 nm, 1 cm path length) of the protein calculated based on the protein primary amino acid sequence using the Expasy Protparam web tool (http://www.expasy.ch/tools/protparam.htlm)
- *c* is the protein concentration,
- *l* is the path length of the cuvette (cm).
- For B6.3 ε280 = 1.9

2.2.4 Human Cell Lines

2.2.4.1 Antibodies and reagents.

The monoclonal antibodies (mAb) used in this study were as follows: 10D5,anti-αvβ6 integrin, from Chemicon International; 2G2, and 6.3G9, anti-human αvβ6 integrin generously provided by S Violette (Biogen Idec). 53a2 rat mAb against human αvβ6 was produced in-house. Anti-c-Met from Invitrogen, anti-E-cadherin from Santa Cruz Biotechnology, anti-HGF/SF from R&D Systems. IA4, anti-smooth muscle actin and AE1/AE3, anti-cytokeratin were from Dako. Polyclonal antibody C-19, anti-human integrin β6 was from Santa Cruz Biotechnology. Human type 1 collagen was obtained from Sigma, Matrigel from BD Biosciences and MET kinase inhibitor SU11274 from Calbiochem.

2.2.4.2 Immunohistochemistry

Antibodies used were anti-αvβ6, 62G2 (0.5μg/ml; Biogen Idec)), anti-smooth muscle actin (SMA), IA4 (1;100; Dako), anti-c-Met (1:50; Zymed) anti-HGF/SF (1:10; R&D Systems), anti-cytokeratin, AE1/AE3 (1:50; Dako), or anti-E-cadherin (1:50; Santa Cruz Biotechnology), phospho-Smad2 (Cell signalling) and Smad4 (sc-7966, Santa Cruz Biotechnology). Immunohistochemistry was performed on 4μm, formalin fixed, paraffin embedded serial sections of tumor blocks. Samples were dewaxed and brought to absolute alcohol using Xylene 5mins x2, 100% EtOH 2mins x2, 95% EtOH 2mins x2, 50% EtOH 2mins, ddH2O 2mins. Antigen retrieval varied according to primary antibody; 0.1% α-chymotrypsin 0.1% calcium chloride pH 7.8 for 20 min at 37°C (AE1/AE3); Digest-All™ 3 Pepsin Solution (Zymed® Laboratories, USA) for 5 min at 37°C (6.2G2), microwaving for 30 minutes in 0.1M citrate buffer, pH 6 (c-Met, SF/HGF, E-cadherin). Endogenous peroxidase was neutralized with 0.45% hydrogen peroxidase in methanol for 15 min and primary antibodies applied in TBS (pH 7.6) for 1 hour. Anti-mouse IgG biotinylated secondary antibody (Vectastain Elite ABC Reagent, Vector Laboratories) was applied for 30 min followed by peroxidase-labelled streptavidin (Vectastain Elite ABC Reagent; Vector Laboratories) for 30 min. Peroxidase was visualized using DAB+ (Dako) for 7 min and counterstained in Mayer's hematoxylin (Sigma, UK). Slides were dehydrated and cleared then mounted using permount (Fischer SP15-500).

2.2.4.3 Human Tissue

Ethical approval was obtained from the National Research Ethics Committee reference number 07/Qo4o5/8. Skin samples were chosen at random from pathology records at Mt Vernon Hospital, Northwood, UK and stained for αvβ6, SMA, c-Met, HGF/SF, E-cadherin and cytokeratin. Samples were scored according to the quickscore method (Detre *et al* 1995). The staining intensity of αvβ6 and SMA was scored out of 3 (0= none, 1=weak, 2=moderate, 3=strong), and the proportion of cells staining positively was scored out of 4 (0=no staining, 1=1-25%, 2=25-50%, 3=51-75%, 4=76-100%). The score for intensity was added to the score for proportion to

give a score in the range of 0-7 and grouped as low (score=0,1), medium (score=1-3), or high (score 4-7).

OSCC samples were obtained from pathology storage at UCLH and Barts Hospitals, London, UK with OSCC patient details obtained from medical records at the relevant hospitals. Patient mortality data were obtained from the Thames Cancer Registry and confirmed with patient records. Patients whose tissue samples were unobtainable were excluded from the study.

2.2.4.4 Cell culture

All cell culture procedures were carried out in a class II hood with humidified air and 5% CO_2. Culture medium (Table 2.4), PBS and Trypsin/EDTA were pre-warmed to 37°C before use. Cell lines were stored in frozen aliquots and brought into culture having been thawed to 37°C and resuspended by drop wise addition of 10 ml culture medium (Table 2.4). The cells were then centrifuged at 1300 x g for 3 min and resuspended in 5 ml of culture medium prior to seeding into T25 culture flasks.

Once confluent, cells were sub-cultured routinely twice weekly; culture medium was poured off and cells washed once in 10 ml PBS and the cells released from the flask with 5 ml trypsin/EDTA for 5 min at 37°C. Next, cells were resuspended in fresh culture medium before 2 ml was drawn off and centrifuged at 1300 x g for 3 min. These cells were then seeded into T75 flasks.

If cells were to be stored, a confluent flask was selected, cells washed and released from the flask as before then centrifuged and resuspended in 5mls freezing medium (Table 2.4). Cells were then aliquoted into 1ml cryovials (Nalgene) and stored at -80°C.

2.2.4.5 Preparation of NTGLi1 and NTGLi2 cell lines

NT-Gli1 cells were generously donated by Dr Graham Neill (Centre for Cutaneous Research, Barts and The London School of Medicine and Dentistry, London, UK). NTGli1 and NTGli2 cell lines were used as a BCC model. Briefly, the coding sequences of GLI1 and an active mutant of GLI2 (DN-GLI2b) were cloned into pBabePuro and retroviral particles made using the Phoenix (amphotropic) packaging cell line as described previously (Regl *et al* 2002). NTert-1 keratinocytes (NTGli1, NTGli2) were selected with puromycin (1 ug/ml) 48 hr after retroviral transduction (for 72 hr) and Gli expression was confirmed by Western Blot analysis (Santa Cruz GLI-1 C18 and GLI-2 H-300 abs). Cells were grown in keratinocyte growth medium (KGM) (Table 2.4). Human Foreskin Fibroblasts (HFF2) were obtained from ATCC (Teddington, Middlesex, UK) and maintained in fibroblast growth medium (DMEM supplemented with 10% fetal calf serum) at 37^{o}C in a humidified atmosphere.

2.2.4.6 RNAi

RNAi SMART pool reagents targeting β6 control (random) sequences were obtained from Dharmacon (Chicago, USA) and used as described previously (Nystrom *et al* 2006). Cells were seeded into 6-well plates and left for 24 hours until approximately 40% confluent, then transfected with 100nmol/ well of the relevant duplex pool using Oligofectamine transfection reagent (Invitrogen, Paisley, UK). Cells were used in assays after 24-48 hours. Cells were also lyzed and used to verify protein knock-down by Western blotting analysis. These experiments were kindly carried out by Professor Gareth Thomas, Centre for Tumour Biology, Institute of Cancer, Bart's and the London School of Medicine and Dentistry,UK.

2.2.4.7 Flow cytometry

Subconfluent cells were washed twice with PBS and harvested by trypsin/EDTA (0.25% w/v, 5 mM). Cells were washed once in PBS containing 10% FCS then resuspended to give concentration of 2.5x10^{6} per ml. 200µl added to each FACS tube (5x10^{5} per tube). FACS media was Dulbecco's modified Eagle's medium (DMEM)

supplemented with 0.1% (w/v) Bovine Serum Albumin (BSA) and 0.1% (w/v) sodium azide (DMEM 0.1/0.1). Next, cells were incubated with primary antibody for 40 min at 4°C and washed twice with PBS. FITC conjugated secondary antibody was applied to the cells for 30 min at 4°C. Cells were washed twice with PBS and resuspended in 0.5 ml PBS with 10% FCS. Labelled cells were analysed on an LSR-1 FACS flow cytometer (Becton Dickinson, Oxford, UK) using CellQuest software, acquiring $1x10^4$ events.

Antibodies used were the anti-αvβ6 antibody (10D5; Chemicon International, Harrow, UK), anti-c-Met antibody (Invitrogen), Alexa 488-conjugated secondary antibody (Dako), rabbit anti human IgG 2.3mg/ml (Jackson ImmunoResearch Laboratories, West Grove, USA), Mouse Tetra-His antibody (Qiagen, Crawley, UK) diluted 1:100 in DMEM. Negative control used secondary antibody only. Results show mean fluorescence (arbitrary units, log scale).

2.2.4.8 TGF-β bioassay

Mink lung epithelial reporter cells (MLEC) stably expressing a TGFβ-responsive luciferase reporter construct (Abe *et al* 1994) were plated overnight in 96-well plates in DMEM, 10% FCS (5×10^4 cells/well). The medium was changed to serum-free α MEM, and NTGli1 or NTGli2 cells (2.5×10^4 cells/well) were added to each well in serum-free α MEM containing anti-αvβ6 antibody (10μg/ml; 10D5; Chemicon) or ctl antibody (10μg/ml; anti-α4 integrin). The cells were co-cultured overnight, washed once in PBS and lysed in reporter lysis buffer (Promega). Luciferase assay buffer (Promega) was added to the supernatant and the luminescence measured using a Wallac platereader. These experiments were kindly carried out by Dr Sarah Dickinson, Centre for Tumour Biology, Institute of Cancer, Bart's and the London School of Medicine and Dentistry, UK.

2.2.4.9 Co-culture experiments

HFF2 Fibroblasts and NTGli1 or NTGli2 cells were plated in 6-well dishes (2.5×10^5 cells per cell type) or on to 13mm glass coverslips in 24 well plates (2.5×10^4 cells of each cell type). Cells were seeded in DMEM, 10% FCS ± antibodies (as above) or TGF-β1 (1ng/ml; R&D Systems) and left to attach. The medium was then changed to serum-free DMEM containing antibodies or TGF-β and cultured for a further 48 hours. The cells were either lyzed for analysis by Western blotting or fixed and processed for immunoflourescence. The supernatant was analyzed by ELISA for HGF/SF.

2.2.4.10 Western blot analysis following cell culture experiments

Cells were lyzed in NP40 buffer (Biosource). Samples containing equal protein were electrophoresed under reducing conditions in 12% SDS-PAGE gels. Protein was electro-blotted to nitrocellulose membranes (Amersham Biosciences). Blots were probed with antibodies against αvβ6 (Santa Cruz) or SMA (Dako). Horseradish peroxidase-conjugated anti-goat or anti-mouse (Dako) were used as secondary antibodies. Bound antibodies were detected with the ECL Western blotting detection kit system (Amersham). Blots were probed for HSP70 (Santa Cruz) as a loading control. Exposures of blots in the linear range were quantified by densitometry software (Scion Corp.).

2.2.4.11 Preparation and use of medium conditioned by fibroblasts and myofibroblasts

$5x10^5$ fibroblasts were plated in fibroblast growth medium in $75cm^2$ culture flasks for 24 hours then washed twice with PBS. To induce a myofibroblastic phenotype cells were incubated for 48 hours in medium containing recombinant TGF-β1 (1ng/ml; R&D Systems), which was acid-activated prior to use (4mM HCl/ 0.1% BSA).

Control cells were cultured in medium alone. After 48 hours the cells were washed twice with PBS, and cultured for a further 72 hours in α-MEM. The control fibroblast (FCM) or myofibroblast-conditioned medium (MCM) was collected, clarified by centrifugation and the cells detached and counted. The volumes of FCM and MCM were corrected for cell number, adjusted to a total volume of 500μl and used in the lower chamber of a Transwell invasion assay as a chemoattractant.

2.2.4.12 Transwell invasion assays

Cell-invasion assays were performed over 72 hours using Matrigel-coated polycarbonate filters (Transwell®, BD Biosciences, Oxford, UK). Matrigel (70 ml, 1:2 dilution in α-MEM) was added to the upper chamber and allowed to set for 1 hr at 37°C. To act as a chemotactant, 500 μl of KGM was placed in the lower chamber. Cells were plated in the upper chamber of quadruplicate wells at a density of $5x10^4$ in 200 ml of α-MEM and incubated at 37°C for 72 hrs. For blocking experiments anti-αvβ6 antibody (6.3G9; 10μg/ml) or control antibody (7.2; 10μg/ml), were added to the cells for 30 minutes at 4°C prior to seeding. For c-Met inhibition, cells were treated with c-Met kinase inhibitor, SU11274 (5μM; Calbiochem) for 24 hours prior to use, and the inhibitor was present throughout the experiment. After 72 hr, cells in the lower chamber (including those attached to the undersurface of the membrane) were trypsinised and counted on a Casy 1 counter (Sharfe, Reutlinger, Germany). Experiments were repeated a minimum of 3 times in quadruplicate.

2.2.4.13 Organotypic culture

To prepare collagen gels, 7 volumes of collagen type 1 (4 mg/ml, Upstate, Lake Placid, NY) were mixed on ice with 1 volume 10× DMEM, 1 volume FCS and 1 volume FGM in which HFF had been suspended at a concentration of $0–5 \times 10^6$ ml^{-1}. Then 1 ml of this solution (5×10^5 HFF unless otherwise stated) was aliquoted into wells of a 24-well plate and allowed to polymerise for 30 min at 37°C. After polymerization, 1ml of FGM was added per well and gels were left for 18 h at 37°C

to equilibrate. Concurrently, a fibroblast-free collagen gel mix was used to coat sterile nylon discs (100 μm pore size; Tetko Inc, New York, USA) which after polymerization at 37°C for 10 min were fixed in 1% glutaraldehyde for 1 h, washed (four times in phosphate-buffered saline (PBS), twice in KGM) and stored at 4°C. Next day, medium was aspirated from the wells of the 24-well plates and 5×10^5 NTGli1 cells (suspended in α-MEM supplemented with 10% FCS and glutamine) were added to each well. The following day, gels were removed from the 24-well plate and placed on to individual collagen coated nylon discs resting on steel grids. These steel grids were made from 2.5 cm^2 squares of stainless steel mesh with the edges bent down to form 4–5 mm high 'legs'. This initial time-point was defined as day 1 of organotypic culture. The steel grids were placed in six-well plates and sufficient KGM (minus the cholera toxin) added to reach the undersurface of the grid, allowing the epithelial layer to grow at an air–liquid interface.

For inhibition studies, the met kinase inhibitor SU11274 (5μM) was added to the KGM. The medium was changed every two days. After six days the gels were bisected, fixed in formal-saline, and processed to paraffin. 4μm sections were immunostained with the pan-cytokeratin antibody AE1/AE3 (Dako) as described previously.

2.2.4.14 Confocal microscopy

Cells were fixed for 10 minutes in 4% formaldehyde in cytoskeletal buffer (10 mM MES, 3 mM $MgCl_2$, 138 mM KCl, 2 mM EGTA, pH 6.1) with 0.32 M sucrose. Cells were permeabilised for 5 minutes with 0.2% Triton X-100 and incubated for 30 minutes in DMEM, 0.1% BSA, 0.1% sodium azide. Non-specific staining was blocked by incubation in 5% normal goat serum. Cells were then incubated with anti-SMA (IA4; Dako) and anti-αvβ6 antibodies (53a; in-house) for 1 hour, and binding detected by incubation with secondary antibodies conjugated with FITC or Cy3 (Jackson ImmunoResearch) for 45 minutes. Nuclei were visualised using DAPI (Invitrogen). Coverslips were mounted onto glass slides using mowiol. All dilutions were in DMEM, 0.1% BSA, 0.1% sodium azide and incubations were at room

temperature. Images were recorded and processed with a confocal laser scanning microscope (Zeiss LSM510). Confocal microscopy was kindly carried out by Dr Sarah Dickinson, Centre for Tumour Biology, Institute of Cancer, Bart's and the London School of Medicine and Dentistry,UK

2.2.5 Preparation of scFv-nanoparticle conjugates

2.2.5.1 Resovist to scFv conjugation

This carbodiimide attachment method was adapted from the method used by De Nardo et al (2005) for attachment of available COO- groups on Resovist particles to the NH_2 groups on scFvs. Firstly, the scFvs were dialysed into 1L 0.1M MES buffer pH 6.3 (=19.5g in 1l ddH_20) for 6hrs at 4ºC using dialysing cassette (3,500MW), 3 buffer changes performed. Next, 1ml of 10mg/ml particles in MES buffer was activated by adding 200µl EDC/NHS activation buffer 1hr at room temp. Activation reaction stopped by running particles through a PD10 desalting column (Amersham Bioscience UK). Next, the particles were eluted off the column with 0.1M MES buffer pH 6.3. To eluted particles 200µl of 1mg/ml scFv/MES added and mixed overnight at room temperature. To block unbound active sites, 100µl 25mM glycine/PBS added and mixed at room temperature for 60 minutes. ScFv-nanoparticles were then washed to remove unbound glycine by running through PD-10 desalting column and particles eluted off with 0.1M MES buffer. Finally, the scFv-Resovist particles were concentrated using Vivaspin 15R concentrators before purification by size exclusion chromatography (section *2.2.3.8*).

2.2.5.2 Chemicell DX to scFv attachment

Attachment of scFvs to the dextran coating of the Chemicell particles was achieved using a two step procedure whereby particles were first 'activated' with cyanogen bromide. Briefly, 10mg Chemicell FluidMAG-DX particles were washed x1 with 1 ml 0.1 M Sodium hydrogen phosphate buffer pH 9.0 using the magnetic separator

(Dynal A.S, Oslo, Norway) and resuspended in 0.25 ml 0.1 M Sodium hydrogen phosphate buffer pH 9.0. 50µl Cyanogen Bromide in 5 M Acetonitrile was added to the particles and mixed by vortex. The tube was then placed in ice cold water for 10 minutes.

After incubation, the activated particles were washed x2 with 1 ml PBS using the magnetic separator and resuspended in 0.25 ml ice cold PBS. Next, 200µl of 1mg/ml scFv (in PBS) was added to the activated particles and mixed overnight at room temperature. Excess reactive sites blocked with 100µl 25mM glycine/PBS and finally particles washed x3 with PBS using the magnetic separator and resuspended in 1ml PBS. Figure 5.24 depicts the steps required for particle attachment.

2.2.5.3 Purification of nanoparticle-scFv conjugates

scFv-nanoparticle conjugates were separated from unbound scFvs and unbound nanoparticles by size exclusion chromatography using an AKTA FPLC system (GE-Healthcare, Amersham, UK) and a 30ml Sephacryl 300 high resolution column (GE Healthcare). The column was calibrated using the Gel Filtration Standard Kit (Bio-Rad) and conjugated particles were loaded onto the column at a constant flow rate of 0.5ml/min in PBS and fractions collected throughout for storage at 4°C.

2.2.5.4 Analysis of scFv – nanoparticle conjugation: The Bradford Assay

The concentration of scFv-nanoparticle conjugates was estimated using the Bradford assay. Firstly, standards of scFv alone were prepared in PBS buffer at concentrations of 0, 2.5, 5, 7.5 and 10µg/ml. 500µl Bradford Reagent (Sigma) was added to 500µl of each standard and samples left to equilibrate to room temp for 15mins. Using a Cecil CE4041 2000 series spectrophotometer, the absorbance of each standard was measured at OD 595nm in quartz cuvettes allowing a plot to be made of the absorbance vs. standard protein concentration.

The concentration of scFv in the scFv-nanoparticle fractions obtained after size exclusion chromatography could then be calculated by repeating the Bradford assay as above then measuring the OD at 595nm and comparing this reading to the calibration curve.

2.2.5.5 Estimation of nanoparticle concentration post scFv-nanoparticle conjugation

The concentration of nanoparticles in the fractions obtained after purification could also be estimated using a spectrophotometer. Nanoparticle concentration standards for both Resovist and Chemicell particles were prepared in PBS at concentrations of 0, 0.125, 0.25, 0.375, 0.5mg/ml. The absorbance was measured at OD 490 on the Cecil CE4041 2000 series spectrophotometer. A plot was then made of the absorbance *v.* standard nanoparticle concentration. Measuring the OD at 490 and comparing this reading to the calibration curve then allowed the nanoparticle concentration in the scFv-nanoparticle fractions to be calculated.

2.2.6 Analysis of scFv-nanoparticle conjugates *in vitro*

Standard cell culture techniques were followed as set out in section *2.2.2.4*. Three αvβ6 expressing cell lines were used for the experiments set out below. VB6 cells were a kind gift from Professor Gareth Thomas, Barts and the London Medical School. HT29 cells were a purchased from ATCC- Promochem, Teddington, UK. A375B6 cell line is a transfected melanoma cell line and was a kind gift from Dr John Marshall, Barts and the London Medical School.

2.2.6.1 Estimation of cellular uptake of nanoparticles: The Ferrozine Assay

The Ferrozine Assay uses an iron detection buffer to form a complex with ferrous iron that absorbs strongly at 550 nm that can be read on a microplate reader – so allowing the detection of small changes in iron concentration within solutions. By using the

assay with a range of standards with known iron concentrations it is possible to prepare a graph from which unknown iron concentrations can be read when the same assay is performed.

100µl $FeCl_3$ standards were prepared at 0, 0.05, 0.1, 0.25, 0.5, 1, 2.5, 5, 7.5 and 10 µg/ml in 10 mM HCL which were then incubated with 100 µl 50 mM NaOH and 100µl iron releasing buffer (Table 2.6) at 60°C for 2 hrs. Once the samples had cooled to room temperature, 30µl iron detection buffer (Table 2.6) was then added and the samples incubated at room temperature for a further 30 min. The iron detection buffer produces a colour change in the solution which was then read by the Opsys MR™ Microplate Reader (Dynex Technologies), absorbance readings taken at 550nm. The absorbance vs. the Fe^{2+} concentration for each standard was plotted. This assay was then performed for both Resovist and Chemicell nanoparticles at concentrations 0, 0.5, 1, 2.5, 5, 10, 2.5, 5, 10, 25, 50 and 100 µg/ml in 10 mM HCL. The absorbance vs. the nanoparticle concentration for each standard was plotted and the nanoparticle concentration was then plotted against its corresponding Fe^{2+} concentration

For analysis of iron uptake by cells after incubation with nanoparticles or nanoparticle-scFv initially cells were seeded in 24 well plates at $5x10^4$/ml, 2mls per well and incubated in culture medium for 5 days. On day 5, the culture media was replaced with either 1ml filter sterilised scFv-nanoparticle conjugates or 1ml of nanoparticles alone at varying concentrations in culture media. Cells were incubated overnight followed by 3 x washes in cold PBS. Next, cells were released from the wells, a haemocytometer cell count performed and remaining cells lysed with 300 µl 50 mM NaOH for 2 hrs on a shaker at room temperature.

Following this, cell lysates were transferred to 1.5 ml eppendorf tubes, mixed with 300 µl of 10 mMHCL and 300µl of the iron releasing reagent (Table 2.6). The samples were then incubated for 2 hrs at 60°C on a heating block. Addition of iron detection buffer and colour change detection at 550nm then allowed the microplate readings to be referenced against the standard nanoparticle concentration curves, giving an estimate of the relative iron uptake.

2.2.6.2 Estimation of cell death after exposure to MACH: The MTT Assay

Cell survival after incubation with nanoparticles and exposure to MACH was assessed using a cell viability assay based on 3-(4,5- Dimethylthiazol-2-yl)-2,5-diphenyltetrazolium bromide (MTT) (Sigma-Aldrich) (Mosmann 1983).

Cells were seeded on 96 well plates at a density of $1x10^5$ cells/ml, 200µl/well and incubated for a minimum of 16 hours to allow adherence of the cells. Once adherent, 100µl culture medium containing either nanoparticles alone, scFv-nanoparticle conjugates or culture media only as a control was added per well. The nanoparticles were added at a range of concentrations, cells returned to the incubator for 1 hr before being exposed to MACH for 20 minutes. In each case, ambient temperature was maintained at 37°C using the Air Therm. Following this, cells were washed and incubated for a further 96hrs with fresh culture media.

20µl of MTT (5mg/ml) was then added to each well and plates returned to the incubator for a further 4hrs. Then, culture media was removed and purple formazan crystals were added to each well along with 100µl of DMSO. The crystals would then induce a colour change indicating cell viability which could be read by the Opsys MR™ Microplate Reader at 550nm as before. Percentage cell survival was then estimated by comparison with untreated control wells. All tests were performed in triplicate.

2.2.7 Statistical Analysis

Statistical analysis was carried out using IBM's SPSS software version 18. Data are expressed as the mean ± SD of a given number of observations. Figures show representative examples of independent repeats with error bars representing SD. Where appropriate, one-way ANOVA was used to compare multiple groups; comparisons between groups were made with Fisher's exact test or the student's T test. $P < 0.05$ was considered to be significant. Five-year survival rates were calculated according to the Kaplan–Meier method using the logrank test with the

endpoint for survival analysis being death from disease. Univariate and multivariate analysis of overall and disease-free survival was performed according to Cox proportional hazard models.

Chapter 3

Expression of αvβ6 in non-melanoma skin cancers and the role of SMA in morphoeic type basal cell carcinoma

3.1 Introduction

The αvβ6 integrin has previously been shown to be over expressed in various epithelial derived malignancies including skin SCC (Thomas *et al* 2005). As previously discussed in the introduction to this thesis, αvβ6 has been implicated in the malignant transformation of oral SCCs from leukoplakia, a premalignant oral lesion (Hamidi *et al* 2000). It is proposed therefore that αvβ6 may be expressed in the premalignant skin lesion Actinic Kerastosis (AK) and that it may play a part in the development of the most common non melanoma skin cancer, basal cell carcinoma.

Although most BCCs (80%) may be described as belonging to the nodular subset that is relatively indolent, there exists a smaller subset that are the highly aggressive morphoeic type (6%) and these are found mostly in the head and neck region (Scrivener *et al* 2002; Walling *et al* 2004). These two subsets may be differentiated histologically; morphoeic type BCCs have an infiltrative growth pattern with small islands of tumour cells in a densely fibrous stroma, whereas nodular type BCCs have pallisading cells arranged as nests within the relatively normal dermal stroma.

To further study the role of αvβ6 in BCCs, cell culture experiments will be carried out using keratinocytes transfected with the Gli-1 transcription factor as currently there are no BCC cell lines available. This model was chosen as BCCs have been shown to develop due to disruption of the sonic hedgehog signalling (Shh) pathway, leading to upregulation of the glioma-associated (Gli) family of transcription factors (Dahmane *et al* 1997). In human BCCs, disorders in the Shh pathway are usually due to mutations in the hedgehog receptor and antagonist Patched 1 (Ptch1) (Evangelista *et al* 2006). Transgenic mouse models have been developed showing the loss of Ptch1 function from the basal keratinocytes of mouse skin is sufficient to induce BCC-like tumour formation (Adolphe *et al* 2006). The importance of the Shh pathway in BCC development has further been confirmed with the development of BCC like tumours in mice which over-express constituents of the abnormal Shh pathway, including Shh, Gli-1 and Gli-2 (Oro *et al* 1997, Grachtchouk *et al* 2000, Nilsson *et al* 2000).

3.2 Aims and Objectives

The aim of this chapter is to determine whether αvβ6 could have potential for future use as a molecular target in patients with non melanoma skin cancers. The objectives of this chapter are to measure αvβ6 expression levels in tissue samples from patients with normal skin, AKs, skin SCCs and BCCs. This chapter's further objectives are to examine the role of αvβ6 in BCCs using transwell invasion assays, confocal microscopy and cell culture experiments.

3.3 Results

3.3.1 Expression of αvβ6 in non-melanoma skin cancers and actinic keratoses

Sections of NMSC, AKs and normal skin were obtained from Mt Vernon Hospital Pathology Dept, subjected to immunohistochemical staining and scored as set out in Chapter 2. For the initial analysis 8 sections of normal skin, 19 AKs, 19 BCCs and 19 SCCs were examined. Table 3.1 shows the differences in expression levels of αvβ6 between the different tissue types, examples of which are shown in Figure 3.1.

Tissue	No of Specimens	αvβ6 expression (no of samples)		
		Low or Negative	Medium	High
Normal skin	8	8	0	0
Actinic Keratosis	19	0	13	6
BCC	19	3	10	6
SCC	19	0	4	15

Table 3.1 - Tissue sections were scored using the quickscore method and the sections were then grouped according to whether the αvβ6 expression was negative/low, medium or high. Equal numbers of AK, SCC and BCC samples were scored.

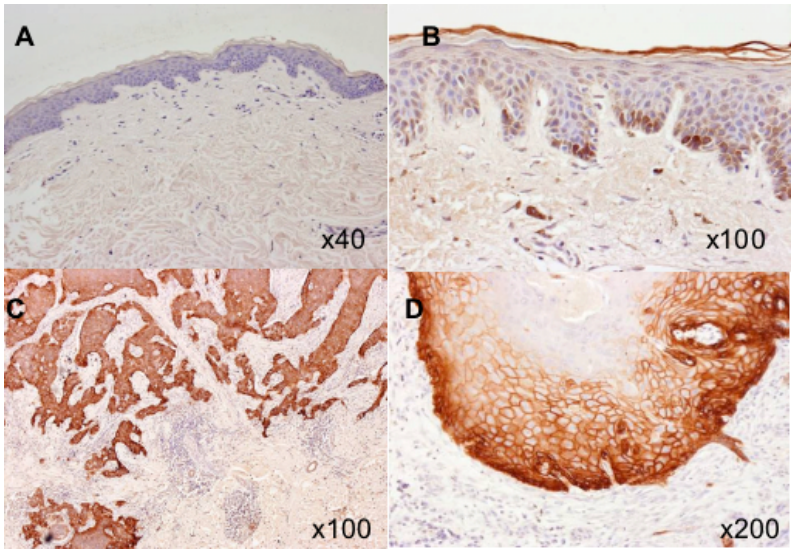

Figure 3.1 - Immunohistochemistry images showing αvβ6 staining (brown). **A** negative expression in normal skin, **B** low expression of αvβ6 in Actinic Keratosis, **C** high αvβ6 expression in SCC at x100 magnification, **D** high αvβ6 expression in SCC at higher magnification.

One of the aims of this chapter is to determine whether premalignant AKs also express αvβ6 and whether the expression level is part way between normal skin and SCC as is found in oral leukoplakia. The results here show that when comparing tumours with high levels of αvβ6 expression, 79% of skin SCCs were found to have high expression levels, compared to just 32% of AK and 0% of normal skin samples. αvβ6 was found to be expressed at high level in 32% of the BCC sections examined (Figure 3.2)

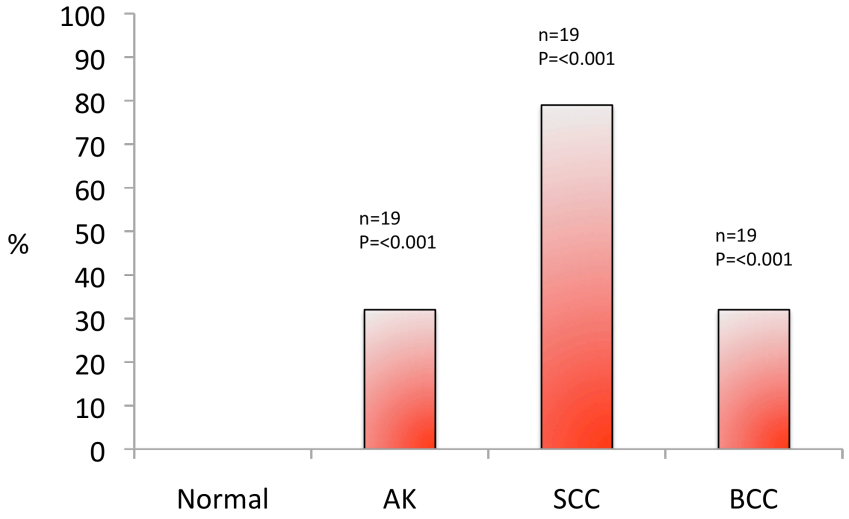

Figure 3.2 - Graph showing percentage of tissue samples with high expression levels of αvβ6.

3.3.2 αvβ6 expression in BCC

Although overall only 32% of BCC samples showed high expression levels of αvβ6 which is comparable to the expression seen in AKs, there was a striking difference in αvβ6 expression seen between morphoeic and nodular type BCC (Figure 3.3).

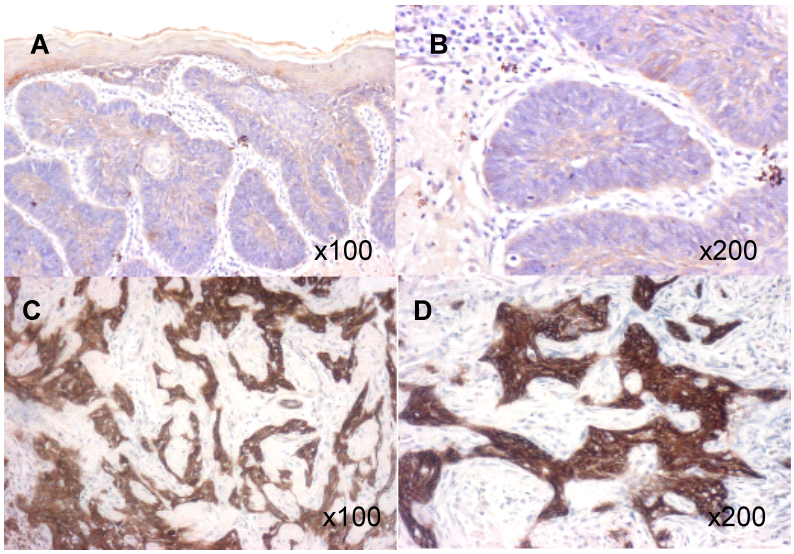

Figure 3.3 - Examples of immunohistochemical staining for αvβ6 expression (brown colour) at x100 and x200 magnification. **A,B:** Nodular type BCCs showing typical pallasading cells and islands of tumour with low levels of αvβ6 expression. This is contrasted to morphoeic type BCC (**C,D**) with fibrotic stroma pattern and high levels of expression of αvβ6.

Of the 19 BCCs initially examined, 16 were of the nodular type and 3 morphoeic. To investigate the differing αvβ6 expression levels seen between nodular and morphoeic BCCs, a further 9 morphoeic BCC specimens were examined giving a total of 12 morphoeic and 16 nodular. In the 16 nodular type, high expression of αvβ6 was present in only 13% of tumours. In contrast, expression of αvβ6 in morphoeic BCC was significantly higher ($p = < 0.001$) with 9 of 12 tumours (75%) expressing the integrin strongly (Figure 3.4).

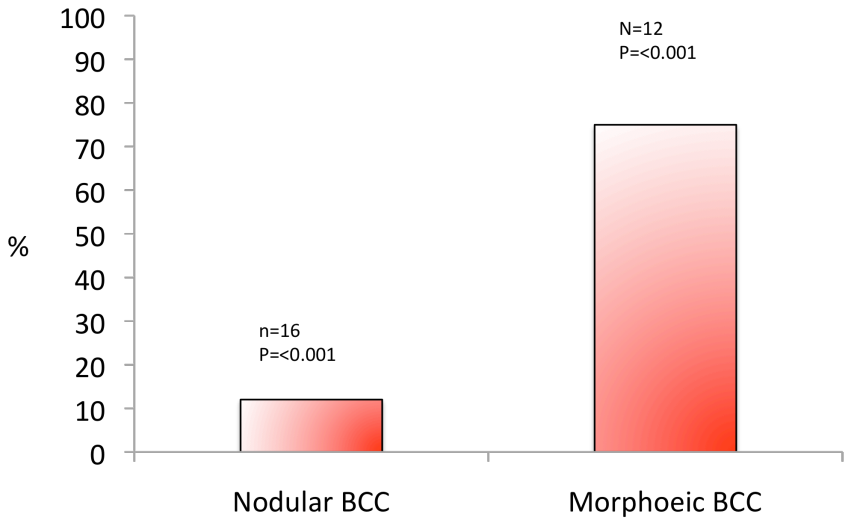

Figure 3.4 - Percentage of BCCs expressing high levels of αvβ6

3.3.3 Generation of the BCC model – NTGli1

The marked differences in αvβ6 expression between nodular and morphoeic BCC variants raises the possibility that the αvβ6 integrin plays a role in generation of the more aggressive tumour phenotype. To further investigate the role of αvβ6 in BCC a BCC model was generated using retrovirally transfected keratinocytes. Abnormal activation of the Shh signaling pathway has been shown to be a major contributing factor in the development of BCCs (Dahmane *et al* 1997). cDNA encoding the Shh transcription factor Gli1 (DN-GLI1b) was retrovirally transduced into NTert-1 skin keratinocytes (Dickson *et al* 2000) to produce the cell line NTGli. Expression of the proteins was confirmed using Western blotting (Figure 3.5).

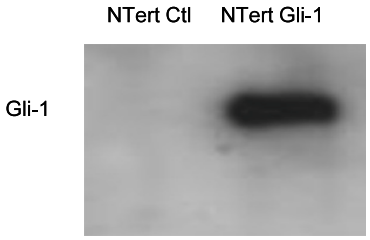

Figure 3.5 - Western blot showing expression of Gli-1 transcription factor in NTert keratinocytes transfected with Gli-1 transcription factors compared to non transfected NTert controls

Flow cytometry and confocal microscopy confirmed that NTGli1 cells expressed αvβ6 (Figure 3.6,3.7).

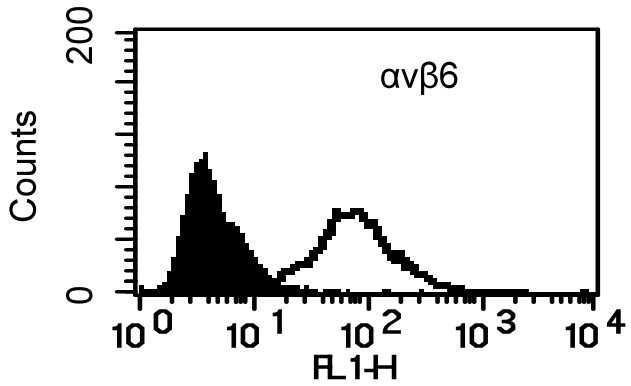

Figure 3.6 - Flow cytometry showing αvβ6 expression on NTGli1 keratinocytes.

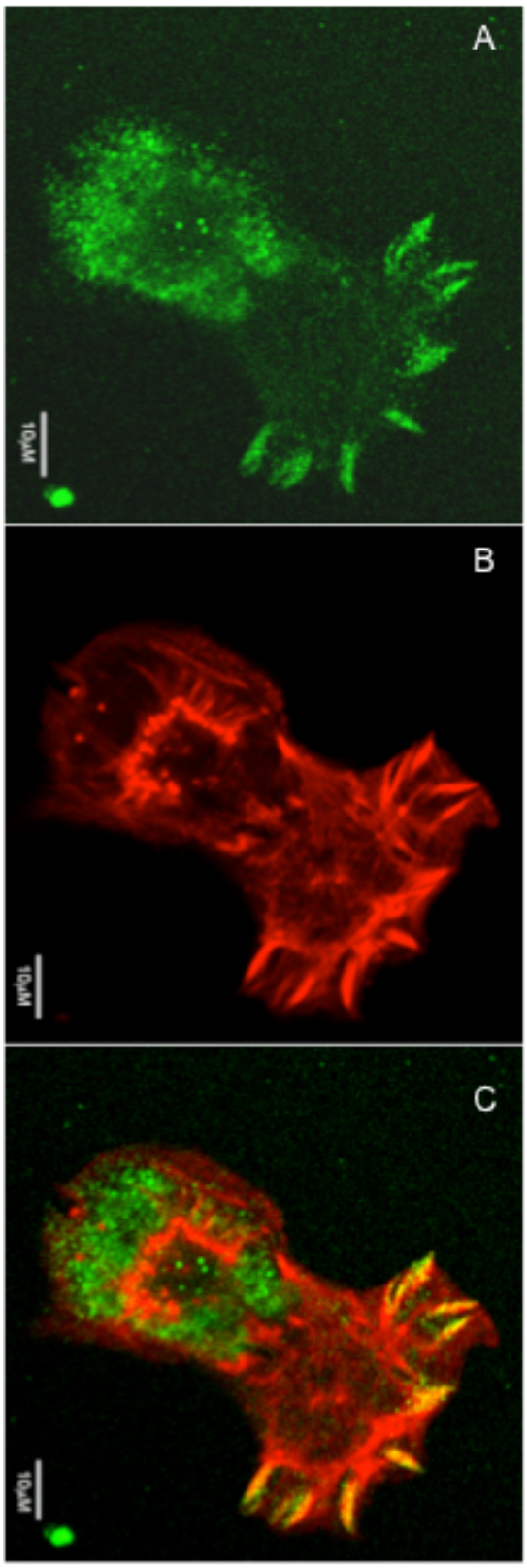

Figure 3.7 - Confocal microscopy of NTGli1 cells showing **A** expression of αvβ6 (green), **B** actin (red) and **C** merged image

3.3.4 Role of αvβ6 in invasion of NTGli1 in Transwell assays

To investigate whether αvβ6 directly promoted invasion of NTGli1 and NTGli1 cells, Transwell assays were run comparing invasion of cells alone with αvβ6 blocking antibodies (Figure 3.8).

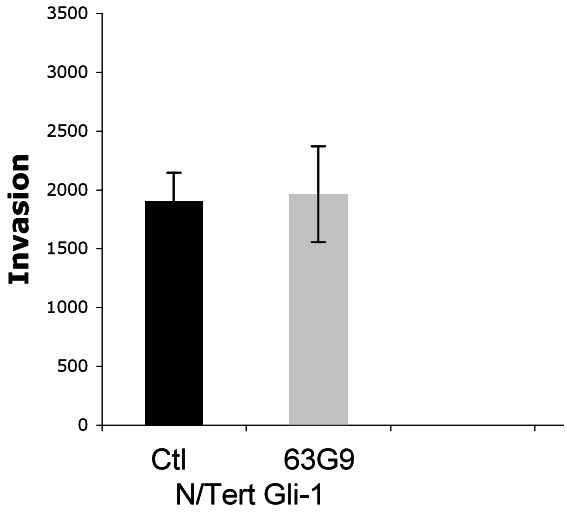

Figure 3.8 - Transwell assays showing inhibition of αvβ6 by the antibody 6.3G9 did not have any effect on invasion of Gli-1 transfected N/tert keratinocytes.

Further Transwell assays comparing antibody 6.3G9 inhibition of αvβ6 with β6 RNAi did not demonstrate suppression of invasion of NTGli1 cells (*p=0.834, p=0.718* respectively; Figure 3.9). In contrast, as has been shown previously, αvβ6 inhibition of carcinoma cells from the head and neck (VB6), breast (BT20) and lung (H441) significantly reduced invasion (*p= 0.0035, p=0.005; p=0.002* respectively). Since it has also been suggested that αvβ6 may promote invasion directly through modulating TGF-β1-dependent EMT, assays were repeated, either adding TGF-β1 or inhibiting TGF-β1 signalling using recombinant soluble TGF-β receptor II (TGF-βrii). Neither treatment had an effect on NTGli1 invasion (Figure 3.9; *p=0.52, p=0.47* respectively).

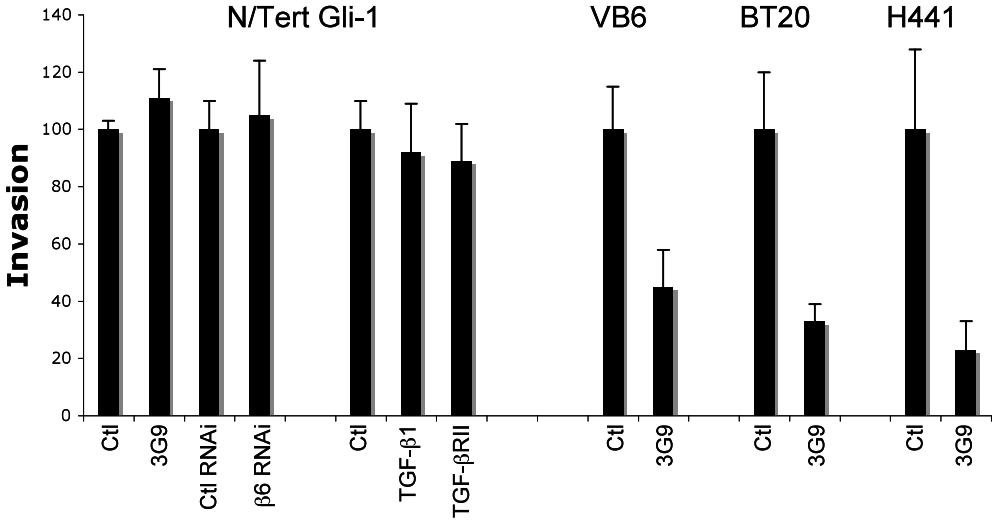

Figure 3.9 - Relative invasion of NTGli1 and comparable SCC cell lines VB6 (head and neck), BT20 (breast), H441 (lung) in Transwell assays alone (ctl) variously following incubation with αvβ6 blocking antibody 3G9, β6 RNA inhibition, TGFβ 1 and recombinant soluble TGF-β receptor II (TGF-βrii). Transwell invasion of NTGli1 cells was not inhibited by blockade of αvβ6 integrin (6.6.3G9) or by transient transfection of cells with β6 RNAi. Treatment of NTGli1 cells with TGF-β1 or inhibition of TGF-β1 using recombinant soluble TGF-β receptor type II (TGF-βRII) did not affect invasion.

3.3.5 αvβ6 mediated TGF-β1 activation in NTGli1 cells

αvβ6 has been shown to modulate several other cell functions, including activation of TGF-β1 (Munger *et al* 1999). To investigate whether αvβ6 activated TGF-β in NTGli1 cells, a TGF-β bioassay was carried out as previously described (Abe *et al* 1994). Inhibition of αvβ6 using antibodies (10D5) or β6 RNAi significantly reduced TGF-β1 activation (by 59% and 37% respectively; *p=<0.0001, p=0.0006*; Figure 3.10). NTGli2 cells activated TGF-β1 similarly (Figure 3.11).

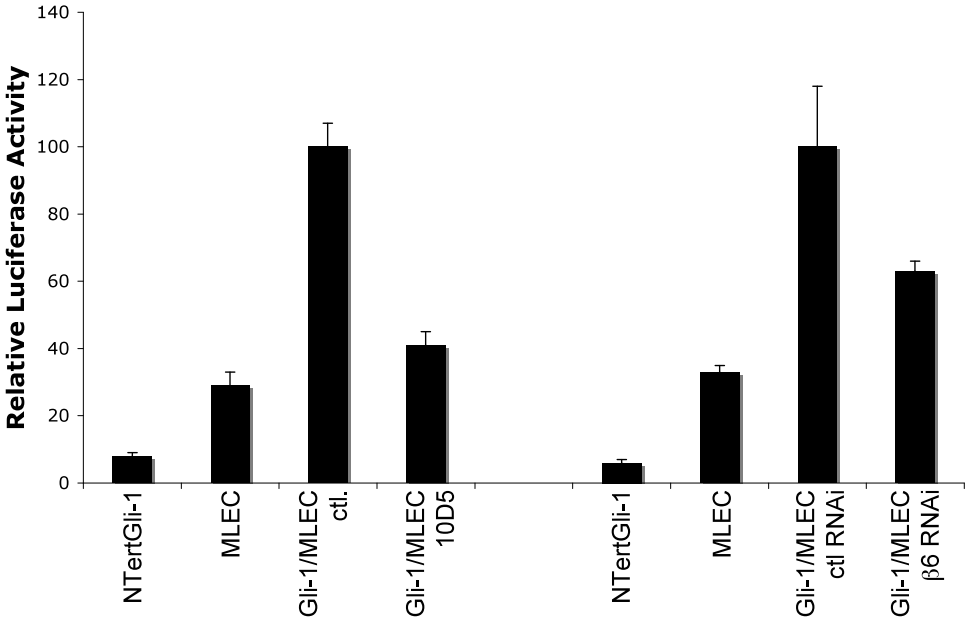

Figure 3.10 - TGF-β activation co-culture assay. Co-culture of NTGli1 with MLEC promoted TGF-β activation, which was suppressed by antibody blockade of αvβ6 integrin (10D5) or by transient transfection of cells with β6 RNAi. Control antibody was anti-β4 integrin, 7.2

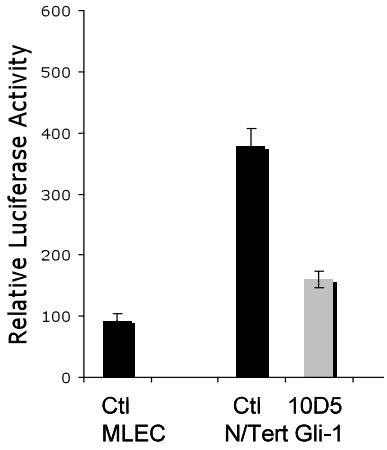

Figure 3.11 - TGF-β activation co-culture assay of NTGli1 with MLEC promoted TGF-β activation, which was suppressed the anti αvβ6 antibody 10D5.

A common finding in many types of carcinoma is that stromal fibroblasts become 'activated' myofibroblasts and express a number of contractile proteins, particularly α-smooth muscle actin (SMA) (Tlsty and Hein 2001). TGF-β1 is considered to have a central role in inducing the myofibroblastic phenotype (Tuxhorn *et al* 2001). To determine whether NTGli1 cells could induce myofibroblast differentiation, co-culture experiments were carried out with HFF2 fibroblasts. Co-culture of HFF2 with NTGli1 cells induced myofibroblast transdifferentiation, producing a significant increase in SMA expression (Figure 3.12, 3.13). SMA was associated with cytoplasmic stress fibres (Figure 3.13). To demonstrate myofibroblast generation was αvβ6-dependent, co-culture assays were repeated in the presence of either 10D5, a αvβ6 inhibitory antibody or a non αvβ6 binding antibody, 7.2 (Figure 3.13). When the anti αvβ6 antibody was included, SMA expression was inhibited significantly. This was confirmed by Western blotting (Figure 3.14; *p= 0.006*). These experiments suggest αvβ6 is important in driving the phenotypic conversion of fibroblasts to myofibroblasts.

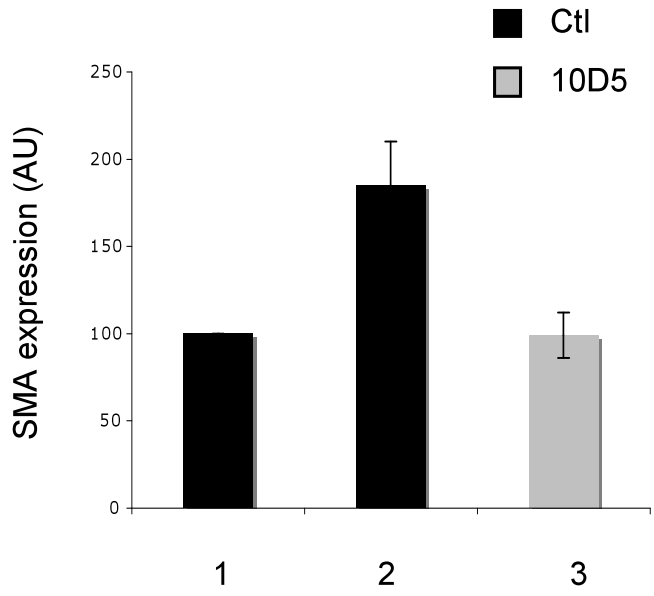

Figure 3.12 - Histogram showing Western blot densitometric expression of SMA in NTGli1 cells alone (1), co-cultures of HFF and NTGli1 cells (2) and after incubation with 10D5 αvβ6 blocking antibody (3)

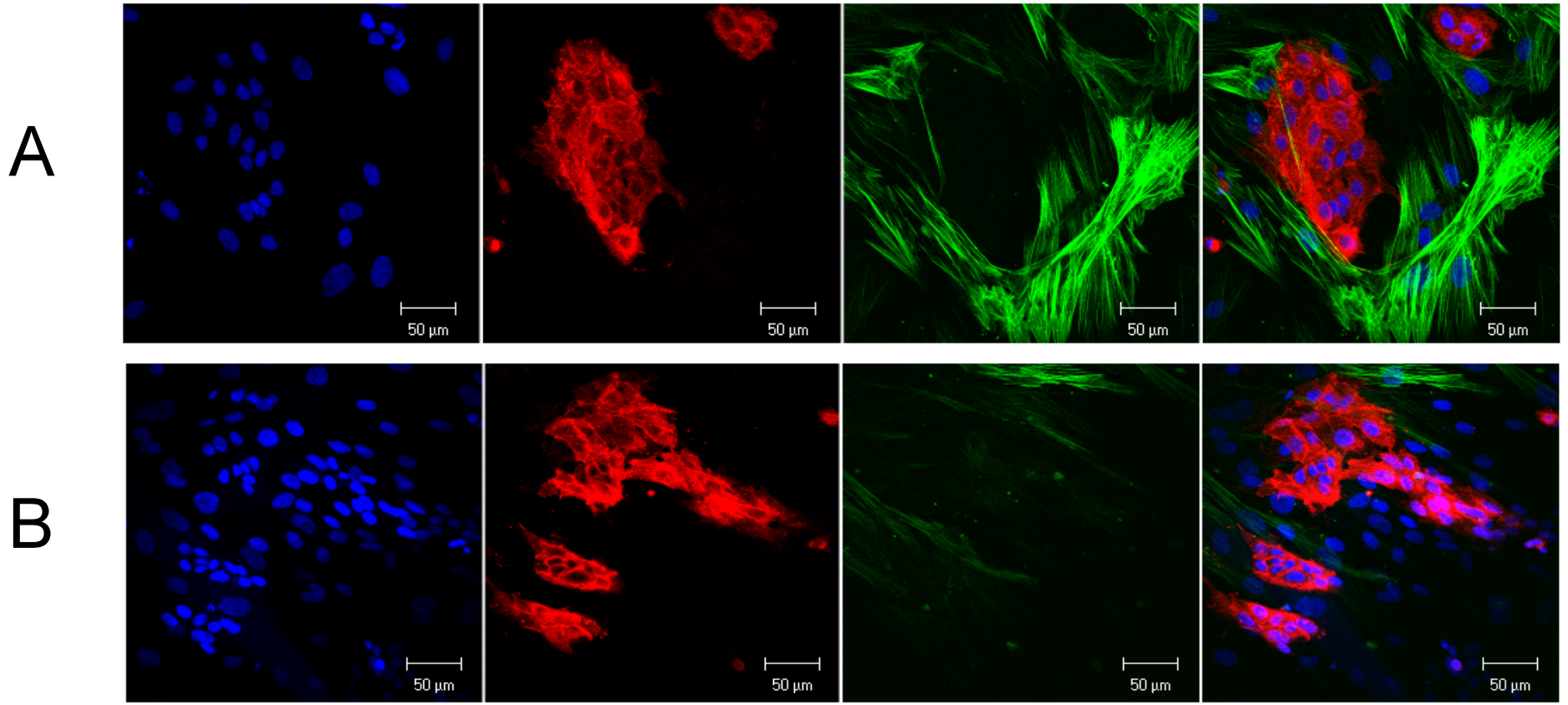

Figure 3.13 - Confocal microscopy of αvβ6-positive NTGli1 cells (red) co-cultured on glass cover slips with HFF2 fibroblasts (blue), showing production of SMA (green). Panal A shows cells cultured in presence of 7.2 (a non αvβ6 binding control antibody). Addition of 10D5 αvβ6 blocking antibody reduces SMA production (panel B), suggesting αvβ6 promotes fibroblast to myofibroblast transition.

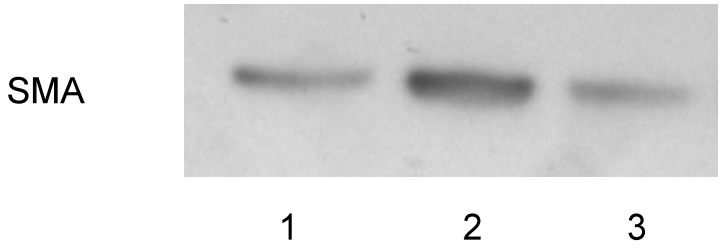

Figure 3.14 - Western blot showing SMA expression in HFF2 fibroblasts alone (1), co-cultures of HFF and NTGli1 cells (2) and suppression of SMA in co-cultures after incubation with 10D5 αvβ6 blocking antibody

3.3.6 Myofibroblast content within the stroma of morphoeic BCC

Morphoeic BCCs are characterised by an infiltrative growth pattern and a densely fibrous stroma. To determine whether this stroma contained myofibroblasts, samples of nodular and morphoeic BCCs were stained and scored for the myofibroblast marker SMA expression using immunohistochemistry (Figure 3.15).

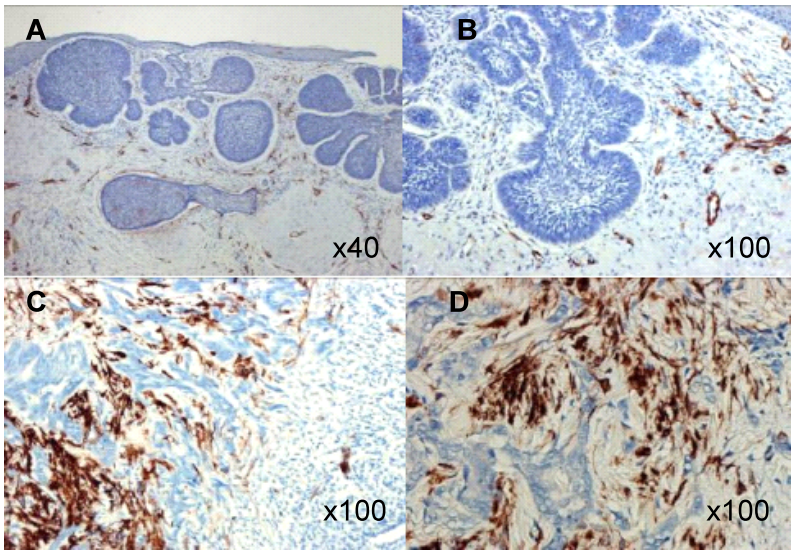

Figure 3.15 - **A, B** Nodular BCC showing tumour islands and low levels of SMA expression (brown staining) **C, D** Morphoeic BCC with fibrotic stroma and high SMA expression.

Similar to αvβ6 expression, expression of SMA was significantly higher in morphoeic BCCs (*p=0.0041*) with 10 of 12 tumours (83%) having stroma with strong SMA expression, indicating myofibroblastic differentiation. In contrast, only 6 of 16

nodular BCC (37.5%) showed strong expression (Table 3.2). No SMA staining was observed in the dermis of normal skin.

		αvβ6 and SMA expression									
		Negative		Low		Medium		High		%High	
	Cases	αvβ6	SMA	αvβ6	SMA	αvβ6	SMA	αvβ6	SMA	αvβ6	SMA
Nodular BCC	16	1	2	5	1	8	7	2	6	13	37.5
Morphoeic BCC	12	0	0	1	0	2	2	9	10	75	83

Table 3.2 - Expression of SMA and αvβ6 in nodular and morphoeic BCC

3.3.7 Effect of myofibroblasts on NTGli1 invasion

Previously it has been shown that myofibroblasts promote invasion of SCC cells through the paracrine secretion of growth factors (Lewis *et al* 2004). Although expression of αvβ6 did not directly modulate Transwell invasion of NTGli1 cells, it can be postulated that generation of a stromal myofibroblastic phenotype would have an invasion-promoting effect. To determine the effect of myofibroblasts on NTGli1 cell invasion, Transwell – Matrigel assays were set up. Myofibroblasts were generated by treating HFF2 fibroblasts with TGF-β1 and cultured for 72 hours in α-MEM. The myofibroblast-conditioned media (MCM) was used as a chemoattractant in the lower chamber of the Transwell, and NTGli1 cells were allowed to invade towards this stimulus for 72 hours before being counted. Untreated fibroblast conditioned medium (FCM) was used for comparison. MCM was found to significantly promote invasion of NTGli1 cells compared with FCM ($p=<00001$; Figure 3.16). Addition of αvβ6 inhibitory antibody (6.3G9) into the assay still did not inhibit invasion.

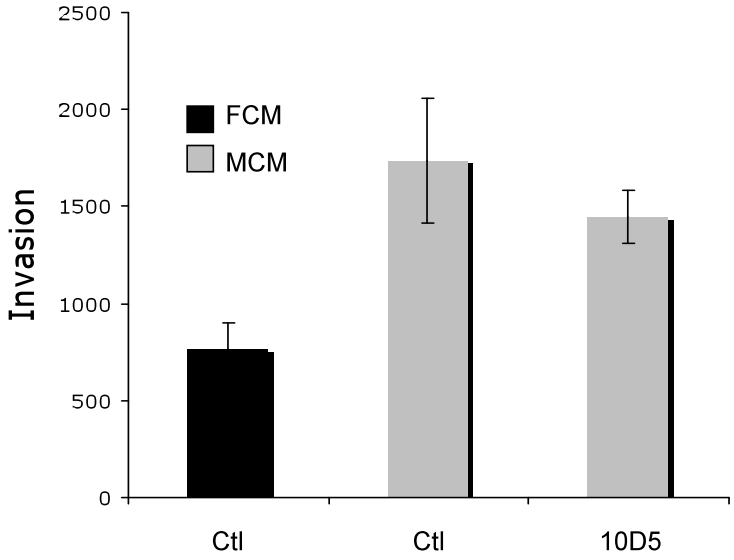

Figure 3.16 - Transwell – Matrigel migration assay comparing migration of NTGli1 cells through Matrigel towards either fibroblast conditioned medium (FCM) or myofibroblast conditioned medium (MCM) with addition of 10D5 αvβ6 blocking antibody. Blockade of αvβ6 (6.6.3G9) did not inhibit invasion MCM-induced invasion. Results are expressed relative to VB6 invasion using SCCM-generated myofibroblast conditioned medium.

To further investigate the interaction between NTGli1 and HFF2 cells in the invasive process, organotypic experiments were set up. In contrast to Transwell invasion, transient transfection of NTGli1 cells with β6 RNAi markedly suppressed invasion (Figure 3.17).

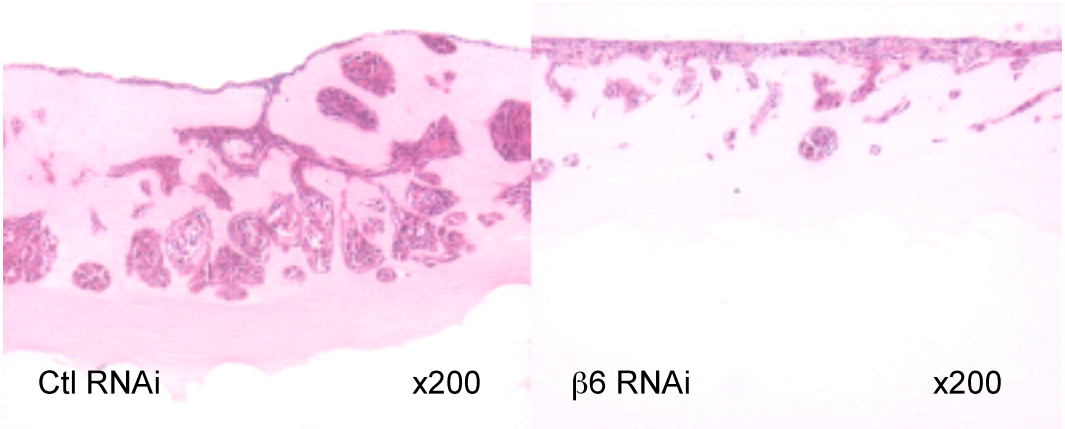

Figure 3.17 - NTGli1 cells were transiently transfected with random or β6 RNAi and then grown in organotypic culture with HFF2 fibroblasts for 6 days. In contrast to Transwell invasion, inhibition of αvβ6 suppressed invasion of NTGli1 cells

3.3.8 Role of myofibroblast secreted HGF/SF in NTGli invasion

Previously, studies have demonstrated that myofibroblasts secrete HGF/SF (Goke *et al* 1998). This cytokine promotes epithelial cell growth and migration and has been shown to stimulate invasion in squamous carcinoma cells (Lewis *et al* 2004). To determine whether induction of a myofibroblastic phenotype was associated with increased production of HGF/SF, medium from co-cultures of NTGli1 and HFF2 cells treated with control or anti- αvβ6 inhibitory antibodies was examined. Figure 3.18 shows that co-culture of NTGli1 and HFF2 induces HGF/SF production which is suppressed when αvβ6 is inhibited.

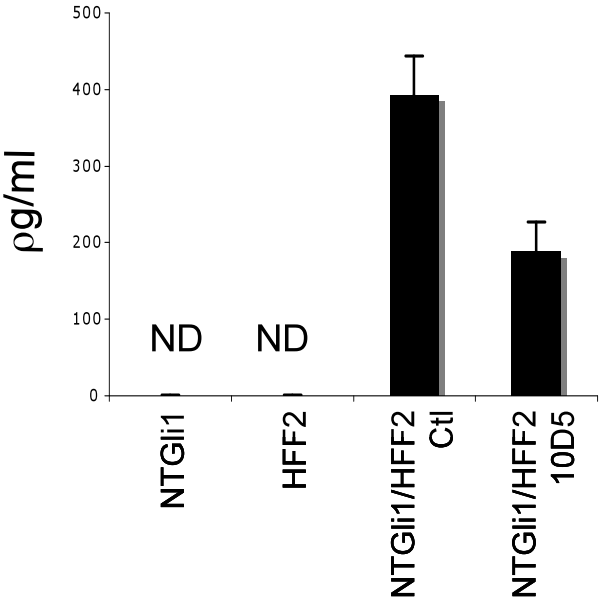

Figure 3.18 - ELISA showing production of HGF when NTGli1 cells are co-cultured with HFF2 cells and the reduction in HGF levels when αvβ6 blocking antibody is added.

To determine whether the invasion-promoting effect of MCM was modulated through HGF/SF, HGF/SF signalling pathway in NTGli1 cells was inhibited using the Met kinase inhibitor, SU11274 (5μg/ml). Flow cytometry confirmed that NTGli1 cells expressed the HGF/SF receptor, c-Met (Figure 3.19).

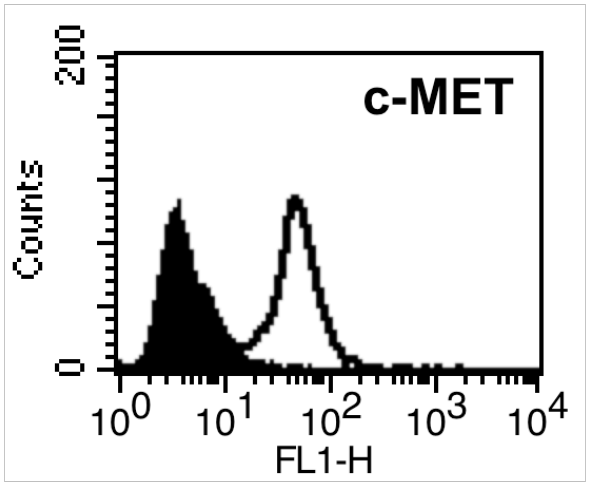

Figure 3.19 - Flow cytometry demonstrating c-Met expression by NTGli1 cells

Inactivation of c-Met significantly reduced invasion of NTGli1 cells towards MCM (*p=0.00002*). Following c-Met inhibition, the level of invasion was similar to that produced by FCM suggesting that the invasion-promoting effect of MCM was mediated by HGF/SF (Figure 3.20).

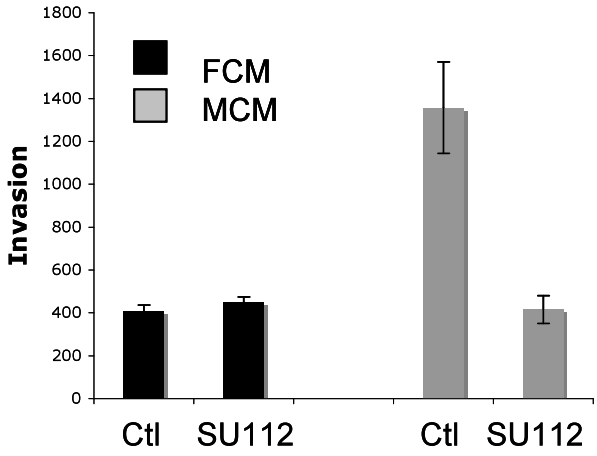

Figure 3.20 - Transwell invasion assay following treatment of NTGli1 cells with Met kinase inhibitor (SU11274) and using conditioned medium from fibroblasts (FCM) or myofibroblasts (MCM).

3.3.9 Expression of c-Met and HGF/SF in morphoeic BCCs

Immunochemistry confirmed that c-Met was expressed strongly (+++) or moderately (++) expressed by all morphoeic BCCs and that HGF/SF was commonly detected in myofibroblasts in the desmoplastic stroma (Figure 3.21). Interestingly, all the nodular BCC also expressed c-Met strongly and expression did not differ significantly from the morphoiec variants (*p=0.69*; Figure 3.22). Normal epidermis was negative for E-Cadherin or showed weak expression in basal keratinocyes only (Figure 3.22).

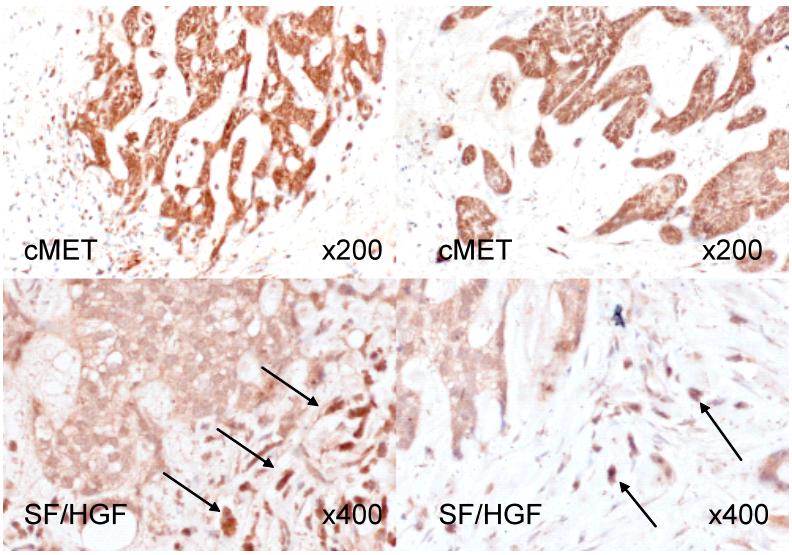

Figure 3.21 - Immunohistochemistry showing representative c-Met (upper panel) and HGF/SF (lower panel) expression in morphoeic BCC. Strong c-Met expression was observed in most tumours. HGF/SF expression was present in stromal cells

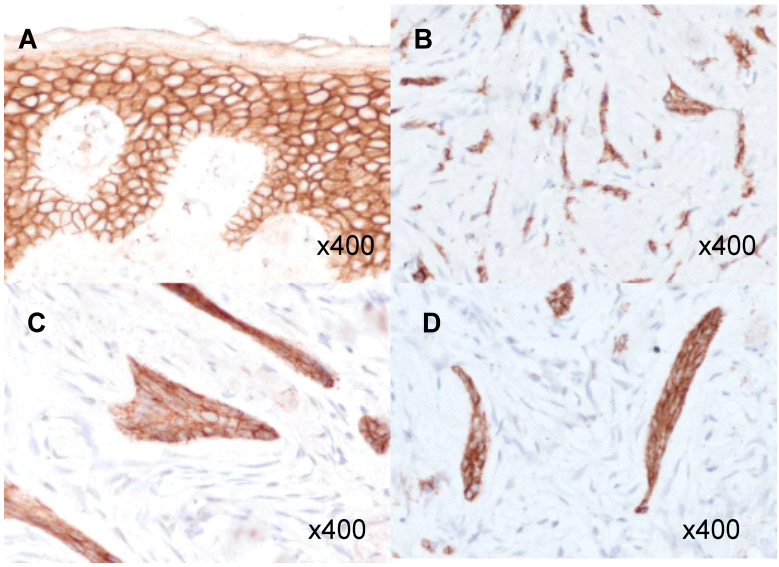

Figure 3.22 - Immunohistochemical staining for E-Cadherin in normal epidermis (**A**), morphoeic (**B,C**) and nodular BCCs (**D**)

3.4 Discussion

The results presented in this chapter show that the integrin αvβ6 is expressed at significantly higher levels in aggressive, infiltrative morphoeic BCC compared with more common nodular BCC. Using Gli-transfected, NTert human skin keratinocytes as a BCC model, the effects of αvβ6 expression in these cells were examined. Antibody inhibition of αvβ6 had no direct effect on cell invasion. However, on co-culture assays, NTGli1 cells seemingly modulate human myofibroblast transdifferentiation through αvβ6-dependent activation of TGF-β1. Data presented here shows that the fibrotic stroma of morphoeic BCC is myofibroblast-rich compared with nodular BCC, and that myofibroblasts promote BCC invasion through secretion of HGF/SF.

Morphoeic BCC account for around 6% of BCCs, and are so-called because of their fibrotic (desmoplastic) stroma. Unlike the more common nodular BCC variant, morphoeic BCCs are aggressively infiltrative, resulting in greater depth of invasion, tissue destruction and recurrence (Walling *et al* 2004). Since 95% of these tumours are located on the face or head this causes significant morbidity (Scrivener *et al* 2002). Immunohistochemical staining of BCC samples showed that 77% of

morphoeic BCC strongly expressed αvβ6. This was similar to expression levels in cutaneous SCC (79% high expression; 15/19 tumours), but was significantly higher than nodular BCC (7%, 2/16 tumours). Interestingly the histological growth pattern of morphoeic BCC more closely resembles SCC than nodular BCC.

Expression of αvβ6 is increasingly described in numerous carcinoma types, often correlating with poor prognosis (Bates *et al* 2005, Elayadi *et al* 2007, Hazelbag *et al* 2007). Workers have shown previously that αvβ6 promotes invasion of head and neck SCC *in vitro* and *in vivo* (Thomas *et al* 2001, Nystrom *et al* 2006). These data suggest that αvβ6 is an attractive tumour target, and several studies have now successfully inhibited tumour growth *in vivo* using treatments directed against the integrin (Zhou *et al* 2004, Koopman *et al* 2007). Surprisingly, inhibition of αvβ6 had no effect on NTGli1 cell Transwell invasion (Figure 4.8). However, αvβ6 modulates several other cell functions including activation of TGF-β1 (Munger *et al* 1999), and these data show that activation of TGF-β1 in NTGli1 cells was αvβ6-dependent (Figure 3.11). The role of TGF-β1 in tumour biology is complex, having both suppressive and promoting effects (Elliot and Blobe 2005). This is explained in part, by observations that most carcinomas become refractory to the anti-proliferative effect of TGF-β1 (Elliot and Blobe 2005). TGF-β1 also has direct pro-oncogenic effects on tumour cells, including promotion of motility through modulating epithelial-to-mesenchymal transition (EMT). However, treatment of NTGli1 cells with recombinant TGF-β1 or inhibition of TGF-β1 signalling using recombinant soluble TGF-βRII receptor had no effect on invasion. These data suggest that activation of TGF-β1 did not promote NTGli1 cell invasion directly.

Another mechanism by which αvβ6-dependent activation of TGF-β1 could promote tumour progression is by modulating the tumour stroma. TGF-β1 is considered to have a central role in inducing the myofibroblastic phenotype, and αvβ6-dependent activation of TGF-β1 results in the pathological fibrosis of several epithelial organs (Munger *et al* 1999, Hahm *et al* 2007). There is now abundant evidence that tumour stroma promotes tumour progression (Liotta and Kohn 2001, Pupa *et al* 2002, De Wever and Mareel 2003), and workers have previously shown a pro-invasive, paracrine interaction between myofibroblasts and head and neck SCC cells (Lewis *et*

al 2004). Transdifferentiation of myofibroblasts is frequently observed associated with the edge of an actively expanding tumour mass, and it is common to find αvβ6 expressed most strongly at this invasive margin (Lewis *et al* 2004, Nystrom *et al* 2006, Koopman *et al* 2007). Co-culture assays suggested that NTGli1 cells modulated myofibroblast transdifferentiation through the αvβ6-dependent activation of TGF-β1, and that conditioned medium from myofibroblasts promoted NTGli1 Transwell invasion. Immunochemistry confirmed that the stroma of morphoeic BCCs is myofibroblastic-rich compared with nodular BCCs. Additionally, although inhibition of αvβ6 had no anti-invasive effect in Transwell assays, when NTGli1 cells were admixed with fibroblasts in organotypic culture, β6 RNAi knockdown markedly reduced invasion. It may be postulated that this effect is modulated through suppression of myofibroblast transdifferentiation.

Myofibroblasts may promote tumour progression in a number of different ways including secretion of proteases, matrix proteins and cytokines (De Wever and Mareel 2003). Co-culture of NTGli1 and HHF2 cells resulted in upregulated secretion of HGF/SF which was suppressed when αvβ6 was inhibited (Fig 3.18). HGF/SF acts through the c-Met tyrosine kinase receptor, and misregulated expression of both cytokine and receptor is a common finding in many tumour types (Peruzzi and Bottaro 2006), although expression has not been described in BCC previously. These data show that inhibition of HGF/SF signaling suppressed the invasion-promoting effect of myofibroblast-conditioned medium in Transwell assays (Figure 3.20). De Wever and colleagues (2004) found that myofibroblasts stimulated invasion of colon carcinoma cells through secretion of a combination of HGF/SF and Tenascin C, and it is possible that a similar mechanism promotes invasion of NTGli1 cells. Immunochemistry showed that morphoeic BCC express both c-Met receptor and stromal HGF/SF (Figure 3.21). Interestingly, c-Met expression was also present in nodular BCC at similar levels, although expression in normal epidermis was negative or weakly basal (Fig 3.21 upper panels).

HGF/SF may induce invasive growth through several mechanisms, including regulation of the expression and function of cadherins, integrins and matrix metalloproteinases (Birchmeier *et al* 2003). It has previously been shown that

HGF/SF promotes invasion of head and neck SCC cells and induces expression of the type IV collagenases MMP-2 and –9 (Lewis *et al* 2004, Bennett *et al* 2000). This latter observation suggesting a possible mechanism for the HGF/SF-dependent invasion through Matrigel (which is composed of predominantly type IV collagen) described in this study. HGF/SF stimulation also promotes tyrosine phosphorylation of b-catenin, resulting loss of E-cadherin binding and nuclear translocation of b-catenin (Monga *et al* 2002). Nuclear localization of b-catenin has been reported to be significantly higher in morphoeic BCC compared with nodular BCC (El-Bahrawy *et al* 2003). Although Gli-1 has been reported to downregulate E-cadherin expression in BCC through induction of the E-cadherin repressor, Snail (Li *et al* 2006), immunochemistry showed that E-cadherin expression was maintained in morphoeic BCC (Figure 3.22). However, there was less membranous and more cytoplasmic staining compared with normal epidermis. These data raise the possibility that altered E-cadherin function may play a role in the morphogenesis of morphoeic BCC, and that this may be modulated through stromal-derived HGF/SF.

3.5 Summary

The aim of this chapter was to examine the expression of αvβ6 in non melanoma skin cancers and in premalignant skin lesions in comparison to normal skin. These results show the novel finding that premalignant AKs express higher levels of αvβ6 than normal skin and lower levels than are seen in skin SCC. These findings can be compared to the expression of αvβ6 seen in leukoplakia, a premalignant oral lesion which can progress on the SCC (Westernoff *et al* 2005) suggesting αvβ6 may be important for the progression of premalignant disease.

The immunohistochemistry revealed that αvβ6 is expressed at significantly higher levels in aggressive morphoeic BCC compared with nodular BCC. Further cell modelling then demonstrated an indirect invasion-promoting effect modulated through stromal cells; αvβ6-dependent TGF-β1 activation induces a myofibroblastic phenotype resulting upregulated HGF/SF secretion which promotes tumour cell invasion. Data here shown also confirms that morphoeic BCC are myofibroblastic-

rich and express HGF/SF and c-Met. These clinical observations support the suggestion that the paracrine interactions observed *in vitro* between BCC cells and fibroblasts may also occur in *vivo*, and may explain the morphological appearance of morphoeic BCCs. As well as emphasizing the importance of the stromal contribution to tumour development, the data show that that αvβ6 may promote tumour invasion through both direct and indirect mechanisms.

Chapter 4

αvβ6 as a prognostic indicator in oral squamous cell carcinoma

4.1 Introduction

Amongst the commonest major cancers, oral SCC has one of the lowest overall 5-year survival rates and there has been no improvement in this over the past two decades (Stewart and Kleihues 2003, Parker *et al* 1996). The standard treatment for patients with this cancer is surgery, radiotherapy, or multiple modalities for high risk patients. For patients with early (stage I or II) disease, these treatments are often successful however 20-30% of these patients will go on to suffer either local tumour or lymph node recurrence (Vikram 1994; Clayman *et al* 1996). For patients with advanced oral carcinoma (stage III or IV), the recurrent rate is approximately 50–60% and 20–35% of these patients will have metastatic disease at first presentation (Clayman *et al* 1996). Furthermore, patients with advanced disease often suffer substantial functional and cosmetic morbidity, which decreases the quality of life. The identification of prognostic factors that may affect disease outcome may lead to improvements in adjuvant systemic therapy and a reduction in the morbidity associated with the disease.

OSCC is usually histological classified as well, moderately or poorly differentiated and this tumour grade is based on degree of squamous differentiation (keratinisation, pearl formation and intercellular bridges), degree of cellular pleomorphism and mitotic index (number of visible mitotic figures). Other histopathologic features have been shown to provide statistically significant prognostic information include the pattern of tumour invasion within the stroma (cohesive or non-cohesive), the maximum depth of tumour invasion and the presence of nodal extracapsular spread (Thomas *et al* 2006).

At present the outcome in patients with OSCC is directly related to the stage at diagnosis and this in turn is related to how early the disease is detected. It is also important to predict which patients are at significantly higher risk of disease recurrence after the primary treatment and the present gold standard for this is clinical stage following the initial endoscopy. Currently, the most significant prognostic indicator of survival in patients with OSCC is the presence of extracapsular spread in cervical lymph node metastasis (Greenberg *et al* 2003, Puri *et al* 2003). Other important factors include tumour size (Tytor and Olofsson 1992), positive margins

after surgical excision (Sutton *et al*. 2003) and the presence of perineural and perivascular invasion (Rahima *et al*. 2004). However, there is no clear consensus however regarding the relative importance of these features and, although attempts have been made to combine various parameters into defined scoring systems, their use has produced unsatisfactory inter-observer agreement.

Numerous molecular markers have been studied in the hope that they may be able to provide more accurate prognostic information for the staging of OSCC. A review by Thomas et al (2005) discusses the conflicting evidence that the cell cycle regulators P16, P53 and CCND1 are shown to be both prognostic and not prognostic in OSCC. Thus there is a marked need to develop new accurate diagnostic tools that can accurately identify aggressive disease, preferably at an early stage, so that patient management can be adjusted accordingly.

4.2 Hypothesis and Aims

The hypothesis proposed in this chapter is that αvβ6 is an independent prognostic marker in OSCC. This will be tested using immunohistochemical staining on tumour specimens from patients with OSCC. Building on results from the previous chapter, the myofibroblastic marker SMA will also be examined as to whether it may yield prognostic information. The aims are to compare selected molecular markers including αvβ6 and SMA with other standard histo-pathological parameters currently used to predict prognosis in OSCC.

4.3 Results

4.3.1 Patient Data

282 consecutive patients were identified from the records at 2 London hospitals (107 patients from University College Hospital (UCL)/Eastman Dental Hospital (EDH), and 175 from Barts and the London Hospital (BLT)). These patients underwent surgery between 1992 and 2005 (UCL/EDH, 1992-2004; BLT, 2000-2005). All patients were treated with surgery with or without radiotherapy and none received chemotherapy. Data were available on age, sex, tumour stage (I-IV), metastatic disease, lymph node status and presence of extracapsular spread. Data were collected also for depth of invasion (mm), tumour grade (well, moderately, poorly differentiated), pattern of invasion (cohesive or discohesive), surgical margins (positive = ≤1mm, close = >1-<5mm, clear = ≥5mm) (Woolgar 2006), inflammation (low, medium or high) and whether patients received radiotherapy. Date of death data were obtained through the Thames Cancer Registry and cases were excluded if complete survival data or pathological archival material were not available. Appropriate ethical approval was obtained (REC reference 07/Q0405/1). The median follow up was 6.4 years (25^{th}-75^{th} centile 4.4-8.2 yrs), with a total of 14,714 person-years. Of the 282 patients, 120 were known to have died from OSCC.

Patient characteristics are summarized below in Table 4.1.

Characteristic	Number of patients (%) N= 282	Number who died from OSCC N=120 (% dying from OSCC within group)
Sex		
Male	179 (63)	77 (43)
Female	103 (37)	43 (42)
Age (yrs)		
<50	49 (17)	16 (33)
50-60	75 (27)	36 (48)
61-70	78 (28)	32 (41)
>70	79 (28)	36 (46)
Disease Stage		
1	98 (35)	21 (21)
2	43 (15)	20 (47)
3	15 (5)	8 (53)
4	125 (44)	70 (56)
Radiotherapy		
Yes	117 (42)	63 (54)
No	162 (58)	56 (35)
Surgical Margins		
Clear (>5mm)	85 (30)	23 (27)
Close (1-5mm)	82 (29)	36 (44)
Involved (<1mm)	113 (40)	61 (54)
Metastasis		
Yes	92 (33)	54 (59)
No	190 (67)	66 (35)
Extracapsular spread		
Yes	40 (14)	25 (63)
No	242 (86)	94 (39)
Cancer site		
Tongue	106 (38)	44 (42)
Floor of Mouth	39 (14)	17 (44)
Buccal Mucosa	30 (11)	13 (43)
Lip	24 (9)	5 (21)
Other	83 (29)	41 (49)

Table 4.1 – Patient characteristics for entire cohort of 282 OSCC patients

4.3.2 Pathological Data

Immunohistochemistry analysis was carried out on the tumour specimens as described in Chapter 2. Tumours were classified as cohesive (Bryne patterns 1 and 2) or discohesive (Bryne patterns 3 and 4) according to their pattern of invasion (Bryne 1992). The inflammatory infiltrate was scored as diffuse (=3), patchy (=2) or weak/absent (=1). Initially, 107 cases were examined for αvβ6, SMA, EGFR and P53; the sections were scored on the basis of extent of staining within the tumor mass (<5%=1 [low], 5-50%=2 [moderate], >50%=3 [high]). To look at activation of the TGF-β pathway, sections were also stained for Smad 4 and Smad 2; these were scored using the same method however were not investigated as potential prognostic indicators. Based upon the findings from the first 107 cases, a further 111 tumour sections were stained for αvβ6 and another 175 cases for SMA, giving a total of 282 for the final analysis. To allow for accurate assessment of staining, scoring was carried out independently by 2 consultant histopathologists (Dr Kim Piper and Professor Gareth Thomas from Barts and The London NHS Trust). Concordance was >95%, the remaining cases were re-analysed and a consensus score agreed.

The table below (Table 4.2) shows the breakdown of the pathological data for the total 282 cases.

Characteristics	Number (%) N =282*	Number who died from OSCC N=120* (% dying from OSCC within group)
Grade		
Well differentiated	53 (19)	14 (26)
Moderately differentiated	169 (60)	72 (43)
Poorly Differentiated	59 (21)	34 (58)
Depth of Invasion (mm)		
<2.0	17	4 (24)
2.0-3.9	43	11 (26)
4.0-8	96	29 (30)
>8	126	76 (60)
Pattern of Invasion		
Cohesive	162 (57)	51 (31)
Discohesive	120 (43)	69 (57)
Extracapsular Spread		
Yes	40 (14)	25 (63)
No	242 (86)	94 (39)
Inflammation		
Low	138 (49)	74 (54)
Moderate	85 (30)	32 (38)
High	59 (21)	14 (24)
αvβ6		
Low	56 (26)	24 (43)
Medium	48 (22)	15 (31)
High	114 (52)	60 (53)
SMA		
Low	130 (46)	33 (25)
Medium	74 (26)	34 (46)
High	78 (24)	53 (68)
EGFR		
Low	49 (46)	18 (37)
Medium	26 (25)	14 (54)
High	31 (29)	17 (55)
P53		
Low	67 (63)	27 (40)
Medium	25 (23)	15 (60)
High	15 (14)	7 (47)

*except for αvβ6 (218 pts, 99 deaths);EGFR and p53 (107 pts, 49 deaths)

Table 4.2 - Pathological characteristics for patient cohort

4.3.3 Statistical Analysis

The endpoint for survival analysis was death from OSCC. Survival time was measured from the date of diagnosis until the time of death or until the time last seen alive. Patients who died from causes other than OSCC were censored at the date of death. Survival analysis using Cox proportional hazards regression was used to examine the association between the risk of dying from OSCC and each of the factors taken independently and together. To evaluate the predictive performance of each factor (i.e. the 1- and 3-year OSCC death rates), the detection rate (DR; also known as sensitivity) and false-positive rate (FPR; also known as 1 minus specificity) was calculated. DR is the proportion of patients who have died by one year with test positive results; FPR is the proportion of patients alive at one year with test-positive results. Likelihood ratios (DR/FPR) were obtained for each marker, which quantifies among patients with a specified characteristic how many times more likely it is that patients will die from OSCC at 3 years compared to those who have not died. The minimum patient follow up was 3.67 years.

To examine the factors in combination and allow for associations between them, a prognostic model was developed using a Cox regression modelling, in which the dataset of 282 patients was divided into two groups in a 2:1 ratio (Royston 2009). Group 1 had patients diagnosed up to and including 9 October 2002, because the first two-thirds of all OSCC deaths occur in this group (these were used as the 'training' set to develop the prognostic model). Group 2 had patients diagnosed after 9 October 2002, ie the last third of OSCC deaths, and these formed the 'validation' set in which the prognostic model was tested. A Cox regression with backward selection and 5% level of statistical significance (Royston 2009) was applied to Group 1, and the parameter estimates were used as scores based on the group of factors that together had the most efficient predictive ability. These scores were then applied to patients in Group 2, in which the predictive performance of the model was evaluated by estimating DR and FPR for censored time-to-event data with 3-year mortality as the time point (Lu 2006 and Heagerty 2000). This receiver operating curve (ROC) analysis also produced an estimate of the area under the curve. Kaplan- Meier survival estimates were also used to provide survival plots. All statistical methods and results

in this chapter were reviewed Dr Alan Hackshaw, Statistician and Deputy Director UCL Cancer Trials Centre).

4.3.4 αvβ6 expression in OSCC

A total of 218 cases were examined for αvβ6 expression and of these cases, 56 (25.7%) were found to have low expression, 48 (21.9%) moderate and 114 (52%) had high expression levels. From the patients with high levels of αvβ6, 52.6% (60 patients) died from OSCC and from the group with low expression levels 42.9% (24 patients) died. The expression levels of αvβ6 was found to be similar to that reported previously in OSCC (Thomas *et al* 2001) and figure 4.1 below shows the typical appearance of sections stained for αvβ6.

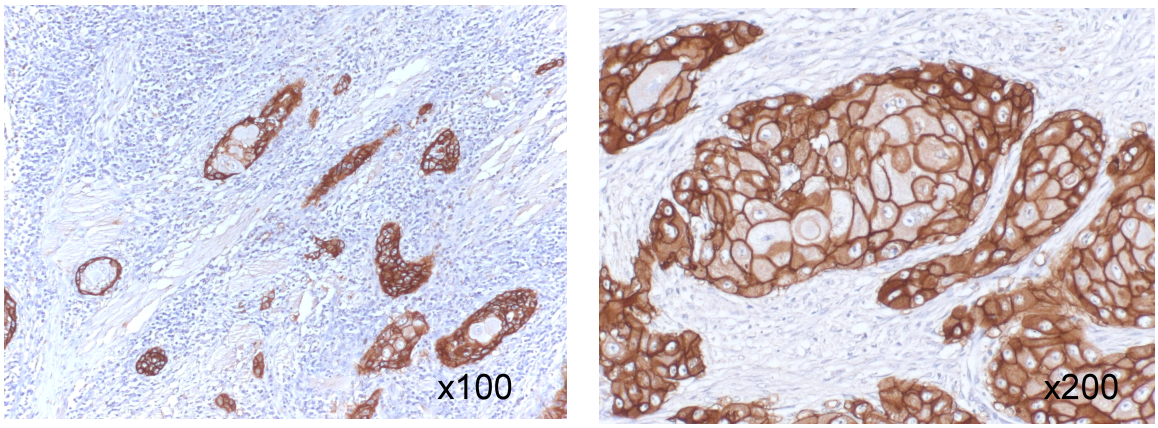

Figure 4.1 – Typical OSCC section stained for αvβ6 at x100 and x200 magnification showing strong intratumoural staining.

Kaplan-Meier plots (figure 4.2) suggested patients with high αvβ6 expression had a poorer prognosis than those with low αvβ6 expression and survival analysis for the total 218 cases showed there to be a 30% (confidence interval 0.84-2.05) increased risk of death with a high level of αvβ6 expression compared to low expression (table 4.5). However these data failed to reach significance on unadjusted or adjusted Cox regression analysis (p=0.029 and p=0.16 respectively).

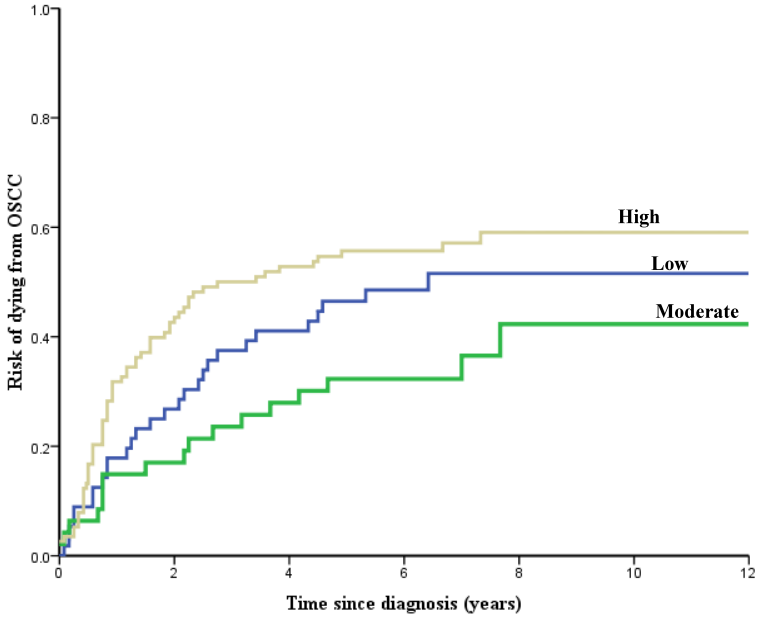

Figure 4.2 – Kaplan-Meir plot showing risk of dying from OSCC against time from diagnosis for patients with strong, moderate and low expression levels of αvβ6.

Table 4.3 below displays the correlation of αvβ6 expression with other pathological factors examined. αvβ6 was found to significantly correlate with depth of invasion (p= 0.013), presence of metastasis (p=0.048) and just failed to reach significance with the correlation with SMA expression (p=0.055). Survival analysis did not reveal any significant association between αvβ6 expression levels and death from OSCC (table 4.5)

		αvβ6			
		Low N=56	Medium N=48	High N=114	P-value for the association between the risk factor and αvB6
Age	Mean age, years	62.9	59	60.4	0.296
Depth of invasion	Mean value, mm	7.4	7.6	9.8	0.013
			Percentage*		
Sex	Male	64	69	66	0.888
	Female	36	31	34	
Disease stage	1	38	40	19	0.106
	2	13	13	19	
	3	5.4	4.2	4.4	
	4	45	43	57	
Radiotherapy	No	61	77	56	0.049
	Yes	38	23	43	
Grade	Well differentiated	27	17	15	0.120
	Moderately differentiated	45	65	65	
	Poorly differentiated	29	19	20	
Surgical margins	Clear	30	27	27	0.878
	Close	30	38	30	
	Involved	39	35	43	
Metastases	No	77	71	59	0.048
	Yes	23	29	41	
ECS	No	91	92	84	0.278
	Yes	9	8	16	
Pattern of invasion	Cohesive	63	56	49	0.244
	Discohesive	37	44	51	
Inflammation	Low	54	42	54	0.488
	Medium	29	31	31	
	High	18	27	16	
SMA	Low	52	58	40	0.055
	Medium	32	19	27	
	High	16	23	33	

*expressed as a percentage of low, medium and high αvβ6 expression respectively.

Table 4.3 – αvβ6 correlation with common pathological indices in OSCC. 218 patients included in analysis.

4.3.5 SMA expression in OSCC

SMA staining was performed on all 282 cases, the numbers staining low, moderate and high were 130 (46.1%), 74 (26.2%) and 78 (27.7%) respectively. Looking at death from OSCC, there were 33 (25.4%), 34 (45.9%), and 53 (67.9%) deaths in the Low, Moderate and High SMA groups respectively. Figure 4.3 shows OSCC section with strong stromal staining for SMA.

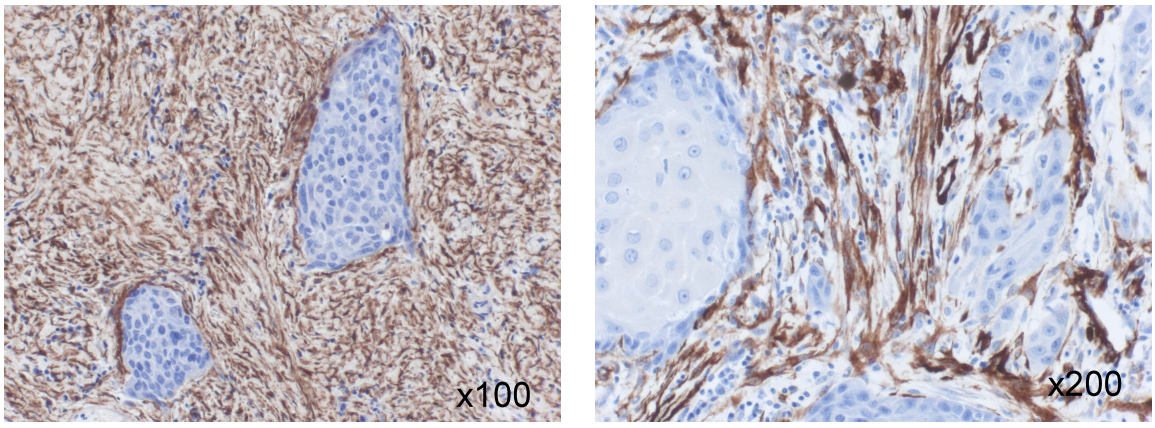

Figure 4.3 – Stromal staining for SMA at x100 and x200 magnification

Ten lymph node metastases were also examined for SMA expression using immunohistochemistry and all were all found to be strongly positive for SMA (figure 4.4).

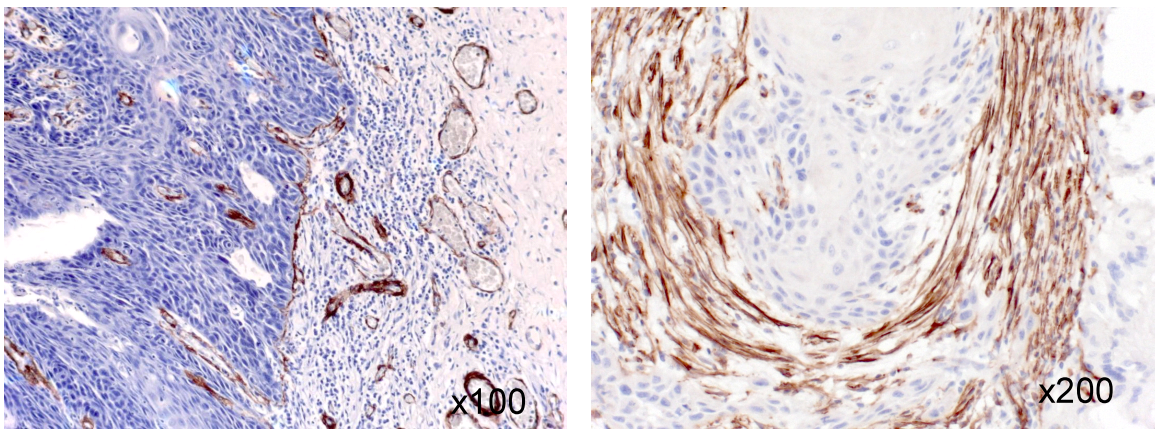

Figure 4.4 – SMA staining showing early invasion with blood vessels identified and LN stromal reaction

Survival analysis revealed a significantly increased risk of death for those patients with tumours showing high stromal levels of SMA expression (figure 4.5). Cox regression analysis confirmed a 4.26 times increased risk of dying from OSCC (unadjusted, confidence interval 2.74-6.61) for those patients with high SMA levels compared to those with low SMA expression (p= 0.002) and a 3.06 times increased risk (confidence interval 1.65 – 5.66) when adjusted for other pathological markers (p=0.002). Data shown in table 4.5.

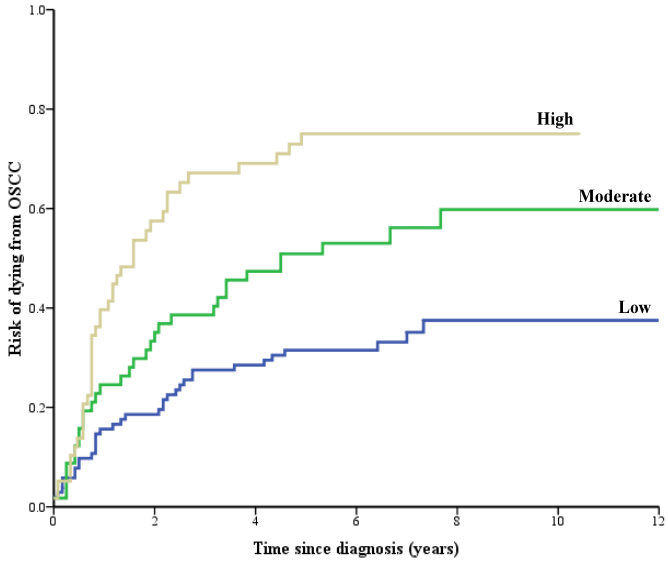

Figure 4.5 – Kaplan-Meir analysis for 282 cases of OSCC examined for SMA expression showing the increased risk of death when tumour stroma has moderate or high levels of SMA expression.

SMA expression correlated strongly with increased depth of tumour invasion (p=<0.001), disease stage (p=<0.001), degree of differentiation (p=0.01), presence of metastasis (p=<0.001), extracapsular spread (p=<0.001) and inversely correlated with inflammation (p=<0.001) (table 4.4).

		SMA			
		Low N=130	Medium N=74	High N=78	P-value for the association between the risk factor and SMA
Age	Mean age, years	62.3	58.5	61.5	0.40
Depth of invasion	Mean value, mm	5.3	9.8	12.6	<0.001
			Percentage*		
Sex	Male	55	72	70	0.11
	Female	45	28	30	
Disease stage	1	56	19	15	<0.001
	2	15	18	13	
	3	6	5	4	
	4	23	58	68	
Radiotherapy	No	65	58	47	0.86
	Yes	35	42	53	
Grade	Well differentiated	22	24	8	0.01
	Moderately differentiated	64	49	64	
	Poorly differentiated	14	27	28	
Surgical margins	Clear	40	22	22	0.048
	Close	29	35	25	
	Involved	31	43	53	
Metastases	No	83	62	47	<0.001
	Yes	17	38	53	
ECS	No	98	85	68	<0.001
	Yes	2	15	32	
Pattern of invasion	Cohesive	69	50	46	0.02
	Discohesive	31	50	54	
Inflammation	Low	30	53	77	<0.001
	Medium	33	35	21	
	High	37	12	2	
αvβ6	Low	28	31	16	0.055
	Medium	28	16	19	
	High	44	53	65	

*expressed as a percentage of low, medium and high SMA expression respectively

Table 4.4 – correlation of SMA expression with αvβ6 and other pathological markers examined. 282 patients included in analysis.

4.3.6 EGFR expression in OSCC

A total of 107 cases were examined for EGFR expression and of these cases 49 had low expression, 26 medium expression and 31 high expression. Of the patients who died from OSCC, 37% had low expression levels, 53% medium and 55% high EGFR expression levels. On Cox regression analysis, although there was an increased risk of death associated with high level of EGFR expression (Hazard Ratio 1.96 for high vs low EGFR expression (unadjusted)) this did not reach significance. Figure 4.6 shows typical staining for EGFR in OSCC and figure 4.7 shows the Kaplan Meier plot for EGFR expression in OSCC.

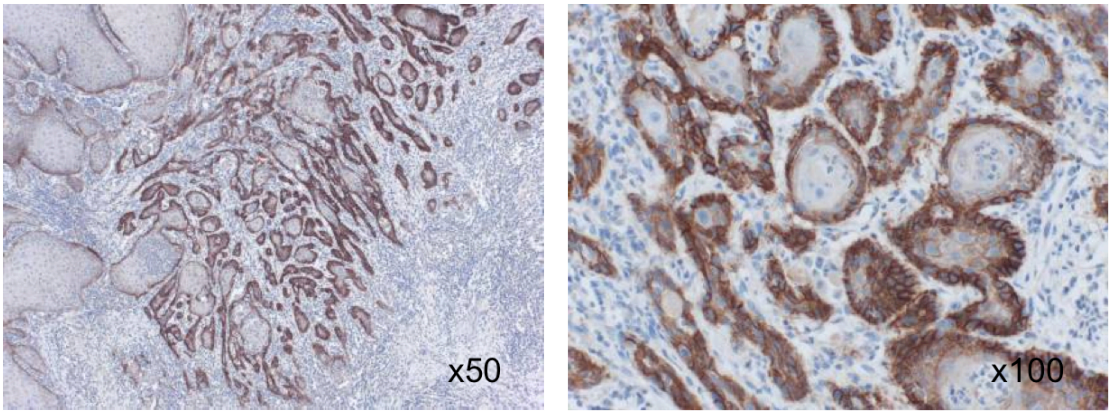

Figure 4.6 – OSCC staining showing medium EGFR expression levels.

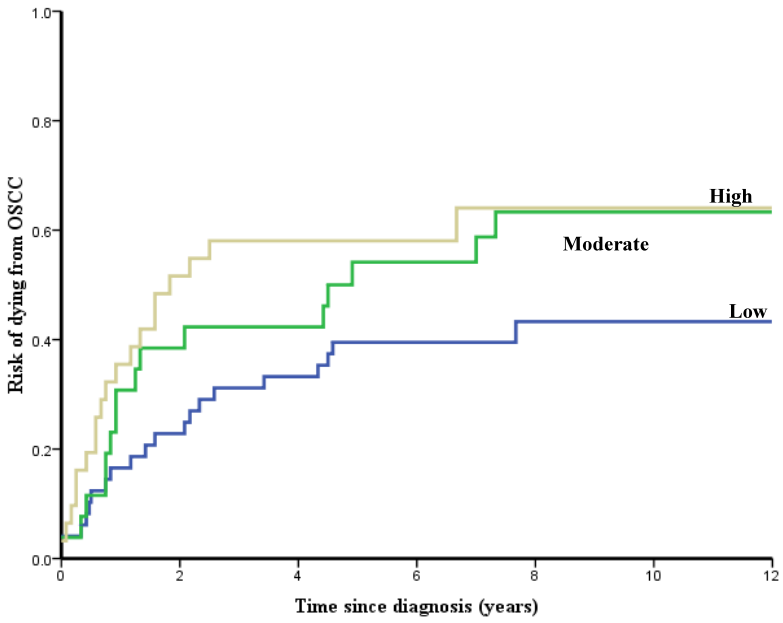

Figure 4.7 – Kaplan Meier plot for EGFR expression in OSCC. No significant difference is seen in survival when comparing patients with low, medium and high levels of EGFR expression.

4.3.7 P53 expression in OSCC

Of the 107 cases examined for p53 expression, 67 were found to have low expression, 25 moderate expression and 15 cases showed strong expression. Percentage of deaths from OSCC in patients with low, medium and high p53 expression levels was 40, 60 and 47% respectively. There was no significant correlation between level of p53 expression and risk of death from OSCC in the 107 cases analysed. Figure 4.8 shows a Kaplan Meir survival plot for p53 expression with sample p53 staining shown in Figure 4.9.

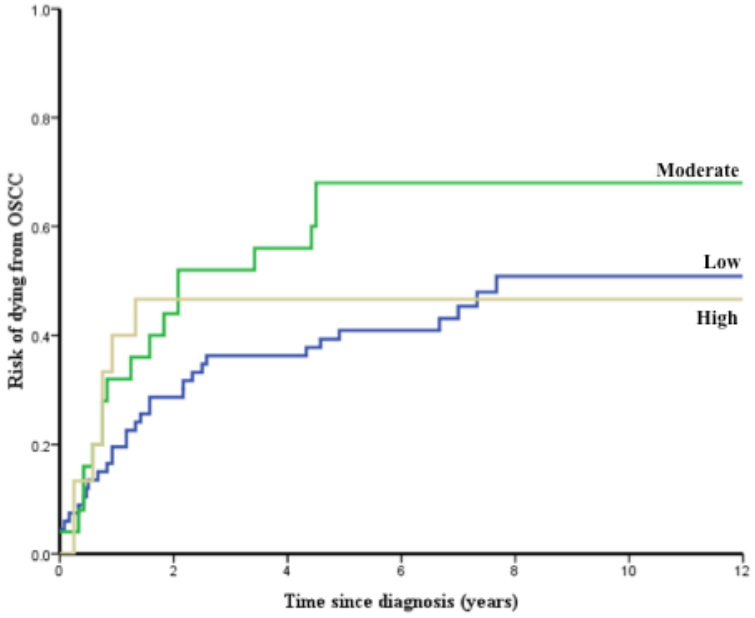

Figure 4.8 – Kaplan Meier plot showing risk of death from OSCC and p53 expression level.

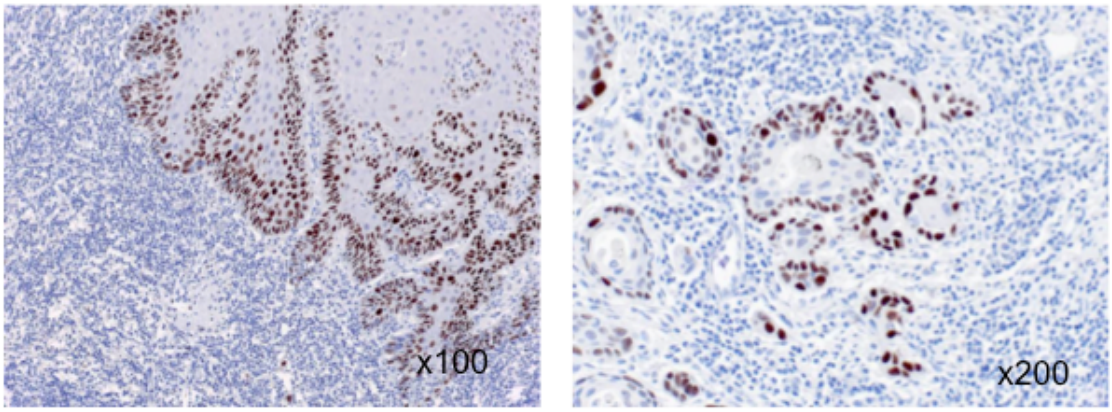

Figure 4.9 – OSCC sections stained for p53

4.3.8 Smad4 and Smad2 expression in OSCC

107 cases were stained for Smad4 and 40 cases for Smad2. Stromal myofibroblasts were highly positive for both markers and there was a strong correlation between SMA expression and phosphorylated Smad2 and 4 ($p<0.001$ for both). Figure 4.10 shows normal mucosa with nuclear positivity for Smad4 compared to OSCC sample showing strong Smad4 expression

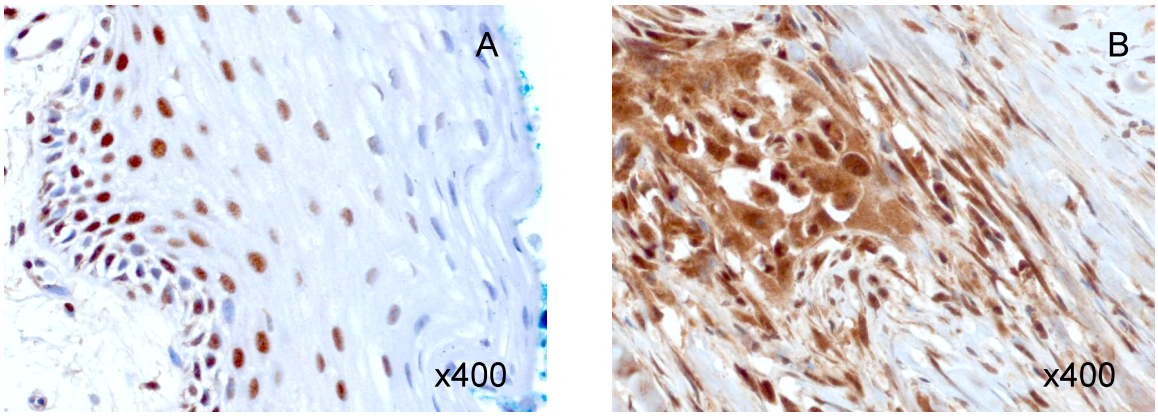

Figure 4.10 – Smad4 staining in normal mucosa showing nuclear Smad4 only (A) compared with smad4 stromal and cytoplasmic upregulation in OSCC.

4.3.9 Comparison of prognostic indictors in OSCC

Table 4.5 shows the hazard ratios for the chance of dying from OSCC for standard clinicopathological indices, SMA and αvB6. Looking at each factor independently (the unadjusted column), risk of death from OSCC was significantly increased with advanced tumour stage, positive resection margins, high tumour grade, an infiltrative, discohesive pattern of invasion and the presence of lymph node metastasis. Again looking at the unadjusted figures, the presence of a strong inflammatory host response conferred a significant survival advantage; patients with a high inflammatory response had a 68% reduction in OSCC mortality (HR=0.32 [95% CI=0.18-0.57]). There was also a weak association between increasing age and poorer prognosis in OSCC. Although extracapsular spead was a significant risk factor for early death from OSCC in the unadjusted column, surprisingly this factor loses significance when adjusted for all the other factors in the table. Patient sex, tumour site, p53, EGFR and αvβ6 expression levels did not have any affect on prognosis in OSCC.

There was a clear association between high stromal SMA expression and increased risk of OSCC death by over 4-fold (HR 4.26 [95% CI= 2.74-6.61], p=<0.001). After adjusting for known risk factors and all other variables considered in this analysis, the risk remained raised and statistically significant (HR 3.06 [95% CI=1.65-5.66; p=0.002]), showing that SMA is an independent risk factor for OSCC mortality. In fact, strong SMA expression had the highest hazard ratio of all the parameters examined in univariate and multivariate analysis, and even medium expression was associated with a significant increase in mortality (HR 2.01; table 4.5). There was also strong correlation between SMA expression and tumour stage, depth of invasion and extracapsular spread ($p<0.001$ for each) and inverse correlation with inflammation ($p<0.001$).

Characteristic	***Unadjusted***		***Adjusted*** *(for all other factors in table)*	
	Hazard Ratio (95% CI)	P value	Hazard Ratio (95% CI)	P value
Age*	1.04 (0.97-1.11)	0.04	1.08 (0.99-1.16)	0.07
Sex				
Male	1.0		1.0	
Female	0.96 (0.66-1.40)	0.72	1.43 (0.94–2.18)	0.10
Disease Stage				
I	1.0	<0.001	1.0	0.20
II	2.61 (1.41-4.82)		1.90(0.99-3.66)	
III	3.02 (1.34-6.82)		1.62 (0.65-4.03)	
IV	3.64 (2.24-5.94)		1.21 (0.62-2.33)	
Radiotherapy				
No	1.0	0.002	1.0	0.41
Yes	1.88 (1.31-2.70)		1.18 (0.80-1.75)	
Surgical Margins				
Clear (>5mm)	1.0	0.004	1.0	0.04
Close (1-5mm)	1.81 (1.07-3.05)		1.98 (1.16-3.38)	
Involved (<1mm)	2.58 (1.60-4.17)		1.68 (0.97-2.93)	
Metastasis				
No	1.0	<0.001	1.0	0.05
Yes	2.31 (1.61-3.32)		1.76 (1.00-3.11)	
Extracapsular Spread				
No	1.0	<0.001	1.0	0.70
Yes	2.54 (1.63-3.96)		1.12 (0.63-1.98)	
Grade				
Well differentiated	1.0	0.015	1.0	0.94
Mod differentiated	1.82 (1.03-3.22)		1.07 (0.51-2.21)	
Poorly differentiated	2.96 (1.59-5.52)		1.11 (0.58-2.12)	
Depth of Invasion **	1.40 (1.23-1.59)	<0.001	0.96 (0.78-1.19)	0.70
Pattern of Invasion				
Cohesive	1.0	<0.001	1.0	0.001
Discohesive	2.46 (1.71-3.54)		2.07 (1.33-3.24)	
Inflammation				
Low	1.0	<0.001	1.0	0.55
Medium	0.58 (0.38-0.88)		0.88 (0.55-1.42)	
High	0.32 (0.18-0.57)		0.69 (0.36-1.35)	
αvβ6				
Low	1.0	0.029	1.0	0.16
Medium	0.66 (0.35-1.27)		1.09 (0.66-1.78)	
High	1.43 (0.80-2.30)		1.00 (0.95-1.04)	
SMA				
Low	1.0	<0.001	1.0	0.002
Medium	2.18 (1.35-3.51)		2.01 (1.14-3.52)	
High	4.26 (2.74-6.61)		3.06 (1.65-5.66)	

* For increases of 5 years ** for increases of 5mm

Table 4.5 – Hazard ratios for each potential prognostic factor in the cohort of 282 patients studied.

The data show that although αvβ6 is not an independent prognostic marker in OSCC, a high level of SMA expression within the tumour stroma is associated with an increased risk of dying from OSCC. At 3 years, the risk (95% CI) of dying from OSCC was 26% (18-34), 44% (32-56) and 74% (63-85) in the low, medium and high SMA groups respectively. The median OSCC-specific survival of the patients whose cancers expressed high levels of SMA was only 22 months (95% CI 13-22), the lowest of all other risk factors other than extracapsular spread (15 months). The median OSCC specific survival for other recognised risk factors were: metastatic disease (25 months), discohesive pattern of invasion (26 months), poorly differentiated tumours (28 months), stage IV disease (32 months) and positive surgical margins (43 months). Table 4.6 shows the OSCC death rates at 1, 2 and 3 years from diagnosis for patients with low, medium and high SMA expression and the median survival times for each group.

	SMA Expression		
	Low	**Medium**	**High**
1 year	12% (7-18)	22% (12-32)	37% (26-48)
2 years	21 % (14-28)	36% (25-47)	65% (54-76)
3 years	26% (18-34)	44% (32-56)	74% (63-85)
Median survival (95% CI)	Not reached	93 months (40-not estimable)	22 months (13-22)

Table 4.6 – OSCC death rates (95% confidence intervals) according to SMA expression

The Kaplan –Meier curves in Figure 4.11 below show that high SMA levels are associated with poor survival irrespective of whether the patients have advanced disease or not.

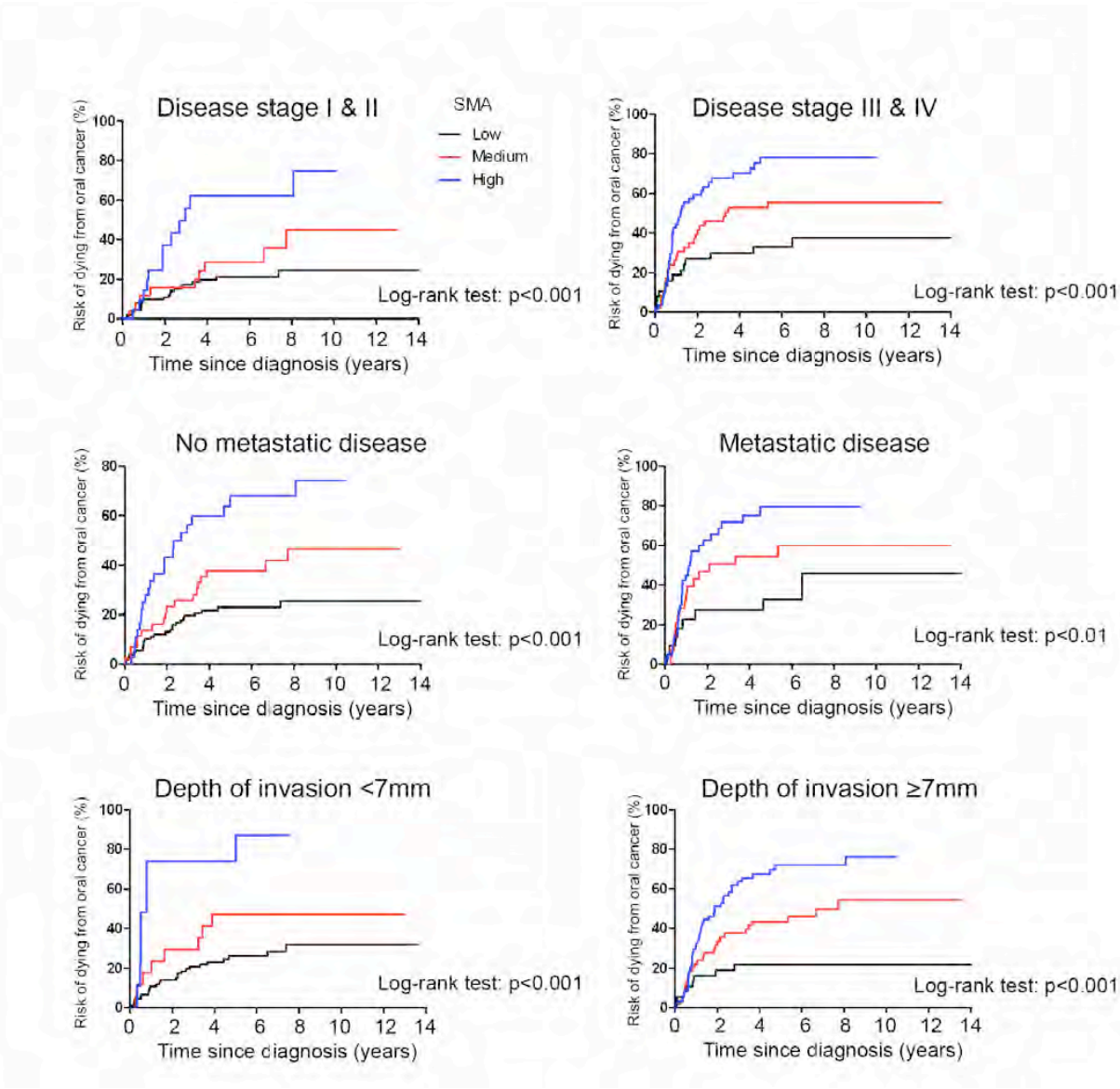

Figure 4.11 – Kaplan –Meier survival curves for varying SMA levels comparing patients with early and advanced disease. Blue line is high SMA, red medium and black low. High SMA is associated with significant OSCC mortality regardless of whether the disease is advanced or not.

The sensitivity and specificity of each predictive marker can also be assessed by generating a 'likelihood ratio' which is the detection rate (DR) divided by the false positive rate (FPR). DR is the percentage of those who have died with the specified characteristic (sensitivity) and FPR is the percentage of those still alive with the specified characteristic (1-specificity) (Deeks and Altman 2004). Table 4.7 shows the DR, FPR and likelihood ratios for each potential prognostic indicator at 1 and 3 years – the higher the likelihood ratio, the more powerful the marker.

Characteristic and definition of test positive	*1 year status*			*3 year status*		
	DR% (60 deaths)	FPR% (214 alive	Likelihood ratio (LR)	DR% (99 deaths)	FPR% (164 alive)	Likelihood ratio (LR)
Age (years)						
≥45	95	90	1.05	95	88	1.1
≥50	85	82	1.04	87	79	1.1
≥55	73	69	1.06	74	67	1.1
≥60	57	56	1.02	58	55	1.1
Sex						
Male	68	63	1.1	64	64	1.0
Disease Stage						
≥II, III, IV	93	57	1.6	88	52	1.7
≥ III, IV	75	43	1.7	69	39	1.8
≥ IV	71	37	1.9	62	34	1.8
Radiotherapy						
Yes	50	39	1.3	53	35	1.5
Surgical Margins						
Close, Involved	87	66	1.3	83	62	1.3
Involved	62	35	1.8	54	32	1.7
Metastasis						
Yes	55	36	1.5	48	23	2.1
Extracapsular Spread						
Yes	27	10	2.7	24	7	3.4
Grade						
Moderate, poor	88	79	1.1	90	76	1.2
Poor	33	17	1.9	31	15	2.1
Depth of Invasion						
≥ 4.0 mm	88	75	1.2	89	71	1.2
≥ 5.0	85	65	1.3	85	60	1.4
≥ 6.0	73	59	1.2	76	52	1.5
≥ 10.0	60	30	2.0	59	23	2.6
Pattern of Invasion						
Discohesive	72	35	2.1	66	30	2.2
Inflammation						
Low, Medium	92	75	1.2	90	71	1.3
Low	63	43	1.5	65	37	1.8
αvβ6	N=27	N=164		N=81	N=125	
Medium, high	83	72	1.2	78	72	1.1
High	69	47	1.5	65	43	1.5
SMA						
Medium, high	73	47	1.6	73	40	1.8
High	47	22	2.1	47	13	3.6

Table 4.7 – Prognostic value of each baseline patient characteristic (for the death rate at 1 and 3 years)

At 3 years from diagnosis, only SMA and extracapsular spread have a likelihood ratio greater than 3 with SMA at 3.6 and extracapsular spread at 3.4. From this analysis,

other important prognostic indicators are depth of invasion >10mm (2.6 LR), presence of metastases (2.1 LR) and poor tumour grade (2.1 LR). Applying the likelihood ratio rather than simply looking at the % of patients dead at 1 or 3 years with a particular prognostic indicator adjusts for the % patients with a prognostic factor who remain alive at 1 or 3 years (i.e. the false positive rate). In the case of patients with high SMA levels, at 3 years from diagnosis 47% had died and only 13% of those still alive had high SMA expression levels. Contrast this with other factors such as stage IV disease which is seen in 62% of patients who die at 3 years, however there is also a high false positive rate with this indicator as of those left alive at 3 years, 34% had stage IV disease. Taking this into consideration, within this patient cohort, SMA is seen to be the most powerful prognostic indicator of those considered.

To assess the validity of the finding that SMA was an independent prognostic marker in OSCC, data from the first 163 cases (80 OSCC related deaths) was used to produce a model to apply to the second data set of 116 patients (40 OSCC deaths). Cox regression modelling with backward elimination selected the most efficient group of prognostic indicators from the first data set. Of all the factors considered, only age, metastatic disease, discohesive growth pattern and SMA expression were selected. The regression parameter estimates were 0.0226 (age), 0.585 (metastatic disease), 0.899 (discohesive pattern of invasion), and 0.731 and 1.186 for medium and high SMA expression.

Using these parameter estimates, a score for each patient in the independent validation set was derived and a ROC analysis performed using time to event data with censoring. Figure 4.12 shows the ROC analysis showing the combined prognostic factors were highly predictive of death from OSCC at 3 years with an area under the curve of 77%. Also from the curve it can be seen that using these factors around 70% of patients who die from OSCC were test positive (DR=0.7) but only 20% of those still alive were test positive (FPR =0.2).

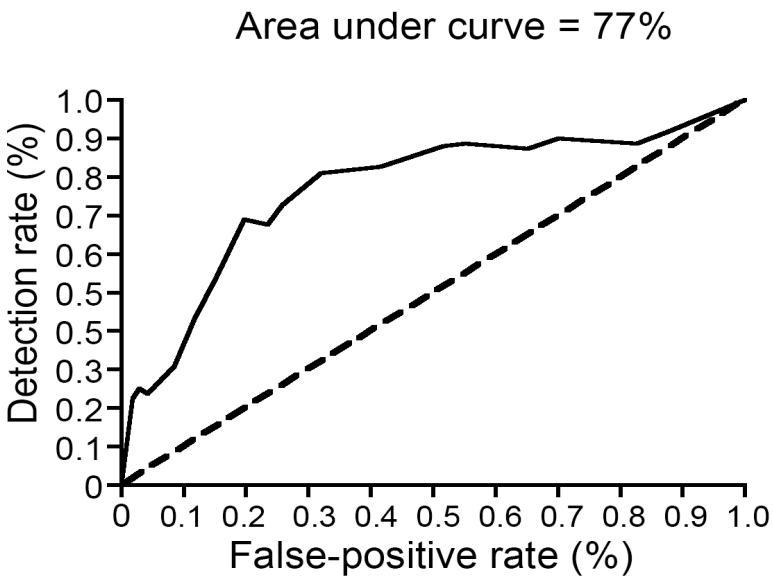

Figure 4.12 – ROC curve for 3-year OSCC mortality derived using a model containing age, metastatic disease status, pattern of invasion and SMA expression, when applied to the independent validation dataset. The dashed line is the line of no effect.

4.4 Discussion

Currently in OSCC, patient management is based on the tumor-node-metastasis (TNM) system, which usually is supplemented with additional histopathological information from the primary tumor and loco-regional lymph nodes (Woolgar 2006). Although patients with advanced stage IV disease and extracapsular spread clearly have a poorer prognostic outlook than those with early disease, there is no clear consensus regarding the relative importance of other tumor features in determining patient prognosis. Most prognostic studies report using relatively low patient numbers and this has hindered the identification of useful biomarkers, limiting the discovery of potential new prognostic markers. Thus there is a marked need to develop new diagnostic tools that can accurately identify aggressive tumours early, so that management can be adjusted accordingly.

In this chapter, the significance of αvβ6, stromal SMA, EGFR and p53 expression in 282 patients with OSCC is analysed, in relation to conventional prognostic indices

and mortality from OSCC. SMA was investigated to follow on from the findings set out in Chapter 3 and based upon evidence that the tumour stroma promotes tumour progression in other tumour types (Liotta and Kohn 2001, Pupa *et al* 2002, De Wever and Mareel 2003, DeWever et al 2008), and in in-vitro findings that myofibroblasts promote cell motility in OSCC cell lines (Lewis *et al* 2004).

Results have shown that although αvβ6 is expressed at high levels in OSCC, it is not an independent prognostic marker as has been suggested in colon, cervical, non small cell lung and gastric cancers (Bates *et al* 2005, Hazelbag *et al* 2007, Elayadi *et al* 2007, Zhang *et al* 2008). Interestingly though, high levels of stromal SMA are seen to be an independent indicator of poor prognosis, and this finding is more significant than any of the other primary tumor indices used currently. The data clearly show that in the OSCC patient cohort analysed, stromal SMA expression is the most significant independent prognostic marker, and is highly predictive of early death. In fact, only patients with extracapsular metastatic spread in the neck had a shorter median survival than those with high stromal levels of SMA (15 months verses 22 months).

As well as being associated with early mortality, SMA expression within the primary tumor correlated significantly with other indicators of adverse outcome including increased depth of tumour invasion advanced disease stage and poor tumour differentiation. Furthermore, high SMA expression correlated with both presence of lymph node metastasis and extracapsular spread. Immunohistochemical staining of lymph node metastases also revealed high levels of SMA, suggesting that myofibroblasts may help promote tumour dissemination.

Expression of EGFR was also examined and not found to be significantly associated with prognosis in OSCC in this patient cohort. Although EGFR overexpression has been reported to be associated with higher grades or reduced survival in a numerous epithelial cancers including HNSCC (Salomon *et al* 1995, Kiyota *et al*. 2000; Putti *et al*. 2002, Laimer *et al* 2007), the clinical relevance of the findings varies. For example, Storkel *et al* (1993) found that overexpression of EGFR was associated with shortened survival whereas Christensen *et al* (1995) and Khan *et al* (2002) could not find significant correlation of EGFR with clinicopathological features or prognosis.

Others have looked specifically at tumour depth, lymph node status, extracapsular invasion, recurrence and survival in specimens from patients with HNSCC and found no significant correlation. (Partridge *et al* 1988, Ishitoya *et al* 1989, Frank *et al* 1993).

The well-known tumour suppressor p53 was also examined as a potential prognostic marker in this OSCC cohort. Previously Nylander et al (2000) have shown that p53 is mutated in over 50% of human HNSCC specimens however again there are conflicting reports about the link between p53 expression and mortality in OSCC (Boslooper et al 2008, Gasco and Crook 2003). Results in this chapter show that although p53 was upregulated in OSCC, there was no significant correlation between p53 levels and mortality. The reasons for this may be manifold but may include that the detection of p53 by immunohistochemistry is not always synonymous with the presence of p53 mutations.

The analysis of 282 OSCC patients has revealed that tumour stage, grade, discohesive growth pattern, depth, incomplete surgical excision, metastatic disease and extracapsular spread are significant risk factors for mortality, which is consistent with previous studies (Brandwein-Gensler et al 2005, Woolgar 2006). However, of all the prognostic indicators looked at, SMA was the single most significant independent predictor of mortality from OSCC and interestingly high SMA levels were indicative of poor outcomes irrespective of disease stage. This is important, as it would allow high risk patients to be identified at the stage of initial biopsy, as SMA expression levels seen on the initial biopsy were consistent with those seen in the subsequent resection specimen.

It is not immediately clear why certain tumours develop with a fibroblast rich stroma. The fibroblasts seen within tumours have an activated phenotype and are similar to those seen within healing wounds however they may be distinguished from normal fibroblasts by the fact they are perpetually activated, neither reverting to a normal phenotype nor undergoing apoptosis and elimination. These tumour fibroblasts can be identified within the tumour stroma by the expression on SMA. Activation of fibroblasts to become SMA positive myofibroblasts is proposed to take place by several mechanisms including activation of a tissue resident fibroblast, local cancer

cells or epithelial cells undergoing epithelial-to-mesenchymal transition (EMT), or the migration and activation of a marrow-derived cell.

TGF-β has previously been shown to be the most potent cytokine driving myofibroblast transdifferentiation (DeWever et al 2008) and high levels of Smad2 and Smad4 seen in OSCC specimens along with the strong correlation with SMA expression would seem to confirm the relationship here. It is likely that a supportive SMA-positive stroma is generated because subsets of tumours are particularly effective at activating TGF-β1 (and probably refractory to its growth-suppressive effect). However, it is also possible that stromal cells from different individuals may vary in their ability to transdifferentiate into myofibroblasts.

TGFβ exists in a latent form and may be activated through several mechanisms, including binding to the αvβ6, which has been shown to be a prognostic marker in several types of carcinoma (Bates et 2005, Hazelbag et al 2007 and Elayadi et al 2007). αvβ6 expression has been shown to be increased in OSCC and to promote tumour invasion both directly and indirectly through stimulating TGF-β-dependent myofibroblastic transdifferentiation (Marsh et al 2008, Nystrom et al 2006). αvβ6 did not correlate significantly with SMA expression on multivariate analysis, nor was αvβ6 an independent prognostic marker in this OSCC patient cohort which suggests that either alternative mechanisms may be more important in activating TGFβ in OSCC, or that the stromal response to TGF-β varies between individuals.

One other interesting finding was that SMA expression correlated inversely with inflammation ($p=<0.001$). The lack of a lymphocytic response in SMA-positive tumours may also be modulated through TGF-β, since this cytokine has also been shown to be a potent immune suppressor (Yang and Moses 2008). SMA expression also significantly correlated with depth and a discohesive pattern of invasion ($p<0.001$, $p=0.02$ respectively). Myofibroblasts have previously been shown to have an invasion promoting role in several tumour types through the upregulation of HGF (Lewis et al 2004, Marsh et al 2008). This growth factor promotes tumor cell motility, in part through downregulating cell cohesion and remodelling the extracellular matrix

(Birchmeier et al 2003), and it is possible a similar mechanism may modulate OSCC invasion in vivo.

SMA status was also associated significantly with metastasis and extracapsular spread (both $p<0.001$). These data raise the possibility that SMA-positive stroma may be involved directly in disease progression and actively promote metastasis. There could be several explanations for this. Conceivably SMA-positive cells within lymph nodes could represent tumour cell EMT, or SMA-positive myofibroblasts may metastasise along with tumour cells. It is more likely that myofibroblasts are generated from local, or circulating mesenchymal cells and support disease progression by generating a supportive environment conducive to disease dissemination and that certain individuals may be more prone to stromal activation by TGFβ.

4.5 Summary

These data suggest that SMA may be the most significant independent prognostic indicator yet identified in OSCC. High SMA is shown here to identify those patients most at risk in OSCC and more importantly identifies aggressive tumours even in patients with early stage disease or at the initial biopsy. Although αvβ6 itself was not found to be an independent prognostic marker, there was a significant correlation between high αvβ6 expression, presence of metastases and depth of invasion suggesting the integrin may have a pro-invasive role in OSCC.

Clearly there needs to be further prospective analysis of the natural progression of SMA positive tumours before suggesting that SMA scoring should take precedence over well established clinicopathological prognostic markers. However the data from this large series of patients suggests that SMA scoring should be added as part of the routine assessment of samples from OSCC patients as those with high SMA scores should perhaps be managed more aggressively than those with low SMA scoring tumours.

Chapter 5

Production of B6.3, a recombinant Ab to αvβ6 for the delivery of targeted magnetic alternating current hyperthermia

5.1 Introduction

The murine scFv MFE-23 is a well characterised anti CEA antibody fragment which has previously been used in clinical trials (Begent *et al* 1996). To minimise the human anti mouse antibody response seen with repeated doses, MFE-23 has been humanised through the replacement of solvent exposed murine residues with human homologues (Graff et al 2004). This new humanised scFv (hMFE-23) was then further stabilised by the same group using affinity maturation and termed shMFE-23. Furthermore, introducing a Tyrosine-H100b to Proline mutation in the H3 loop of VH domain has been shown to prevent MFE-23 binding to CEA without affecting the overall structure of MFE-23 (Boehm *et al* 2000).

The integrin αvβ6 is utilised by the Foot and Mouth Disease Virus (FMDV) serotype O1 BFS as a vector by which to enter bovine epithelial cells (Monaghan *et al* 2005). FMDV is an RNA virus that is replicated in epithelial cells of domestic livestock and the primary route of infection is through epithelial cells in the animal's oropharynx. The FMDV capsid consists of 60 copies each of the proteins VP1-VP4 which surround a single stranded positive sense RNA genome. Crystal structures of these have shown the VP1 peptide contains a surface exposed conformationally flexible loop, the GH loop which has at its apex a highly conserved RGD motif (Acharya *et al* 1989). In cattle, the cells targeted by FMDV during the acute phase of infection have been shown to constitutively express αvβ6 suggesting that the integrin is important for the uptake of FMDV into cells (Monaghan *et al* 2005). Binding of RGD motifs on the VP1 capsule peptide to αvβ6 stimulates a clathrin dependent uptake of the integrin-FMDV complex into cytoplasmic endosomes prior to transfer of the viral RNA into the cytoplasm (Berryman *et al* 2005).

Although many integrins have RGD as a ligand, not all will recognise FMDV and there is evidence that other amino acids either side of the RGD sequence are important for intracellular uptake of FMDV. Consistently across FMDV strains, a leucine residue is seen at the RGD+1 and RGD+4 positions which is similar to the RGDLXXI sequence found in the LAP peptide associated with TGFβ (Munger *et al* 1999). Mateu *et al* (1996) showed that substituting various amino acids at the RGD+1 and RGD+4 sites of synthetic peptides derived from the GH loop of VP1 of a

particular FMDV strain reduced the ability of the peptides to inhibit infection of cells by the same strain of the FMDV. More recently, alanine substitution of the residues at RGD+1 and RGD+4 sites in a 17-mer peptide corresponding to the GH sequence of the VP1 loop of FMDV reduced the ability of the peptide to bind αvβ6 (Burman *et al* 2006). Although the contribution made by each individual residues of the GH loop to binding of αvβ6 is not fully understood, it is clear that residues either side of the RGD are also important for high affinity binding to αvβ6. A recent study looking at peptides generated from αvβ6 specific ligands with the sequence RGDLXXL (ie Leucine at RGD +1 and +4) and analysis of their binding to αvβ6 shows that the sequence is important for formation of a post RGD helix in the secondary structure of the peptide. This helix is shown to be functionally important for stabilising the interaction of the RGD containing ligand with αvβ6 and for maintaining high affinity binding (DiCara *et al* 2007)

The CDR3 loop of the VH domain of antibodies has previously been used as a site for insertion of peptides to successfully alter the specificity of a human/mouse chimeric heavy chain antibody (Lanza *et al* 1997). The conformationally exposed position of the CDR3 loop within the VH domain of shMFE-23 also means it is an ideal site for a similarly structural based approach of peptide insertion to alter the specificity of the scFv. Knowledge of the sequence of the VP1 peptide and evidence that it shows high affinity for αvβ6 gives rise to the possibility that by grafting the peptide into the CDR3 loop of shMFE-23, we can create a new scFv specific for αvβ6. Furthermore, by mutating the H3 loop with substitution of tyrosine residue for a proline residue, the new scFv should not bind to CEA.

Ferric nanoparticles have been shown to generate heat when placed within an alternating magnetic field (Kallumadil *et al* 2009, Cantillon-Murphy *et al* 2010) and magnetic alternating current hyperthermia (MACH) has been successfully used *in vivo* to reduce tumour bulk (Jordan *et al* 1997, deNardo *et al* 2005, Balivada *et al* 2010). Single chain antibody fragments have previously been conjugated to many types anticancer therapies, including to nanoparticles (deNardo *et al* 2005, Dobson 2010).

5.2 Aims and Objectives

Work in this chapter builds upon previous data on magnetic alternating current hyperthermia and the chapter aims are to produce novel αvβ6 specific scFv in large scale and to attach commercially available magnetic nanoparticles to the αvβ6 specific scFv. The objective is to determine whether the scFv-nanoparticle conjugates can then be used to deliver targeted hyperthermia against αvβ6 expressing cell lines.

5.3 Results

5.3.1 Insertion of VP1 peptide into CDR3 loop of shMFE-23

DNA encoding the 17- mer peptide sequence from A140 to A156 of VP1 was inserted at the tip of CDR-H3 of MFE-23, between T98 and G99 (Kabat nomenclature). This was done using overlapping PCR reactions as described below. The first PCR reaction was designed to produce N terminus of desired sequence and to include Nco1 restriction enzyme site in final product (CCATG). Primers used were shMFE sense (**5**^{1}CATGCCATGGCCCAAGTTAAACTGGAACAGTCC**3**^{1}) andVP1 antisense (**5**^{1}GAGCCAGCACCTGCAGATCACCTCGCAGATTCGGAACTGCAGTTGGTG TCCCTTCGTTGC **3**^{1}) Figure 5.1 shows the results of the PCR reaction run on 1% agarose gel.

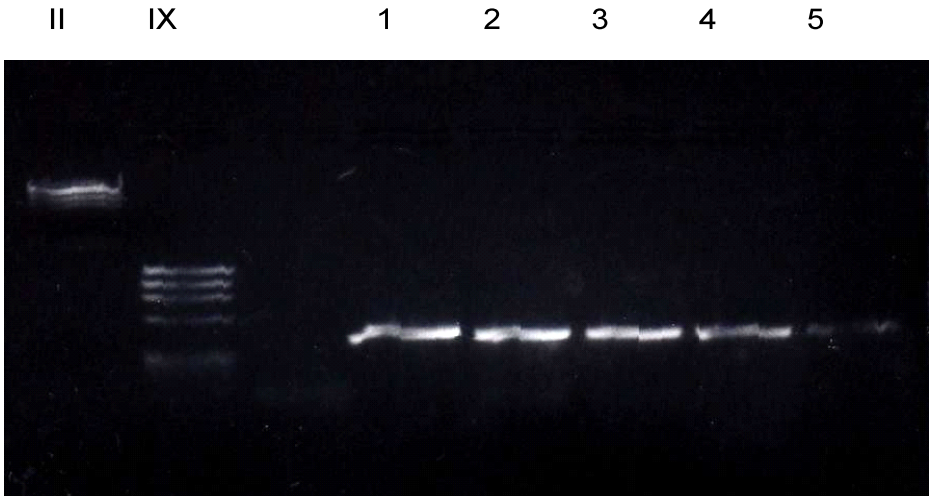

Figure 5.1 - 1% agarose gel showing PCR products from first PCR reaction to generate N terminal end of shMFE with varying amounts of plasmid template (1µl – 5µl) diluted 1:1000 and molecular weight markers II, IX.

The second PCR reaction was designed to produce C terminus of desired sequence using primers shMFE antisense (**5**^{1}ATAGTTTAGCGGCCGCAGCCTTGATTTC**3**^{1}) and VP1 sense (**5**^{1}CTGCGAGGTGATCTGCAGGTCGTGGCTCAGAA

AGTTGCAGGTCCTTACCCTTTCGACTACTGGGGACAAGG **3**[1]). Figure 5.2 shows the PCR products run on agarose gel.

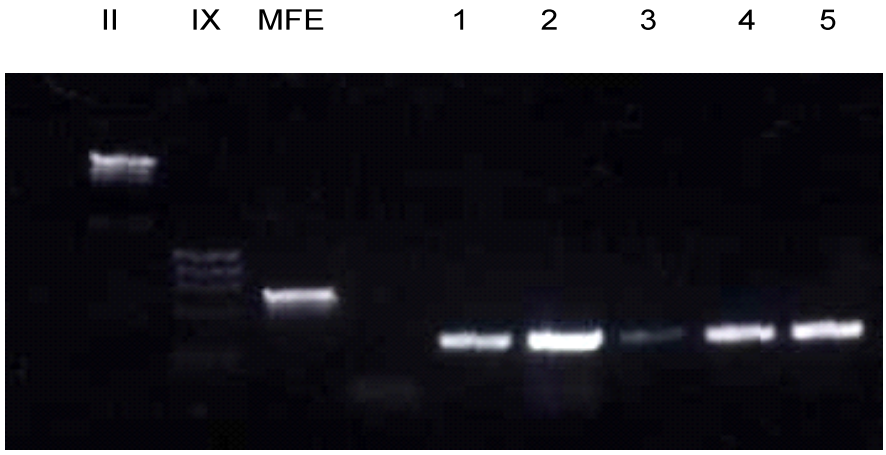

Figure 5.2 - 1% agarose gel showing PCR products from second PCR reaction to generate C terminal end of shMFE with varying amounts of plasmid template (1µl – 5µl) diluted 1:1000, MFE as control and molecular weight markers II, IX.

The two separate PCR reactions have generated N and C terminal ends of B6.3 which were then combined in a third PCR reaction using primers shMFE sense and shMFE antisense to produce sequence coding for shMFE-23 with VP1 peptide in the CDR3 region of VH chain as shown in figure 5.3.

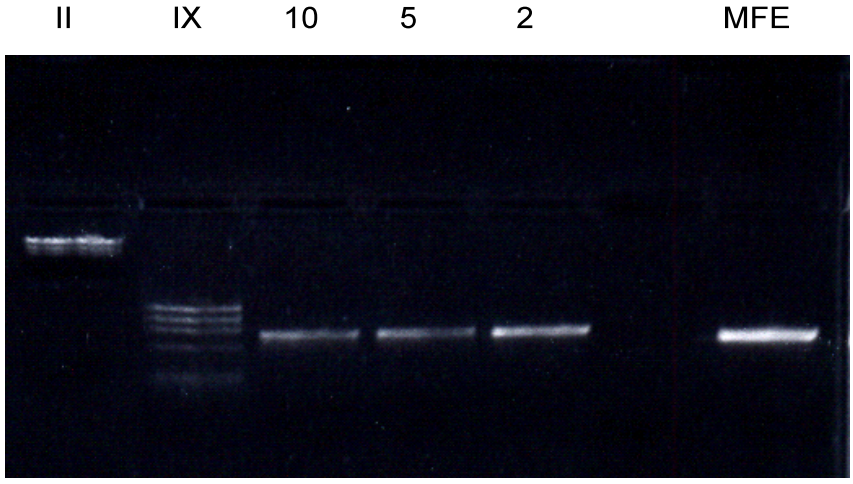

Figure 5.3 - 1% agarose gel showing PCR products from third PCR reaction at 2,5,10µl to produce DNA sequence encoding desired product B6.3, MFE as control and molecular weight markers II, IX.

Having produced the sequence for B6.3, restriction enzymes Not1 and Nco1 were used to cut the PCR product and the *E. coli* vector puc119 (figure 5.4) prior to ligation

of digested B6.3 and puc119 vector, phenol extraction of the DNA and electroporation into TG1 *E. coli* cells.

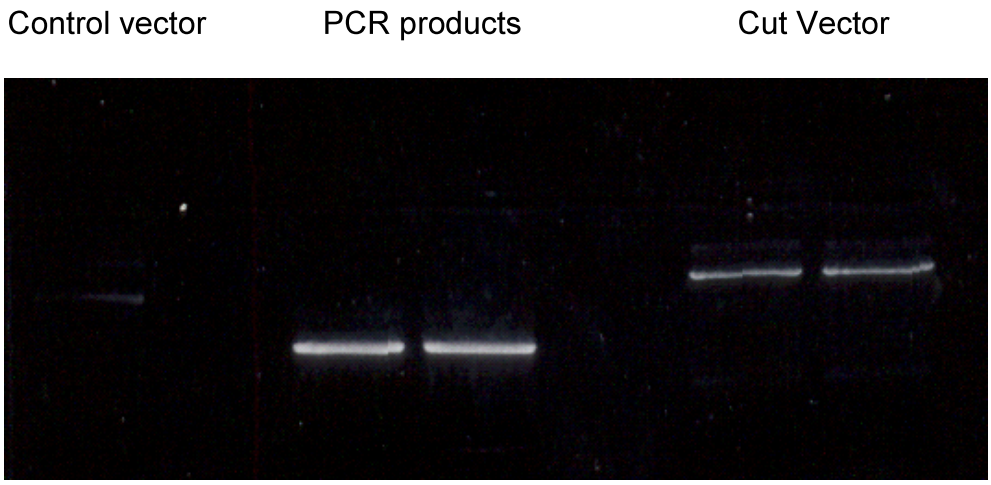

Figure 5.4 - 1% agarose gel showing PCR products and puc119 vector after digestion with enzymes Nco1 and Not 1 as compared to the un-cut control puc119 vector.

Transformed cells were plated and left to grow overnight, from these plates, 20 colonies were selected for PCR screening using primers shMFE sense and shMFE antisense. Five colonies were found to be positive for the insert B6.3 on colony screening; these were then selected for plasmid extraction and sent for sequencing. Initial sequence result showed peptide insertion, proline mutation and two unexpected errors at position 82 and 162. These errors were corrected using site directed mutagenesis as shown in Appendix 1 (Figure A1.1). Repeated sequence data showed the desired sequence for B6.3 as shown in figure 5.5.

10
CAA GTT AAA CTG GAA CAG TCC GGT GCT GAA GTT
gln val lys leu glu gln ser gly ala glu val
21
GTC AAA CCA GGT GCT TCC GTG AAG TTG TCC TGT AAA GCC TCT GGT TTT AAC ATC AAG GAT
val lys pro gly ala ser val lys leu ser cys lys ala ser gly phe asn ile lys asp
41
TCG TAT ATG CAT TGG TTG AGA CAA GGG CCA GGA CAA AGA TTG GAA TGG ATT GGC TGG ATT
ser tyr met his trp leu arg gln gly pro gly gln arg leu glu trp ile gly trp ile
61
GAT CCA GAG AAT GGT GAT ACC GAG TAC GCT CCT AAA TTT CAG GGA AAG GCT ACT TTT ACT
asp pro glu asn gly asp thr glu tyr ala pro lys phe gln gly lys ala thr phe thr
81
ACC GAC ACT TCC GCT AAT ACC GCA TAC TTG GGC TTA TCT TCC TTG AGA CCA GAG GAC ACT
thr asp thr ser ala asn thr ala tyr leu gly leu ser ser leu arg pro glu asp thr
101
GCC GTA TAC TAC TGC AAC GAA GGG ACA CCA ACT GCA GTT CCG AAC CTG CGA GGT GAT CTG
ala val tyr tyr cys asn glu gly thr pro thr Ala Val Pro Asn Leu Arg Gly Asp Leu

CAG GTG CTG GCT CAG AAA GTT GCA GGT CCT TAC CCT TTC GAC TAC TGG GGA
Gln Val Leu Ala Gln Lys Val Ala gly pro tyr pro phe asp tyr trp gly
121
CAA GGT ACC TTA GTT ACT GTC TCT AGC GGT GGC GGA GGT TCA GGC GGT GGA GGG TCT GGA
gln gly thr leu val thr val ser ser gly gly gly gly ser gly gly gly gly ser gly
141
GGT GGC GGT AGT GAA AAT GTG CTG ACC CAA TCT CCA AGC TCC ATG TCT GCT TCT GTT GGC
gly gly gly ser glu asn val leu thr gln ser pro ser ser met ser ala ser val gly
161
GAT AGA GTA ACC ATC GCT TGT AGC GCA TCC TCT AGT GTC CCA TAT ATG CAC TGG TTT CAA
asp arg val thr ile ala cys ser ala ser ser ser val pro tyr met his trp phe gln
181
CAG AAG CCA GGT AAA AGC CCA AAG TTG TTG ATT TAT TCG ACA TCC AAC TTG GCT TCT GGA
gln lys pro gly lys ser pro lys leu leu ile tyr ser thr ser asn leu ala ser gly

201
GTG CCT TCA AGG TTT TCT GGT TCC GGC TCA GGA ACC GAT TAT AGT TTG ACT ATT AGC TCA
val pro ser arg phe ser gly ser gly ser gly thr asp tyr ser leu thr ile ser ser
221
GTG CAG CCA GAG GAT GCT GCA ACC TAC TAT TGC CAG CAA AGG TCC TCA TAT CCA CTG ACT
val gln pro glu asp ala ala thr tyr tyr cys gln gln arg ser ser tyr pro leu thr
241
TTC GGG GGT GGA ACG AAG TTG GAA ATC AAG GCT GCG GCC
phe gly gly gly thr lys leu glu ile lys ala ala ala

Figure 5.5 - Sequence of B6.3 - VP1 peptide sequence insertion is in red and proline mutation shown in green.

After sequence data confirmed the desired DNA sequence, electroporation was used to insert the sequence into TG1 *E. coli* cells which were then grown in the presence of IPTG to stimulate protein expression. Initially, expression was very weak however on concentration of the samples, the His tag on the protein could be detected on Western blot (figure 5.6).

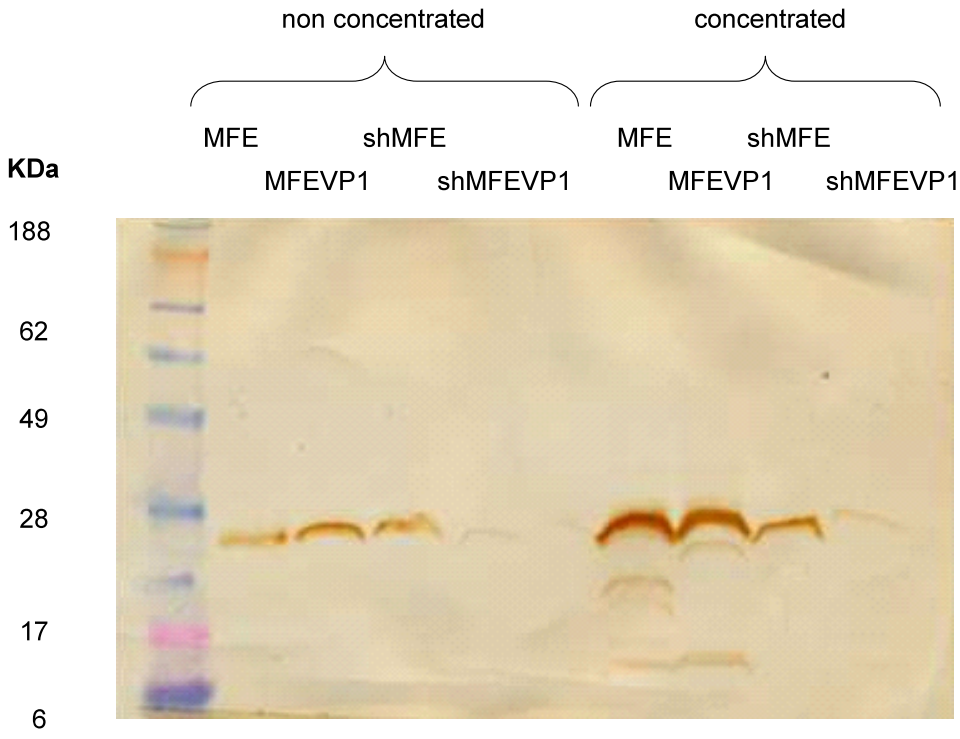

Figure 5.6 - Western blot showing expression of MFE, MFEVP1, shMFE and MFEVP1 in *E. coli* with IPTG. There is weak expression of B6.3 (labelled shMFEVP1) in the concentrated sample.

5.3.2 Insertion of free cystine into *P.pastoris* vector PPiczαB

The aim of the work in this chapter is to produce αvβ6 specific single chain antibodies that can be attached to magnetic nanoparticles for the delivery of targeted magnetic fluid hyperthermia. Proteins can be attached to magnetic nanoparticles either non-specifically via amine groups or using site-specific attachments via the –SH groups found on a free cystine molecule. Large scale single chain production can be carried out in the yeast *P.pastoris* and to do this, the B6.3 construct should be transferred in a yeast vector such as PPICZαB. To allow for site specific attachment of magnetic nanoparticles to the B6.3 scFv and to any future antibodies, using PCR, a cystine residue was inserted into the *P.pastoris* vector PPICZαB. To facilitate transfer from puc119 *E. coli* vector to the yeast vector, primers were designed to add a Not1 restriction enzyme site and to remove the myc tag in a single step PCR reaction. Primers used were Ppic cys Sense (**5**^{1}GTACCTCGAGCCGCGGCGGCCGC CTGTCATCATCATCATCATCATTGATTTGTAGCCTTAGA**3**^{1}) and Ppic cys

Antisense (**5**[1] TGTGGGGGATCCGCACAAACGAAGGT**3**[1]) Not 1 site shown in green, cystine in red and his tag in blue. Results from the PCR reaction are shown on the agarose gel in figure 5.7.

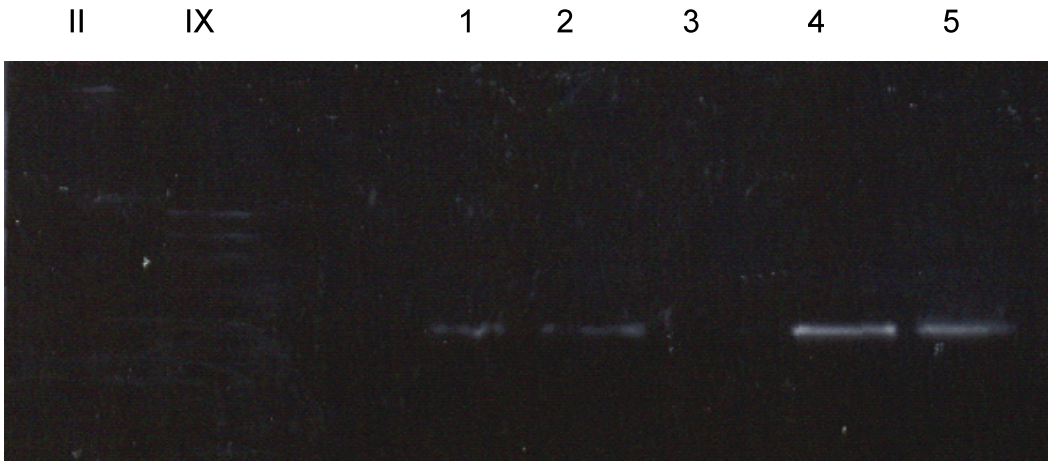

Figure 5.7 - 1% agarose gel showing PCR products with varying template concentrations (1µl – 5µl) diluted 1:1000 and molecular weight markers II,IX.

Having generated DNA sequence to be inserted into the PPICZαB vector by PCR, samples of the PCR reactions were run on agarose gel and then digested using enzymes BamHI and Not 1. Figure 5.8 shows the digested products of original PPICZαB vector and the PCR products from the above gel.

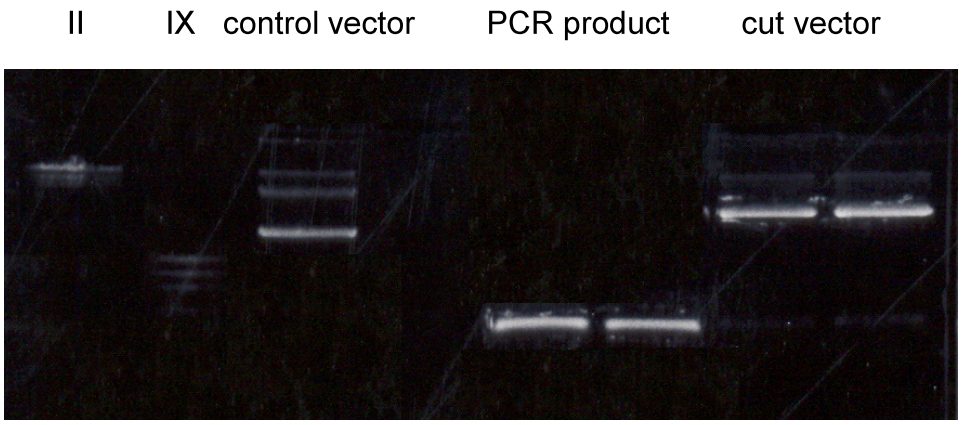

Figure 5.8 - 1% agarose gel showing digested PCR products, digested PPICZαB vector compared to control undigested vector and molecular weight markers II,IX

Digested PCR product and vector were run on agarose gel, the DNA was then excised and extracted from the gel. The products were ligated together then transformed into TOP 10F[1] *E. coli* cells by electroporation. Transformed cells were grown on LB plates in the presence of zeocin and colonies checked for insert acceptance by PCR screening using the primers Ppic cys sense and antisense as above. Colonies which had accepted the insert on PCR screening were sent for sequencing, results shown below in figure 5.9.

Original sequence

GCT GCT AAA GAA GAA GGG GTA TCT CTC GAG AAA AGA GAG GCT GAA GC TGCAG GAATTCAC
ala ala lys glu glu gly val ser leu glu lys arg glu ala glu ala
SfiI NotI
GGCCCAGCC GGC CGTC TCGGATCGGTACCTC GAGCCGCG GCG GCC GCCAGC TTTCTA

c-myc tag
GAA CAA AAA CTC ATC TCA GAA GAG GAT CTG AAT AGC GCC GTC GAC
glu gln lys leu ile ser glu glu asp leu asn ser ala val asp

Poly His tag Stop
CAT CAT CAT CAT CAT CAT TGA GTTTGTAGCCTTAGACATGACTGTTCCTCAGTTCAA
His His His His His His ***

GTTGGGCACTTACGAGAAGACCGGTCTTGCTAGATTCTAATCAAGAGGATGT CAGAATGCC

Sequence data after PCR to remove myc tag and insert cystine residue

GCT GCT AAA GAA GAA GGG GTA TCT CTC GAG AAA AGA GAG GCT GAA GC TGAAT TCA CGT
ala ala lys glu glu gly val ser leu glu lys arg glu ala glu ala
SfiI NotI
GGC CCA GCC GGC CGT CTC GGA TCG GTA CCT CGA GCC GCG GCG GCC GCC TGT
Ala Ala Ala cys

Poly His tag Stop
CAT CAT CAT CAT CAT CAT TGA GTTTGTAGCCTTAGACATGACTGTTCCTCAGTTCAA
His His His His His His ***

GTTGGGCACTTACGAGAAGACCGGTCTTGCTAGATTCTAATCAAGAGGATGT CAGAATGCC

Figure 5.9 - Sequence data showing removal of c-myc tag and insertion of cystine. Sequencing primers used were 5^{1}AOX (5^{1}GACTGGTTCCAATTGACAAGC3^{1}) and Ppic cys reverse (5^{1}AAATGAAGCCTGCATCTCTC3^{1})

Entire sequencing results for original PPICZαB vector, PPICZαBcys and are available in appendix 1 (Figures A1.2, A1.3).

5.3.3 Subcloning of B6.3 into PPICZαBcys vector

Having now produced a new *P.pastoris* vector PPICZαBcys which would add a free cysteine residue to the single chain, I wanted to insert the DNA coding for B6.3 into the new vector ready for production of the scFv in yeast. To begin with, B6.3 in puc119 vector and the newly produced PPICZαBcys vector were digested using the restriction enzymes Sfi and Not1. Figure 5.10 shows the products of digestion reaction run on agarose gel.

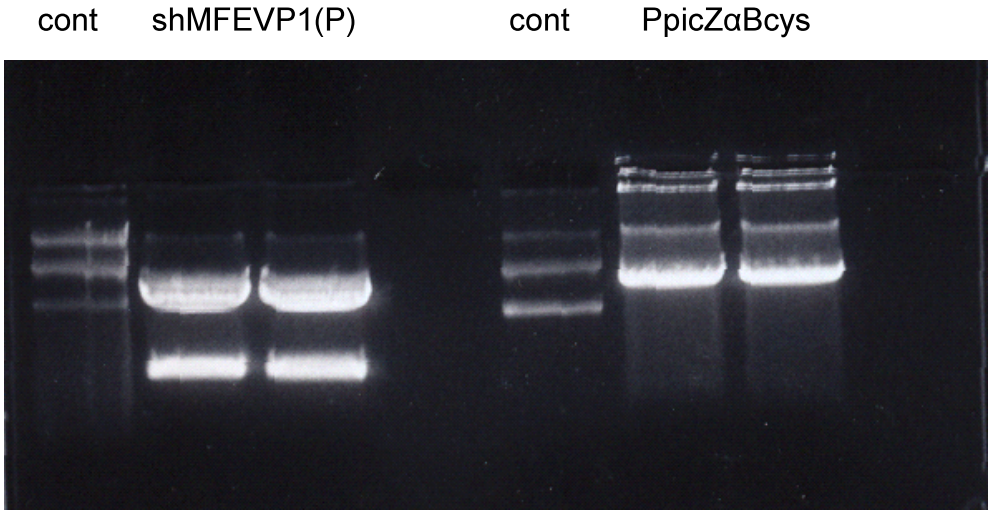

Figure 5.10 - % agarose gel showing products after digestion of B6.3 and PPICZαBcys compared to undigested controls.

Following digestion, the bands containing the products of digestion were excised from gel and ligated together. Ligated product was extracted using phenol and electroporated into TOP 10F[1] *E. coli* cells for growth on LB/zeocin plates. Colonies were selected to be sent for sequencing following PCR colony screening. Sequencing results shown in figure 5.11 below used primers 5[1]AOX (5[1]GACTGGTTCCAATTGACAAGC3[1]) and Ppic cys reverse (5[1]AAATGAAGCCTGCATCTCTC3[1]). Full sequence data is shown in appendix 1 (figure A1.4)

101
GCC GTA TAC TAC TGC AAC GAA GGG ACA CCA ACT GCA GTT CCG AAC CTG CGA GGT GAT CTG
ala val tyr tyr cys asn glu gly thr pro thr Ala Val Pro Asn Leu Arg Gly Asp Leu

CAG GTG CTG GCT CAG AAA GTT GCA GGT CCT TAC CCT TTC GAC TAC TGG GGA
Gln Val Leu Ala Gln Lys Val Ala gly pro tyr pro phe asp tyr trp gly
121
CAA GGT ACC TTA GTT ACT GTC TCT AGC GGT GGC GGA GGT TCA GGC GGT GGA GGG TCT GGA
gln gly thr leu val thr val ser ser gly gly gly gly ser gly gly gly gly ser gly
141
GGT GGC GGT AGT GAA AAT GTG CTG ACC CAA TCT CCA AGC TCC ATG TCT GCT TCT GTT GGC
gly gly gly ser glu asn val leu thr gln ser pro ser ser met ser ala ser val gly
161
GAT AGA GTA ACC ATC GCT TGT AGC GCA TCC TCT AGT GTC CCA TAT ATG CAC TGG TTT CAA
asp arg val thr ile ala cys ser ala ser ser ser val pro tyr met his trp phe gln
181
CAG AAG CCA GGT AAA AGC CCA AAG TTG TTG ATT TAT TCG ACA TCC AAC TTG GCT TCT GGA
gln lys pro gly lys ser pro lys leu leu ile tyr ser thr ser asn leu ala ser gly
201
GTG CCT TCA AGG TTT TCT GGT TCC GGC TCA GGA ACC GAT TAT AGT TTG ACT ATT AGC TCA
val pro ser arg phe ser gly ser gly ser gly thr asp tyr ser leu thr ile ser ser
221
GTG CAG CCA GAG GAT GCT GCA ACC TAC TAT TGC CAG CAA AGG TCC TCA TAT CCA CTG ACT
val gln pro glu asp ala ala thr tyr tyr cys gln gln arg ser ser tyr pro leu thr
241 Not1
TTC GGG GGT GGA ACG AAG TTG GAA ATC AAG GCT GCGGCCGCCTGTCATCATCATCATCATCAT
phe gly gly gly thr lys leu glu ile lys ala cys

Figure 5.11 - Sequencing results for insertion of B6.3 into PPICZαBcys showing VP1 peptide and proline mutation (red), Not 1 restriction enzyme site (green) and cystine (blue)

5.3.4 Production of shMFE in puc 119 vector then in PPICZαcys vector

For control experiments, the original CEA binding scFv shMFE without VP1 insert or proline mutation needed to be inserted into the modified PPICZαBcys vector. First, shMFE was amplified using PCR from PTCON vector and inserted into puc119 vector using primers shMFE sense (**5**^{1}CATGCCATGGCCCAAGTTAA ACTGGAACAGTCC**3**^{1}) and shMFE antisense (**5**^{1}ATAGTTTAGCGGCCGCAG CCTTGATTTC3^{1}).

The PCR products and puc119 vector then cut using restriction enzymes Nco1 and Not1. The products of digestion were then ligated and the new construct shMFE/puc119 was transformed into TG1 cells. The cells were grown overnight then colonies picked for PCR screening and subsequently sent for sequencing (Appendix 1, Figure A1.5).

Having inserted shMFE into puc119 vector, the DNA encoding for shMFE can now be cut from the vector and inserted into PPICZαBcys vector using restriction enzymes Sfi1 and Not1. Figure 5.12 shows the products of digestion run on agarose gel.

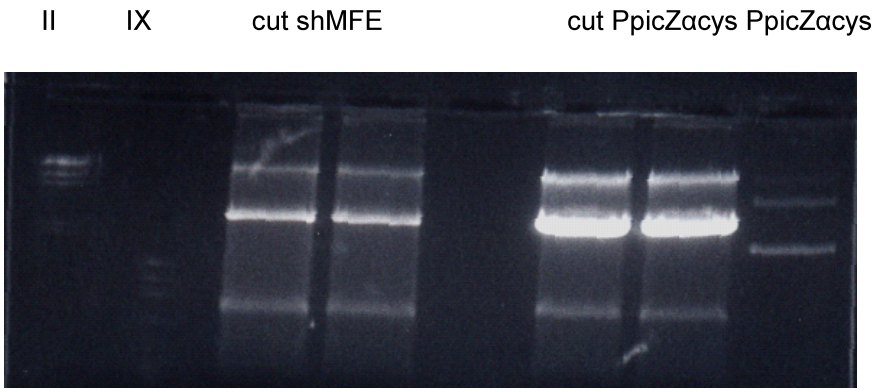

Figure 5.12 - 1% agarose gel showing products after digestion of shMFE and PPICZαBcys compared to undigested controls.

Following digestion, the bands containing the products of digestion were excised from gel and ligated together. Ligated product was extracted using phenol and electroporated into TOP 10F[1] *E. coli* cells for growth on LB/zeocin plates. Colonies were selected to be sent for sequencing following PCR colony screening using shMFE sense and shMFE antisense primers. Figure 5.13 shows sequencing results with original tyrosine residue in red in position 115, no VP1 insert and cystine residue shown in blue. Entire sequence data can be seen in appendix 1 (Figure A1.6)

101
GCC GTA TAC TAC TGC AAC GAA GGG ACA CCA ACT GGT CCT TAC TAT TTC GAC TAC TGG GGA
ala val tyr tyr cys asn glu gly thr pro thr gly pro tyr tyr phe asp tyr trp gly
121
CAA GGT ACC TTA GTT ACT GTC TCT AGC GGT GGC GGA GGT TCA GGC GGT GGA GGG TCT GGA
gln gly thr leu val thr val ser ser gly gly gly gly ser gly gly gly gly ser gly
141
GGT GGC GGT AGT GAA AAT GTG CTG ACC CAA TCT CCA AGC TCC ATG TCT GCT TCT GTT GGC
gly gly gly ser glu asn val leu thr gln ser pro ser ser met ser ala ser val gly
161
GAT AGA GTA ACC ATC GCT TGT AGC GCA TCC TCT AGT GTC CCA TAT ATG CAC TGG TTT CAA
asp arg val thr ile ala cys ser ala ser ser ser val pro tyr met his trp phe gln
181
CAG AAG CCA GGT AAA AGC CCA AAG TTG TTG ATT TAT TCG ACA TCC AAC TTG GCT TCT GGA
gln lys pro gly lys ser pro lys leu leu ile tyr ser thr ser asn leu ala ser gly
201
GTG CCT TCA AGG TTT TCT GGT TCC GGC TCA GGA ACC GAT TAT AGT TTG ACT ATT AGC TCA
val pro ser arg phe ser gly ser gly ser gly thr asp tyr ser leu thr ile ser ser
221
GTG CAG CCA GAG GAT GCT GCA ACC TAC TAT TGC CAG CAA AGG TCC TCA TAT CCA CTG ACT
val gln pro glu asp ala ala thr tyr tyr cys gln gln arg ser ser tyr pro leu thr
241 Not1
TTC GGG GGT GGA ACG AAG TTG GAA ATC AAG GCT GCGGCCGCCTGTCATCATCATCATCATCAT
phe gly gly gly thr lys leu glu ile lys ala cys

Figure 5.13 - Sequencing results for insertion of shMFE into PPICZαBcys showing original tyrosine (red), Not 1 restriction enzyme site (green) and cystine (blue). Compare to sequencing in section 5.3.3.

5.3.5 Transformation of B6.3 and shMFE into X33 cells for production in *Pichia pastoris*

Sequencing confirmed the correct sequence of B6.3 and shMFE in the PPICZαBcys vector so allow large scale production of the scFv in *P.pastoris,* the construct was first linearised using Pme1 enzyme and run on agarose gel (figure 5.14).

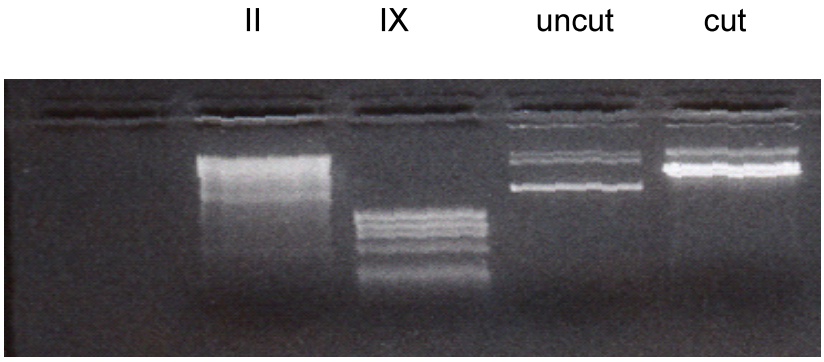

Figure 5.14 - 1% agarose gel showing B6.3/PPICZαBcys after digestion with Pme1, compared to control uncut B6.3/PPICZαBcys and molecular weight markers II, IX.

Similarly, to produce shMFEcys in large scale and having confirmed the correct sequence above, Pme1 enzyme was used to linearise shMFE/PPICZαBcys construct, the results of which are shown below in figure 5.15.

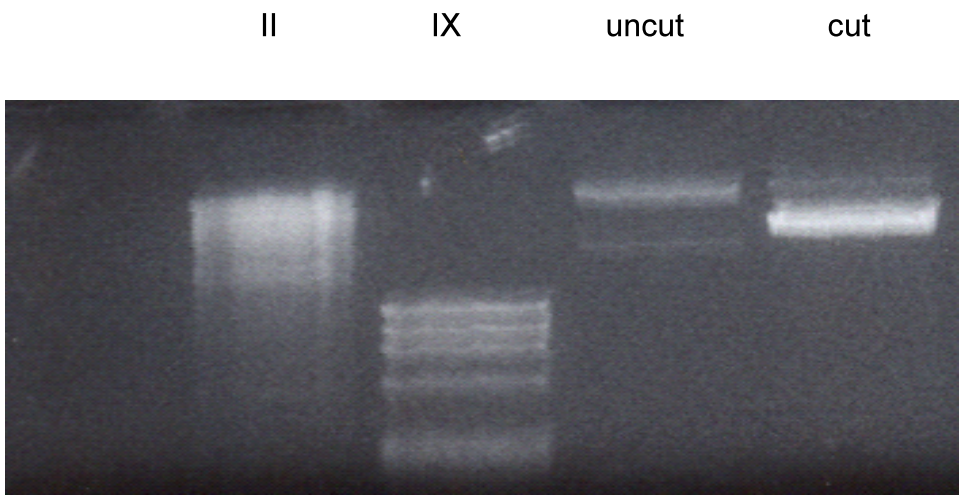

Figure 5.15 - 1% agarose gel showing shMFE/PPICZαBcys after digestion with Pme1, compared to control un cut shMFE/PPICZαBcys and molecular weight markers II, IX.

For both the shMFE and B6.3, the linearised DNA was cut from agarose gel, purified and transformed into X33 cells which were grown on YPD/zeocin plates. 10 colonies were selected for PCR colony screening using primers 5^1AOX (**5^1**GACTGGTTCCAATTGACAAGC**3^1**) and 3^1AOX (**5^1**GCAAATGGCATTCTGACATCC**3^1**) and colonies grown in BMGY media to check for protein expression. Figures 5.16 and 5.17 show expression of B6.3 and shMFE detected by western blot following incubation with methanol.

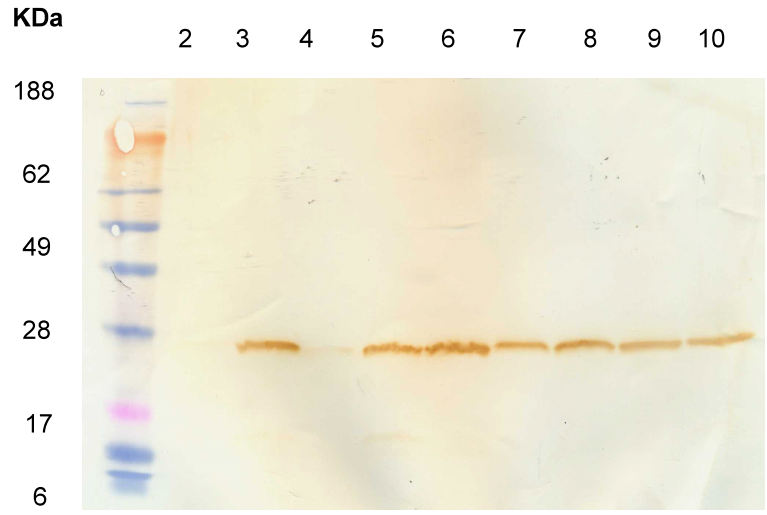

Figure 5.16 - Western blot showing expression of B6.3 in separate colonies labelled 2-10 after 33 hrs incubation. All colonies except for 2,4 show good expression levels

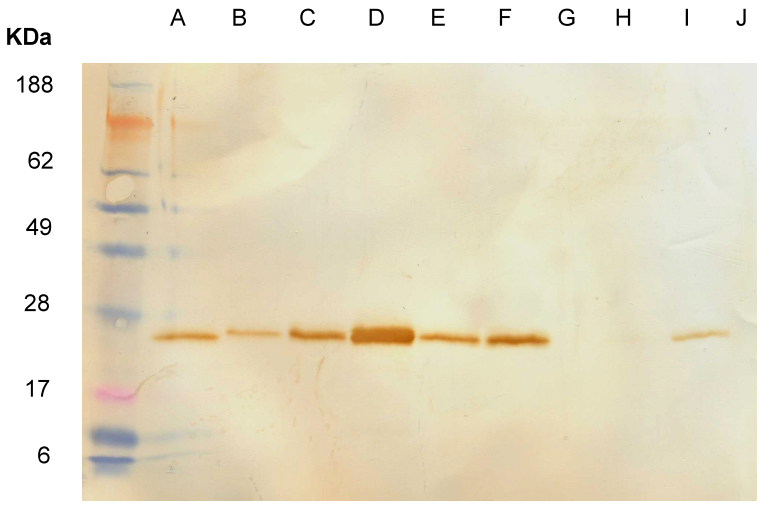

Figure 5.17 - Western blot showing expression of shMFE in separate colonies labelled A-J after 33 hrs incubation. Colony D shows a particularly high level of expression.

The colony which showed high levels of protein expression was then grown and large scale production continued. Fermentation in *P.pastoris* produced yields of 0.98mg/ml after initial expanded bed-IMAC chromatography. Size exclusion chromatography using Superdex 75 column revealed B6.3 eluted almost exclusively as a non-covalent dimer (Figure 5.18). This was unexpected as previously, the non humanised MFEVP1(P) was produced in *P.pastoris* as a monomer (Kogelberg *et al* 2008). The

purified dimer was a stable construct and could not be split into monomeric form even after freeze thawing, exposure to 3 M urea, in extremes of both acidic and basic pH.

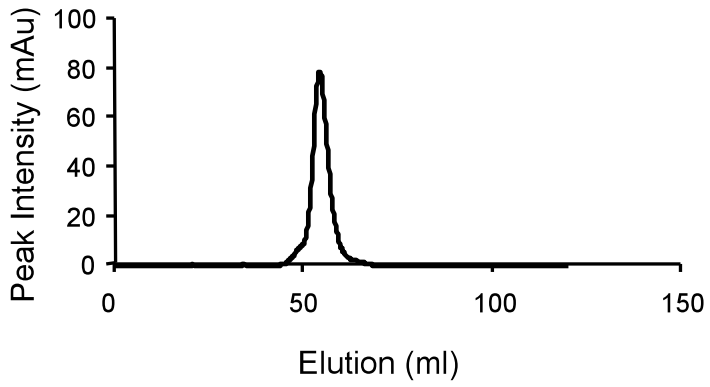

Figure 5.18 - B6.3 seen produced almost exclusively as a dimer following size exclusion chromatography using a Superdex 75 column.

5.3.6 B6.3 specifically binds its ligand αvβ6

To examine the specificity of B6.3 to it's ligand αvβ6, ELISAs were set up which showed B6.3 bound to immobilized αvβ6. Figure 5.19 shows binding of B6.3 in comparison to the murine MFEVP1(P) and MFE with TBS as a control.

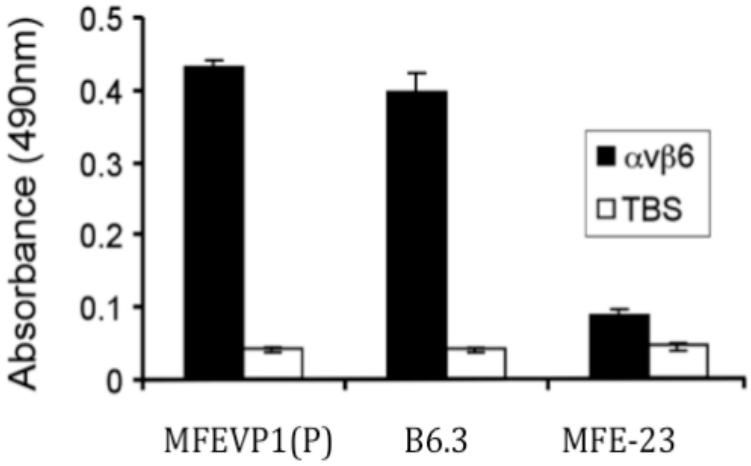

Figure 5.19 - ELISA showing B6.3 bound to immobilized αvβ6. B6.3, MFEVP1(P) and MFE-23 were applied at 20µg/ml to immobilized αvβ6. Binding was detected with mouse anti-Tetra-His IgG followed by sheep anti-mouse horseradish peroxidase (HRP) linked secondary antibody. The data represent the mean of triplicate measurements and error bars represent the standard deviation at each data point.

This ELISA confirms B6.3 binds immobilised αvβ6 in comparison to MFEVP1(P) and in comparison to MFE which shows minimal binding only. Specificity of B6.3 for the ligand αvβ6 was also confirmed on flow cytometry using the αvβ6 expressing cell line HT29 (Fig 5.20)

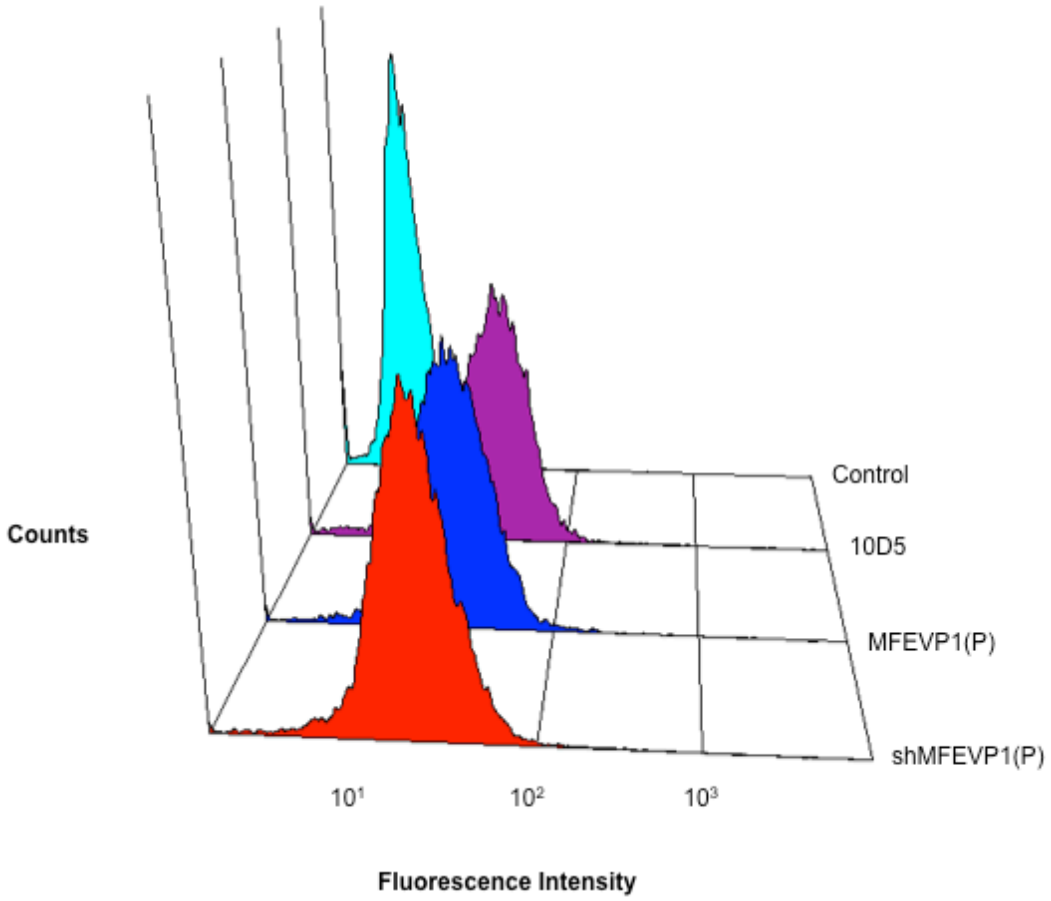

Fig 5.20 - FACS - HT 29 cells were incubated with B6.3, MFEVP1(P), 10D5 and MFE-23 (all at 100 µg/ml). Binding was detected with monoclonal mouse anti-polyhistidine followed by PE- labeled anti-mouse IgG. In the omission control shown, cells were incubated with MFE-23 at 50 µg/ml followed by R-PE-labeled goat anti-rabbit IgG.

5.4 Magnetic Alternating Current Hyperthermia (MACH)

The second aim of this chapter is to investigate the potential for the use of B6.3 to target αvβ6 expressing cells for the delivery of MACH. MACH requires the use of superparamagnetic nanoparticles and two particles were investigated, Chemicell DX and FDA approved Resovist. MACH was generated using the Magnetic Alternating Current Hyperthermia (MACH) system kindly supplied by Professor Quentin Pankhurst of the Royal Institution of Great Britain.

5.4.1 Heating of nanoparticles using the MACH system

Nanoparticles at concentrations between 0.1mg/ml and 10mg/ml were placed within the alternating magnetic field at 150V, 0.74A, 1 Mhz and temperature measurements were taken from a starting temperature of 37°C to simulate human body temperature. Chemicell DX particles achieved a maximum temperature of 61.5°C at 10mg/ml after 6 mins and at 1mg/ml, the maximum temperature reached was 43°C (Figure 5.21 and Figure 5.23).

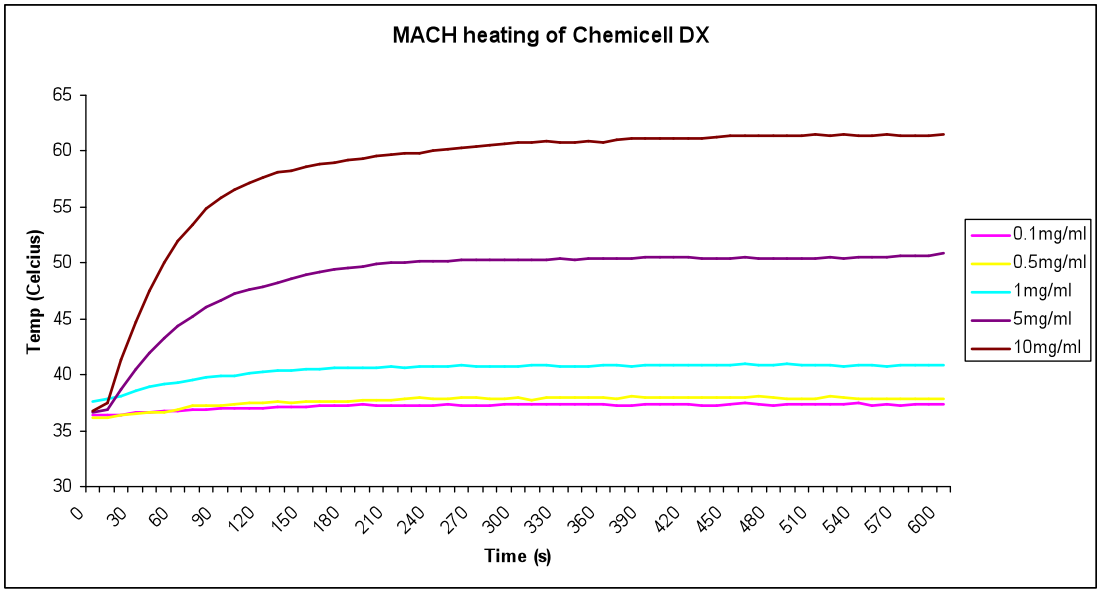

Figure 5.21 - Graph showing heating of Chemicell DX particles at concentrations from 0.1mg/ml to 10mg/ml. Particles were suspended in 0.5mls of water in 1.5ml eppendorf tubes and temperature measurements taken using the Luxtron probe.

Resovist heating at 10mg/ml resulted in a maximum temperature of 70°C and of 41°C at 1mg/ml giving temperature increases of 33 °C and 4°C respectively (Figure 5.22 and Figure 5.23)

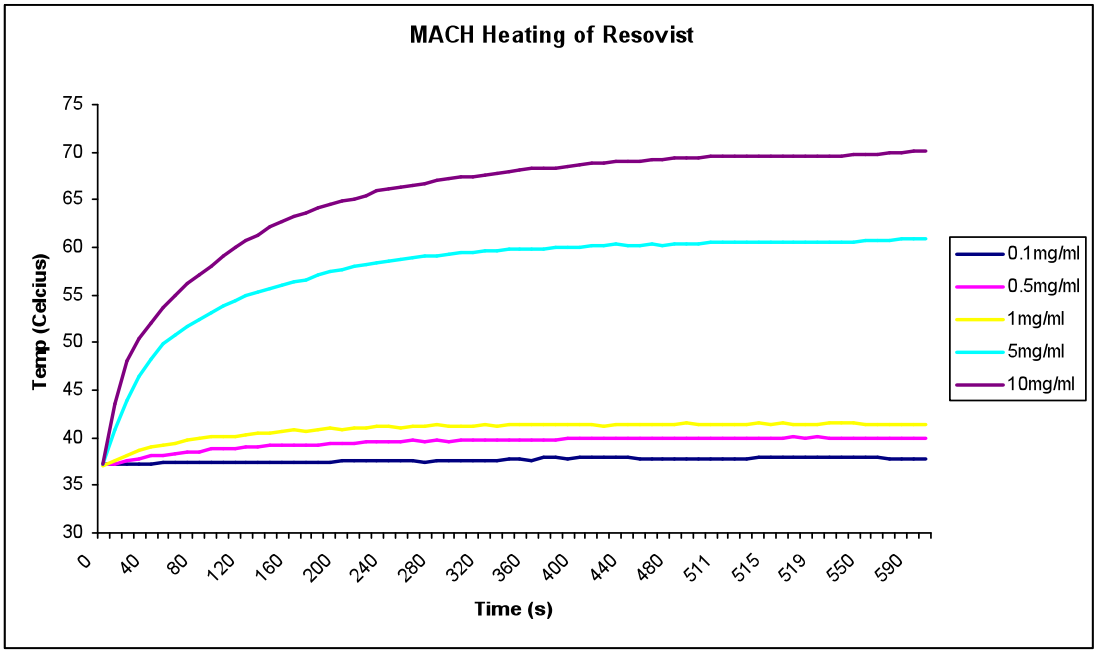

Figure 5.22 - Graph showing heating of Resovist particles at concentrations from 0.1mg/ml to 10mg/ml. Temperature increases were measured using the Luxtron probe and particles were suspended in 0.5mls water in 1.5ml eppendorf tubes as before.

The Figure 5.23 below shows the maximum temperatures reached for both Chemicell DX and Resovist when starting from 37°C. The increasing maximum temperature reflects the increasing concentration of iron found at higher nanoparticles concentration levels. For therapeutic hyperthermia the temperature increase would need to be at least 4°C as significant cell death is only seen at temperatures of 41°C and above (Jordan *et al*., 1999).

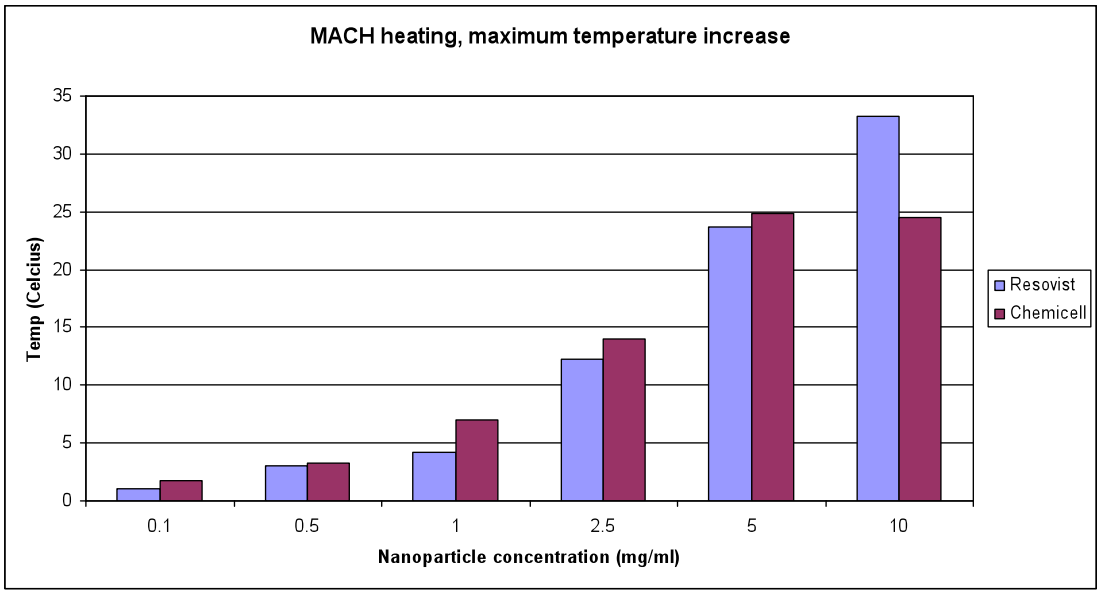

Figure 5.23 - Graph showing maximum temperature increases achieved for Resovist and Chemicell DX nanoparticles at concentrations from 01.mg/ml to 10mg/ml when placed within an alternating magnetic field at 1Mhz.

5.4.2 Heating of B6.3-nanoparticle conjugates

Resovist and Chemicell DX both display superparamagnetic properties enabling their use in the generation of MFH however each particle has a different coating. Resovist has a dextran COO- coating and Chemicell a Dextran OH- coating. Chemicell particles were conjugated using the cyanogen bromide method and Resovist using carbodiimide activation (Figure 5.24).

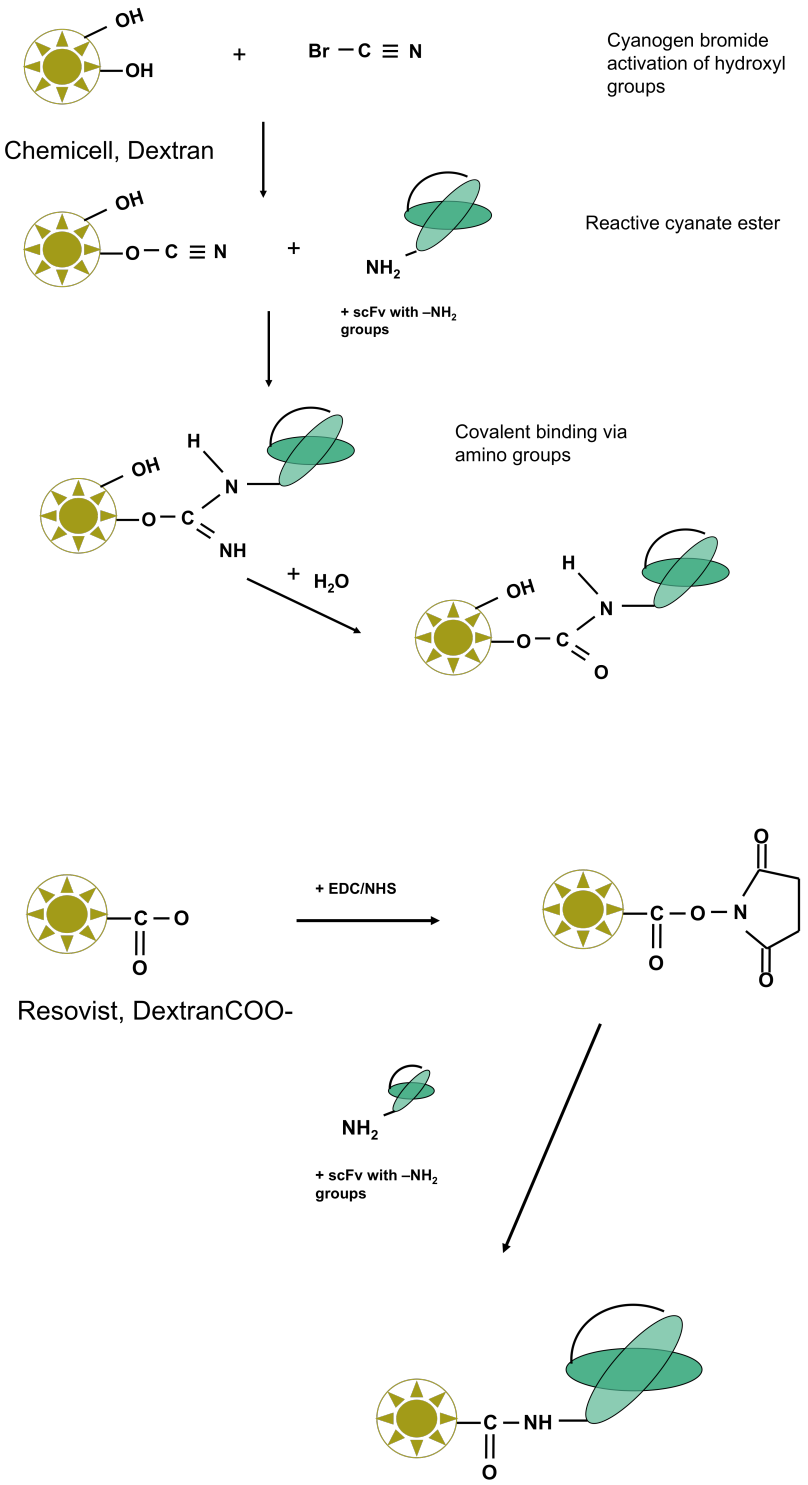

Figure 5.24 – Alternative conjugation methods used for joining B6.3 and Cemicell and Resovist nanoparticles.

Results below indicate that the scFv-nanoparticle conjugates retain the ability to generate heat when placed within the alternating magnetic field of the MACH machine. The particle concentration used were 0.25mg/ml to 1.25mg/ml to reflect potential in vivo situation, as it is unlikely that intravenously delivered scFv-nanoparticle conjugates would accumulate at the tumour site at concentrations higher than this. Figures 5.25 and 5.27 show increases in heating potential of B6.3-Chemicell DX conjugates to a maximum of 44.8°C at 1.25 mg/ml after 4mins 20 sec.

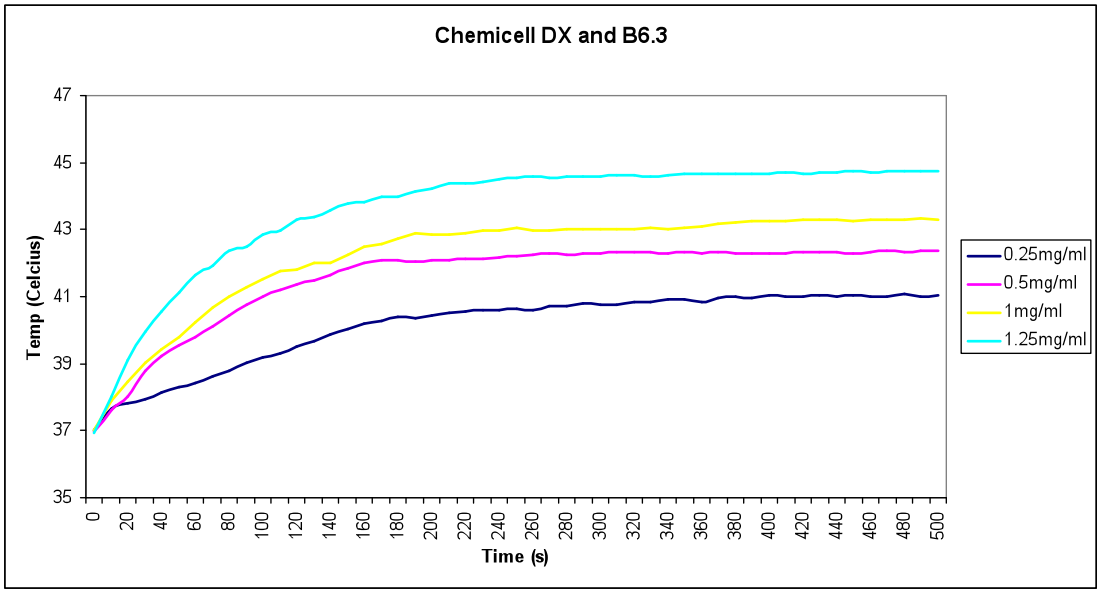

Figure 5.25 – Heating potential of conjugates of B6.3 and Chemicell DX particles at varying concentrations. Maximal heating achieved was 44.8°C at 1.25mg/ml of Chemicell nanoparticles. Temperature required for cell death (>41°C) was reached at concentration of 0.5mg/ml after less than 2 minutes exposure to MFH. ScFv-nanoparticle conjugates were suspended in 0.5mls water in 1.5ml eppendorf tubes.

MACH heating of Resovist and B6.3 conjugates showed that concentrations of greater than 0.5mg/ml were required to reach temperatures of over 41°C. There was little difference seen in the behaviour of conjugates at 0.25mg/ml and 0.5mg/ml although the rate of temperature increase at concentrations of 1 and 1.25mg/ml of B6.3 and Resovist was faster than that seen with the B6.3 and Chemicell-DX conjugates (Figure 5.26 and 5.27).

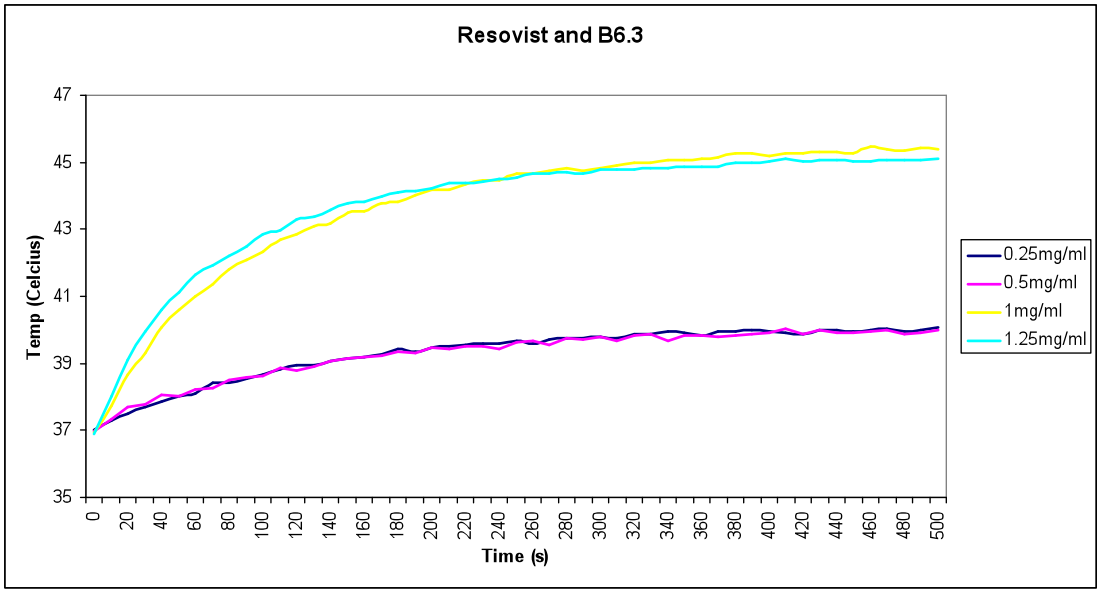

Figure 5.26 – Heating potential of conjugates of B6.3 and Resovist particles at varying concentrations. At concentrations of 0.5mg/ml the maximum temperature achieved was 40°C however at 1mg/ml, 41°C was reached after only 68 seconds heating. Temperature measurements were taken using the Luxtron temperature probes placed in the 1.5ml eppendorf tubes used to contain the 0.5mls water in which the conjugates were suspended.

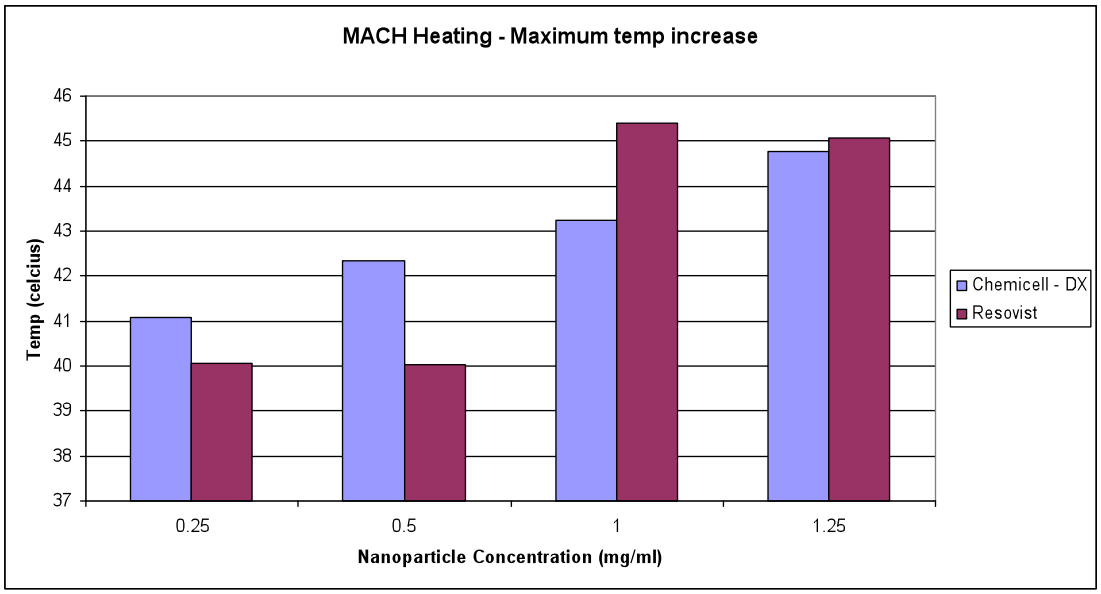

Figure 5.27 – Graph showing the maximum temperature increases seen when Resovist and Chemicell – B6.3 conjugates were exposed to MACH at varying concentrations. Maximal heating was seen with Resovist-B6.3 at 1mg/ml with a temperature increase to 45.3°C from a baseline of 37°C.

5.4.3 Iron uptake Assay

To investigate whether the conjugation of B6.3 to the nanoparticles increased the cellular uptake of nanoparticles compared to nanoparticles alone, B6.3 -nanoparticle conjugates were incubated with αvβ6 expressing cell lines and the amount of iron in the cell was measured using a Ferrozine assay as described in chapter 2. Experiments were repeated in triplicate and at varying concentrations. Figure 5.28 shows the colour change seen at the end of the assay with the darker colour indicating increasing iron uptake.

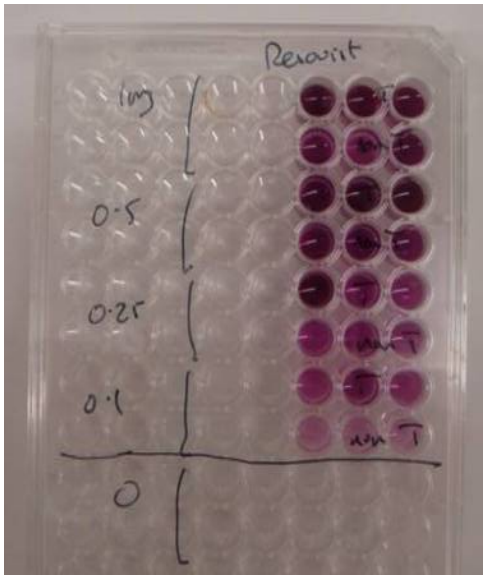

Figure 5.28 – Example of the final stage of a Ferrozine iron uptake assay showing varying concentrations of 'targeted' B6.3-Resovist conjugates alongside varying concentrations of non targeted Resovist ('non-T'). As the concentration of nanoparticles increases from 0.1mg/ml to 1mg/ml, there is a darker colour seen, indicating a greater concentration of iron is present.

When B6.3-Chemicell-DX conjugates were incubated with the αvβ6 expressing A375 cell line, there was a clear increase in relative iron uptake compared to when Chemicell-DX alone was incubated with A375 cells. Figure 5.29 shows the relative iron uptake of targeted and non-targeted Chemicell-DX nanoparticles at concentrations from 0.1mg/ml through to 2.5mg/ml.

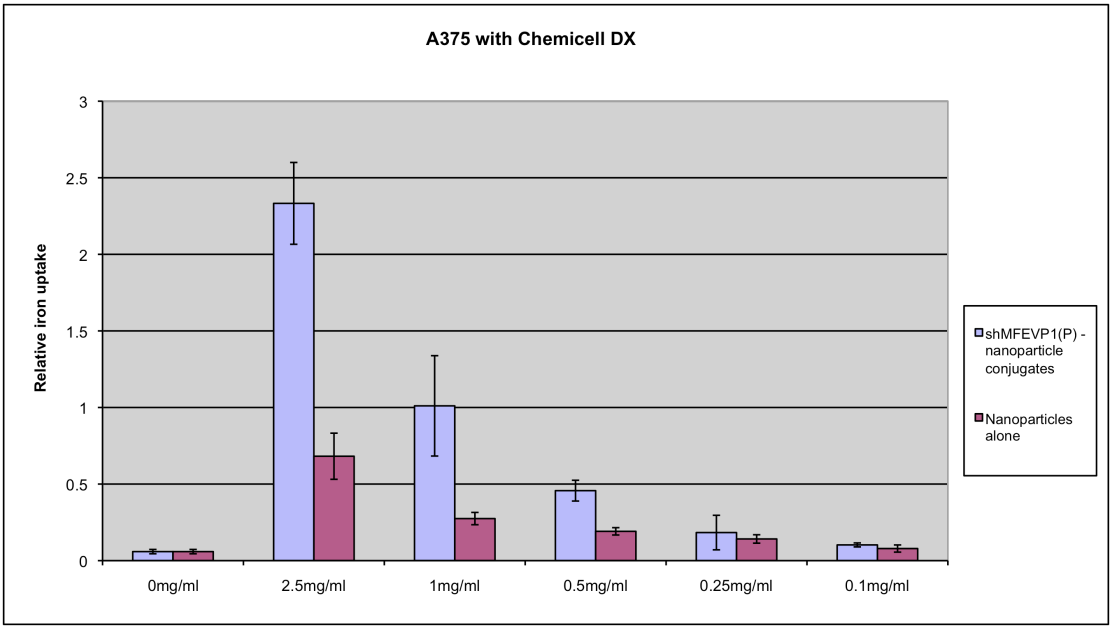

Figure 5.29 – Results of Ferrozine assay showing relative iron uptake by αvβ6 expressing cell line when cells were incubated with targeted B6.3 – Chemicell DX conjugates compared to Chemicell DX alone. Experiments were done in triplicate and show that targeted nanoparticles are better taken up than non-targeted at each concentration tested.

Looking at iron uptake by A375 cells after incubation with Resovist and with B6.3-Resovist conjugates, there was again increased uptake with targeted compared to the non targeted nanoparticles and this observation was again seen at every concentration (Figure 5.30).

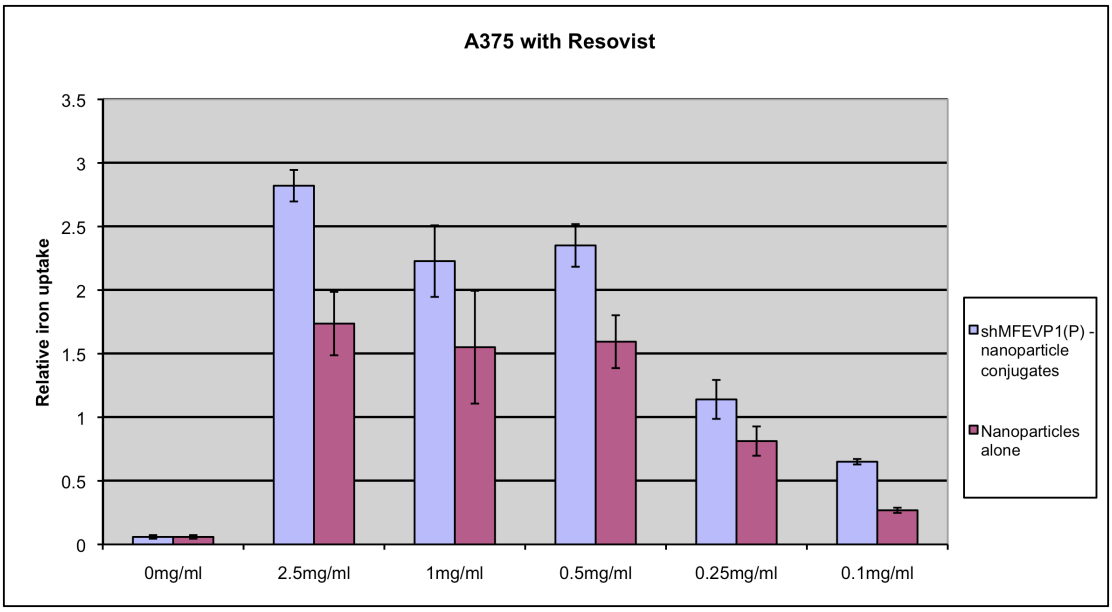

Figure 5.30 – Relative iron uptake seen with the Ferrozine assay comparing targeted and non targeted Resovist nanoparticles at varying concentrations. Experiments again carried out in triplicate. Maximal iron uptake is seen at concentrations of 2.5mg/ml.

5.4.4 MACH directed cell death

This series of experiments was set up to investigate whether there was any difference in cell death when cells incubated with targeted or non targeted nanoparticles were exposed to MACH. Three different αvβ6 expressing cell lines were selected; HT29, VB6, A375 and both Chemicell-DX and Resovist nanoparticles were tested with each cell line. Cells were then incubated with either targeted B6.3 conjugated nanoparticles or non-targeted nanoparticles with cells alone used as a control. Cells that were incubated with nanoparticles were then split into two groups – a 'wash' and 'non-wash' group to remove any non specific binding of nanoparticles to the cells. Cells were then exposed to MACH and cell survival estimated using a standard MTT assay. Full experimental details are set out in Chapter 2.

Figure 5.31 shows the MACH machine and cells being placed with the coil which generates the alternating magnetic current and Figure 5.32 shows 96 well plates with cells plated out at varying concentrations from which strips of cells were removed to be placed within the MACH coil. In all cases, the ambient temperature was

maintained at 37°C using the Air Therm to simulate the *in-vivo* situation and results from these experiments are presented in Figures 5.33 to 5.35.

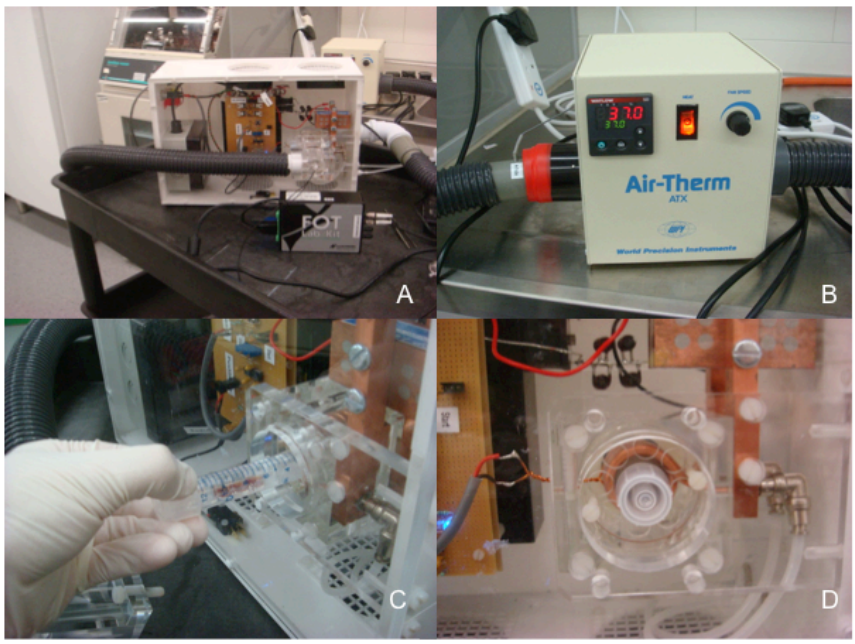

Figure 5.31 – Experimental set up: A) MACH machine, B) Airtherm unit keeping baseline temperature at 37°C to simulate in-vivo situation, C) Single strip from 96 well plate containing cells within sterile tube, D) Cells placed within the coil where they are exposed to an alternating magnetic current.

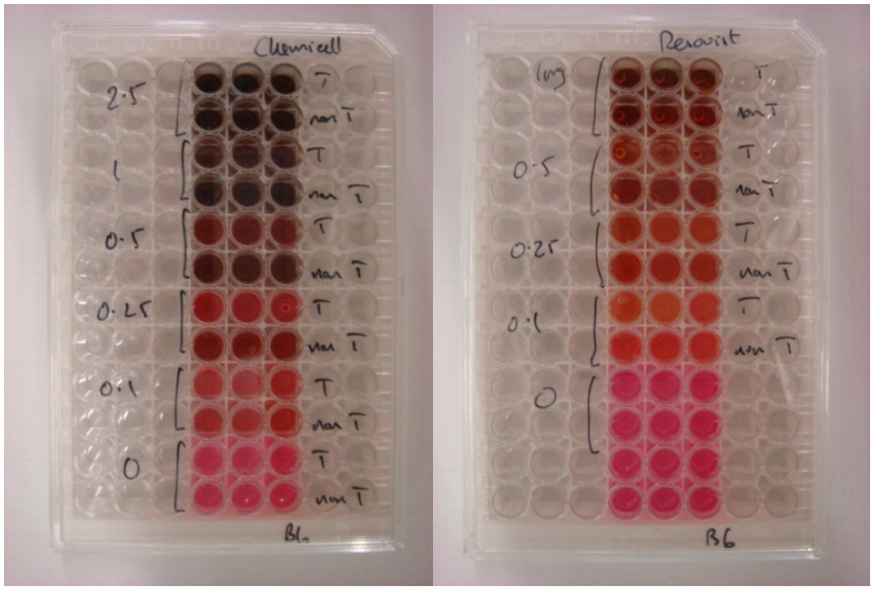

Figure 5.32 – 96 well plates showing VB6 cells incubated with varying concentrations of nanoparticles, both B6.3 conjugated ('T') alone ('non T'). The experiments were repeated in triplicate and horizontal rows of wells were removed in turn to be exposed to MACH before being returned to the incubator.

Chemicell

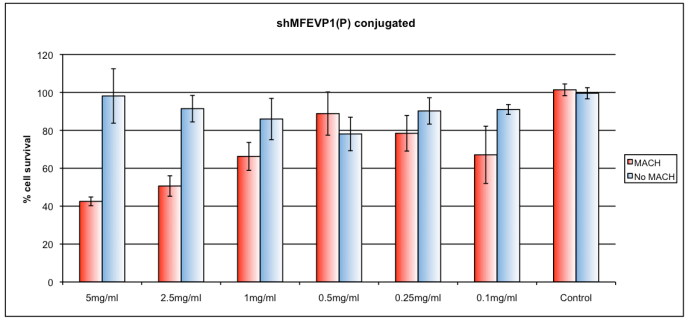

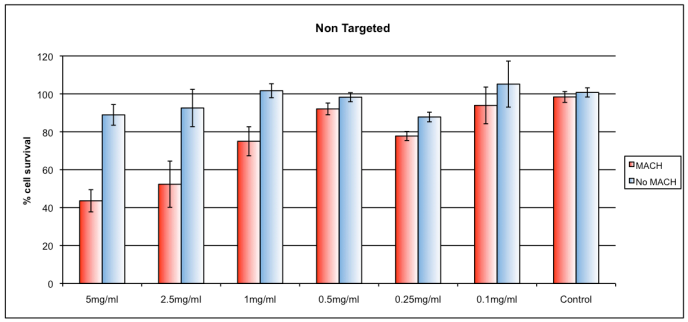

Resovist

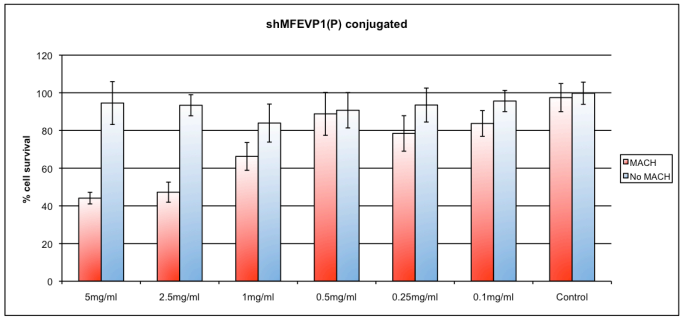

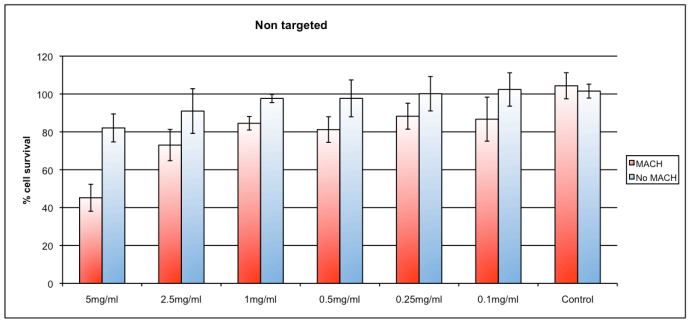

Figure 5.33 – VB6 cells with targeted and non targeted Chemicell and Resovist particles

Chemicell

Resovist

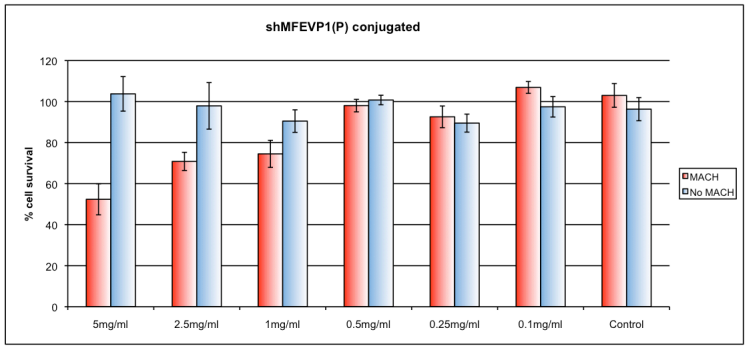

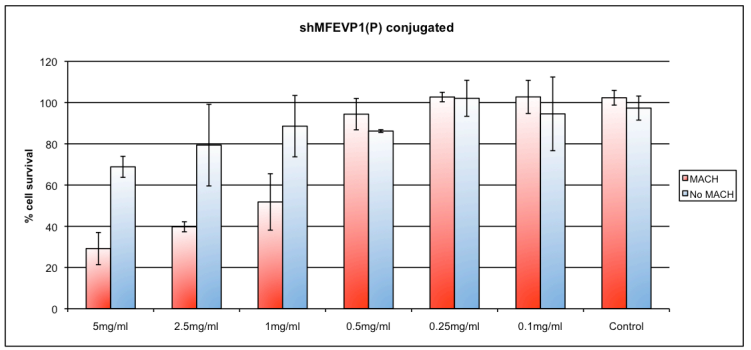

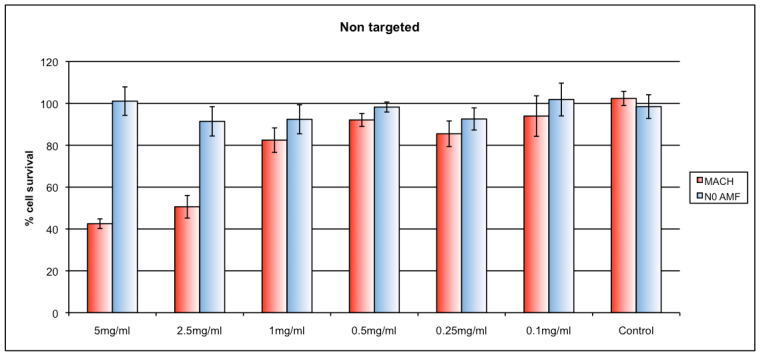

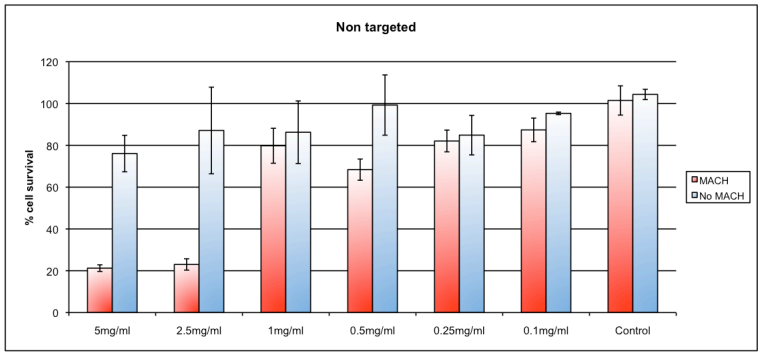

Figure 5.34 – A375 cells with targeted and non targeted Chemicell and Resovist particles

Chemicell

Resovist

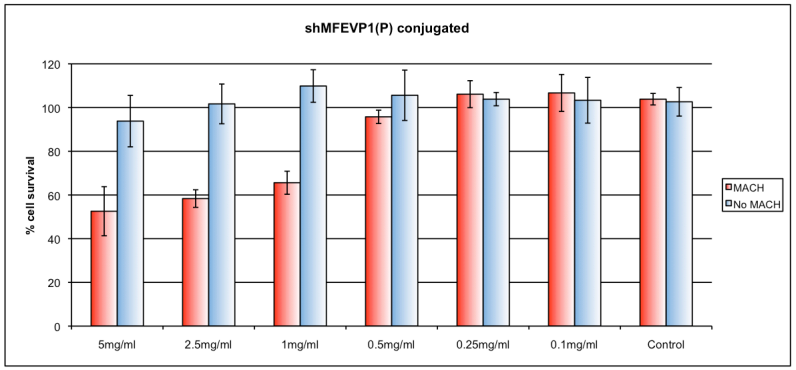

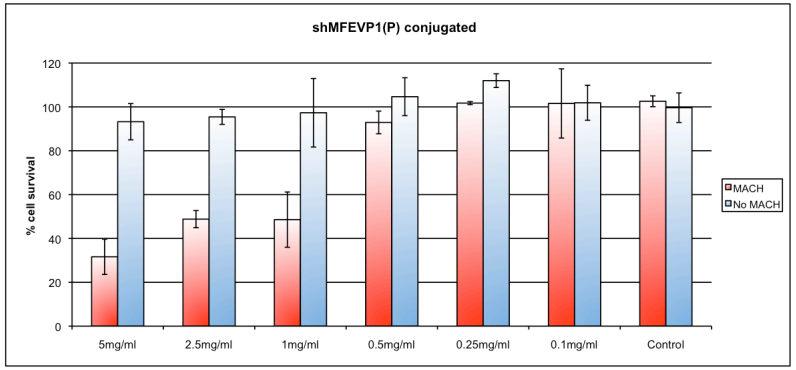

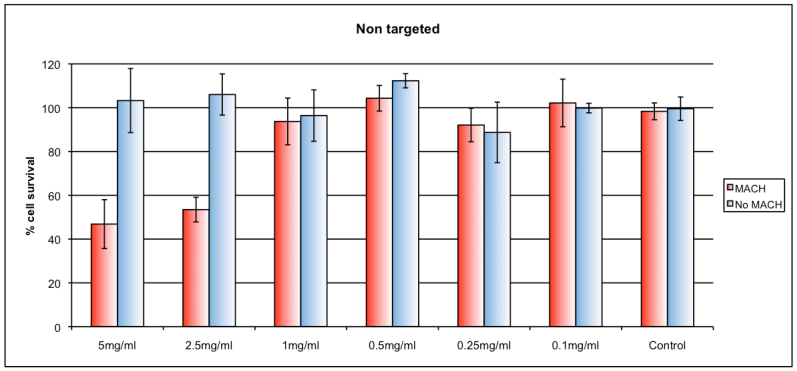

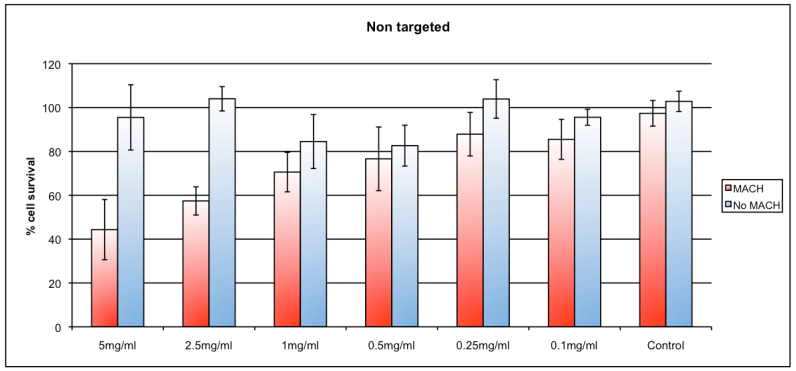

Figure 5.35 – HT29 cells with targeted and non targeted Chemicell and Resovist particles

Taking an overview of the data produced from these cell death experiments, there is a clear reduction in cell survival following exposure to MACH at particles concentrations of 2.5mg/ml and 5mg/ml when compared to cell survival in the 'no MACH' group. This observation is consistently seen in all three cell types, with both Chemicell and Resovist nanoparticles and the effect appears to be irrespective of whether the nanoparticles are targeted or not. A second conclusion that can be drawn from the experiments is that MACH itself does not appear to be harmful to the cells as cell survival in the control groups (cells only) remains at around100% again for all three cell types and in each separate experiment.

Looking at potentially more physiologically more feasible nanoparticle concentrations of 1mg/ml and below, for all cell types at 1mg/ml there remains a reduction in cell survival when cells incubated with nanoparticles are exposed to MACH compared to the 'no MACH' group. Table 5.1 shows the % cell survival of all three cell types and shows a significantly increased cell kill with targeted Resovist particles and A375 cells (p=0.01), this effect is also seen with HT29 cells and targeted Chemicell particles (p=0.04).

	Chemicell		**Resovist**	
	Cell Survival (%)	P value	Cell Survival (%)	P value
VB6				
Targeted	66.2		66.2	
Non targeted	75.0	0.35	84.5	0.08
A375				
Targeted	74.5		51.8	
Non targeted	82.4	0.33	79.8	*0.01
HT29				
Targeted	65.6		48.6	
Non targeted	93.7	*0.04	70.6	0.11

Table 5.1: Comparison of % cell survival seen when cells are incubated with 1mg/ml either non targeted or targeted (B6.3 conjugated) nanoparticles and exposed to MACH. Significant findings asterisked.

At concentrations less than 1mg/ml there was no significant differences seen in cell survival rates for any cell type between cells exposed to MACH and those not exposed to MACH for either targeted or non targeted particles.

5.5 Discussion

Using a stepwise, rational structure based design approach, the novel scFv B6.3 has been manufactured using the CEA binding MFE-23 scFv as a scaffold. MFE-23 was chosen as it is has been used in clinical trials and is well characterized (Boehm *et al* 2000, Lee at al 2002, Sainz-Pastor *et al* 2006).

The first aim of this chapter was to insert the GH loop of the VP1 FMDV peptide into the CDR3 loop of shMFE-23 and to generate a novel scFv specific for αvβ6. Previously, it has been shown that αvβ6 strongly binds the FMDV using β6 transfected cells whereas other integrins such as α5β1 and αvβ6 were not seen to be important for FMDV to bind epithelial cells (Jackson *et al* 2000). Thus, it was predicted that the αvβ6 binding capacity of VP1 peptide could be conferred to the scFv shMFE.

To increase the specificity of the novel peptide, a proline to tyrosine mutation was introduced using the same PCR reaction to introduce the VP1 peptide sequence. Previously this single residue mutation at Y100bP was predicted to reduce CEA binding and has since been shown to eliminate binding of MFE-23 to CEA (Boehm and Perkins 2000, Read *et al* 1995). Throughout this chapter, the humanised version of MFE-23 has been used in an attempt to minimise anti-mouse antibody production if this construct is to be used in human trials in the future.

The αvβ6 specific scFv was produced in yeast *P.pastoris* to GMP standards at concentrations of 0.98mg/ml and this antibody was subsequently shown to bind αvβ6 on ELISA. The ultimate aim of the work presented in this thesis is to produce a scFv which may ultimately be used for anti cancer therapies, in particular in OSCC. To this end,

αvβ6 was chosen as a target as the integrin has previously been shown to modulate tumour cell invasion, inhibit apoptosis, regulate protease expression and activate TGF-β1 and importantly, there is minimal expression on healthy epithelium (Ahmed *et al* 2002).

Magnetic fluid hyperthermia is a novel approach to cancer therapy using an externally generated alternating magnetic field to excite and generate heat on nanometre sized iron particles which are in close proximity to tumour cells. Previously this approach has been shown to be feasible and safe when delivered by direct intratumoural injection in clinical trials in patients with brain and prostate cancers (van Landeghem *et al* 2009, Johannsen *et al* 2006). An alternative to direct intratumoural injection is to attach MNPs to scFvs with the aim of using the scFvs to target tumour cells and deliver the nanoparticles directly to the tumour.

There are several methods to attach scFvs to MNPs, including non-specific amine attachments between the $–NH_2$ groups on the scFv and –COOH groups found on the dextran coating on MNPs. An alternative method is to use site-specific attachments between the scFv and the MNPs, to this end *P.pastoris* vector PPICZαB was successfully manipulated so that a free terminal cystine residue would be introduced when the vector was used for scFv production in *P.pastoris*. The sequencing data presented above confirm that the cystine is present in the vector. This cystine residue could be used for future experiments where site specific attachment between free –SH groups present on the cystine and the –COOH groups on dextran coated nanoparticles are required.

The second aim of this chapter was to attach commercially available magnetic nanoparticles to B6.3 and to investigate potential hyperthermia mediated cell kill. Using two alternate attachment methods, B6.3 was successfully conjugated to Resovist and Chemicell DX nanoparticles. The new conjugates were then shown to generate heat when placed within an alternating magnetic field and also greater cellular uptake of iron was seen with the scFv-conjugated particles compared to particles alone. Assessing cell death following exposure to MACH, there was a clear effect seen at concentrations of

greater than 2.5mg/ml and even at 1mg/ml a significant reduction in cell viability was seen in two out of six cell death experiments.

These data suggest that conjugating nanoparticles to scFvs results in an increased cellular uptake of nanoparticles in vitro and at concentrations greater than 1mg/ml nanoparticles combined with MACH does effect cell death in vitro compared to MACH alone. Given that intravenously delivered scFv-nanoparticle concentrations would be unlikely to reach concentrations of 1mg/ml and are more likely to be measured in nanograms/ml, perhaps a more feasible method of delivering nanoparticles to the tumour bed in vivo situation would be direct intratumoural injection as used by van Landeghem *et al* (2009). A separate possibility is that the scFv/nanoparticle conjugates could be used to treat metastases in a similar way to the detection of sentinal node with radioactive tracers or blue dye. These two methods could be considered as ways of accumulating sufficient nanoparticles to generate sufficient hyperthermia required to cause cell death.

5.6 Summary

The αvβ6 integrin is an exciting new target for SCC cancer therapy and results set out in earlier chapters have shown that the integrin is over expressed in non-melanoma skin cancers as well as in oral SCC. In this chapter, the novel scFv B6.3 has been manufactured and shown to bind αvβ6 on ELISA and FACS analysis. Further, B6.3 has been successfully conjugated to two commercially available magnetic nanoparticles, demonstrating the potential application of these new conjugates for the delivery of targeted MACH against αvβ6 expressing cell lines.

In conclusion, the results set out above have shown the successful design and manufacture of B6.3 and its potential for use in the development of MACH driven personalised medical therapies in patients with OSCC.

Chapter 6

Conclusions and Future Challenges

The aim of this thesis is to investigate the clinical usefulness of the αvβ6 integrin and it role as a potential target for antibody delivered MACH, a novel anticancer therapy. This chapter aims to review the findings presented in this thesis and to suggest potential further avenues of research.

The αvβ6 integrin is known to be over-expressed in many types of carcinoma with minimal expression in normal healthy tissues. Whilst it has previously been reported that αvβ6 is over expressed in skin SCC (Thomas et al 2006), the expression in BCC and pre-malignant actinic keratoses (AK) has not previously been studied. The results presented in chapter 3 show 32% of AK express high αvβ6 levels compared to 79% of skin SCC and 32% of BCC. Within the BCCs, the morphoeic subset were seen to show very high levels of αvβ6 expression and it was postulated that there may be a link between αvβ6 and the production of a myofibroblast rich fibrotic stroma seen in morphoeic BCCs.

Using a BCC model, data presented in Chapter 3 is suggestive that αvβ6 may activate TGF-β1 which in turn promotes invasion through the transdifferentiation of myofibroblasts. TGF-β1 is known to have a complex role in tumourigenesis and increased expression levels have been linked to cancer progression and metastatic spread in colorectal and prostate cancers (Tsushima et al 1996, Wikstrom et al 1998, Friedman et al 1995), further TGFβ has been shown to have complex interactions with the tumour microenvironment (reviewed in Bierie and Moses 2006) and to promote cell motility through the modulation of epithelial to mesenchymal transition (EMT). The concept that the tumour stroma itself can have effects on the rate of tumour progression is gaining credence and there is strong evidence that TGFβ has a role in driving myofibroblast transdifferentiation, particularly in squamous cell carcinoma (Lewis et al 2004).

The novel findings presented in Chapter 3 further support the idea that there is a synergistic relationship between tumour and tumour stroma which is in part regulated by TGFβ and highlights a possible role of αvβ6 as a pro-invasive factor in morphoeic BCC. This finding raises the possibility of targeted therapies against BCC which can be used to

modulate disease progression or recurrence, particularly in morphoeic type BCC which is often refractive to current therapies.

Considering the clinical utility of αvβ6 not only as a potential target for anti cancer therapies but also as a potential prognostic marker for advanced disease, the hypothesis 'αvβ6 is an independent prognostic marker in OSCC' was proposed and tested on a retrospective cohort of 282 patients with OSCC in Chapter 4. OSCC was selected as a cancer type to study as the 5-year survival rates remain at under 50% with very little improvement over the past 25 years. Furthermore, the integrin has recently been shown to be an independent prognostic marker in colon, cervical and gastric carcinomas (Bates et al 2005, Hazelbag et al 2007 and Zhang *et al* 2008) and is known to be over expressed in OSCC.

Following on from the identification of the importance of αvβ6 in the formation of a pro-invasive myofibroblast rich tumour stroma in Chapter 3, the myofibroblast marker SMA was also examined as a potential prognostic marker in the same cohort of patients along with standard histopathological parameters. The findings from Chapter 4 were that αvβ6 was not an independent prognostic marker however, high SMA levels were strongly and significantly associated with adverse outcomes in the group of patients studied.

Histological techniques are commonly used for analysing tumour samples due to the availability of formalin fixed paraffin embedded tissue and relative ease of application. Currently in OSCC there is no single prognostic marker in routine clinical use and the prognosis of OSCC patients is derived from the combination of several recognised pathological features (TNM staging). Weaknesses with the TNM system for OSCC include the fact that it only includes the tumour diameter and not tumour depth which is the measurement found to consistently predict significantly poorer outcomes in OSCC however there is no clear consensus on the cut off point for tumour depth after which patients have a clearly adverse prognosis (Asakage *et al* 1998, Jung *et al* 2009). Broders classification of well, moderate or poorly differentiated tumours has been used since 1920 to provide prognostic information for various tumour types but has been shown to

be of limited value in predicting prognosis in OSCC (Okamoto et al 2002, Woolgar 2006). Many molecular markers in OSCC have been examined and to date no one marker has been confirmed as providing accurate prognostic information. Clearly if there were a single marker that could be routinely examined for in laboratories and could provide an accurate prediction of prognosis this would greatly aid with the planning of future treatment strategies.

Data presented in this thesis is in agreement with Vered *et al* (2010) who have recently shown that cancer associated fibroblasts as detected by SMA staining are an independent predictor of tumour recurrence in OSCC and they have also shown the persistence of these cells in OSCC metastases. Similarly, data from this cohort of patients shows that high SMA expression is significantly associated with metastasis and extracapsular spread, raising the possibility that the myofibroblastic rich stroma may promote tumour dissemination. These findings tie in with the results from chapter 3, again highlighting the importance of the tumour stroma in modulating disease progression and identifying SMA as a possible target for future therapies.

The final step in testing the clinical utility of αvβ6 integrin was to develop a technique to target the integrin and to use this to deliver anticancer therapy directly to tumour cells expressing αvβ6. Targeted hyperthermia was selected as the anticancer therapy of choice as it was felt that the heat might also affect the tumour stromal cells that had been identified as important for the promotion of tumourigenesis and to be indicators of adverse prognosis in the previous chapters. The work presented in Chapter 5 therefore details the design of a scFv antibody fragment specific for the αvβ6 integrin and the subsequent conjugation to nanoparticles for the generation of targeted hyperthermia.

Clearly there are many challenges to overcome before we are able to effectively treat OSCC patients with targeted MACH driven therapies. Data from Chapter 5 shows that the B6.3 scFv binds αvβ6 and that *in-vitro* B6.3-nanoparticle conjugates show increased cellular uptake. Furthermore, significant cell death is seen when cells and nanoparticles are exposed to MACH at concentrations of greater than 1mg/ml. These findings can be

compared to results from human experiments in patients with glioblastoma multiforma and prostate cancer in which nanoparticles were directly injected into the tumour giving very high particle/tumour concentrations of 10mg/ml (Maier-Hauff et al 2007, Johannsen et al 2010). Other groups have achieved significant heating of tumours in murine experiments using nanoparticle concentrations were around 315ug per ml of tumour in which nanoparticle/antibody conjugates were delivered intravenously (DeNardo et al 2005).

The particles used in this thesis were chosen for their heating ability using the MACH system available and the ability to conjugate the particles to scFvs (Vigor 2010 PhD thesis). New particles are constantly becoming available and in the future it may be possible to increase the frequency and power delivered by MACH machine which may also effect greater heat generation. Possible future directions for research in this area include *in-vivo* experiments using the current B6.3-nanoparticle conjugates looking at biodistribution and histological effects of MACH using SCC tumour xenographs. One area where the use of MACH would be exciting is for the treatment of metastatic tumours in the draining lymph node basins. One possible mechanism of delivery would be the injection of targeted nanoparticles into the tumour itself along the lines of sentinel node studies and then the nodal basin could be exposed to MACH. This raises the possibility of treating subclinical micro-metastases that currently are undetectable.

In conclusion, this thesis has produced some novel findings highlighting the clinical utility of the αvβ6 integrin as a potential target in cancers overexpressing αvβ6. The identification of SMA as an independent prognostic marker merits further investigation, ideally in a prospectively designed multicentre study. Finally, the single chain antibody B6.3 has potential for use in its current form or as part of a whole antibody for the development of personalised medicine in αvβ6 expressing cancers.

Appendix 1

Supplementary data

10
CAA GTT AAA CTG GAA CAG TCC GGT GCT GAA GTT
gln val lys leu glu gln ser gly ala glu val
21
GTC AAA CCA GGT GCT TCC GTG AAG TTG TCC TGT AAA GCC TCT GGT TTT AAC ATC AAG GAT
val lys pro gly ala ser val lys leu ser cys lys ala ser gly phe asn ile lys asp
41
TCG TAT ATG CAT TGG TTG AGA CAA GGG CCA GGA CAA AGA TTG GAA TGG ATT GGC TGG ATT
ser tyr met his trp leu arg gln gly pro gly gln arg leu glu trp ile gly trp ile
61
GAT CCA GAG AAT GGT GAT ACC GAG TAC GCT CCT AAA TTT CAG GGA AAG GCT ACT TTT ACT
asp pro glu asn gly asp thr glu tyr ala pro lys phe gln gly lys ala thr phe thr
81
ACC GGC ACT TCC GCT AAT ACC GCA TAC TTG GGC TTA TCT TCC TTG AGA CCA GAG GAC ACT
thr gly thr ser ala asn thr ala tyr leu gly leu ser ser leu arg pro glu asp thr
101
GCC GTA TAC TAC TGC AAC GAA GGG ACA CCA ACT GCA GTT CCG AAC CTG CGA GGT GAT CTG
ala val tyr tyr cys asn glu gly thr pro thr Ala Val Pro Asn Leu Arg Gly Asp Leu

CAG GTG CTG GCT CAG AAA GTT GCA GGT CCT TAC CCT TTC GAC TAC TGG GGA
Gln Val Leu Ala Gln Lys Val Ala gly pro tyr pro phe asp tyr trp gly
121
CAA GGT ACC TTA GTT ACT GTC TCT AGC GGT GGC GGA GGT TCA GGC GGT GGA GGG TCT GGA
gln gly thr leu val thr val ser ser gly gly gly gly ser gly gly gly gly ser gly
141
GGT GGC GGT AGT GAA AAT GTG CTG ACC CAA TCT CCA AGC TCC ATG TCT GCT TCT GTT GGC
gly gly gly ser glu asn val leu thr gln ser pro ser ser met ser ala ser val gly
161
GAT GGA GTA ACC ATC GCT TGT AGC GCA TCC TCT AGT GTC CCA TAT ATG CAC TGG TTT CAA
asp gly val thr ile ala cys ser ala ser ser ser val pro tyr met his trp phe gln
181
CAG AAG CCA GGT AAA AGC CCA AAG TTG TTG ATT TAT TCG ACA TCC AAC TTG GCT TCT GGA
gln lys pro gly lys ser pro lys leu leu ile tyr ser thr ser asn leu ala ser gly

201
GTG CCT TCA AGG TTT TCT GGT TCC GGC TCA GGA ACC GAT TAT AGT TTG ACT ATT AGC TCA
val pro ser arg phe ser gly ser gly ser gly thr asp tyr ser leu thr ile ser ser
221
GTG CAG CCA GAG GAT GCT GCA ACC TAC TAT TGC CAG CAA AGG TCC TCA TAT CCA CTG ACT
val gln pro glu asp ala ala thr tyr tyr cys gln gln arg ser ser tyr pro leu thr
241
TTC GGG GGT GGA ACG AAG TTG GAA ATC AAG GCT GCG GCC
phe gly gly gly thr lys leu glu ile lys ala ala ala

Figure A1.1 VP1 peptide sequence shown in red, proline mutation in green. Errors in sequence shown in blue at position 82 and 162. Subsequently altered using site directed mutatgenesis: GGC (Glycine) corrected to GAC (Aspartate) using primers (5^{1}GCTACTTTTACTACCGACACTTCCGCTAATACC3^{1}) and (5^{1}GGTATTAGCGGAAGTGTCCGTAGTAAAAGTAGC3^{1}). Second, GGA (Glycine) corrected to AGA (Argenine) using primers (5^{1}GTTTCTGTTGGCGATAGAGTAACCATCGC3^{1}) and shMFE antisense G to A (5^{1}GCGATGGTTACTCTATCGCCAACAGAAAC3^{1})

5¹ AOX1 priming
TTGCGACTGG TTCCA
site
ATTGACAAGCTTTTGATTTTAACGA CTTTTAACGA CAACTTGAGA AGATCAAAAA ACAACTAATTA

TTCGAAACG **ATG** AGA TTT CCT TCA ATT TTT ACT GCT GTT TTA TTC GCA GCA TCC TCC GCA
met arg phe pro ser ile phe thr ala val leu phe ala ala ser ser ala

--- TTA GCT GCT CCA GTC AAC ACT ACA ACA GAA GAT GAA ACG GCA CAA ATT CCG GCT
leu ala ala pro val asn thr thr thr glu asp glu thr ala gln ile pro ala

GAA GCT GTC ATC GGT TAC TCA GAT TTA GAA GGG GAT TTC GAT GTT GCT GTT TTG CCA
glu ala val ile gly tyr ser asp leu glu gly asp phe asp val ala val leu pro

TTT TCC AAC AGC ACA AAT AAC GGG TTA TTG TTT ATA AAT ACT ACT ATT GCC AGC ATT
phe ser asn ser thr asn asn gly leu leu phe ile asn thr thr ile ala ser ile

GCT GCT AAA GAA GAA GGG GTA TCT CTC GAG AAA AGA GAG GCT GAA GC TGCAG GAATTCAC
ala ala lys glu glu gly val ser leu glu lys arg glu ala glu ala
SfiI NotI
GGCCCAGCC GGC CGTC TCGGATCGGTACCTC GAGCCGCG GCG GCC GCCAGC TTTCTA

c-myc tag
GAA CAA AAA CTC ATC TCA GAA GAG GAT CTG AAT AGC GCC GTC GAC
glu gln lys leu ile ser glu glu asp leu asn ser ala val asp

Poly His tag Stop
CAT CAT CAT CAT CAT CAT TGA GTTTGTAGCCTTAGACATGACTGTTCCTCAGTTCAA
His His His His His His ***
3¹ AOX1 priming
GTTGGGCACTTACGAGAAGACCGGTCTTGCTAGATTCTAATCAAGAGGATGT CAGAATGCC

site
ATTTGCCTGAGAGATGCAGGCTTCATTTTTGATACTTTTTTATTTGTAACCTATATGTATAGGAT

TTTTTTTGTCATTTTGTTTCTTCTCGTACGAGCTTGCTCCTGATCAGCCTATCTCGCAGCTGATGA

ATATCTTGTGGTAGGGGTTTGGGAAAATCATTCGAGTTTGATGTTTTTCTTGGTATTTCCCACTCC
BamH
TCTTCAGAGTACAGAAGATTAAGTGAGACCTTCGTTTGTGCGGATCCCCCACACACCATAGCTTC

AAAATGTTTCTACTCCTTTTTTACTCTTCCAGATTTTCTCGGACTCCGCGCATCGCCGTACCACTTC

Figure A1.2 Original PpicZαB vector sequence showing c-myc and His tags in blue, Sfi, Not1 and BamH restriction enzyme sites in green and 3^1 and 5^1 AOX1 priming sites (from Invitrogen catalogue)

5¹ AOX1 priming
TTGCGACTGG TTCCA
site
ATTGACAAGCTTTTGATTTTAACGA CTTTTAACGA CAACTTGAGA AGATCAAAAA ACAACTAATTA

TTCGAAACG **ATG** AGA TTT CCT TCA ATT TTT ACT GCT GTT TTA TTC GCA GCA TCC TCC GCA
met arg phe pro ser ile phe thr ala val leu phe ala ala ser ser ala

--- TTA GCT GCT CCA GTC AAC ACT ACA ACA GAA GAT GAA ACG GCA CAA ATT CCG GCT
leu ala ala pro val asn thr thr thr glu asp glu thr ala gln ile pro ala

GAA GCT GTC ATC GGT TAC TCA GAT TTA GAA GGG GAT TTC GAT GTT GCT GTT TTG CCA
glu ala val ile gly tyr ser asp leu glu gly asp phe asp val ala val leu pro

TTT TCC AAC AGC ACA AAT AAC GGG TTA TTG TTT ATA AAT ACT ACT ATT GCC AGC ATT
phe ser asn ser thr asn asn gly leu leu phe ile asn thr thr ile ala ser ile

GCT GCT AAA GAA GAA GGG GTA TCT CTC GAG AAA AGA GAG GCT GAA GC TGAAT TCA CGT
ala ala lys glu glu gly val ser leu glu lys arg glu ala glu ala
SfiI NotI
GGC CCA GCC GGC CGT CTC GGA TCG GTA CCT CGA GCC GCG GCG GCC GCC TGT
Ala Ala Ala cys
Poly His tag Stop
CAT CAT CAT CAT CAT CAT TGA GTTTGTAGCCTTAGACATGACTGTTCCTCAGTTCAA
His His His His His His ***
3¹ AOX1 priming
GTTGGGCACTTACGAGAAGACCGGTCTTGCTAGATTCTAATCAAGAGGATGT CAGAATGCC

site
ATTTGCCTGAGAGATGCAGGCTTCATTTTTGATACTTTTTTATTTGTAACCTATATGTATAGGAT

TTTTTTTGTCATTTTGTTTCTTCTCGTACGAGCTTGCTCCTGATCAGCCTATCTCGCAGCTGATGA

ATATCTTGTGGTAGGGGTTTGGGAAAATCATTCGAGTTTGATGTTTTTCTTGGTATTTCCCACTCC
BamH
TCTTCAGAGTACAGAAGATTAAGTGAGACCTTCGTTTGTGCGGATCCCCCACACACCATAGCTTC

AAAATGTTTCTACTCCTTTTTTACTCTTCCAGATTTTCTCGGACTCCGCGCATCGCCGTACCACTTC

Figure A1.3 Sequencing data of PpicZαBcys vector showing removal of c-myc tag, insertion of cystine residue in red, His tag in blue, Sfi, Not1 and BamH restriction enzyme sites in green and 3¹ and 5¹ AOX1 priming sites

```
TTCAATTTTTACTGCTGTTTTATTCGCAGCATCCTCCGCATTAGCTGCTCCAGTCAACACTACAACAGAA
GATGAAACGGCACAAATTCCGGCTGAAGCTGTCATCGGTTACTCAGATTTAGAAGGGGATTTCGATGT
TGCTGTTTTGCCATTTTCCAACAGCACAAATAACGGGTTATTGTTTATAAATACTACTATTGCCAGCATT
GCTGCTAAAGAAGAAGGGGTATCTCTCGAGAAAAGAGAGGCTGAAGCTGCAGGAAT
                          Sfi1
   TCACGTGGCCCA GCCGGCC ATG GCC CAA GTT AAA CTG GAA CAG TCC GGT GCT GAA  GTT
                                 met  ala  gln  val  lys  leu  glu  gln  ser  gly  ala  glu  val
21
GTC AAA CCA GGT GCT TCC GTG AAG TTG TCC TGT AAA GCC TCT GGT TTT AAC ATC AAG GAT
 val  lys  pro  gly  ala  ser  val  lys  leu  ser  cys  lys  ala  ser  gly  phe  asn  ile  lys  asp
41
TCG TAT ATG CAT TGG TTG AGA CAA GGG CCA GGA CAA AGA TTG GAA TGG ATT GGC TGG ATT
 ser  tyr  met  his  trp  leu  arg  gln  gly  pro  gly  gln  arg  leu  glu  trp  ile  gly  trp  ile
61
GAT CCA GAG AAT GGT GAT ACC GAG TAC GCT CCT AAA TTT CAG GGA AAG GCT ACT TTT ACT
 asp  pro  glu  asn  gly  asp  thr  glu  tyr  ala  pro  lys  phe  gln  gly  lys  ala  thr  phe  thr
81
ACC GAC ACT TCC GCT AAT ACC GCA TAC TTG GGC TTA TCT TCC TTG AGA CCA GAG GAC ACT
 thr  asp  thr  ser  ala  asn  thr  ala  tyr  leu  gly  leu  ser  ser  leu  arg  pro  glu  asp  thr
101
GCC GTA TAC TAC TGC AAC GAA GGG ACA CCA ACT GCA GTT CCG AAC CTG CGA GGT GAT CTG
 ala  val  tyr  tyr  cys  asn  glu  gly  thr  pro  thr  Ala  Val  Pro  Asn  Leu  Arg  Gly  Asp  Leu

CAG GTG CTG GCT CAG AAA GTT GCA GGT CCT TAC CCT TTC GAC TAC TGG GGA
 Gln  Val  Leu  Ala  Gln  Lys  Val  Ala  gly  pro  tyr  pro  phe  asp  tyr  trp  gly
121
CAA GGT ACC TTA GTT ACT GTC TCT AGC GGT GGC GGA GGT TCA GGC GGT GGA GGG TCT GGA
 gln  gly  thr  leu  val  thr  val  ser  ser  gly  gly  gly  gly  ser  gly  gly  gly  gly  ser  gly
141
GGT GGC GGT AGT GAA AAT GTG CTG ACC CAA TCT CCA AGC TCC ATG TCT GCT TCT GTT GGC
 gly  gly  gly  ser  glu  asn  val  leu  thr  gln  ser  pro  ser  ser  met  ser  ala  ser  val  gly
161
GAT AGA GTA ACC ATC GCT TGT AGC GCA TCC TCT AGT GTC CCA TAT ATG CAC TGG TTT CAA
 asp  arg  val  thr  ile  ala  cys  ser  ala  ser  ser  ser  val  pro  tyr  met  his  trp  phe  gln
181
CAG AAG CCA GGT AAA AGC CCA AAG TTG TTG ATT TAT TCG ACA TCC AAC TTG GCT TCT GGA
 gln  lys  pro  gly  lys  ser  pro  lys  leu  leu  ile  tyr  ser  thr  ser  asn  leu  ala  ser  gly
201
GTG CCT TCA AGG TTT TCT GGT TCC GGC TCA GGA ACC GAT TAT AGT TTG ACT ATT AGC TCA
 val  pro  ser  arg  phe  ser  gly  ser  gly  ser  gly  thr  asp  tyr  ser  leu  thr  ile  ser  ser
221
GTG CAG CCA GAG GAT GCT GCA ACC TAC TAT TGC CAG CAA AGG TCC TCA TAT CCA CTG ACT
 val  gln  pro  glu  asp  ala  ala  thr  tyr  tyr  cys  gln  gln  arg  ser  ser  tyr  pro  leu  thr
241                                                    Not1
TTC GGG GGT GGA ACG AAG TTG GAA ATC AAG GCT GCGGCCGCCTGTCATCATCATCATCATCAT
phe  gly  gly  gly  thr  lys  leu  glu  ile  lys  ala                  cys
TGAGTTTGTAGCCTTAGACATGACTGTTCCTCAGTTCAAGTTGGGCACTTACGAGAAGACCGGTC
```

Figure A1.4 : Sequencing results for insertion of shMFEVP1(P) into PpicZαBcys showing VP1 peptide and proline mutation (red), restriction enzyme sites (green) and cystine (blue)

10
CAA GTT AAA CTG GAA CAG TCC GGT GCT GAA GTT
gln val lys leu glu gln ser gly ala glu val
21
GTC AAA CCA GGT GCT TCC GTG AAG TTG TCC TGT AAA GCC TCT GGT TTT AAC ATC AAG GAT
val lys pro gly ala ser val lys leu ser cys lys ala ser gly phe asn ile lys asp
41
TCG TAT ATG CAT TGG TTG AGA CAA GGG CCA GGA CAA AGA TTG GAA TGG ATT GGC TGG ATT
ser tyr met his trp leu arg gln gly pro gly gln arg leu glu trp ile gly trp ile
61
GAT CCA GAG AAT GGT GAT ACC GAG TAC GCT CCT AAA TTT CAG GGA AAG GCT ACT TTT ACT
asp pro glu asn gly asp thr glu tyr ala pro lys phe gln gly lys ala thr phe thr
81
ACC GGC ACT TCC GCT AAT ACC GCA TAC TTG GGC TTA TCT TCC TTG AGA CCA GAG GAC ACT
thr asp thr ser ala asn thr ala tyr leu gly leu ser ser leu arg pro glu asp thr
101
GCC GTA TAC TAC TGC AAC GAA GGG ACA CCA ACT GGT CCT TAC TAT TTC GAC TAC TGG GGA
ala val tyr tyr cys asn glu gly thr pro thr gly pro tyr tyr phe asp tyr trp gly
121
CAA GGT ACC TTA GTT ACT GTC TCT AGC GGT GGC GGA GGT TCA GGC GGT GGA GGG TCT GGA
gln gly thr leu val thr val ser ser gly gly gly gly ser gly gly gly gly ser gly
141
GGT GGC GGT AGT GAA AAT GTG CTG ACC CAA TCT CCA AGC TCC ATG TCT GCT TCT GTT GGC
gly gly gly ser glu asn val leu thr gln ser pro ser ser met ser ala ser val gly
161
GAT AGA GTA ACC ATC GCT TGT AGC GCA TCC TCT AGT GTC CCA TAT ATG CAC TGG TTT CAA
asp arg val thr ile ala cys ser ala ser ser ser val pro tyr met his trp phe gln
181
CAG AAG CCA GGT AAA AGC CCA AAG TTG TTG ATT TAT TCG ACA TCC AAC TTG GCT TCT GGA
gln lys pro gly lys ser pro lys leu leu ile tyr ser thr ser asn leu ala ser gly
201
GTG CCT TCA AGG TTT TCT GGT TCC GGC TCA GGA ACC GAT TAT AGT TTG ACT ATT AGC TCA
val pro ser arg phe ser gly ser gly ser gly thr asp tyr ser leu thr ile ser ser
221
GTG CAG CCA GAG GAT GCT GCA ACC TAC TAT TGC CAG CAA AGG TCC TCA TAT CCA CTG ACT
val gln pro glu asp ala ala thr tyr tyr cys gln gln arg ser ser tyr pro leu thr
241
TTC GGG GGT GGA ACG AAG TTG GAA ATC AAG GCT GCG GCC
phe gly gly gly thr lys leu glu ile lys ala ala ala

Figure A1.5 : Sequencing results of shMFE in puc119 showing original tyrosine without proline mutation as in shMFEVP1(P)

```
TTCAATTTTTACTGCTGTTTTATTCGCAGCATCCTCCGCATTAGCTGCTCCAGTCAACACTACAACAGAA
GATGAAACGGCACAAATTCCGGCTGAAGCTGTCATCGGTTACTCAGATTTAGAAGGGGATTTCGATGT
TGCTGTTTTGCCATTTTCCAACAGCACAAATAACGGGTTATTGTTTATAAATACTACTATTGCCAGCATT
GCTGCTAAAGAAGAAGGGGTATCTCTCGAGAAAAGAGAGGCTGAAGCTGCAGGAAT
                    Sfi1
   TCACGTGGCCCA GCCGGCC ATG GCC CAA GTT AAA CTG GAA CAG TCC GGT GCT GAA  GTT
                                 met  ala  gln  val  lys  leu  glu  gln  ser  gly  ala  glu  val
21
GTC AAA CCA GGT GCT TCC GTG AAG TTG TCC TGT AAA GCC TCT GGT TTT AAC ATC AAG GAT
 val  lys  pro  gly  ala  ser  val  lys  leu  ser  cys  lys  ala  ser  gly  phe  asn  ile  lys  asp
41
TCG TAT ATG CAT TGG TTG AGA CAA GGG CCA GGA CAA AGA TTG GAA TGG ATT GGC TGG ATT
 ser  tyr  met  his  trp  leu  arg  gln  gly  pro  gly  gln  arg  leu  glu  trp  ile  gly  trp  ile
61
GAT CCA GAG AAT GGT GAT ACC GAG TAC GCT CCT AAA TTT CAG GGA AAG GCT ACT TTT ACT
 asp  pro  glu  asn  gly  asp  thr  glu  tyr  ala  pro  lys  phe  gln  gly  lys  ala  thr  phe  thr
81
ACC GAC ACT TCC GCT AAT ACC GCA TAC TTG GGC TTA TCT TCC TTG AGA CCA GAG GAC ACT
 thr  asp  thr  ser  ala  asn  thr  ala  tyr  leu  gly  leu  ser  ser  leu  arg  pro  glu  asp  thr
101
GCC GTA TAC TAC TGC AAC GAA GGG ACA CCA ACT GGT CCT TAC TAT TTC GAC TAC TGG GGA
ala  val  tyr  tyr  cys  asn  glu  gly  thr  pro  thr  gly  pro  tyr  tyr  phe  asp  tyr  trp  gly
121
CAA GGT ACC TTA GTT ACT GTC TCT AGC GGT GGC GGA GGT TCA GGC GGT GGA GGG TCT GGA
 gln  gly  thr  leu  val  thr  val  ser  ser  gly  gly  gly  gly  ser  gly  gly  gly  gly  ser  gly
141
GGT GGC GGT AGT GAA AAT GTG CTG ACC CAA TCT CCA AGC TCC ATG TCT GCT TCT GTT GGC
 gly  gly  gly  ser  glu  asn  val  leu  thr  gln  ser  pro  ser  ser  met  ser  ala  ser  val  gly
161
GAT AGA GTA ACC ATC GCT TGT AGC GCA TCC TCT AGT GTC CCA TAT ATG CAC TGG TTT CAA
 asp  arg  val  thr  ile  ala  cys  ser  ala  ser  ser  ser  val  pro  tyr  met  his  trp  phe  gln
181
CAG AAG CCA GGT AAA AGC CCA AAG TTG TTG ATT TAT TCG ACA TCC AAC TTG GCT TCT GGA
 gln  lys  pro  gly  lys  ser  pro  lys  leu  leu  ile  tyr  ser  thr  ser  asn  leu  ala  ser  gly
201
GTG CCT TCA AGG TTT TCT GGT TCC GGC TCA GGA ACC GAT TAT AGT TTG ACT ATT AGC TCA
 val  pro  ser  arg  phe  ser  gly  ser  gly  ser  gly  thr  asp  tyr  ser  leu  thr  ile  ser  ser
221
GTG CAG CCA GAG GAT GCT GCA ACC TAC TAT TGC CAG CAA AGG TCC TCA TAT CCA CTG ACT
 val  gln  pro  glu  asp  ala  ala  thr  tyr  tyr  cys  gln  gln  arg  ser  ser  tyr  pro  leu  thr
241                                                    Not1
TTC GGG GGT GGA ACG AAG TTG GAA ATC AAG GCT GCGGCCGCCTGTCATCATCATCATCATCAT
phe  gly  gly  gly  thr  lys  leu  glu  ile  lys  ala                  cys
TGAGTTTGTAGCCTTAGACATGACTGTTCCTCAGTTCAAGTTGGGCACTTACGAGAAGACCGGTC
```

Figure A1.6 : Sequencing results of shMFE PpicZα cys showing original tyrosine without proline mutation and cystine residue in blue.

Appendix 2

References

Abe M, Harpel JG, Metz CN, Nunes I, Loskutoff DJ, Rifkin DB (1994) An assay for transforming growth factor-beta using cells transfected with a plasminogen activator inhibitor-1 promoter-luciferase construct. *Anal Biochem* **216**: 276–284

Acharya R, Fry E, Stuart D, Fox G, Rowlands D, Brown F (1989) The three-dimensional structure of foot-and-mouth disease virus at 2.9 A resolution. *Nature* **337(6209):**709-716

Adams GP and Schier R (1999) Generating improved single-chain Fv molecules for tumor targeting. *J Immunol Methods* **231(1-2)**: 249-260

Adolphe C, Hetherington R, Ellis T, Wainwright B (2006) Patched1 functions as a gatekeeper by promoting cell cycle progression. *Cancer Res*. **66**: 2081-2088

Ahmed N, Riley C, Rice GE, Quinn MA, Baker MS (2002) Alphavbeta6 integrin – A marker for the malignant potential of epithelial ovarian cancer *J Histochem Cytochem* **50**: 1371-1380

Ahmed N, Pansino F, Clyde R, Murthi P, Quinn MA, Rice GE, Agrez MV, Mok S, and Baker MS (2002) Overexpression of alpha(v)beta6 integrin in serous epithelial ovarian cancer regulates extracellular matrix degradation via the plasminogen activation cascade *Carcinogenesis* **23:** 237-244

Akhurst RJ, Derynck R (2001) TGF-beta signaling in cancer–a double-edged sword. *Trends Cell Biol* **11**: S44–51.

Akiyama SK, Olden K, Yamada KM (1995) Fibronectin and integrins in invasion and metastasis *Cancer Metastasis Rev* **14**: 173-189

Albanell J, Codony-Servat J, Rojo F, Del Campo JM, Sauleda S, Anido J, Raspall G, Giralt J, Roselló J, Nicholson RI, Mendelsohn J, Baselga J (2001) Activated extracellular

signal-regulated kinases: association with epidermal growth factor receptor/transforming growth factor alpha expression in head and neck squamous carcinoma and inhibition by anti-epidermal growth factor receptor treatments. *Cancer Res*. **61**: 6500-6510

Alexiou C, Jurgons R, Schmid RJ, Bergemann C, Henke J, Erhardt W, Huenges E, Parak F (2003) Magnetic drug targeting—biodistribution of the magnetic carrier and the chemotherapeutic agent mitoxantrone after locoregional cancer treatment. *J Drug Target* **11**:139–149

Annes JP, Rifkin DB, Munger JS (2002) The integrin alphavbeta6 binds and activates latent TGFβ3 *FEBS Lett.* **511**: 65-68

Arihiro K, Kaneko M, Fujii S, Inai K, Yokosaki Y (2000) Significance of alpha 9 beta 1 and alpha v beta 6 integrin expression in breast carcinoma. *Breast Cancer* **7(1)**:19-26

Asakage T, Yokose T, Mukai K, Tsugane S, Tsubono Y, Asai M, Ebihara S. (1998) Tumor thickness predicts cervical metastasis in patients with stage I/II carcinoma of the tongue. *Cancer* **82(8):** 1443–8.

Atri M (2006) New Technologies and Directed Agents for Applications of Cancer Imaging *J Clin Oncol.* **24(20)**: 3299-3308

Balivada S, Rachakatla RS, Wang H, Samarakoon TN, Dani RK, Pyle M, Kroh FO, Walker B, Leaym X, Koper OB, Tamura M, Chikan V, Bossmann SH, Troyer D (2010) A/C magnetic hyperthermia of melanoma mediated by iron/iron oxide core/shell magnetic nanoparticles: a mouse study. *BMC Cancer* **10:**119.

Barr RJ. (1991) Classification of cutaneous squamous cell carcinoma. *J Cutan Pathol* **18**: 225

Barnes CJ, Ohshiro K, Rayala SK, El-Naggar AK, Kumar R (2007) Insulin-like Growth Factor Receptor as a Therapeutic Target in Head and Neck Cancer *Clin Cancer Res*.**13(14)**: 4291-4299

Bates RC, Bellovin DI, Brown C, Maynard E, Wu B, Kawakatsu H, Sheppard D, Oettgen P, Mercurio AM (2005) Transcriptional activation of integrin beat6 during the epithelial mesenchymal transition defines a novel prognostic indicator of aggressive colon carcinoma *J Clin Invest* **115**: 339-347

Batra SK, Jain M, Wittel UA, Chauhan SC, Colcher D (2002) Pharmacokinetics and biodistribution of genetically engineered antibodies. *Curr. Opin. Biotechnol*. **13**: 603–608

Begent RH, Verhaar MJ, Chester KA, Casey JL, Green AJ, Napier MP, Hope-Stone LD, Cushen N, Keep PA, Johnson CJ, Hawkins RE, Hilson AJ, Robson L (1996) Clinical evidence of efficient tumor targeting based on single-chain Fv antibody selected from a combinatorial library *Nat. Med*. **2** 979-984

Bennett JH, Morgan MJ, Whawell SA, Atkin P, Roblin P, Furness J, Speight PM (2000) Metalloproteinase expression in normal and malignant oral keratinocytes: stimulation of MMP-2 and -9 by scatter factor. *Eur J Oral Sci* **108**: 281-291.

Bernier J, Domenge C, Ozsahin M, Matuszewska K, Lefèbvre JL, Greiner RH, Giralt J, Maingon P, Rolland F, Bolla M, Cognetti F, Bourhis J, Kirkpatrick A, van Glabbeke M; European Organization for Research and Treatment of Cancer Trial 22931 (2004) Postoperative irradiation with or without concomitant chemotherapy for locally advanced head and neck cancer. *N Engl J Med.* **350**:1945-1952

Bernstein SC, Lim KK, Brodland DG, Heidelberg KA. (1996) The many faces of cutaneous squamous cell carcinoma. *Dermatol Surg* **22**: 243

Berry CC, Wells S, Charles S, Curtis ASG. (2003) Dextran and albumin derivatised iron oxide nanoparticles: influence on fibroblasts in vitro. *Biomaterials* **24(25)**: 4551–4557

Berryman S, Clark S, Monaghan P, Jackson T (2005) Early events in integrin αvβ6 mediated cell entry of foot and mouth disease virus *J.Virol* **79**: 8519-8534

Bierie B, Moses HL. (2006) Tumour microenvironment: TGFβ: the molecular Jekyll and Hyde of cancer. *Nat Rev Cancer* **6(7)**: 506-520

Billetta R, Hollingdale MR, Zanetti M (1991) Immunogenicity of an engineered internal image antibody *Proc Natl Acad Sci U S A*. **88(11)**: 4713-4717

Birchmeier C, Birchmeier W, Gherardi E, Vande Woude GF (2003). Met, metastasis, motility and more. *Nat Rev Mol Cell Biol.* **4(12)**: 915-25

Bird RE, Hardman KD, Jacobson JW, Johnson S, Kaufman BM, Lee SM, Lee T, Pope SH, Riordan GS, Whitlow M (1988) Single-chain antigen-binding proteins *Science*. **242(4877)**: 423-6

Bock JM, Menon SG, Sinclair LL, Bedford NS, Goswami PC, Domann FE, Trask DK (2007) Celecoxib toxicity is cell cycle phase specific *Cancer Res*. **67(8)**: 3801-8

Boehm MK, Corper AL, Wan T, Sohi MK, Sutton BJ, Thornton JD, Keep PA, Chester KA, Begent RH, Perkins SJ (2000) Crystal structure of the anti-(carcinoembryonic antigen) single-chain Fv antibody MFE-23 and a model for antigen binding based on intermolecular contacts *Biochem. J.* **346 Pt 2:** 519-528

Boehm MK, Perkins SJ (2000) Structural models for carcinoembryonic antigen and its complex with the single-chain Fv antibody molecule MFE23. *FEBS Lett.* **475,** 11-1

Bonnemain B (1998) Superparamagnetic agents in magnetic resonance imaging, physicochemical characteristics and clinical applications. A review, *J. Drug Target*. **6**: 167–174

Bonner JA, Harari PM, Giralt J, Azarnia N, Shin DM, Cohen RB, Jones CU, Sur R, Raben D, Jassem J, Ove R, Kies MS, Baselga J, Youssoufian H, Amellal N, Rowinsky EK, Ang KK (2006) Radiotherapy plus cetuximab for squamous-cell carcinoma of the head and neck. *N Engl J Med* **354**: 567–578

Bosch FX, Lorincz A, Muñoz N, Meijer CJ, Shah KV (2002). The causal relation between human papillomavirus and cervical cancer. *J Clin Pathol* **55**: 244-265

Boslooper K, King-Yin Lam A, Gao J, Weinstein S, Johnson N (2008) The clinicopathological roles of alpha-B-crystallin and p53 expression in patients with head and neck squamous cell carcinoma *Pathology* **40(5)**:500-4

Boyer C, Whittaker MR, Chuah K, Liu J, Davis TP (2010) Modulation of the surface charge on polymer-stabilized gold nanoparticles by the application of an external stimulus. *Langmuir* **26(4):**2721-2730

Bradbury ARM, Marks JD (2004) Antibodies from phage antibody libraries. *Journal of Immunological Methods* **290:** 29–49

Brandwein-Gensler M, Teixeira MS, Lewis CM, Lee B, Rolnitzky L, Hille JJ, Genden E, Urken ML, Wang BY (2005) Oral squamous cell carcinoma: histologic risk assessment, but not margin status, is strongly predictive of local disease-free and overall survival. *Am J Surg Pathol*. **29(2):**167-178

Breasted JH (1931) The Rise of Man. *Science* **74**: 639-640

Brennan JA, Boyle JO, Koch WM, Goodman SN, Hruban RH, Eby YJ, Couch MJ, Forastiere AA, Sidransky D (1995). Association between cigarette smoking and mutation of the p53 gene in squamous-cell carcinoma of the head and neck. *N Engl J Med* **332**:712-717.

Breuss JM, Gallo J, DeLisser HM, Klimanskaya IV, Folkesson HG, Pittet JF, Nishimura SL, Aldape K, Landers DV, Carpenter W, Gillett N, Sheppard D, Matthay MA, Albelda SM, Kramer RH, Pytela R (1995) 'Expression of the beta 6 integrin subunit in development, neoplasia and tissue repair suggests a role in epithelial remodelling' *J Cell Sci* **108**:22241-22251

Bryne M, Koppang HS, Lilleng R, Kjaerheim A (1992) Malignancy grading of the deep invasive margins of oral squamous cell carcinomas has high prognostic value. *J Pathol*. **166**:375–381

Buettner PG, Raasch BA (1998) Incidence rates of skin cancer in Townsville, Australia. *Int J Cancer* **78**: 587–593

Burman A, Clark S, Abrescia NG, Fry EE, Stuart DI, Jackson T (2006) Specificity of the VP1 GH loop of Foot and Mouth Disease Virus for αv Integrins *J. Virol* **80:** 9798-9810

Burtness B, Goldwasser MA, Flood W, Mattar B, Forastiere AA. (2005) Eastern Cooperative Oncology Group Phase III randomized trial of cisplatin plus placebo compared with cisplatin plus cetuximab in metastatic/ recurrent head and neck cancer: an Eastern Cooperative Oncology Group Study. *J Clin Oncol*. **23**:8646–8654

Burton DR, Barbas CF 3rd, Persson MA, Koenig S, Chanock RM, Lerner RA (1991) A large array of human monoclonal antibodies to type 1 human immunodeficiency virus from combinatorial libraries of asymptomatic individuals. *Proc. Natl. Acad. Sci. U. S.A*. **88:** 10134–10137

Busk M, Pytela R, Sheppard D (1992) Characterization of the integrin alpha v beta 6 as a fibronectin-binding protein. *J Biol Chem*; **267:** 5790–5796.

Callen JP, Bickers DR, Moy RL. Actinic keratoses. (1997) *J Am Acad Dermatol*. **36**: 650–653

Cai W and Chen X (2007) Nanoplatforms for Targeted Molecular Imaging in Living Subjects *Small* **3(11)**: 1840-1854

Cai X, Garen A (1995) Anti-melanoma antibodies from melanoma patients immunised with genetically modified autologous tumor cells: selection of specific antibodies from single-chain Fv fusion phage libraries. *Proc. Natl. Acad. Sci. U. S. A.* **92:** 6537–6541

Cantillon-Murphy P, Wald LL, Adalsteinsson E, Zahn M (2010) Heating in the MRI environment due to superparamagnetic fluid suspensions in a rotating magnetic field *J Magn Magn Mater* **322(6):**727-733

Chan DCF, Kiroptin DB, Bunn PA (1997) Physical chemistry and in vivo tissue heating properties of colloidal magnetic iron oxides with increased power absorption rates. *In: Hafeli U, Schutt W, Teller J, Zborowski M, eds. Scientific and Clinical Applications of Magnetic Carriers. New York: Plenum Press*: 607-18

Chan G, Boyle JO, Yang EK, Zhang F, Sacks PG, Shah JP, Edelstein D, Soslow RA, Koki AT, Woerner BM, Masferrer JL, Dannenberg AJ (1999) Cyclooxygenase-2 expression is up-regulated in squamous cell carcinoma of the head and neck. *Cancer Res*. **59(5)**:991-994.

Charles SW, Popplewell J. (1980) Progress in the development of ferromagneticliquids. *IEEE Trans Magn* **16(2)**:172–177

Chaussy C, Thuroff S. (2001) Results and side effects of high-intensity focused ultrasound in localized prostate cancer. *J. Endourology*. **15**:437–440

Chester KA, Begent RH, Robson L, Keep P, Pedley RB, Boden JA, Boxer G, Green A, Winter G, Cochet O (1994) Phage libraries for generation of clinically useful antibodies *Lancet* **343**: 455-456

Chen W, Jarzyna PA, van Tilborg GA, Nguyen VA, Cormode DP, Klink A, Griffioen AW, Randolph GJ, Fisher EA, Mulder WJ, Fayad ZA. (2010) RGD peptide functionalized and reconstituted high-density lipoprotein nanoparticles as a versatile and multimodal tumor targeting molecular imaging probe. *FASEB J*. **24(6):**1689-1699

Choi SY, Kahyo H (1991). Effect of cigarette smoking and alcohol consumption in the aetiology of cancer of the oral cavity, pharynx and larynx. *Int J Epidemiol* **20**: 878-885.

Christensen ME, Engbaek F, Therkildsen MH, Bretlau P, Nexo E (1995) A sensitive enzyme-linked immunosorbent assay used for quantitation of epidermal growth factor receptor protein in head and neck carcinomas: evaluation, interpretations and limitations. *Br J Cancer* **72**: 1487–1493

Chung CH, Ely K, McGavran L, Varella-Garcia M, Parker J, Parker N, Jarrett C, Carter J, Murphy BA, Netterville J, Burkey BB, Sinard R, Cmelak A, Levy S, Yarbrough WG, Slebos RJ, Hirsch FR (2006) Increased epidermal growth factor receptor gene copy number is associated with poor prognosis in head and neck squamous cell carcinomas. *J Clin Oncol* **24**: 4170– 4176.

Clackson T, Hoogenboom HR, Griffiths AD, Winter G (1991) Making antibody fragments using phage display libraries. Nature **352**: 624–628

Clark RA, Ashcroft GS, Spencer MJ, Larjava H, Ferguson MW. (1996) Re-epithelialization of normal human excisional wounds is associated with a switch from alpha v beta 5 to alpha v beta 6 integrins. *British J Dermatol* **135:**46–51

Clayman GL, Lippman SM, Laramore GE, Hong WK (1996) Head and neck cancer. *In: Cancer Medicine, Holland JF, Frei E, Bast RC, Kufe DW, Morton DL, Weichselbaum R (eds). Philadelphia: Williams and Wilkins:* 1645–1709

Cohen EE, Lingen MW, Vokes EE (2004) The expanding role of systemic therapy in head and neck cancer. *J Clin Oncol*. **22**: 1743-1752

Cohen EE, Rosen F, Stadler WM, Recant W, Stenson K, Huo D, Vokes EE (2003) Phase II trial of ZD1839 in recurrent or metastatic squamous cell carcinoma of the head and neck. *J Clin Oncol.* **21:**1980-1987

Colcher D, Pavlinkova G, Beresford G, Booth BJ, Choudhury A, Batra SK. (1998) Pharmacokinetics and biodistribution of genetically-engineered antibodies *J Nucl Med*. **42(4)**: 225-241.

Cooper JS, Pajak TF, Forastiere AA, Jacobs J, Campbell BH, Saxman SB, Kish JA, Kim HE, Cmelak AJ, Rotman M, Machtay M, Ensley JF, Chao KS, Schultz CJ, Lee N, Fu KK; Radiation Therapy Oncology Group 9501/Intergroup (2004) Postoperative concurrent radiotherapy and chemotherapy for high-risk squamous-cell carcinoma of the head and neck. *N Engl J Med* **350**: 1937-1944.

D'Souza AJ, Schowen RL, Topp EM (2004) Polyvinylpyrrolidone– drug conjugate: synthesis and release mechanism. J Cont Rel **94(1)**:91–100

Dahmane N, Lee J, Robins P, Heller P, Ruiz i Altaba A (1997) Activation of the transcription factor Gli1 and hedgehog signaling pathway in skin tumours. *Nature* **389**: 876-881.

Davies DR, Padlan EA, Segal DM (1975) Three-dimensional structure of immunoglobulins *Annu Rev Biochem*. **44**:639-667

Dayhoff MO, Eck RV, Park CM (1972) A model of evolutionary change in proteins. *Dayhoff, M.O., ed., Atlas of Protein Sequence and Structure. National Biomedical Research Foundation, Washington, D.C.* **Vol. 5:** 89–99

de Bondt RB, Nelemans PJ, Hofman PA, Casselman JW, Kremer B, van Engelshoven JM, Beets-Tan RG. (2007) Detection of lymph node metastases in head and neck cancer: a meta-analysis comparing US, USgFNAC, CT and MR imaging. *Eur J Radiol*. **64(2):**266-272

De Lorenzo C, Tedesco A, Terrazzano G, Cozzolino R, Laccetti P, Piccoli R, D'Alessio G (2004) A human, compact, fully functional anti- ErbB2 antibody as a novel antitumour agent. *Br. J. Cancer* **91**: 1200–1204

DeNardo SJ, DeNardo GL, Miers LA, Natarajan A, Foreman AR, Gruettner C, Adamson GN, Ivkov R (2005) Development of tumour targeting bioprobes ((111) in-chimeric L6 monoclonal antibody nanoparticles) for alternating magnetic field cancer therapy. *Clin Cancer Res*. **11** (19 Pt 2): 7087s-7092s

Detre S, Jotti GS, Dowsett M (1995) A 'quickscore' method for immunohistochemical semiquantitation: validation for oestrogen receptor in breast carcinomas. *J Clin Pathol.* **48:** 876-878

De Wever O, Mareel M (2003) Role of tissue stroma in cancer cell invasion. *J Pathol* **200(4):** 429-447.

De Wever O, Nguyen Q-D, Hoorde LV, Bracke M, Bruyneel E, Gespach C, Mareel M (2004) Tenascin-C and SF/HGF produced by myofibroblasts in vitro provide convergent

pro-invasive signals to human colon cancer cells through RhoA and Rac. *FASEB J*, **18:** 1016-1018.

De Wever O, Demetter P, Mareel M, Bracke M (2008) Stromal myofibroblasts are drivers of invasive cancer growth. *Int J Cancer* **123:** 2229-2238

Dewey WC, Hopwood LE, Sapareto SA, Gerweck LE (1977) Cellular responses to combinations of hyperthermia and radiation. *Radiology* **123**: 463–474

Dewey W. (1994) Arrhenius relationships from the molecule and cell to the clinic. *Int J Hyperthermia*; **10:** 457-83.

DiCara D, Rapisarda C, Sutcliffe JL, Violette SM, Weinreb PH, Hart IR, Howard MJ, Marshall JF (2007) Structure-function analysis of RGD-helix motifs in αvβ6 integrin ligands' *J. Cell Biol*. **282(13):** 9657-65

Dickson MA, Hahn WC, Ino Y, Ronfard V, Wu JY, Weinberg RA, Louis DN, Li FP,Rheinwald JG (2000) Human Keratinocytes That Express hTERT and Also Bypass a p16INK4a-Enforced Mechanism That Limits Life Span Become Immortal yet Retain Normal Growth and Differentiation Characteristics. *Molecular and Cellular Biology* **20:** 1436–1447

Diepgen TL, Mahler V (2002) The epidemiology of skin cancer. *British Journal of Dermatology* **146 (Suppl. 61):** 1–6

di Tomaso E, Capen D, Haskell A, Hart J, Logie JJ, Jain RK, McDonald DM, Jones R, Munn LL (2005) Mosaic tumor vessels: cellular basis and ultrastructure of focal regions lacking endothelial cell markers. *Cancer Res*. **65:** 5740–5749

Dobson J (2010) Cancer therapy: A twist on tumour targeting. *Nat Mater*. **9(2):**95-96

Dodson JM, DeSpain J, Hewett JE, Clark DP (1991) Malignant potential of actinic keratoses and the controversy over treatment. A patient oriented perspective. *Arch Dermatol* **127:** 1029–1031

Dreyer WJ, Bennett JC (1965) The molecular basis of antibody formation: a paradox. *Proc Natl Acad Sci U S A* **54:** 864-869.

Dubel S (2007) Recombinant therapeutic antibodies *Appl Microbiol Biotechnol* **74:**723–729

Dvorak HF, Nagy JA, Feng D, Dvorak AM (2000) Tumor architecture and targeted delivery. *In: Abrams, P.G., Fritzberg, A.R. (Eds.), Radioimmunotherapy of Cancer. Marcel Dekker, Inc., New York* 107–135

Elayadi AN, Samli KN, Prudkin L, Liu YH, Bian A, Xie XJ, Wistuba II, Roth JA, McGuire MJ, Brown KC (2007) A peptide selected by biopanning identifies the integrin alphavbeta6 as a prognostic biomarker for nonsmall cell lung cancer *Cancer Res*. **67(12)**: 5889-5895

El-Bahrawy M, El-Masry N, Alison M, Poulsom R, Fallowfield M (2003) Expression of beta-catenin in basal cell carcinoma. *Br J Dermatol.* **148(5):**964-70

Elliott RL, Blobe GC (2005) Role of transforming growth factor Beta in human cancer. *J Clin Oncol* **23:** 2078–2093.

Elster A, Burdette J (2001) *Questions and Answers in Magnetic Resonance Imaging (St Louis, USA:Mosby)* 273-280

Evangelista M, Tian H, Sauvage FJ (2006) The hedgehog signalling pathway in Cancer. *Clin Cancer Res* **12:** 5924-5928

Fears TR (1983) Estimating increase in skin cancer morbidity due to increase in ultraviolet radiation exposure. *Cancer Invest* **1:** 119–126

Fitzpatrick TB (1988) The validity and practicality of sun-reactive skin types I through VI *Arch Dermatol*. **124(6)**: 869-871

Forastiere AA, Metch B, Schuller DE, Ensley JF, Hutchins LF, Triozzi P, Kish JA, McClure S, VonFeldt E, Williamson SK (1992) Randomized comparison of cisplatin plus fluorouracil and carboplatin plus fluorouracil versus methotrexate in advanced squamous-cell carcinoma of the head and neck: a Southwest Oncology Group study. *J Clin Oncol*. **10:** 1245-1251

Fouchier F, Penel C, Pierre Montero M, Bremond P, Champion S. (2007) Integrin alphavbeta6 mediates HT29-D4 cell adhesion to MMP-processed fibrinogen in the presence of Mn2+ *Eur J Cell Biol* ;**86**:143–60

Frank JL, Garb JL, Banson BB, Peterman J, Neifeld JP, Kay S, Kornstein MJ, Sismanis A, Ware JL (1993) Epidermal growth factor receptor expression in squamous cell carcinoma of the hypopharynx. *Surg Oncol.* **2(3):**161-7

Frankel DH, Hanusa BH, Zitelli JA (1992) New primary nonmelanoma skin cancer in patients with a history of squamous cell carcinoma of the skin. Implications and recommendations for follow-up. *J Am Acad Dermatol* **26:** 720–726

Friedman E, Gold LI, Klimstra D, Zeng ZS, Winawer S, Cohen A. High levels of transforming growth factor β1 correlate with disease progression in human colon cancer (1995) *Cancer Epidemiol Biomarkers Prev.* **4**: 549–554

Fujita K, Sano D, Kimura M, Yamashita Y, Kawakami M, Ishiguro Y, Nishimura G, Matsuda H, Tsukuda M (2007) Anti-tumor effects of bevacizumab in combination with paclitaxel on head and neck squamous cell carcinoma. *Oncol Rep*. **18(1):**47-51

Fukumura D, Jain RK (2007) Tumor microvasculature and microenvironment: targets for anti-angiogenesis and normalization. *Microvasc Res*. **74(2-3)**: 72-84

García-Echeverría C, Pearson MA, Marti A, Meyer T, Mestan J, Zimmermann J, Gao J, Brueggen J, Capraro HG, Cozens R, Evans DB, Fabbro D, Furet P, Porta DG, Liebetanz J, Martiny-Baron G, Ruetz S, Hofmann F. (2004) In vivo antitumor activity of NVP-AEW541-A novel, potent, and selective inhibitor of the IGF-IR kinase. *Cancer Cell*. **5(3):**231-9

Gasco M, Crook T (2003) p53 family members and chemoresistance in cancer: what we know and what we need to know *Drug Resist Updat.* **6(6):**323-8

Gibson MK, Li Y, Murphy B, Hussain MH, DeConti RC, Ensley J, Forastiere AA; Eastern Cooperative Oncology Group (2004) Randomized phase III evaluation of cisplatin plus fluorouracil versus cisplatin plus paclitaxel in advanced head and neck cancer (E1395): an intergroup trial of the Eastern Cooperative Oncology Group. *J Clin Oncol*. **23:** 3562-3567

Gilchrist RK, Medal R, Shorey WD, Hanselman RC, Parrott JC, Taylor CB (1957) Selective inductive heating of lymph nodes. *Ann Surgy* **146:** 59-66

Giles G, Marks R, Foley P. (1988) Incidence of non-melanocytic skin cancer treated in Australia. *Br Med J* **269:** 13–17

Glockshuber R, Malia M, Pfitzinger I, Plückthun A (1990) A Comparison of Strategies To Stabilize Immunoglobulin Fv Fragments *Biochemistry* **29**: 1362-1367

Goel A, Colcher D, Baranowska-Kortylewicz J, Augustine S, Booth BJ, Pavlinkova G, Batra SK (2000) Genetically engineered tetravalent single-chain Fv of the pancarcinoma

monoclonal antibody CC49: improved biodistribution and potential for therapeutic application. *Cancer Res*. **60**: 6964–6971

Grachtchouk M, Mo R, Yu S, Zhang X, Sasaki H, Hui CC, Dlugosz AA (2000) Basal Cell Carcinomas in mice overexpressing Gli2 in skin. *Nature Genetics* **24:** 216-217

Graff CP, Chester K, Begent R, Wittrup KD (2004) Directed evolution of an anti-carcinoembryonic antigen scFv with a 4-day monovalent dissociation half-time at 37 degrees *C Protein Eng Des Sel*. **17(4)**: 293-304

Grau JJ, Monzó M, Caballero M, Carles J, Palmero R, Artells R, Pico C, Gascon P (2004) Expression of cyclooxygenase2 mRNA (COX2-mRNA) in peripheral blood of head and neck cancer patents and healthy controls. *J Clin Oncol*. **22 (14 S):** 5521-7

Graus YF, de Baets MH, Parren PW, Berrih-Aknin S, Wokke J, van Breda Vriesman PJ, Burton DR (1997) Human anti-nicotinic acetylcholine receptor recombinant Fab fragments isolated from thymus-derived phage display libraries from myasthenia gravis patients reflect predominant specificities in serum and block the action of pathogenic serum antibodies. *J. Immunol.* **158:** 1919–1929

Green A. (1992) Changing patterns in incidence of nonmelanoma skin cancer. *Epithelial Cell Biol*. **1:** 47–51.

Greenberg JS, Fowler R, Gomez J, Mo V, Roberts D, El Naggar AK, Myers JN (2003) Extent of extracapsular spread: a critical prognosticator in oral tongue cancer. *Cancer* **97(6):**1464-1470

Griffiths AD, Williams SC, Hartley O, Tomlinson IM, Waterhouse P, Crosby WL, Kontermann RE, Jones PT, Low NM, Allison TJ (1994) Isolation of high affinity human antibodies directly from large synthetic repertoires. *EMBO J.* **13:** 3245-9

Guo W, Giancotti FG. (2004) Integrin signalling during tumour progression. *Nat Rev* **5:**816–26

Haapasalmi K, Zhang K, Tonnesen M, Olerud J, Sheppard D, Salo T, Kramer R, Clark RA, Uitto VJ, Larjava H (1996) Keratinocytes in human wounds express alphavbeta6 integrins. *J Invest Dermatol* **106:** 42-8

Hahm K, Lukashev ME, Luo Y, Yang WJ, Dolinski BM, Weinreb PH, Simon KJ, Chun Wang L, Leone DR, Lobb RR, McCrann DJ, Allaire NE, Horan GS, Fogo A, Kalluri R, Shield CF 3rd, Sheppard D, Gardner HA, Violette SM (2007) αvβ6 Integrin Regulates Renal Fibrosis and Inflammation in Alport Mouse. *Am J Path* **170:** 110-125

Häkkinen L, Koivisto L, Gardner H, Saarialho-Kere U, Carroll JM, Lakso M, Rauvala H, Laato M, Heino J, Larjava H (2004) Increased expression of beta6-integrin in skin leads to spontaneous development of chronic wounds. *Am J Pathol* **164:** 229–242.

Hamidi S, Salo T, Kainulainen T, Epstein J, Lerner K, Larjava H (2000) Expression of alphaVbeta6 integrin in oral leukoplakia *Br J of Cancer* **82:** 1433-1440

Hazelbag S, Kenter GG, Gorter A, Dreef EJ, Koopman LA, Violette SM, Weinreb PH, Fleuren GJ (2007) Overexpression of the alphaVbeta6 integrin in cervical squamous cell carcinoma is a prognostic factor for decreased survival *J Pathol.* **212(3):** 316-24.

Heagerty PJ, Lumley T, Pepe MS. (2000) Time dependent ROC curves for censored survival data and a diagnostic marker. *Biometrics* **56:** 337–344

Hecht JL, Dolinski BM, Gardner HA, Violette SM, Weinreb PH (2008) Overexpression of the alphavbeta6 integrin in endometrial cancer. *Appl Immunohistochem Mol Morphol.* **16(6):**543-547

Hilger I, Hergt R, Kaiser WA (2000) Effects of magnetic thermoablation in muscle tissue using iron oxide particles, an in vitro study. *Invest Radiol* **35**: 170-179

Hilger I, Andra W, Hergt R, Hiergeist R, Schubert H, Kaiser WA (2001) Electromagnetic heating of breast tumours in interventional radiology: in vitro and in vivo studies in human cadavers and mice. *Radiol* **218:** 570-575

Hilschmann N, Craig LC (1965) Amino acid sequence studies with Bence-Jones proteins. *Proc Natl Acad Sci U S A* **53**: 1403-1409

Hinz B, Dugina V, Ballestrem C, Wehrle-Haller B, Chaponnier C (2003) Alpha-smooth muscle actin is crucial for focal adhesion maturation in myofibroblasts. *Mol. Biol. Cell* **14**: 2508– 2519

Holme SA, Malinovszky K, Roberts DL (2000) Changing trends in non-melanoma skin cancer in South Wales 1988–98. *Br J Dermatol* **143:** 1224–1229

Hoogenboom HR (2005) Selecting and screening recombinant antibody libraries. *Nat. Biotechnol*. **23:** 1105–1116

Hoover LA, Wortham DG, Lufkin RB, Hanafee WN (1987) Magnetic resonance imaging of the larynx and tongue base: clinical applications. *Otolaryngol Head Neck Surg*. **97:** 245–256

Hsiao JR, Chang Y, Chen YL, Hsieh SH, Hsu KF, Wang CF, Tsai ST, Jin YT (2010) Cyclic alphavbeta6-targeting peptide selected from biopanning with clinical potential for head and neck squamous cell carcinoma. *Head Neck.* **32(2):**160-172

Hu F, Neoh KG, Cen L, Kang E-T (2006) Cellular response to magnetic nanoparticles "PEGylated" via surface-initiated atom transfer radical polymerization. *Biomacromolecules* **7:** 809–816

Huang X, Wu J, Spong S, Sheppard D (1998) The integrin alphavbeta6 is critical for keratinocyte migration on both its known ligand fibronectin and on *vitronectin* *J Cell Sci* **111(Pt15):** 2189-2195

Hume DA, Ross IL, Himes SR, Sasmono RT, Wells CA, Ravasi T (2002) The mononuclear phagocyte system revisited *J Leukocyte Biol* **72**: 621-627

Huston JS, Levinson D, Mudgett-Hunter M, Tai MS, Novotný J, Margolies MN, Ridge RJ, Bruccoleri RE, Haber E, Crea R (1988) Protein engineering of antibody binding sites: recovery of specific activity in an anti-digoxin single-chain Fv analogue produced in Escherichia coli. *Proc Natl Acad Sci U S A*. **85(16):** 5879-5883

Hynes RO (2002) Integrins : bidirectional, allosteric signalling machines *Cell* **110**: 673-687

Impola U, Uitto VJ, Hietanen J, Hakkinen L, Zhang L, Larjava H, Isaka K, Saarialho-kere U. (2004) Differential expression of matrilysin-1 (MMP-7), 92 kD gelatinase (MMP-9), and metalloelastase (MMP-12) in oral verrucous and squamous cell cancer. *J Pathol* **202**: 14–22.

Inbar D, Hochman J, Givol D Localization of Antibody-Combining Sites within the Variable Portions of Heavy and Light Chains *Proc. Nat. Acad. Sci. USA* **69(9):** 2659-2662.

Ishitoya J, Toriyama M, Oguchi N, Kitamura K, Ohshima M, Asano K, Yamamoto T. (1989) Gene amplification and overexpression of EGF receptor in squamous cell carcinomas of the head and neck. *Br J Cancer* **59(4):**559-562

Jackson T, King AM, Stuart DI, Fry E (2003) Structure and receptor binding. *Virus Res.* **91**: 33-46

Jain RK (1988) Determinants of tumor blood flow: a review. *Cancer Res.* **48**: 2641–2658

Johannsen M, Gneveckow U, Thiesen B, Taymoorian K, Cho CH, Waldöfner N, Scholz R, Jordan A, Loening SA, Wust P (2006) Thermotherapy of Prostate Cancer Using Magnetic Nanoparticles: Feasibility, Imaging, and Three-Dimensional Temperature Distribution *Eur Urol* **52(6):** 1653-61

Johannsen M, Thiesen B, Wust P, Jordan A (2010) Magnetic nanoparticle hyperthermia for prostate cancer *Int J Hyperthermia*. *Int J Hyperthermia*. **26(8):**790-795

Jordan A, Wust P, Fähling H, John W, Hinz A, Felix R (1993) Inductive heating of ferrimagnetic particles and magnetic fluids: physical evaluation of their potential for hyperthermia. *Int J Hyperthermia*. **9(1):** 51-68

Jordan A, Wust P, Scholz R, Faehling H, Krause J, Felix R (1997) Magnetic Fuid hyperthermia. *In: Hafeli U, Schutt W, Teller J, Zborowski M, eds. Scientific and Clinical Applications of Magnetic Carriers. New York: Plenum Press*: 569-95

Jordan A, Scholz R, Wust P, Fähling H, Felix R (1999) Magnetic fluid hyperthermia (MFH): Cancer treatment with AC magnetic field induced excitation of biocompatible superparamagnetic nanoparticles. *J Magn Magn Mater* **201**: 413-419

Jones J, Watt, FM, Speight PM (1997) Changes in the expression of alpha v integrins in oral squamous cell carcinomas *J Oral Pathol Med* **26:** 63 – 68

Jones J, Sugiyama M, Watt FM, Speight PM (1993) Integrin expression on normal, hyperplastic, dysplastic and malignant oral epithelium. *J Pathol* **169:** 235-243

Jung J, Cho NH, Kim J, Choi EC, Lee SY, Byeon HK, Park YM, Yang WS, Kim SH. (2009) Significant invasion depth of early oral tongue cancer originated from the lateral

border to predict regional metastases and prognosis. *Int J Oral Maxillofac Surg* **38(6):** 653–60

Kabat EA, Wu TT (1971) Attempts to locate complementary-determining residues in the variable positions of light and heavy chains. *Ann N Y Acad Sci* **(190):** 382-393.

Kallumadil M, Tada M, Nakagawa T, Abe M, Southern p, Pankhurst Q (2009) Suitability of commercial colloids for magnetic hyperthermia *J. Magn. Magn. Mater*. **321** 1509–13

Kawashima A, Tsugawa S, Boku A, Kobayashi M, Minamoto T, Nakanishi I, Oda Y (2003) Expression of alpha v integrin family in gastric carcinoma: increased alphavbeta6 is associated with lymph node metastasis *Pathol Res Pract* **199:** 57-64

Khan AJ, King BL, Smith BD, Smith GL, DiGiovanna MP, Carter D, Haffty BG (2002) Characterization of the HER-2/neu oncogene by immunohistochemical and fluorescence in situ hybridization analysis in oral and oropharyngeal squamous cell carcinoma. *Clin Cancer Res* **8:** 540–548

Khuri FR, Nemunaitis J, Ganly I, Arseneau J, Tannock IF, Romel L, Gore M, Ironside J, MacDougall RH, Heise C, Randlev B, Gillenwater AM, Bruso P, Kaye SB, Hong WK, Kirn DH (2000) A controlled trial of intratumoural ONYX-015, a selectively-replicating adenovirus, in combination with cisplatin and 5-fluorouracil in patients with recurrent head and neck cancer. *Nat Med* **6:** 879–885

Kiyota A, Shintani S, Mihara M, Nakahara Y, Ueyama Y, Matsumura T, Todd R, Wong DT (2000) Expression of a truncated epidermal growth factor receptor in oral squamous cell carcinomas. *Cancer Lett*. ; **161(1)**:9-15

Klucznik RP, Carrier DA, Pyka R, Haid RW (1993) Placement of a ferromagnetic intracerebral aneurysm clip in a magnetic field with a fatal outcome. *Radiology* **187:** 855–856

Köhler G and Milstein C (1975) Continuous cultures of fused cells secreting antibody of predefined specificity. *Nature* **256**: (5517) 495-7.

Koivisto L, Larjava K, Hakkinen L, Uitto VJ, Heino J, Larjava H (1999) Different integrins mediate cell spreading, haptotaxis and lateral migration of HaCaT keratinocytes on fibronectin. *Cell Adhes Commun* **7:** 245–257

Kotitz R, Fannin PC, Trahms L(1995) Time-Domain Study of Brownian and Neel Relaxation in Ferrofluids. *Journal of Magnetism and Magnetic Materials* **149:**42-46

Kyzas PA, Stefanou D, Batistatou A, Agnantis NJ (2005) Prognostic significance of VEGF immunohistochemical expression and tumor angiogenesis in head and neck squamous cell carcinoma *J Cancer Res Clin Oncol* **131:** 624–630

Laimer K, Spizzo G, Gastl G, Obrist P, Brunhuber T, Fong D, Barbieri V, Jank S, Doppler W, Rasse M, Norer B (2007) High EGFR expression predicts poor prognosis in patients with squamous cell carcinoma of the oral cavity and oropharynx: a TMA-based immunohistochemical analysis. *Oral Oncol*. ;**43(2):**193-8

Lanza P, Felding-Habermann B, Ruggeri ZM, Zanetti, M, Billetta R (1997) Selective interaction of a conformationally-constrained Arg-Gly-Asp (RGD) motif with the integrin receptor alphavbeta3 expressed on human tumor cells *Blood Cells Mol. Dis*. **23**: 230-241

Lanzetti L, Di Fiore PP. (2008) Endocytosis and cancer: an 'insider' network with dangerous liaisons. *Traffic;***9:**2011–21

Lee J-H, Lee K, Moon SH, Lee Y, Park TG, Cheon J (2009) All-in-one target-cell-specific magnetic nanoparticles for simultaneous molecular imaging and siRNA delivery. *Angew. Chem. Int. Ed*. **48:** 4174–4179

Lee S, Chon H, Lee M (2009) Surface-enhanced Raman scattering imaging of HER2 cancer markers overexpressed in single MCF7 cells using antibody conjugated hollow gold nanoparticles. *Biosens. Bioelectron*. **24:** 2260–2263

Lee YC, Boehm MK, Chester KA, Begent RH, Perkins SJ (2002) Reversible dimer formation and stability of the anti-tumour single-chain Fv antibody MFE-23 by neutron scattering, analytical ultracentrifugation, and NMR and FT-IR spectroscopy *J. Mol. Biol.* **320**: 107-127

Lewin F, Norell SE, Johansson H, Gustavsson P, Wennerberg J, Biörklund A, Rutqvist LE (1998) Smoking tobacco, oral snuff, and alcohol in the aetiology of squamous cell carcinoma of the head and neck: a population-based case-referent study in Sweden. *Cancer* **82**:1367-1375

Lewis MP, Lygoe K, Nystrom ML, Anderson WP, Speight PM, Thomas GJ (2004) SCC-derived TGF-β1 promotes myofibroblast differentiation and modulates scatter factor–dependent tumour invasion. *Br J Cancer* **90:** 822-832

Li X, Deng W, Nail CD, Bailey SK, Kraus MH, Ruppert JM, Lobo-Ruppert SM (2006) Snail induction is an early response to Gli1 that determines the efficiency of epithelial transformation *Oncogene* **25:** 609-21

Lin MM, Li S, Kim H-H, Kim H, Lee H-B, Muhammed M (2010) Complete separation of magnetic nanoparticles via chemical cleavage of dextran by ethylenediamine for intracellular uptake. *J. Mater. Chem*.; **20:** 444-7

Liotta LA, Kohn EC (2001) The microenvironment of the tumour-host interface. *Nature* **411:** 375-379.

Lohmann CM, Solomon AR. (2001) Clinicopathological variants of cutaneous squamous cell carcinoma. *Adv Anat Pathol* **8:** 27-34

Loo C, Lowery A, Halas N, West J, Drezek R (2005) Immunotargeted nanoshells for integrated cancer imaging and therapy. *Nano Lett*. **5:** 709–711

Lu L, Liu C. Using the time dependent ROC curve to build a better survival model in SAS [Internet]. North East SAS Users group (NESUG) 2006; http://www.nesug.org/Proceedings/nesug06/an/da29.pdf

Lyons AJ, Jones J (2007) Cell adhesion molecules, the extracellular matrix and oral squamous carcinoma *Int. J. Oral Maxillofac. Surg*. **36:** 671–679

Maeda H, Matsumura Y (1989) Tumoritropic and lymphotropic principles of macromolecular drugs. *Crit Rev Ther Drug Carrier Syst* **6:** 193–210.

Maier-Hauff K, Rothe R, Scholz R, Gneveckow U, Wust P, Thiesen B, Feussner A, von Deimling A, Waldoefner N, Felix R, Jordan A (2007) Intracranial thermotherapy using magnetic nanoparticles combined with external beam radiotherapy: results of a feasibility study on patients with glioblastoma multiforme *J Neurooncol.* **81(1):** 53-60

Mansour AM, Drevs J, Esser N, Hamada FM, Badary OA, Unger C, Fichtner I, Kratz F (2003) A new approach for the treatment of malignant melanoma: enhanced antitumor efficacy of an albuminbinding doxorubicin prodrug that is cleaved by matrix metalloproteinase *Cancer Res* **63:** 4062–4066

Marks JD, Hoogenboom HR, Bonnert TP, McCafferty J, Griffiths AD, Winter G (1991) By-passing immunization. Human antibodies from V-gene libraries displayed on phage. *J. Mol. Biol.* **222**: 581.

Marks R, Rennie G, Selwood TS. (1988) Malignant transformation of solar keratoses to squamous cell carcinoma. *Lancet* **1:** 795–797.

Marsh D, Dickinson S, Neill GW, Marshall JF, Hart IR, Thomas GJ (2008) alpha vbeta 6 Integrin promotes the invasion of morphoeic basal cell carcinoma through stromal modulation. *Cancer Res.*;**68(9):**3295-3303

Mateu MG, Valero ML, Andreu D, Domingo E (1996) Systematic replacement of amino acid residues within an Arg-Gly-Asp containing loop of foot and mouth disease virus and effect on cell recognition *J. Biol. Chem.* **271:** 12814-12819

Mayer A, Tsiompanou E, O'Malley D, Boxer GM, Bhatia J, Flynn AA, Chester KA, Davidson BR, Lewis AA, Winslet MC, Dhillon AP, Hilson AJ, Begent RH (2000) Radioimmunoguided Surgery in Colorectal Cancer Using a Genetically Engineered Anti-CEA Single-Chain Fv Antibody. *Clin Cancer Res*. **6(5):** 1711-1719

Mazzola L (2003) Commercialising nanotechnology. *Nature Biotechnology* **21:** 1137-1143

McCafferty J, Griffiths AD, Winter G, Chiswell DJ (1990) Phage antibodies: filamentous phage displaying antibody variable domains. *Nature* **348:** 552–554.

McDonald DM, Choyke PL (2003) Imaging of angiogenesis: from microscope to clinic. *Nat. Med.* **9:** 713–725

Medal R, Shorey WD, Gilchrist RK, Barker W, Hanselman R (1959) Controlled radiofrequency generator for production of localized heat in intact animal. *Arch Surg* **79:** 427-431

Meredith JR, Fazeli B, Schwartz MA (1993) The extracellular matrix as a cell survival factor *Mol Biol Cell* **4 :** 953-961

Miller DL, Weinstock MA. (1994) Nonmelanoma skin cancer in the United States: Incidence. *J Am Acad Dermatol* **30:** 774–778.

Mirick GR, Bradt BM, Denardo SJ, Denardo GL (2004) A review of human anti-globulin antibody (HAGA, HAMA, HACA, HAHA) responses to monoclonal antibodies. Not four letter words. *Q. J. Nucl. Med. Mol. Imaging* **48**: 251–257

Mitsumori M, Hiraoka M, Shibata T, Okuna Y, Masunaga S, Koishi M, Okajima K, Nagata Y, Nishimura Y, Abe M, Ohura K, Hasegawa M, Nagae H, Ebisawa Y (1994) Development of intra-arterial hyperthermia using a dextran magnetite complex. *Intl J Hyperthermia* **10:** 785-793.

Monaghan P, Gold S, Simpson J, Zhang Z, Weinreb PH, Violette SM, Alexandersen S, Jackson T (2005) The alpha(v)beta6 integrin receptor for FMDV is expressed constitutively on the oral epithelial cells targeted in cattle *J. Gen Virol.* **86:** 2769-2780

Monga SPS, Mars WM, Pediaditakis P, Bell A, Mulé K, Bowen WC, Wang X, Zarnegar R, Michalopoulos GK (2002) Hepatocyte growth factor induces Wnt-independent nuclear translocation of β-catenin dissociation in hepatocytes. *Cancer Res* **62:** 2064–2071.

Mornet S, Vasseur S, Grasset F, Duguet E (2004) Magnetic nanoparticle design for medical diagnosis and therapy. *J Mater Chem* **14**: 2161-2175

Mrhalova M, Plzak J, Betka J, Kodet R (2005) Epidermal growth factor receptor: its expression and copy numbers of EGFR gene in patients with head and neck squamous cell carcinomas. *Neoplasma* **52:** 338–343.

Munger JS, Huang X, Kawakatsu H, Griffiths MJ, Dalton SL, Wu J, Pittet JF, Kaminski N, Garat C, Matthay MA, Rifkin DB, Sheppard D (1999) The integrin alphavbeta6 binds

and activates latent TGFB1 : A mechanism for regulating pulmonary inflammation and fibrosis *Cell* **96:** 319-328

Munshi HG, Stack MS. (2006) Reciprocal interactions between adhesion receptor signaling and MMP regulation. *Cancer Metastasis Rev*;**25**:45–56

Muyldermans S (2001) Single domain camel antibodies: current status. *J.Biotechnol.* **74:** 277–302

Nilsson M, Unden AB, Krause D, Malmqwist U, Raza K, Zaphiropoulos PG, Toftgard R (2000). Induction of basal cell carcinomas and trichoepitheliomas in mice overexpressing GLI-1. *Proc Natl Acad Sci U S A*. **97:** 3438-3443

Niu J, Dorahy DJ, Gu X, Scott RJ, Draganic B, Ahmed N, Agrez MV (2002) Integrin expression in colon cancer cells is regulated by the cytoplasmic domain of the beta6 integrin subunit. *Int J Cancer* **99:** 529–537.

Nomura T, Saikawa A, Morita S, Sakaeda Kakutani T, Yamashita F, Honda K, Takakura Y, Hashida M (1998) Pharmacokinetic characteristics and therapeutic effects of mitomycin C-dextran conjugates after intratumoural injection. *J Control Release* **52**: 239–252

Nylander K, Dabelsteen E, Hall PA (2000) The p53 molecule and its prognostic role in squamous cell carcinomas of the head and neck. *J Oral Pathol Med*. **29(9):**413-425

Nystrom ML, McCulloch D, Weinreb PH, Violette SM, Speight PM, Marshall JF, Hart IR, Thomas GJ (2006). Cyclooxygenase-2 inhibition suppresses αvβ6 integrin-dependent oral squamous carcinoma invasion. *Cancer Res* **66:** 10833–10842

Nystrom ML, Thomas GJ, Stone M, Mackenzie IC, Hart IR, Marshall JF (2005) Development of a quantitative method to analyse cell invasion in organotypic culture. *J Pathol* **205:** 468-475.

Oikarinen A, Raitio A (2000) Melanoma and other skin cancers in circumpolar areas. *Int J Circumpolar Health* **59:** 52–56

Okamoto M, Nishimine M, Kishi M, Kirita T, Sugimura M, Nakamura M, Konishi N. (2002) Prediction of delayed neck metastasis in patients with stage I/II squamous cell carcinoma of the tongue. *J Oral Pathol Med* **31(4):** 227–33.

Orgill D, Porter S, Taylor H (2005) Heat injury to cells in perfused systems. *Ann N Y Acad Sci* **1066:**106-118.

Oro AE, Higgins KM, Hu Z, Bonifas JM, Epstein EH Jr, Scott MP (1997) Basal cell carcinomas in mice over-expressing Sonic hedgehog. *Science* **276**: 817–821

Pakhomov A, Bao Y, Krishnan K (2005) Effects of surfactant friction on Brownian magnetic relaxation in nanoparticle ferrofluids. *J Appl Phys* **97:**310

Pankhurst QA, Thanh NKT, Jones SK, Dobson J (2009) Progress in applications of magnetic nanoparticles in biomedicine *J. Phys. D: Appl. Phys*. **42**

Parker SL, Tong T, Bolden S, Wingo PA (1996) Cancer statistics. *CA Cancer J Clin* **46:** 5–27

Parkin DM, Whelan SL, Ferlay J, Teppo L, Thomas, DB (2002) Cancer Incidence in Five Continents*, Vol. VIII. IARC Scientific Publications No. 155, Lyon, IARC*

Partridge M, Gullick WJ, Langdon JD, Sherriff M (1988) Expression of epidermal growth factor receptor on oral squamous cell carcinoma. *Br J Oral Maxillofac Surg*. **26(5):**381-389.

Pavlicek W, Geisinger M, Castle L, Borkowski GP, Meaney TF, Bream BL, Gallagher JH (1983) The effects of nuclear magnetic resonance on patients with cardiac pacemakers. *Radiology* **147:** 149–153

Persic L, Roberts A, Wilton J, Cattaneo A, Bradbury A, Hoogenboom HR (1997) An integrated vector system for the eukaryotic expression of antibodies or their fragments after selection from phage display libraries. *Gene* **187**: 9–18

Persson MA (1991) Generation of diverse high-affinity human monoclonal antibodies by repertoire cloning. *Proc. Natl. Acad. Sci. U. S. A.* **88**: 2432–2436

Peruzzi B, Bottaro DP (2006) Targeting the c-Met signaling pathway in cancer. *Clin Cancer Res.* **12(12):** 3657-3660

Pignon JP, Bourhis J, Domenge C, Designé L (2000) Chemotherapy added to locoregional treatment for head and neck squamous-cell carcinoma: Three meta-analyses of updated individual data. MACH-NC Collaborative Group—Meta-Analysis of Chemotherapy on Head and Neck Cancer. *Lancet* **355:** 949-955

Poljak RJ (1973) X-ray crystallographic studies of immunoglobulins. *Contemp Top Mol Immuno*l **2**: 1-26.

Poljak RJ, Amzel LM, Avery HP, Becka LN, Nisonoff A (1972) Structure of Fab' New at 6 A resolution. *Nature New Biol.* **235**: 137-140.

Porter RR (1959) The hydrolysis of rabbit y-globulin and antibodies with crystalline papain. *Biochem J.* **73:** 119-126.

Pupa SM, Menard S, Forti S, Tagliabue E (2002) New insights into the role of extracellular matrix during tumour onset and progression. *J Cell Physiol* **192:** 259-267.

Puri SK, Fan CY, Hanna E (2003)(Significance of extracapsular lymph node metastases in patients with head and neck squamous cell carcinoma. *Curr Opin Otolaryngol Head Neck Surg.* **11(2):** 119-23

Putti TC, To KF, Hsu HC, Chan AT, Lai GM, Tse G, Lee YS, Whang-Peng J, Millward M, Lin L, Lin X, Lee CS (2002) Expression of epidermal growth factor receptor in head and neck cancers correlates with clinical progression: a multicentre immunohistochemical study in the Asia-Pacific region. *Histopathology* ;**41(2):**144-51

Rabinovitz I, Mercurio AM (1996) The integrin α6β4 and the biology of carcinoma. *Biochem. Cell Biol*. **74:** 811–821

Radisky DC, Kenny PA, Bissell MJ. (2007) Fibrosis and cancer: do myofibroblasts come also from epithelial cells via EMT? *J Cell Biochem* **101:** 830-839

Ragin CC, Modugno F, Gollin SM (2007) The epidemiology and risk factors of head and neck cancer: a focus on human papillomavirus *J Dent Res*. **86(2):** 104-114

Rahima B, Shingaki S, Nagata M, Saito C. (2004) Prognostic significance of perineural invasion in oral and oropharyngeal carcinoma. *Oral Surg Oral Med Oral Pathol Oral Radiol Endod.* **97(4):**423-31

Ramos DM, But M, Regezi J, Schmidt BL, Atakilit A, Dang D, Ellis D, Jordan R, Li X (2007) Expression of integrin beta6 enhances invasive behaviour in oral squamous cell carcinoma *Matrix Biology* **21:** 297-307

Ramos DM, Dang D, Sadler S (2009). The role of the integrin alpha v beta6 in regulating

the epithelial to mesenchymal transition in oral cancer. *Anticancer Res* **29:** 125-30

Ramsay AG, Keppler MD, Jazayeri M, Thomas GJ, Parsons M, Violette S (2007) HS1-associated protein X-1 regulates carcinoma cell migration and invasion via clathrin-mediated endocytosis of integrin alphavbeta6. *Cancer Res* **67:**5275–84

Rand RW, Snyder M, Elliot D, Snow H (1976) Selective radiofrequency heating of ferrosilicone occluded tissue. *Bull LA Neurol Soc* **41:** 154-159

Rand RW, Snow HD, Brown WJ (1982) Thermomagnetic surgery for cancer. *J Surg Res* **33:** 177-183

Read DA, Chester KA, Keep PA, Begent RH, Pedersen JT, Rees AR (1995) Br. J. Cancer 71, Suppl. XIV, 57 (abstr. P132)

Regezi JA, Ramos DM, Pytela R, Dekker NP, Jordan RC. (2002) Tenascin and beta 6 integrin are overexpressed in floor of mouth in situ carcinomas and invasive squamous cell carcinomas. *Oral Oncol* **38:** 332–336

Regl G, Neil GW, Eichberger T, Kasper M, Ikram MS, Koller J, Hintner H, Quinn AG, Frischauf AM and Aberger F. (2002) Human GLI2 and GLI1 are part of a positive feedback mechanism in Basal Cell Carcinoma. *Oncogene* **21**: 5529-5539.

Reichart PA (2001) Identification of risk groups for oral pre-cancer and cancer and preventive measures *Clin Oral Investig* **5(4):** 207-213

Revets H, De Baetselier P, Muyldermans S (2005) Nanobodies as novel agents for cancer therapy. *Expert Opin. Biol. Ther.* **5**: 111–124

Ries LAG, Eisner MP, Kosary CL, Hankey BF, Miller BA, Clegg L, Mariotto A, Feuer EJ, Edwards BK (2005) *SEER Cancer Statistics Review*, 1975-2002. Bethesda, MD: National Cancer Institute

Royston P, Moons KG, Altman DG, Vergouwe Y (2009) Prognosis and prognostic research: Developing a prognostic model. *BMJ.* **31**: 338-339
Ryle AP, Porter RR (1959) Parapepsins: two proteolytic enzymes associated with porcine pepsin. *Biochem J.* **73**:75-86.

Sachelarie I, Kerr K, Ghesani M, Blum RH (2005) Integrated PET-CT: evidence-based review of oncology indications *Oncology* **19(4):** 481-490

Sahoo Y, Pizem H, Fried T, Golodnitsky D, Burstein L, Sukenik CN, Markovich G (2001) Alkyl phosphonate/phosphate coating on magnetite nanoparticles: a comparison with fatty acids. *Langmuir* **17:**7907–11

Sainz-Pastor N, Tolner B, Huhalov A, Kogelberg H, Lee YC, Zhu D, Begent RH, Chester KA (2006) Deglycosylation to obtain stable and homogeneous Pichia pastoris-expressed N-A1 domains of carcinoembryonic antigen *Int. J. Biol. Macromol.* **39:** 141-150

Salomon DS, Brandt R, Ciardiello F, Normanno N (1995) Epidermal growth factor-related peptides and their receptors in human malignancies. *Crit Rev Oncol Hematol* **19:** 183–232

Sblattero D, Bradbury A (2000) Exploiting recombination in single bacteria to make large phage antibody libraries. *Nat. Biotechnol*. **18:** 75-80

Scapin G (2006) Structural biology and drug discovery. *Curr. Pharm. Des.* **12(17):** 2087-2097

Schipper ML, Lyer G, Koh AL(2009) Particle size, surface coating, and PEGylation influence the biodistribution of quantum dots in living mice. *Small* **5,** 126–134

Scrivener Y, Grosshans E, Cribier B (2002) Variations of basal cell carcinomas according to gender, age, location, and histopathological subtype. *Br J Dermatol* **147:** 41–47

Sedlacek HH, Gronski P, Hofstaetter T, Kanzy EJ, Schorlemmer HU, Seiler FR. (1983) The biological properties of immunoglobulin G and its split products [F(ab')2 and Fab]. *Klin Wochenschr*. **61(15)**:723-736.

Shibuya K, Mathers CD, Boschi-Pinto C, Lopez AD, Murray CJ. Global and regional estimates of cancer mortality and incidence by site: II. Results for the global burden of disease (2002) *BMC Cancer* **26**:2:37

Siegel RW (1999) In: Siegel RW, Hu E, Roco MC Nanostructure science and technology. A worldwide study. *WTEC, Loyola College in Maryland*

Sipos B, Hahn D, Carceller A, Piulats J, Hedderich J, Kalthoff H, Goodman SL, Kosmahl M, Klöppel G (2004) Immunohistochemical screening for the beta 6 integrin subunit expression in adenocarcinomas using a novel monoclonal antibody reveals strong up-regulation in pancreatic ductal adenocarcinomas in vivo and in vitro. *Histopathology* **45**: 226-236

Sjogren CE, Briley-Saebo K, Hanson M, Johansson C (1994) Magnetic characterization of iron oxides for magnetic resonance imaging. *Magn Reson Med* **31(3):** 268–272

Skerra A, Plückthun A (1988) Assembly of a functional immunoglobulin Fv fragment in Escherichia coli. *Science* **240:** 1038-41

Smid EJ, Stoter TR, Bloemena E, Lafleur MV, Leemans CR, van der Waal I, Slotman BJ, Langendijk JA (2006) The importance of immunohistochemical expression of EGFr in

squamous cell carcinoma of the oral cavity treated with surgery and postoperative radiotherapy *Int J Radiat Oncol Biol Phys*.**65(5):** 1323-1329

Smythe WR, LeBel E, Bavaria JE, Kaiser LR, Albelda SM (1995) Integrin Expression in Non small cell carcinoma of the lung *Cancer metastasis review* **14:** 229-239

Söderlind E, Strandberg L, Jirholt P, Kobayashi N, Alexeiva V, Aberg AM, Nilsson A, Jansson B, Ohlin M, Wingren C, Danielsson L, Carlsson R, Borrebaeck CA (2000) Recombining germline-derived CDR sequences for creating diverse single-framework antibody libraries. *Nat. Biotechnol.* **18:** 852-856

Soulieres D, Senzer NN, Vokes EE, Hidalgo M, Agarwala SS, Siu LL (2004) Multicenter phase II study of erlotinib, an oral epidermal growth factor receptor tyrosine kinase inhibitor, in patients with recurrent or metastatic squamous cell cancer of the head and neck. *J Clin Oncol*. **22:** 77-85

Stark DD, Weissleder R, Elizondo G, Hahn PF, Saini S, Todd LE, Wittenberg J, Ferrucci JT (1988) Superparamagnetic iron oxide: clinical application as a contrast agent for MR imaging of the liver *Radiology* **168:** 297-301

Stewart BW, Kleihues P (2003) World Cancer Report. *Lyon: WHO International Agency for Research on Cancer*

Stoecklein NH, Siegmund A, Scheunemann P, Luebke AM, Erbersdobler A, Verde PE, Eisenberger CF, Peiper M, Rehders A, Esch JS, Knoefel WT, Hosch SB (2006) Ep-CAM expression in squamous cell carcinoma of the esophagus: a potential therapeutic target and prognostic marker. *BMC Cancer* **6:** 165–172

Storkel S, Reichert T, Reiffen KA, Wagner W (1993) EGFR and PCNA expression in oral squamous cell carcinomas–a valuable tool in estimating the patient's prognosis. *Eur J Cancer B Oral Oncol* **29B:** 273–277

Storm FK (1983) Background, principles, and practice. *In: Storm FK, editor. Hyperthermia in cancer therapy. Boston: G.K. Hall*

Sun J, Zhou S, Hou P, Yang Y, Weng J, Li X, Li M. (2007) Synthesis and characterization of biocompatible Fe3O4 nanoparticles. *J Biomed Mater Res A.* **80(2):** 333-41

Sutton DN, Brown JS, Rogers SN, Vaughan ED, Woolgar JA (2003) The prognostic implications of the surgical margin in oral squamous cell carcinoma. *Int J Oral Maxillofac Surg*. **32(1):**30-34

Suzuki C, Matsumoto T, Sonoue H, Arakawa A, Furugen Y, Kinoshita K (2003) Prognostic significance of the infiltrative pattern invasion in endometrioid adenocarcinoma of the endometrium. *Pathology International* **53:** 495-500

Suzuki M, Shinkai M, Kamihira M, Kobayashi T. (1995) Preparation and characteristics of magnetite-labelled antibody with the use of poly(ethylene glycol) derivatives. *Biotechnol Appl Biochem :***21 (Pt 3):**335-345

Tartaj P, Gonzalez-Carreno T, Serna CJ (2001) Single-step nanoengineering of silica coated maghemite hollow spheres with tunable magnetic properties. *Adv Mater* **13:** 1620–1624.

Tazawa K, Takemori S, Yamashita I, Kato H, Kasagi T, Saito T, Yamamoto K, Katsuyama S, Maeda M, Honda T, Kimura E, Fujimaki M (1988) Intracellular hyperthermia by fixated submicron particle exciting in inductive field of 500 kHz. *In: Hyperthermic Oncology. London: Taylor & Francis*: 869-870

Thomas GJ, Lewis MP, Whawell SA, Russell A, Sheppard D, Hart IR, Speight PM, Marshall JF (2001) Expression of the alphavbeta6 integrin promotes migration and invasion in squamous cell carcinoma cells *J Invest Dermatology* **117(1):** 67-73

Thomas GJ, Lewis MP, Hart IR, Marshall JF, Speight PM (2001) αvβ6 integrin promotes invasion of squamous carcinoma cells through up-regulation of matrix metalloproteinase-9. *Int J Cancer* **92:** 641-665.

Thomas GJ, Nystrom ML, Marshall JF (2006) αvβ6 integrin in wound healing and cancer of the oral cavity. *J Oral Pathol Med* **35:** 1–10.

Thomas GJ, Poomsawat S, Lewis MP, Hart IR, Speight PM, Marshall JF (2001) alphavbeta6 integrin upregulates matrix metalloproteinase 9 and promotes migration of normal oral keratinocytes *J Invest Dermatology* **116:** 898-904

Thomas GR, Nadiminti H, Gegalado J (2005) Molecular predictors of clinical outcome in patients with head and neck squamous cell carcinoma. *Int J Exp Path* **86**: 347-363

Tlsty TD, Hein PW (2001) Know thy neighbour: stromal cells can contribute oncogenic signals. *Current Opin Genetics and Development* **11:** 54-59.

Tsushima H, Kawata S, Tamura S, Ito N, Shirai Y, Kiso S, Imai Y, Shimomukai H, Nomura Y, Matsuda Y, Matsuzawa Y. High levels of transforming growth factor beta 1 in patients with colorectal cancer: association with disease progression (1996) *Gastroenterology* **110(2)**: 375-382

Tuxhorn JA, Ayala GE, Rowley DR (2001) Reactive stroma in prostate cancer progression. *J Urology* **166:** 2472−2483.

Tytor M, Olofsson J. (1992) Prognostic factors in oral cavity carcinomas. *Acta Otolaryngol Suppl*. **492**:75-78

Uchida T, Sanghvi NT, Gardner TA, Koch MO, Ishii D, Minei S, Satoh T, Hyodo T, Irie A, Baba S (2002) Transrectal high-intensity focused ultrasound for treatment of patients with stage T1b-2n0m0 localized prostate cancer: A preliminary report. *Urology* **59:**394–398

Ullrich A. (2002) Molecular targets in cancer therapy and their impact on cancer management. *Oncology* **63 (suppl 1):**1-5

Valdagni R, Amichetti M (1994) Report of long-term follow-up in a randomized trial comparing radiation therapy and radiation therapy plus hyperthermia to metastatic lymphnodes in stage IV head and neck patients. *Int J Radiat Oncol Biol Phys* **28:** 163-168

Van Aarsen LA, Leone DR, Ho S, Dolinski BM, McCoon PE, LePage DJ, Kelly R, Heaney G, Rayhorn P, Reid C, Simon KJ, Horan GS, Tao N, Gardner HA, Skelly MM, Gown AM, Thomas GJ, Weinreb PH, Fawell SE, Violette SM (2008) Antibody-mediated blockade of integrin alpha v beta 6 inhibits tumor progression in vivo by a transforming growth factor-beta-regulated mechanism *Cancer Res*. **68(2):**561-70

van Landeghem FK, Maier-Hauff K, Jordan A, Hoffmann KT, Gneveckow U, Scholz R, Thiesen B, Brück W, von Deimling A (2009) Post-mortem studies in glioblastoma patients treated with thermotherapy using magnetic nanoparticles. *Biomaterials* **30(1):**52-7

van Waes C, Surh DM, Chen Z, Kirby M, Rhim JS, Brager R, Sessions RB, Poore J, Wolf GT, Carey TE. (1995) Increase in suprabasilar integrin adhesion molecule expression in human epidermal neoplasms accompanies increased proliferation occurring with immortalization and tumor progression. *Cancer Res*. **55:** 5434–5444

Vaupel P (2000) Tumour blood Flow. *In: Molls M, Vaupel P, eds. Blood Perfusion and Microenvironment of Human Tumours. Berlin: Springer-Verlag*: 41-5

Vermorken JB, Remenar E, van Herpen C, Gorlia T, Mesia R, Degardin M, Stewart JS, Jelic S, Betka J, Preiss JH, van den Weyngaert D, Awada A, Cupissol D, Kienzer HR, Rey A, Desaunois I, Bernier J, Lefebvre JL; EORTC 24971/TAX 323 Study Group (2007) Cisplatin, fluorouracil, and docetaxel in unresectable head and neck cancer *N Engl J Med*. **357(17):** 1695-1704

Verrecchia F, Mauvial A (2002) Transforming Growth Factor Beta signalling through Smad pathway: role in extracellular matrix gene expression and regulation *J Invest Dermatology* **118**:211-215

Vered M, Dobriyan A, Dayan D, Yahalom R, Talmi YP, Bedrin L, Barshack I, Taicher S. (2010) Tumorhost histopathologic variables, stromal myofibroblasts and risk score, are significantly associated with recurrent disease in tongue cancer. *Cancer Sci* **101(1):** 274–80.

Vikram B (1994) Changing patterns of failure in advanced head and neck cancer. *Arch Otolaryngol Head Neck Surg* **110:** 564–565

Vigor KL (2010) Antibody Targeted Nanoparticles for Imaging and Therapy of Cancer. *PhD thesis*, University College London
Vladimir S, Zaitsev V, Dmitry S, Filimonov I, Gambino RJ, Chu B, Presnyakov A (1999) Physical and chemical properties of magnetite and magnetite-polymer nanoparticles and their colloidal dispersions. *J Coll Interf Sci* **212:** 49-54

Walling HW, Fosko SW, Geraminejad PA,Whitaker DC, Arpey CJ (2004) Aggressive basal cell carcinoma: Presentation, pathogenesis, and management. *Cancer and Metastasis Reviews* **23:** 389–402.

Wängler C, Buchmann I, Eisenhut M Haberkorn U, Mier W (2007) Radiolabeled peptides and proteins in cancer therapy *Protein Pept Lett*. **14(3):** 273-279.

Watt FM (2002) Role of integrins in regulating epidermal adhesion, growth and differentiation. *EMBO J*. **21:** 3919–3926

Weiner LM, Surana R, Wang S (2010) Monoclonal antibodies: versatile platforms for cancer immunotherapy *Nat Rev Immunol.* **10(5):**317-27

Weinstock MA (1989) The epidemic of squamous cell carcinoma. *JAMA* **262:** 2138-40

Werb Z, Tremble PM, Behrendtsen O (1989) Signal transduction through the fibronectin receptor induces collagenase and stromelysin gene expression *J Cell Biol*. **109:** 877-89

Westernoff TH, Jordan CK, Regezi JA Ramos DM, Schmidt BL. (2005) β6 intehrin, tenascin C and MMP-1 expression in salivary gland noplasms' *Oral Oncol.* **41**:170-4

Wikstrom P, Stattin P, Franck-Lissbrant I, Damber JE, Bergh A. (1998) Transforming growth factor beta 1 is a ssociated with angiogenesis, metastasis and poor clinical outcome in prostate cancer. *Prostate* **37(1)**: 19-29

Wipff PJ and Hinz B (2008) Integrins and the activation of latent transforming growth factor beta1 - an intimate relationship. *Eur J Cell Biol* **87:** 601–15

Woolgar JA(2006) Histopathological prognosticators in oral and oropharyngeal squamous cell carcinoma. *Oral Oncol* **42:** 229-39

Wu AM, Senter PD (2005) Arming antibodies: prospects and challenges for immunoconjugates. *Nat. Biotechnol*. **23**: 1137–1146

Wu AM, Chen W, Raubitschek A, Williams LE, Neumaier M, Fischer R, Hu SZ, Odom-Maryon T, Wong JY, Shively JE (1996) Tumor localization of anti-CEA single-chain Fvs: improved targeting by non-covalent dimers. *Immunotechnology* **2:** 21–36

Wu TT, Kabat EA (1970) An analysis of the sequences of the variable regions of Bence Jones proteins and myeloma light chains and their implications for antibody complementarity. *J Exp Med* **132:** 211-250.

Wynder EL, Bross IJ (1957) Aetiological factors in mouth cancer; an approach to its prevention. *Br Med J* **1:**1137-1143.

Xu J, Lamouille S, Derynck R. (2009) TGF-beta-induced epithelial to mesenchymal transition. *Cell Res* **9(2):** 156-72

Yang L (2010) TGFβ and cancer metastasis: an inflammation link *Cancer metastasis Rev* **29:** 263-71

Yang L, Mao H, Wang YA et al. (2009) Single chain epidermal growth factor receptor antibody conjugated nanoparticles for in vivo tumor targeting and imaging. *Small* **5:** 235–243

Yang L, Moses HL (2008) Transforming growth factor beta: tumor suppressor or promoter? Are host immune cells the answer? *Cancer Res.* **68(22):** 9107-11

Zanetti M (1992) Antigenized antibodies *Nature* **355(6359):** 476-477

van der Zee J (2002) Heating the patient: A promising approach? *Annals of Oncology* **13:** 1173–1184

Zhang ZY, Xu KS, Wang JS, Yang GY, Wang W, Wang JY, Niu WB, Liu EY, Mi YT, Niu J (2008) Integrin avh6 acts as a prognostic indicator in gastric carcinoma. *Clin*

Oncol **20:** 61–6.

Zhou X, Chang Y, Oyama T, McGuire MJ, Brown KC (2004) Cell-specific delivery of a chemotherapeutic to lung cancer cells. *J Am Chem Soc* **129:**15656–15657.

Appendix 3

Publications

Presentations

Publications

Marsh D, Suchak K, Moutasim K, Vallath S, Hopper C, Jerjes W, Uplie T, Kalavrezos N, Violette S, Weinreb P, Chester K, Chana J, Marshall J, Hart I, Hackshaw A, Piper K, Thomas G (2011) Stromal features are predictive of disease mortality in oral cancer patients *J Pathol.* **223(4):** 470-81

Marsh D, Dickson S, Neill G, Marshall J, Hart I, Thomas G (2008) Upregulation of avb6 integrin in morphoeic BCC promotes invasion indirectly through generation of a myofibroblastic stroma' *Cancer Res*. **68(9):**3295-3303

Kogelberg H, Tolner B, Thomas G, DiCara D, Minogue S, Ramesh B, Sodha S, Marsh D, Lowdell M, Meyer T, Begent R, Hart I, Marshall J, Chester K (2008) Engineering a Single Chain Fv Antibody to αvβ6 Integrin using the Specificity-Determining Loop of a Foot-and-Mouth Disease Virus *J Mol Biol*. **382(2)**:385-401

Oral and Poster Presentations

Targeted Magnetic Fluid Hyperthermia - A Novel Therapy in Morphoeic Type Basal Cell Carcinoma Oral Presentation BAPRAS, London Dec 2009

Antibody Targeted Magnetic Fluid Hyperthermia for Therapy in Oral Cancer Oral Presentation BAPRAS, London Dec 2009

Antibody targeted magnetic fluid hyperthermia for therapy in squamous cell carcinoma Sylvia Lawler Prize Presentation, RSM Oncology Section, London July 2009

'Antibody targeted magnetic fluid hyperthermia in oral SCC' European Plastic Surgery Research Council Meeting. Hamburg August 2009

‘The αvβ6 integrin - a potential target for antibody conjugated magnetic fluid hyperthermia in head and neck squamous cell carcinoma’ Oral Presentation. British Association of Surgical Oncology, RCS London. November 2008 Published Abstract EJSO 2008 Oct; 34 (10): 1161

‘The αvβ6 integrin - a novel target for antibody conjugated magnetic fluid hyperthermia in squamous cell carcinoma’ Poster Presentation. National Cancer Research Institute Annual Conference Birmingham, October 2008

‘Upregulation of αvβ6 integrin promotes invasion in morphoeic BCC’
Oral presentation 17th EADV Congress, Paris Sept 2008

‘Expression of αvβ6 Integrin in Non-melanoma Skin Cancer’
Oral Presentation BAPRAS Winter meeting Dec 2007

‘Antibody-nanoparticle conjugates for targeted theragnosis in cancer’
Invited Speaker World BioPharm Forum: New Frontiers in Nanomedicine
Hammersmith hospital Conference Centre, London, UK 16 Oct 2007

‘Expression of αvβ6 Integrin in Squamous Cell Carcinoma of the skin’ Oral Presentation ECSAPS, Aachen, Germany Sept 2007

‘Antibody Targeted Magnetic Nanoparticles for Theragnosis in Cancer’ Poster Presentation. National Cancer Research Institute Annual Conference Birmingham, October 2007.